



Lynch, Ailsa S. (2014) *Base-metal catalysis for the hydrogenation of acetic acid*. PhD thesis.

<http://theses.gla.ac.uk/5162/>

Copyright and moral rights for this work are retained by the author

A copy can be downloaded for personal non-commercial research or study, without prior permission or charge

This work cannot be reproduced or quoted extensively from without first obtaining permission in writing from the author

The content must not be changed in any way or sold commercially in any format or medium without the formal permission of the author

When referring to this work, full bibliographic details including the author, title, awarding institution and date of the thesis must be given

Enlighten:Theses
<http://theses.gla.ac.uk/>
theses@gla.ac.uk

Base - Metal Catalysis for the Hydrogenation of Acetic Acid



Ailsa S. Lynch

A Thesis Presented to the University of Glasgow
for the Degree of Doctor of Philosophy

Abstract

Increasing global ethanol consumption has revived research into a variety of route for the synthesis of ethanol. One such route is via the hydrogenation of acetic acid, for which a catalyst with significant acid tolerance is required. The objective of finding an active, acid tolerant base metal catalyst was central to this project.

In this study, a commercial methanol synthesis catalyst was initially investigated for its viability as an acid hydrogenation catalyst, following the production of ethanol when acetic acid was passed over it in a different study [1]. The methanol synthesis catalyst was not a viable option due to deactivation, but the use of a copper based system was shown to be active, in line with other studies [2].

Copper based catalysts were tested in both integral and differential reactor systems. The copper catalysts, with metal loadings of 5 wt.% and 10 wt.%, showed some activity towards the production of ethanol, but not in comparable quantities to those observed with the high copper content methanol synthesis catalyst.

The effect of higher acetic acid concentrations, up to 20 mol.%, within an atmospheric fixed bed system were investigated, and showed that copper based catalysts were physically compromised by the presence of acetic acid. Deactivation and degradation of this catalyst upon exposure to acetic acid, especially at higher concentrations, meant that it was not appropriate for this process.

The propensity of the copper catalysts to degrade in the presence of acetic acid led to other base metal systems being investigated, in the form of nickel and cobalt catalysts. All three base metal systems were investigated within a differential reactor to show direct comparisons of each catalyst at 10 wt.% and 20 wt.% metal loadings. This research showed that cobalt based systems were the most active of the metals tested at the two separate loadings.

A study into the effect of the catalyst support using an 10 wt.% cobalt loading, on a range of supports, showed that alumina was the superior support for the selective hydrogenation of acetic acid to ethanol. The other supports investigated were silica, titania and zinc oxide.

Comprehensive testing of the catalysts prepared with cobalt, copper and nickel, identified that the 20 wt.% cobalt on alumina was the most stable, in terms of activity and catalyst integrity, and active catalyst of those investigated at an optimal reaction temperature of 250 °C.

Table of Contents

List of Tables.....	7
List of Figures.....	9
Acknowledgements.....	12
Author's Declaration.....	13
Abbreviations.....	14
1 Introduction.....	15
1.1 Ethanol.....	15
1.1.1 Fermentation.....	17
1.1.2 Synthesis.....	18
1.2 Acetic Acid Hydrogenation.....	18
1.3 Acetic Acid Production.....	23
1.4 Catalysts.....	23
1.4.1 Precious Metal Catalysts.....	23
1.4.2 Base-Metal Catalysts.....	24
1.4.3 Supports.....	25
1.5 Catalyst Deactivation.....	26
1.6 Project Background.....	27
1.7 Project Aims.....	28
2 Experimental.....	30
2.1 Catalyst Preparation.....	30
2.1.1 Supports.....	30
2.1.2 Preparation Procedures.....	30
2.1.3 Commercial Catalysts.....	36
2.2 Catalyst Characterisation.....	37
2.2.1 Surface Area Determination.....	37
2.2.2 Thermogravimetric Analysis.....	39
2.2.3 Powder X-Ray Diffraction.....	39
2.2.4 Microanalysis (CHN).....	40
2.2.5 Nuclear Magnetic Resonance Spectroscopy.....	40
2.3 Catalyst Testing.....	40
2.3.1 Berty Reactor.....	40
2.3.2 Low Pressure Microreactor.....	44
2.3.3 HRTC Atmospheric Fixed Bed Reactor.....	48
2.3.4 Materials.....	54
3 Results and Discussion.....	56
3.1 Copper Catalysts.....	56

3.1.1	Methanol Synthesis Catalyst	56
3.1.2	Impregnated Copper Catalysts.....	65
3.1.3	Catalytic Testing: BERTY reactor	78
3.1.4	10 wt.% Copper Catalyst.....	90
3.1.5	Catalyst Testing: Low pressure microreactor.....	90
3.1.6	Copper Chromite catalysts	101
3.1.7	Summary	102
3.2	High Acetic Acid Concentration Reactions.....	104
3.2.1	Reduction Conditions	104
3.2.2	Reactions	105
3.2.3	Liquid Samples	105
3.2.4	Gas Samples	112
3.2.5	ICP-MS Results.....	114
3.2.6	Post reaction characterisation: MeOHSC	119
3.2.7	Post-reaction characterisation	122
3.2.8	Conclusions	125
3.3	Alternative Base Metal Catalysts	127
3.3.1	10 wt.% Nickel catalyst	127
3.3.2	10 wt.% Cobalt catalyst.....	129
3.3.3	Comparing 10 wt.% catalysts.....	130
3.3.4	Conclusions	133
3.4	20 wt.% Metal Catalysts	135
3.4.1	Alumina SA6X75	135
3.4.2	20 wt.% Nickel Catalyst.....	136
3.4.3	20 wt.% Cobalt Catalyst	138
3.4.4	20 wt.% Copper Catalyst.....	139
3.4.5	Comparing 20 wt.% catalysts.....	139
3.4.6	Bimetallic catalysts	143
3.4.7	Conclusions	145
3.5	Optimisation Studies	148
3.5.1	Temperature Dependence.....	148
3.5.2	Sintering	160
3.5.3	Bed Profiling.....	164
3.5.4	Effect of Support Study.....	165
3.5.5	Supports.....	166
3.5.6	Comparison of 10 wt.% cobalt catalysts.....	167
3.5.7	Post-reaction characterisation	172
3.5.8	Summary	181
4	Conclusions	183

References.....186

List of Tables

Table 2-1: Support pore volume values used for impregnated catalyst preparation.....	31
Table 2-2: Impregnated catalysts prepared	32
Table 2-3: Mono- and bi-metallic precipitation catalysts prepared	34
Table 2-4: Mono-metallic and bi-metallic precipitation catalysts prepared.....	36
Table 2-5: Composition of typical Methanol Synthesis Catalyst [44]	37
Table 2-6: Percentage of components in Sud-Chemie copper chromite	37
Table 2-7: Standard reduction parameters for glassline reactions.....	46
Table 2-8: Standard reaction conditions for Glassline reactions	46
Table 2-9: Standard reduction conditions for HRTC atmospheric fixed bed reactions.....	51
Table 2-10: Standard reaction conditions for Hull Glassware reactions.....	52
Table 2-11: Gases used for the reactions, calibrations and characterisation techniques.....	54
Table 2-12: Reactants and products used for reactions and GC calibrations.....	54
Table 2-13: Materials used for the preparation of catalysts and the supplied catalyst supports used	55
Table 2-14: Commercially available catalysts used within the project	55
Table 3-1: BET analysis of commercial methanol synthesis catalyst	57
Table 3-2: Conditions for the reduction of methanol synthesis catalyst	60
Table 3-3: Reaction conditions for MeOHSC tested in BERTY reactor (B1)	60
Table 3-4: Conversion and selectivities from reaction B1	61
Table 3-5: BET data for comparison of pre- and post- reaction samples	64
Table 3-6: Silica Q10 BET data	66
Table 3-7: Reduction conditions for CuAQ10c and CuNQ10c.....	73
Table 3-8: Standard reaction conditions for testing in the BERTY reactor	78
Table 3-9: Selectivities and conversions of the 5 wt.% Cu catalysts.....	80
Table 3-10: Selectivities.....	85
Table 3-11: Selectivities for CuNQ10rB9 (CuNQ10 at 30 barg).....	88
Table 3-12: Standard reaction conditions for microreactor reactions with copper catalysts	92
Table 3-13: Selectivities and conversions of copper catalysts in low pressure microreactor	92
Table 3-14: BET data of copper catalyst, pre and post reaction	97
Table 3-15: Conversion and selectivities of 10 wt.% copper on silica catalyst ...	99
Table 3-16: BET analysis of pre- and post-reaction 10 wt.% copper catalyst....	100
Table 3-17: Copper catalysts conversions and selectivities	102
Table 3-18: Universal reduction conditions for all copper catalyst in the low pressure fixed bed reactor	105
Table 3-19: Reaction conditions for all materials tested in low pressure HRTC reactor	105
Table 3-20: GC analysis high level results (% m/m)	106
Table 3-21: GC analysis low level results (ppm m/m)	107
Table 3-22: Numerical comparison of the ethanol production values between the methanol synthesis catalyst reactions.....	111
Table 3-23: Gas sample GC results.....	113
Table 3-24: ICP-MS values.....	114
Table 3-25: BET data for post reaction samples from HRTC	123
Table 3-26: Reaction data for 10 wt.% catalysts.....	131
Table 3-27: BET data for Alumina SA6X75	136

Table 3-28: Conversions and selectivities for bimetallic catalysts.....	144
Table 3-29: Conversions and selectivities of the most active catalysts	147
Table 3-30: Selectivities on day averages at end and start of reaction	150
Table 3-31: BET data for 20CoSA6X75c tested at a range of temperatures	154
Table 3-32: BET data of post-reaction 20CoSA6X75, reactions at varying temperatures.....	159
Table 3-33: HS XRD particle sizes for CuNQ10	161
Table 3-34: HS XRD particle sizes for 10 wt.% Ni on silica catalyst	162
Table 3-35: 10 wt.% cobalt catalysts with different supports	166
Table 3-36: Reduction conditions for cobalt based catalysts in catalyst support study	167
Table 3-37: Table of reaction conditions for 10 wt.% cobalt catalysts	168
Table 3-38: Table of results for each 10 wt.% Co catalyst on days one and four	169
Table 3-39: BET results pre- and post-reaction for 10 wt.% Co on alumina SA6X75	173
Table 3-40: BET results pre- and post-reaction for 10 wt.% Co on silica Q10 ...	175
Table 3-41: BET results for pre- and post-reaction 10 wt.% Co on titania ST61120 catalyst	177
Table 3-42: BET results for pre-and post-reactions for 10 wt.% Co on ZnO.....	180

List of Figures

Figure 1-1: Global ethanol production by type [7]	16
Figure 1-2: Global ethanol production by country or region [4].....	16
Figure 1-3: Possible routes from Syn-Gas to ethanol.....	20
Figure 2-1 Schematic of BERTY reactor system	41
Figure 2-2: Method from BERTY GC	43
Figure 2-3: GC Calibration graph.....	43
Figure 2-4: Schematic of low pressure microreactor system.....	45
Figure 2-5: Schematic of HRTC glass atmospheric fixed bed reactor system.....	50
Figure 2-6: Photo of HRTC atmospheric fixed bed reactor (when loaded) (40 mm diameter, 1 m length quartz tube)	51
Figure 3-1: XRD pattern of commercial methanol synthesis catalyst	57
Figure 3-2: TPR of commercial methanol synthesis catalyst	58
Figure 3-3: MS Summary for Methanol Synthesis catalyst TPR	59
Figure 3-4: Reaction profile of B1.....	61
Figure 3-5: TPO of post-reaction MeOHSCrB1	62
Figure 3-6: MS (44) for methanol synthesis catalyst post-reaction B1	63
Figure 3-7: XRD pattern and assignment for post-reaction MeOHSCrB1	64
Figure 3-8: XRD pattern of uncalcined silica Q10.....	66
Figure 3-9: TPR profile of silica Q10.....	67
Figure 3-10: TGA profile of uncalcined CuAQ10	68
Figure 3-11: TGA-MS profile of uncalcined CuAQ10	69
Figure 3-12: TGA profile of uncalcined CuNQ10	70
Figure 3-13: TGA-MS profile of uncalcined CuNQ10	71
Figure 3-14: TPR profile of calcined CuAQ10.....	72
Figure 3-15: TPR of calcined CuNQ10	73
Figure 3-16: XRD pattern of uncalcined and calcined CuNQ10	74
Figure 3-17: Hot-Stage XRD patterns of CuNQ10c at 25°C, 100°C, 200°C, 300°C and 400°C	75
Figure 3-18: XRD patterns of uncalcined and calcined CuAQ10 samples	76
Figure 3-19: Hot-stage XRD patterns of CuAQ10c at 25 °C, 100 °C, 200 °C, 300 °C and 400 °C	77
Figure 3-20: Copper reduction routes	77
Figure 3-21: Reaction profile for CuNQ10 BERTY reaction	79
Figure 3-22: Reaction profile for CuNQ10 BERTY reaction, normalised to nitrogen feed marker	79
Figure 3-23: TPO analysis of post reaction CuNQ10	81
Figure 3-24: XRD pattern of post-reaction CuNQ10	82
Figure 3-25: TPO analysis of post-reaction CuAQ10	83
Figure 3-26: XRD pattern of post-reaction CuAQ10.....	83
Figure 3-27: Reaction profile for CuNQ10 with <i>n</i> -octane (B6)	84
Figure 3-28: TPO analysis of post-reaction CuAQ10	86
Figure 3-29: XRD analysis of post-reaction CuAQ10	87
Figure 3-30: Reaction profile for CuNQ10 at 30 barg.	88
Figure 3-31: TPO analysis of CuNQ10 (reaction at 30barg).....	89
Figure 3-32: TPO profile of post-reaction silica Q10	94
Figure 3-33: MS data for Q10rG4	94
Figure 3-34: TPO profile of CuN2Q10rG2.....	95
Figure 3-35: MS data of CuN2Q10rG2.....	96
Figure 3-36: XRD pattern of CuN2Q10rG2.....	96
Figure 3-37: TPO profile of MeOHSCrG5.....	98

Figure 3-38: XRD pattern of MeOHSCrG5.....	99
Figure 3-39: XRD pattern for 10 wt.% copper on silica catalyst	100
Figure 3-40: GC analysis results for all materials tested and acetic acid reference	108
Figure 3-41: GC analysis results for supports and lab prepped copper catalysts	109
Figure 3-42: Liquid sample data for two methanol synthesis catalyst reactions	110
Figure 3-43: All ICP-MS data (ppb) above the standard <25 ppb threshold for all elements analysed.....	115
Figure 3-44: ICP-MS data (ppb)(zinc removed).....	116
Figure 3-45: ICP-MS data for expected elemental contributions from the catalysts	117
Figure 3-46: ICP-MS for Al, Cu and Mg contributions	118
Figure 3-47: ICP-MS data for aluminium and copper	119
Figure 3-48: Photograph of cooled inverted HRTC glass reactor tube (40 mm diameter, 1 m length quartz tube)	120
Figure 3-49: XRD patter of zinc acetate hydrate sample	122
Figure 3-50: XRD pattern of post-reaction CuN(10)Q10.....	124
Figure 3-51: XRD pattern of post-reaction methanol synthesis catalyst	124
Figure 3-52: TPR analysis of 10 wt.% nickel on silica catalyst	128
Figure 3-53: XRD patterns of 10 wt.% nickel on silica catalysts	128
Figure 3-54: XRD analysis of uncalcined and calcined 10 wt.% cobalt on silica catalyst	129
Figure 3-55: Rates of ethanol production for 10 wt.% catalysts	130
Figure 3-56: XRD patterns for pre and post reaction 10 wt.% nickel on silica catalyst	132
Figure 3-57: XRD patterns of calcined and post-reaction 10 wt.% cobalt on silica	133
Figure 3-58: XRD pattern of SA6X75 alumina.....	136
Figure 3-59: HS XRD patterns for 20 wt.% Ni catalyst.....	137
Figure 3-60: TPR profile of 20NiSA6X75c.....	137
Figure 3-61: TPR analysis of 20 wt.% Co catalyst	138
Figure 3-62: Rates of ethanol production for 20 wt.% catalysts	139
Figure 3-63: XRD patterns of calcined and post reaction 20CuSA6X75	140
Figure 3-64: XRD patterns for post reaction 20 wt.% alumina catalysts	141
Figure 3-65: TPO analysis of 20 wt.% Co catalyst.....	142
Figure 3-66: TPO analysis of 20 wt.% Cu catalyst.....	142
Figure 3-67: TPO analysis of 20 wt.% Ni catalyst	143
Figure 3-68: Rates of ethanol production for bimetallic catalysts	144
Figure 3-69: Lines of best fit for all 20 wt.% mono and bimetallic catalysts ...	145
Figure 3-70: Best of each category for rates of ethanol production	146
Figure 3-71: Best fits for temperature study for rates of ethanol production...	149
Figure 3-72: MS data for day one of 20CoSA6X75c 250 °C reaction	151
Figure 3-73: MS data for day one of 20CoSA6X75c 300 °C reaction	151
Figure 3-74: MS data for day four of 20CoSA6X75c 300 °C reaction.....	152
Figure 3-75: XRD patterns of the various temperature samples post-reaction..	153
Figure 3-76: TPO data of post-reaction 20CoSA6X75 for 250 and 300 °C reactions	154
Figure 3-77: MS data of post-reaction 20CoSA6X75 for 250 and 300 °C reactions	155
Figure 3-78: MS data of 20CoSA6X75 reaction at 300 °C.....	156
Figure 3-79: XRD patterns of post-reaction 20CoSA6X75, reactions at varying temperatures.....	157
Figure 3-80: TPO profile of post 300 °C reaction 20CoSA6X75	158

Figure 3-81: HS XRD patterns for CuNQ10c	161
Figure 3-82: HS XRD patterns for 10 wt.% Ni on silica catalyst	162
Figure 3-83: Hot-Stage XRD patterns for 20CuSA6X75	163
Figure 3-84: Bed profile relating bed depth to conversion to ethanol using 20CoSA6X75 catalyst	164
Figure 3-85: Bed profile summary using 20CoSA6X75	165
Figure 3-86: Trend lines for the rates of ethanol production for 10 wt.% cobalt catalysts	168
Figure 3-87: Day one of reaction MS data for CoA(10)Q10c	170
Figure 3-88: Day one of reaction MS data for CoN(10)SA6X75c	170
Figure 3-89: Day one of reaction MS data for CoN(10)ST61120c	171
Figure 3-90: Day one of reaction MS data for CoZnO.....	171
Figure 3-91: TPO of post-reaction 10 wt.% Co on SA6X75	172
Figure 3-92: TPO-MS of post-reaction 10 wt.% Co on SA6X75	173
Figure 3-93: XRD patterns of calcined and post-reaction 10 wt.%Co on silica catalyst samples	174
Figure 3-94: XRD patterns of 10 wt.% Co on titania; calcined and post-reaction	175
Figure 3-95: TPO for post-reaction 10 wt.% Co on ST61120.....	176
Figure 3-96: TPO-MS for post-reaction 10 wt.% Co on ST61120.....	177
Figure 3-97: XRD patterns for 10% Co on Zinc Oxide; calcined and post-reaction	178
Figure 3-98: TPO of post-reaction 10% Co on ZnO	179
Figure 3-99: TPO-MS of post-reaction 10 wt.% Co on ZnO.....	179

Acknowledgements

My thanks go to Professor S. David Jackson for the PhD opportunity to begin with and his unwavering help, guidance and patience throughout the project.

I would also like to thank my industrial supervisor, Dr. Jon Deeley, for the effort he put into this project, our helpful discussions and for organising for me to visit and complete some of my research at the BP Research Centre in Hull.

There are a few people within the University of Glasgow without whom this research would not have been possible; Ron Spence, Andy Monaghan, Jim Gallagher and Jim Bannon. I thank them for their help, expertise and for always making time to show me the way to fix things.

This PhD thesis is not just the product of four years of my life but is also the support and guidance offered to me by my friends and family, especially my parents and Scott. For that, I will be ever grateful.

Author's Declaration

This work contained in this thesis, submitted for the degree of Doctor of Philosophy, is my own work except where due reference is made to other authors. No material within this thesis has been previously submitted for a degree at this or any other university.

Ailsa S. Lynch

Abbreviations

Av.	Average
BERTY	Stationary Basket Catalytic Testing Reactor produced by Autoclave Engineers
BET	Brunauer, Emmett and Teller theory
CHN	Carbon, Hydrogen and Nitrogen Content, determined by microanalysis
DSC	Differential Scanning Calorimetry
ESS	European Spectroscopy Systems (MS manufacturer)
GC	Gas Chromatography
GHSV	Gas Hour Space Velocity
FID	Flame Ionisation Detector
HPLC	High Pressure Liquid Chromatography
HRTC	Hull Research and Technology Centre
ICDD	International Centre for Diffraction Data
ICP-MS	Inductively Coupled Plasma - Mass Spectrometry
ICP-OES	Inductively Coupled Plasma - Optical Emission Spectroscopy
MFCs	Mass Flow Controllers
m/m %	Mass/Mass %
MS	Mass Spectrometry
m/z	Mass/Charge Ratio
NMR	Nuclear Magnetic Resonance Spectroscopy
TCD	Thermal Conductivity Detector
TGA	Thermo-Gravimetric Analysis
TPO	Temperature Programmed Oxidation
TPR	Temperature Programmed Reduction
v/v %	Volume/Volume %
XRD	X-Ray Diffraction (HS XRD - Hot- Stage X-Ray Diffraction)

1 Introduction

“The reduction of carboxylic acid and their derivatives to alcohols, diols, and lactones under high pressure is of considerable commercial importance” [3] and has long been recognised as such. There are a range of chemicals that can be produced from the reduction of carboxylic acids, and the production of ethanol from acetic acid is one such commercially important process.

1.1 Ethanol

Ethanol is a primary alcohol, with a chemical formula of $\text{CH}_3\text{CH}_2\text{OH}$, which can be produced via traditional fermentation methods or synthetic routes. The traditional route for alcohol production by the fermentation of sugars works well for the food and manufacturing industry. However, the needs of the manufacturing and chemical industry require large quantities of a purer, cleaner, analytical grade ethanol. As such, synthetic routes, such as the direct hydration of ethene, are used to produce a purer, more desirable product. These synthetic routes tend to use precious metal catalysts as opposed to the enzymatic catalysts used in fermentation.

Ethanol was produced on a global scale of 21,812 million gallons in 2012 [4] and is most commonly viewed as a solvent, chemical intermediate or fuel. Ethanol is frequently used as a chemical intermediate, second only to water as a solvent, and as a raw material in the manufacture of drugs, plastics, lacquers, plasticizers, perfumes, cosmetics, detergents and rubber accelerators [5].

By far, the largest use of ethanol is within automotive fuel, especially in South American countries such as Brazil. Ethanol, as a low molecular weight alcohol, is replacing other additives as an octane booster in automotive fuels in most economies [6]. Figure 1-1 shows that ethanol production for industrial and beverage purposes has remained relatively consistent between 1975 and 2010, whilst the production of ethanol for fuel has been steadily increasing over the same period.

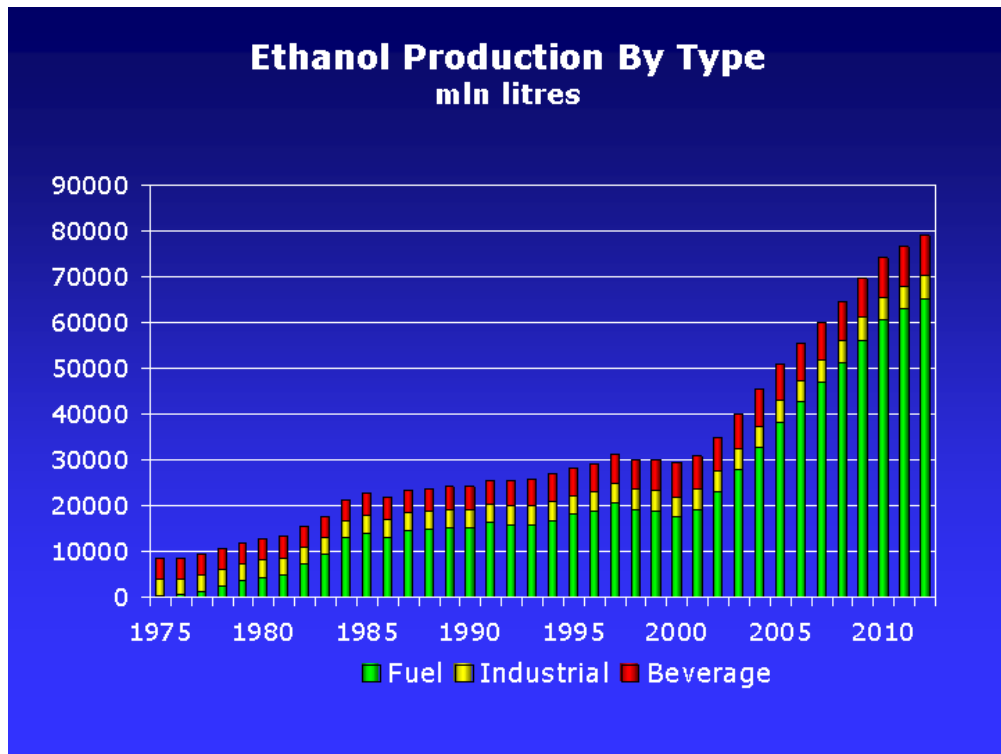


Figure 1-1: Global ethanol production by type [7]

Reflecting ethanol’s primary use as an automotive fuel, the quantities for worldwide production and consumption are heavily weighted to Brazil and USA, as seen in the global production values by country and/or region below in figure 1-2. This reflects the utilisation of ethanol as a motor fuel in Brazil, and increasing bioethanol production for fuel additives in the USA.

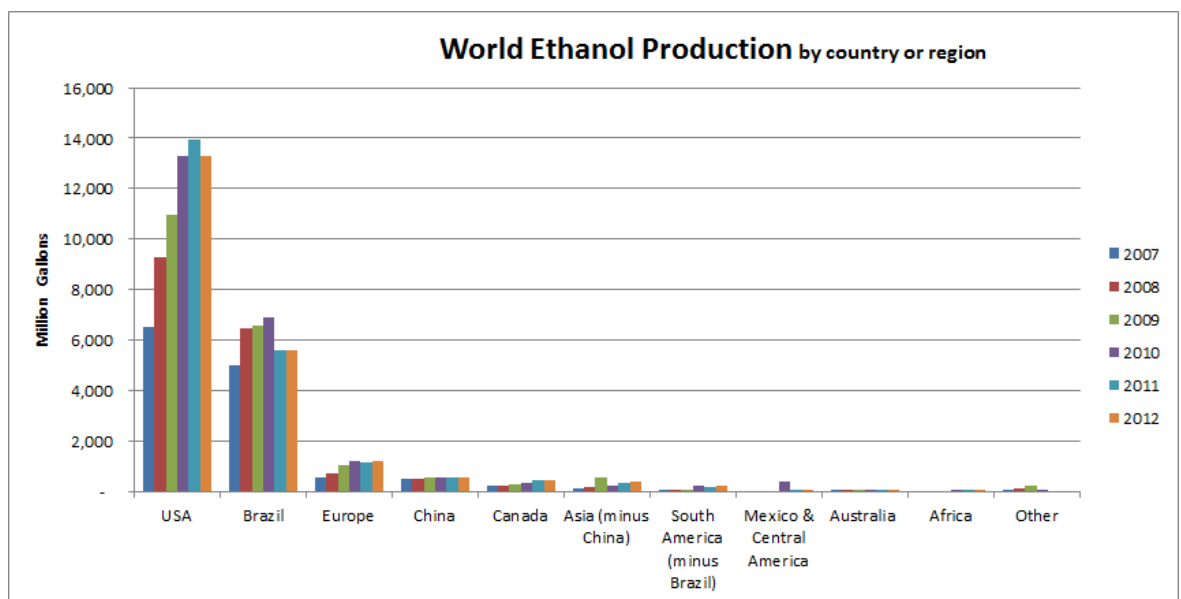


Figure 1-2: Global ethanol production by country or region [4]

The steady increase seen between 1975 and 2010 is also visible in the production values from 2007 to 2010 in figure 1-2 for the USA, Brazil and to a lesser extent Europe. The slight dip and stagnation in production from 2010 onwards can be explained as a response to the global economic events of 2008 but more significantly as a direct consequence of a sharp increase in the price of sugar (beet and cane) and grains (corn, rye, and wheat) at this time, that are used for the production of fermented ethanol [6]. The volatility of the feedstock markets for the traditional fermentation route prompted an increase in the production of alcohols, including ethanol, from developments in petroleum chemistry [6, 7].

Industrial ethanol is a mature market, although the markets are mobile and dynamic given the shift and increase in the use of ethanol within traditional automotive fuel blends. Suppliers in the industrial ethanol market include a range of synthetic and fermentation operators and ethanol synthesis will remain of particular interest due to increasing petroleum prices, environmental concerns and automotive fuel octane additive demands.

1.1.1 Fermentation

Fermentation can be used to produce ethanol through microbial conversion of natural products, such as carbohydrates. This can be done in two major ways via the fermentation of sugar, the source of which is either sugar crops or grain starches such as wheat [6]. In addition the fermentation of non-sugar ligno-cellulose fractions of crops also produces ethanol and is more colloquially described as 'surplus wine ethanol'.

Producers are aware that given the sharp increase in the demand for ethanol, both fermentation and synthetic routes are required to feed the market. Maintained global commitment to the production of ethanol originates from the desire to reduce greenhouse gases within the automotive sector, with legislation necessitating its inclusion in Europe [8] and the USA [9].

Fermentation, despite its many benefits, is often seen as a volatile process given the direct link to feedstock prices, combined with the often reduced product purity continuing to be an issue for certain uses.

1.1.2 Synthesis

There are various examples of synthetic ethanol producers and processes. Each fuelled by a growing demand for an industrial process that can synthesise ethanol both cheaply and efficiently.

The first synthetic route to ethanol was developed by Michael Faraday in 1825 which used the acid-catalysed hydration of ethene.



The catalyst used was phosphoric acid absorbed onto diatomaceous earth or charcoal. This phosphoric acid catalyst was used in the first large scale ethanol production by the Shell Oil Company in 1947. The reaction was carried out with an excess of high pressure steam at 300 °C. In the USA, the process was used on an industrial scale by Union Carbide Corporation and others; Lyondell Basell continues to use it commercially. Today, Ineos Enterprises is the world's largest producer of synthetic and fermentation ethanol with over 300,000 tonnes produced per annum at the plants in Grangemouth [10]. Here, synthetic ethanol production is via the direct gas phase hydration of ethene.

Furthermore, Sasol manufactures ethanol through the direct catalytic hydration of ethene in the presence of steam, using phosphoric acid adsorbed onto silica as a catalyst [11]. In addition, a significant amount of ethanol is produced from Sasol's Fischer-Tropsch process as a co-product.

1.2 Acetic Acid Hydrogenation

There are current catalytic processes for the hydrogenation of acetic acid conversion on an industrial scale [12]. However, the catalysts used in those reactions involve the use of precious metals, specifically palladium and platinum. These precious metal catalytic reactions were heavily researched by BP in the 1980s and resulted in patents relating directly to catalyst composition and process technology [13-15].

The research into non-precious metal catalysis for this process and specifically the use of base metals has been investigated too, although the significant volume of literature related to the reduction of acetic acid to acetaldehyde rather than to ethanol.

Initial consideration of the thermodynamics of the reaction is important in order to establish viability of the system and some reaction parameters. The hydrogenation of acetic acid to ethanol can be expressed as:



The thermodynamics tell us that the reaction is spontaneous at low temperatures and exothermic with a ΔH^0 value of $-41.8 \text{ kJ mol}^{-1}$. As the reaction is exothermic, and proceeds with a reduction in the number of moles, the highest yields of ethanol are obtained at low temperatures and high pressures.

The literature and patent reviews reveal that most of the catalyst studies performed have used Group VIII metals supported on oxides [13, 14, 16, 17] and specifically used palladium systems. The aim of this project, however, was to investigate viable catalyst alternatives to the traditional precious metals used for the selective hydrogenation of acetic acid to ethanol. The use of palladium or platinum catalysts for hydrogenation roles provide high selectivity to the processes, using catalysts with high surface areas through the use of silica or alumina support materials and low metal loadings. The cost implications of using a precious metal however, even at low loadings, can make the use of a base-metal an attractive alternative. For the current routes to ethanol from acetic acid, the patent literature reveals that Celanese [12] have a process using a platinum/tin (Pt/Sn) catalyst.

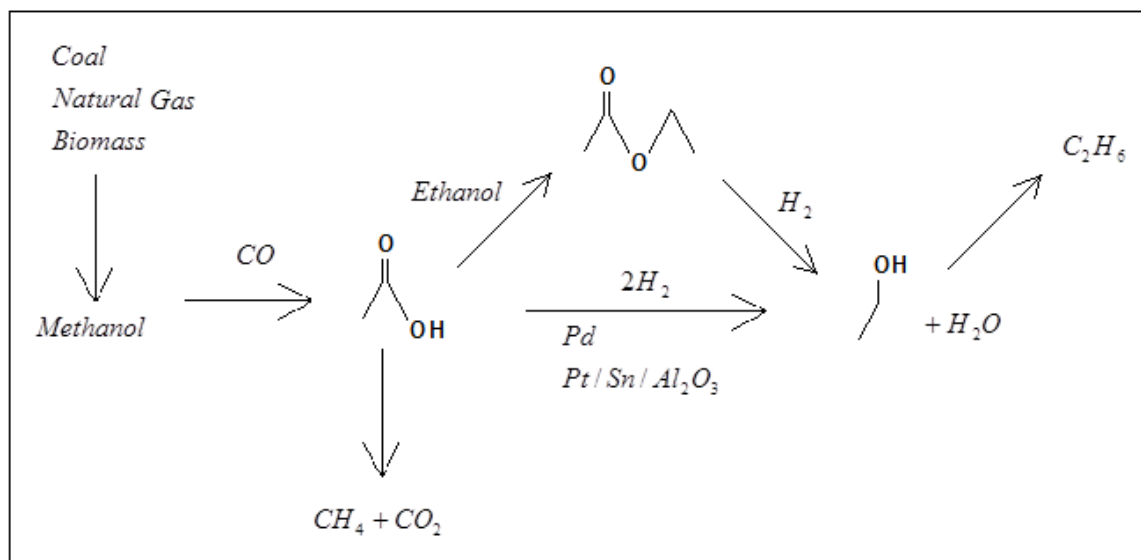


Figure 1-3: Possible routes from Syn-Gas to ethanol

An alternative synthetic route for ethanol is the production of the acetate species (methyl acetate or ethyl acetate) through the esterification of acetic acid, and then synthesis of ethanol through catalytic hydrogenation of the acetate, as seen in figure 1-3.

The production of ethanol as a significant product was observed within a study by Blain *et al.* [1] when acetic acid was passed over a commercial methanol synthesis catalyst under a reducing atmosphere. This observation automatically posed a question regarding the ability of copper catalysts, and this methanol synthesis catalyst in particular, as acetic acid hydrogenation catalysts. The production of ethanol over copper catalysts had been previously observed and reported by Cressely *et al.* [2], along with other products such as acetaldehyde and ethyl acetate.

Acetic acid is commonly used as a model system which can then be expanded to other C₂₊ oxygenates studies. Decomposition studies have frequently taken place on single crystal systems and also the decomposition of adsorbed acetate groups were investigated [16]. The authors concluded that the acetic acid was able to adsorb onto both the alumina support component and the rhodium surface. They also identified that three types of acetates were present on the

rhodium surface, with each being responsible for a unique acetic acid decomposition route.

As well as vapour-phase hydrogenation, acetic acid hydrogenation has been looked at within the aqueous phase [18]. Olcay *et al.* [18] observed that the activity for the hydrogenation of acetic acid to ethanol decreased with the following trend: Ru > Rh ≈ Pt > Pd ≈ Ir > Ni > Cu. The ethanol selectivity of Ru was highest when it reached above 80 % with temperatures below 175 °C. The reaction side products were identified as ethyl acetate, acetaldehyde and the alkane product plus CO₂. The Cu and Ni catalysts investigated were in the form of Raney catalysts to avoid sintering and dissolution, and also to maintain the high surface area required for activity with these base metal catalysts. Variations in the mechanisms for hydrogenation and decomposition are suggested to be dependent upon the active metal phase [18-20].

Base metals, in particular, have grown as an area of development, from when this process was initially being published by Cressely [2] in 1984. In this paper, the activities and selectivities of Cu, Co and Fe based catalyst systems in the form of impregnated metal catalysts using a silica support, generally from the metal nitrate salt, were investigated. The research clearly identifies the activity of base metal systems, with a range of reaction temperatures and metal loadings investigated.

The copper based catalysts were calcined at temperatures ranging within 300 °C to 1050 °C. The copper catalysts heated to above 1050 °C were seen to exhibit increased selectivity to acetaldehyde with the product range severely diminishing compared to the 300, 500 and 850 °C counterparts. Each reaction was carried out at a reactor temperature of 350 °C, which is above the 300 °C limitation used within this project's testwork for copper based catalysts. The data in the Cressely's work does not display any information as to the deactivation of the catalyst either from the presence of the acetic acid or the temperatures used.

It was with a 6.85 % Co/SiO₂ catalyst at 200 °C that ethanol was identified as the primary product within the same paper. Significant conversion to methane was also observed, ranging from 33.5 to 75.8 % depending on metal loading and

temperature, but was observed for both the bulk cobalt and supported cobalt catalysts. A significant decrease in activity and shift towards methane production was seen when cobalt acetate salt was used instead of the nitrate salt in the production of the supported catalysts.

The iron based systems were active for the production of acetone from acetic acid and the desired ethanol production was only observed at higher temperatures. With the use of higher temperatures, up to 400 °C, the amount of methanation increased, giving equal amounts of ethanol and methane production of 3 % at 400 °C.

The three base metals investigated by Cressely [2] showed variance in their product profiles which was postulated to be due to the acetate species forming on the metal surfaces. Research into base metal catalysts was further continued by Cressely *et al.* who subsequently published a paper [21] which commented upon the effect of the support used, alkalisation and the use of bimetallic systems.

Recent patents [12] pertaining to acetic acid hydrogenation have shown that this is an area of expanding research. Celanese International Corporation [12] have patented significantly in the area of acetic acid hydrogenation, detailing the use of Pt/Sn and cobalt based catalyst systems [22-25]. The patent [12] states that ‘the catalyst employed in the process comprises at least one metal, a siliceous support, and at least one support modifier.’ This varied scope included the use of alkali promoter such as those investigated by Cressely [21] but the use of promoters was not encompassed by the remit of the research completed for this project. In addition, Celanese have also patented the use of a stacked bed reactor system using a combination of a Pt/Sn catalyst system in the first bed and a copper catalyst in the second bed [25]. Process developments such as these and improvements to product separation and tolerance for recycle streams have also been heavily patented within the last four years [25-27].

The Pt/Sn catalysts, as outlined in the Celanese patents [23, 25], are traditionally used as dehydrogenation catalysts, but in this instance are highlighted for their activity in the production of ethanol and ethyl acetate. The figures quoted in US Patent 2010/0197485 [23], show that the selectivity of the

catalyst toward ethanol is high with an ethanol selectivity of ~95 % over a 1m catalyst bed at 225 °C. The catalyst quoted in terms of productivity and selectivity was doped with CaSiO_3 , and the effect of doping within the range of 0 -10 wt.% was demonstrated at both 250 °C and 275 °C. The optimal doping to produce the highest selectivity to ethanol was 5 wt.% CaSiO_3 at 275°C.

Recent literature also starts to look at more complex systems using novel $\text{Cu}_2\text{In}/\text{Al}_2\text{O}_3$ catalysts [28]. The indium doping appears to be highly efficient for the reduction of acetic acid to ethanol through the formation of the Cu_2In alloy within the catalyst. Additionally carbide based catalysts have also proved to be effective for the hydrogenation of acetic acid to ethanol with molybdenum carbide recently being identified by Celanese [29] as active.

1.3 Acetic Acid Production

It is unsurprising that the companies researching the hydrogenation of acetic acid to ethanol are also the major acetic acid manufacturers, namely BP and Celanese. Virtually all new acetic acid production routes make use of the homogeneous methanol carbonylation technology developed by Monsanto [30] in the 1970s. Acetic acid itself is used for a variety of applications: for example, as a raw material for vinyl acetate monomer and acetic anhydride synthesis, and as a solvent for purified terephthalic acid production [30].

1.4 Catalysts

The main scope of this study was to look at the gas-phase hydrogenation of acetic acid under relatively mild catalytic conditions for a selective reaction to ethanol.

1.4.1 Precious Metal Catalysts

Significant research has gone into investigating precious metals as hydrogenation catalysts. Palladium systems, both single crystal faces and supported metal catalyst systems [12, 17] have been published showing significant activity for the selective hydrogenation of acetic acid to ethanol.

The viability of palladium has been researched for the upstream processes such as methanol synthesis from syngas. The high cost of the palladium metal and its slow rate of reaction relative to commercial Cu/ZnO/Al₂O₃ alternatives, have stopped further use.

Supported platinum catalysts with a range of supports were tested to probe the kinetic behaviour of carboxylic acid hydrogenation [31, 32]. Rhodium based catalysts have shown significant promise for alcohol production, where selectivity to ethanol is favoured [33].

1.4.2 Base-Metal Catalysts

Cressely *et al.* studied the hydrogenation over Cu/SiO₂ catalysts and reported results of high ethanol yields, along with the detection of additional products such as acetaldehyde and ethyl acetate [2]. Ethyl acetate is produced as a result of the esterification reaction between the ethanol and acetic acid. Furthermore, both the hydrogenation and esterification reactions produce water as a side product.

Commercial methanol synthesis catalysts have been extensively characterised and well documented in many papers. A review of the development on industrial methanol synthesis catalysts shows the catalyst originally used was Fe/K/Al₂O₃ [34]. The activity of ZnO was realised and investigated but not utilised until in 1966 when ICI developed a high content copper methanol synthesis catalyst with the formulation Cu/ZnO/Al₂O₃ via a co-precipitation method [34-36].

Optimisation of a catalyst can be particularly difficult when the preparation technique and metal precursor used can have a profound effect on activity. Examples of this are seen with cobalt catalysts for Fischer-Tropsch synthesis. Techniques for preparation and activation can have a significant impact on the activity of the catalyst [37]. Interestingly, attempts to modify the behaviour of base metals to mimic the catalytic abilities of their precious metal counterparts have been successful, involving nickel with a Sn coating to act like platinum [38].

Acetic acid reduction over iron catalysts has shown very high selectivities to acetaldehyde [39, 40]. Iron oxide has regularly been reported and used for the hydrogenation of carboxylic acids to their corresponding aldehydes. One of the first industrial examples of this was by GAF Corporation in 1935 [41].

Research into bimetallic base metal catalyst systems for acetic acid hydrogenation has its precedent established by Cressely [21]. He observed that of the couplings made between Co, Cu and Fe, the Fe-Co coupling displayed a surprising selectivity to reduction, where the individual metal catalysts directed the reaction towards methanation and ketonisation respectively. Additional synergistic effects were not observed with the other metal couplings tested.

1.4.3 Supports

A catalyst support for this system will need to offer a high surface area to allow significant distribution of the metal particles over the support area. The texture and surface acidity of a support can influence metal dispersion and ability to be reduced, as well as the interaction between the metal and the support [6].

There are specific desirable characteristics with a support. It is pertinent to highlight the importance of the stability of the support as part of its role and the contribution this gives to the viability of a catalyst. Additionally, within this reducing system, hydrogen uptake is an important issue as a readily-available hydrogen supply to the active metal sites is required. Within the context of an acidic system, the use of a basic support would be counter-productive to the acid-based process.

Other systems have seen significant differences with changes in the catalyst support. Conversely to the studies performed by Cressely *et al.* on the effect of metals, Vannice *et al.* [32] studied acetic acid hydrogenation over a range of supported platinum catalysts on various supports (TiO_2 , SiO_2 , $\eta\text{-Al}_2\text{O}_3$ and Fe_2O_3). Dependence of the product selectivity was seen to be directly linked to the oxide support used for the platinum catalysts. Other support studies included looking at SiO_2 , Al_2O_3 , La_2O_3 and ZnO for the reduction of acetic acid with base metal catalysts [21], for which only the silica supported catalysts did not show an increase in the amount of ketonisation at the expense of acid reduction.

Traditional support options include silica, which in its amorphous form does not crystallize upon annealing, and is acidic in nature. Other widely used metal oxide support options include alumina and titania.

1.5 Catalyst Deactivation

The structural engineering of a catalyst plays a large part in controlling the vulnerabilities of a catalyst. A successful catalyst must not only be capable of catalysing the desired reactions selectively but it must also display mechanical robustness.

Ideal catalyst attributes include:

- High Activity
- Adequate Porosity
- High Specific Surface Area
- Stable Structure
- Long Life
- Strong Pellet Bonding
- Optimum Pellet Shape
- Correct fluid-flow properties

When acknowledging the requirements of the catalyst composition, structure and design, a variety of potential causes for deactivation are identified. This includes: mechanical causes including erosion and attrition, specifically pellet attrition; integrity of the pellet both in terms of structure and shape; and a structure's stability in the presence of reactants and products.

Thermal deactivation causes include crystallite growth and pore collapse caused by sintering. This is particularly pertinent when working with copper containing catalysts as the upper operating temperature limit is often indicated as 300 °C [6]. Chemical transformations occurring within the catalyst can include integration of the metal species into the bulk and typically the production of metal -aluminate or silicate species. Extreme thermal activity can also induce the degradation of the stabiliser component of a catalyst.

Chemical causes can be split into three separate subsections: poisoning, carbon laydown and loss of catalytic phase. Poisoning of a catalyst can be either reversible or irreversible. Reversible poisoning can also be competitive between the species present within the reactor system. Traditional poisons for catalysts are sulphur, mercury and chlorine, which contain compounds that irreversibly bind to the catalyst leading to rapid and severe deactivation. Organic compound poisoning also occurs. Fouling, coking and carbon deposition are all routes through which the catalyst is altered by the presence of additional, quite frequently organic, species on the surface of the catalysts. 'Coking' is the presence of aromatic compounds on the surface, 'carbon deposition' encompasses carbon species on the catalyst surface and 'fouling' is everything else although the term 'deactivation' tends to be used. The third chemical route of catalyst deactivation is by loss of the catalytic phase, which directly correlates to a loss in the number of active sites available for the reaction to proceed. Frequently the removal of the active metal phase from the catalyst framework through sintering or extraction causes deactivation of the catalyst. Decreases in activity are further compounded by the reduction in surface area both of the support and active phase, experienced when sintering and extraction occurs. Additionally, changes to the active phase may produce a non-catalytically active compound in lieu of the active phase.

1.6 Project Background

Previous studies by BP involved the establishment of the effect of acetic acid and methyl acetate on a methanol synthesis catalyst [1]. The investigation was to ascertain the viability of a CO/CO₂ recycle stream to carbonylation which may contain trace amounts of acetic acid or methyl acetate and the impact of these species on the activity of the catalyst.

Blain *et al.* [1] observed that the addition of acetic acid into the working methanol system had a number of effects, including decreasing methanol production. It was also observed that the acetate species was highly reactive and formed non-trivial amounts of ethanol through hydrogenation of the acid, as well as methyl acetate and CO/CO₂. From this observation, it was clear that a copper-containing catalyst was active for the hydrogenation of acetic acid to ethanol. Viable catalyst alternatives to the traditional precious metals used for

the selective hydrogenation of acetic acid to ethanol were therefore of interest and were to be investigated. An acetic acid concentration of 1 mol.% was frequently used by Blain, and although a significant decrease in the methanol production was observed with this acid content, the more profound effect on the deactivation of the catalyst was observed with 5 mol.% acetic acid in the system.

There are a variety of points relating specifically to the acetic acid hydrogenation system that need to be considered when investigating this reaction.

- The hydrogenation of acetic acid can lead to a variety of products including, and not exclusively, methanol, ethanol, ethyl acetate, methyl acetate, acetaldehyde and methyl formate. From this range of short chain hydrocarbon derivative products, ethanol was the only desired product, making selectivity as well as activity important.
- The corrosive nature of using an acetic acid feed would have a limiting factor in the amount used. Continued use at high concentrations would damage the reactor system and associated analytical equipment.
- Testing of the catalysts by varying both the pressures used and reactor types, leading to optimisation of parameters such as temperature and pressure.
- The type of catalyst support used can have a significant effect on both catalyst activity but also catalyst stability.
- Investigate overall catalyst stability, including the effect of acetic acid on the catalyst sample post reaction. The requirement for this reaction is an active acid tolerant catalyst.

1.7 Project Aims

The aims of this project were:

- Develop an understanding of why copper catalysts have been found to be unsuitable for acetic acid hydrogenation to ethanol.
- Investigate the role of the catalyst support and determine the stability to acetic acid of a variety of catalyst supports.
- Investigate the ability of base metal supported catalysts to facilitate the hydrogenation of acetic acid to produce ethanol and to ultimately design and synthesise novel acetic acid tolerant base metal hydrogenation catalysts.

2 Experimental

A key aspect of this investigation was the development, preparation and characterisation of alternative base-metal catalysts and comparing those to commercially available alternatives. As such, a number of catalysts were prepared via a range of methods described below, and subsequently characterised.

2.1 Catalyst Preparation

A series of base-metal catalysts were prepared via either an impregnation method using metal salt precursors, or a precipitation method.

2.1.1 Supports

A variety of supports were used for the different catalyst preparations. The majority of catalysts were prepared with either Θ -alumina or amorphous silica, as supplied by BP. The Θ -alumina used was Saint-Gobain Norpro SA6X75 and the silica was Fuji-Silysia CARiACT Q10. Additionally Saint-Gobain Norpro Titania ST61120 was also supplied. The titania support was used for the preparation of an impregnated 10 wt.% cobalt catalyst. The alumina and titania were provided as pellets and the silica was provided in sphere form.

The supports were characterised prior to metal loading to allow for analysis and comparison of the supports at the pre- and post-reaction stages. Depending upon the reactor system being used for catalytic testing, the catalysts were left as either the preformed structures or crushed to a particle size range of 250-425 μm . All catalysts were crushed for characterisation.

2.1.2 Preparation Procedures

The technique employed for catalyst preparation was dependent upon the total metal loading. For total metal loadings of ≤ 10 wt.%, a spray impregnation technique was used, whilst for higher total metal loadings of 20 wt.% a precipitation technique was used. The prepared catalysts were all calcined to the metal oxide and activated by reduction to the metal prior to testing.

2.1.2.1 Impregnation Procedure

Two different nominal metal loaded catalysts, 5 wt.% and 10 wt.%, were prepared via the impregnation route. The impregnated catalysts were prepared using a spray impregnation technique [42], where the volume of the metal solution matched that of the support pore volume. Surface area analysis was performed on the supports prior to calcination to determine the pore volumes for use in the impregnation catalyst preparation. The pore volume values used can be seen in table 2-1.

Table 2-1: Support pore volume values used for impregnated catalyst preparation

	Silica Q10	Alumina SA6X75	Titania ST61120
Pore Volume (cm ³ /g)	1.0	0.71	0.38

The catalysts were prepared in batches of 100 g. Depending upon the support pore volume, the corresponding volume in water to the total pore volume was used to dissolve the metal precursor in an aqueous solution. For example, a 5 wt.% copper on silica catalyst was prepared by dissolving copper (II) nitrate hemipentahydrate (18.3 g) precursor in 95 ml of H₂O. The silica support (95 g) was placed into the drum of a Pascall Lab-Mixer (Model 1664_00_A), which was rotated to agitate the catalyst support, whilst the metal precursor solution was sprayed onto the support using a battery operated Desaga Sarstedt-Gruppe SG1 spray gun fitted with a 50 mL Schott Duran flask. Once all of the aqueous solution had been added, the catalyst was left in the tumbling drum for an additional 30 minutes to aid full and even dispersion of the metal precursor solution. After being removed from the mixer, the catalysts were dried overnight in an oven at 115 °C.

The catalysts prepared are listed in table 2-2, along with their metal loading, the metal precursor and support used in the preparation. In addition, the given names used throughout the results section for the prepared catalysts are listed.

Table 2-2: Impregnated catalysts prepared

Metal	Loading (%)	Metal Precursor	Support	Name
Copper	5	Copper Nitrate Hemipentahydrate	Silica Q10	CuNQ10
Copper	5	Copper Acetate Tetrahydrate	Silica Q10	CuAQ10
Copper	10	Copper Nitrate Hemipentahydrate	Silica Q10	CuN(10)Q10
Nickel	5	Nickel Nitrate Hexahydrate	Silica Q10	NiNQ10
Nickel	10	Nickel Nitrate Hexahydrate	Silica Q10	NiN(10)Q10
Cobalt	5	Cobalt Acetate Tetrahydrate	Silica Q10	CoAQ10
Cobalt	10	Cobalt Acetate Tetrahydrate	Silica Q10	CoA(10)Q10
Cobalt	10	Cobalt Nitrate Hexahydrate	Alumina SA6X75	CoN(10)SA6X75
Cobalt	10	Cobalt Nitrate Hexahydrate	Titania ST61120	CoN(10)ST61120

The calcination and reduction steps are described for each catalyst in the results and discussion sections.

2.1.2.2 Precipitation Procedure

An alternative catalyst preparation technique used was for the production of 20 wt.% catalysts. The precipitation technique used was the HDC or ‘Highly Dispersed Catalyst’ production method [43], which was adapted to either mono-

or bi-metallic catalyst preparation. The technique describes the preparation of high dispersion cobalt catalysts and uses laboratory prepared metal hexamine solutions.

Metal Ammine Solution Preparation

The cobalt hexamine solution was prepared with a cobalt content of ~ 2.9 w/w % Co by the following method. Ammonium hydroxide solution (ca. 25 v/v % NH_3) (1.918 L) and deionised water (1.877 L) were combined and mixed in a large conical flask with the use of a stirrer plate and magnetic stirrer bar. Once thoroughly mixed, ammonium carbonate chip (198 g) was added to the solution and left to stir until all the chips had completely dissolved. Subsequently, cobalt (II) carbonate (218 g) was then added in small portions of ~ 25 g over several hours to allow for full dissolution. The solution was left to stir overnight and subsequently filtered to remove any undissolved material. The solution produced was a crimson red colour attributable to the cobalt hexamine complex.

The nickel hexamine and copper tetrammine solutions were prepared by a similar route. The production of the copper tetrammine solution used ammonium hydroxide solution (ca. 25 v/v % NH_3) (0.688 L), deionised water (2.997 L), ammonium carbonate chip (233 g) and copper (II) carbonate (177 g). The resulting solution, prepared by the same method as for Co, was a blue attributable to the copper ammine complex and corresponded to a copper content of ~ 2.36 w/w % Cu.

The corresponding nickel hexamine solution with a content of ~ 2.5 w/w % Ni was also prepared. The constituent parts for the preparation of the solution were ammonium hydroxide solution (ca. 25 v/v % NH_3) (0.563 L), water (1.877 L), ammonium carbonate chip (152 g) and nickel (II) carbonate hydroxide tetrahydrate (205 g). The same method was employed as for the cobalt and copper complex solutions outlined above. The nickel complex formation was observable through a colour change from green to blue during the solution preparation.

Preparation of the HDC catalysts

The catalysts were prepared with the pelletized Saint-Gobain Norpro SA6X75 alumina which was desiccated prior to catalyst preparation. Three single metal and three mixed metal catalysts were prepared using the alumina support and are listed in table 2-3. For both the mono-metallic and bi-metallic catalysts, the total metal loading was fixed to 20 % by weight, and the methodology was maintained for each preparation.

Table 2-3: Mono- and bi-metallic precipitation catalysts prepared

1 st Metal		2 nd Metal		Support	Name
Metal	Loading (%)	Metal	Loading (%)		
Copper	20			Alumina SA6X75	20CuSA6X75
Cobalt	20			Alumina SA6X75	20CoSA6X75
Nickel	20			Alumina SA6X75	20NiSA6X75
Copper	20			Silica Q10	20CuQ10
Nickel	20			Silica Q10	20NiQ10
Cobalt	20			Silica Q10	20CoQ10
Copper	10	Cobalt	10	Alumina SA6X75	10Cu-10Co-SA6X75
Cobalt	10	Nickel	10	Alumina SA6X75	10Co-10Ni-SA6X75
Nickel	10	Copper	10	Alumina SA6X75	10Ni-10Cu-SA6X75

Preparation Method

The catalysts were prepared in batches of 100 g, using 80 g of SA6X75 alumina. Volumes of the prepared metal ammine solutions, calculated for a metal contribution equivalent to 20 g (or 20 wt. %), were measured out and added to a

5 litre round-bottomed flask. For the bi-metallic catalysts, the volume of each of the two desired metal hexamine solutions was calculated for a 10 wt.% (or 10 g) contribution. The two solutions were then combined in the round-bottomed flask. The round-bottomed flask was attached to a rotary evaporator and placed within a water bath set to 35 °C. The flask was set to rotate and the alumina support added in small batches over the space of an hour. The metal ammine solution and support mixture was then refluxed under vacuum at 40-45 °C to allow for the evaporation of the ammonia and the subsequent metal deposition on the support material. The completion of the metal deposition during the catalyst preparation was visible by a distinctive change in the colour of the solution. The pH of the solution was also checked using a pH meter both prior to the reaction and once metal deposition was indicated to be complete.

Following full metal deposition, the mixture was further refluxed for 15 minutes to age the mixture. The reaction mixtures were then removed from the rotary evaporator and filtered using a Buchner flask. The coloured metal supported catalysts were then washed repeatedly and left to dry on the Buchner apparatus for 30 minutes. Once air dry, the catalysts were then dried in the oven overnight at 200 °C.

Table 2-4: Mono-metallic and bi-metallic precipitation catalysts prepared

Catalyst	Metal(s)	Initial Solution Colour	pH	Catalyst colour post deposition	pH
20CuSA6X75	20% copper on alumina	Blue	12.1	Light blue	9.2
20CoSA6X75	20% cobalt on alumina	Crimson Red	11.6	Red/purple	9.4
20NiSA6X75	20% nickel on alumina	Green	11.8	Light green	9.5
10Cu-10Co-SA6X75	10% copper and 10% cobalt on alumina	Deep Purple (Blue)	11.9	Red-Purple	9.4
10Co-10Ni-SA6X75	10% cobalt and 10% nickel on alumina	Deep Purple (Fuschia)	11.7	Red - Brown	9.9
10Ni-10Cu-SA6X75	10% nickel and 10% copper on alumina	Deep Blue	11.9	Blue/Green	9.5

Once each catalyst was dry, a small sample was crushed and analysed on the TGA-DSC-MS to establish the appropriate calcination temperature for that catalyst. For the calcination step, the catalyst was placed in a quartz weighing boat within a quartz tube and was heated within a Carbolite (MTF 12/38/400) tube furnace. An Interpet Airvolution Mini 2505 peristaltic pump was attached to the quartz furnace tube to push an air supply over the catalyst throughout the calcination programme, with the exit flow being vented externally.

2.1.3 Commercial Catalysts

2.1.3.1 Katalco 51-8 (Methanol Synthesis Catalyst)

The commercial methanol synthesis catalyst tested was Johnson Matthey's Katalco 51-8 which was provided as 5 mm pellets. The typical formulation for methanol synthesis catalysts is Cu/ZnO/Al₂O₃ [34, 44]. Methanol synthesis catalysts often contain additional stabilisers such as magnesium oxide [34] or are doped with rare-earth metals [45].

Table 2-5: Composition of typical Methanol Synthesis Catalyst [44]

Component	Amount (wt.%)
Copper	40-80
Zinc Oxide	10-30
Aluminum Oxide (Alumina)	5-10

2.1.3.2 Copper Chromite

Three copper chromite catalysts were tested, including two modified Na doped species. The two modified catalysts were copper chromite with 120 ppm Na and copper chromite modified with 1600 ppm. Their compositions as reported by Sud-Chemie are shown in table 2-6.

Table 2-6: Percentage of components in Sud-Chemie copper chromite

Component	Concentration (wt%)
Copper oxide	40-50
Chromium (III) oxide	40-50
Manganese dioxide	<5
Barium chromate	3-4
Chromia (VI) compounds, with the exception of barium chromate	<0.2

Additionally, another copper chromite catalyst was tested. This catalyst was also an industrial catalyst and was available in pelletized form. The catalyst was crushed to produce a particle fraction of 250-425 μm .

2.2 Catalyst Characterisation

2.2.1 Surface Area Determination

The Brunauer, Emmett and Teller (BET) analysis technique was used to determine the total surface area, pore volume and average pore diameter of the catalysts. The equipment used for analysis was a Micromeritics Gemini III 2375 surface area analyser. Prior to analysis, a catalyst sample of approximately

0.05 g, was placed in a glass tube and purged overnight under a flow of nitrogen at 110 °C.

This gas volumetric method takes a known quantity of N₂ admitted to the sample tube containing the absorbent at a constant temperature of -196 °C. As the N₂ adsorbs to the sample, the pressure within the sample tube drops until equilibrium is established. Helium is added to the vessel to equal the pressure within both the sample tube and the reference tube. This method uses multipoints for free space analysis including the volume of the solid and also the volume of the reactor tube. The equation below is the final expression which gives the summation of the assumptions of the BET method over an infinite number of adsorbed layers [44] linking together the volume of gas adsorbed and the pressure.

$$\frac{P}{V(P_0 - P)} = \frac{1}{V_m C} + \frac{(C - 1)P}{V_m C P_0}$$

Equation 1: Brunauer, Emmett and Teller (BET) adsorption isotherm equation

Where: V = volume of gas adsorbed at pressure P
 V_m = volume of gas adsorbed in monolayer, same units as V
 P_0 = saturation pressure of adsorbate gas at the experimental temperature
 C = a constant related exponentially to the heats of adsorption and liquefaction of the gas ($C = e^{(q_1 - q_L)/RT}$)
 Where q_1 = heat of adsorption on the first layer
 q_L = heat of liquefaction of adsorbed gas on all other layers
 R = gas constant

When equation 1 is used, plotting the $P/V(P_0 - P)$ against P/P_0 should yield a straight line, specifically in the P/P_0 range of 0.05 - 0.3 where the slope is given by $(C - 1)/V_m C$ and the intercept by $1/V_m C$. These calculations are completed internally by the Micrometric software.

2.2.2 Thermogravimetric Analysis

Thermogravimetric analysis was performed the catalysts at various stages of preparation and testing. The analysis was carried out using a combined TGA/DSC SDT Q600 thermal analyser coupled to an ESS mass spectrometer for evolved gas analysis. Temperature programmed analyses (TGAs) were carried out using argon, temperature programmed reductions (TPRs) were carried out using a 5 % H₂/N₂ gas mix and temperature programmed oxidations (TPOs) were carried out using a 2 % O₂/Ar gas mix. For each analysis, a standard ramp rate of 10 °C min⁻¹ was used for the heating profile.

For the mass spectroscopic analysis, various relevant mass fragments were monitored. Typical values included, 2 (H₂), 14 (CH₂), 15 (CH₃), 16 (CH₄), 28 (CO), 32 (O₂), 44 (CO₂), 45 (CH₃OH), and 60 (CH₃COOH).

2.2.3 Powder X-Ray Diffraction

X-ray diffraction patterns were obtained using a Siemens D5000 X-ray diffractometer (40 kV, 40 mA, monochromatised) with a CuK alpha source (1.5418 Å). The scanning range was 5 - 85° 2θ with a scanning rate of 1 second/step and a step size of 0.02°.

Hot-stage XRD analysis was also carried out on the D5000. The same process conditions were used for the flat plate analysis, however the sample was heated in a 5 % H₂/N₂ atmosphere (flow rate 20 ml min⁻¹). Scans of the sample were taken at room temperature and then at subsequent 100 °C increments with a ramp rate of 12 °C min⁻¹.

All assignments for XRD patterns were completed using the ICDD relational database (PDF-4⁺ 2007).

Average particle sizes were calculated using the Scherrer equation:

$$D_v = k\lambda / (\beta \cos \theta)$$

Equation 2: Scherrer Equation

Where: $\lambda = 1.54 \text{ \AA}$ Cu K_{α} = wavelength of radiation (X-Ray wavelength)
 D_v = crystallite size weighted by volume (average dimension of crystallites)
 k = Scherrer constant
 B = integral breadth of peak (in radians 2θ) located at angle θ (integral reflection of a reflection in radians at 2θ)
 θ = Bragg angle

2.2.4 Microanalysis (CHN)

Catalyst samples were submitted for microanalysis or elemental analysis on an Exeter Analytical CE-440 Elemental Analyser for the quantification of the carbon, hydrogen and nitrogen contents.

2.2.5 Nuclear Magnetic Resonance Spectroscopy

NMR spectra were recorded on a Bruker 400 MHz Spectrospin spectrometer (^1H NMR at 400 MHz and ^{13}C NMR at 400 MHz or 500 MHz). Chemical shifts are reported in ppm. ^1H NMR spectra were recorded with DMSO as solvent using ($\delta = 2.50$) as internal standard, and for ^{13}C NMR spectra, the chemical shifts are reported relative to the central resonance of DMSO ($\delta = 39.52$).

2.3 Catalyst Testing

Catalyst testing for the process of acetic acid hydrogenation was carried out in a variety of reactor types. These included a range of low and high pressure reactor systems, with both differential and integral reactor designs.

2.3.1 Bertly Reactor

2.3.1.1 Apparatus

A 300 ml Bertly reactor (Autoclave Engineers) fitted with a mangedrive 075-MKII impeller for agitation was used for catalyst testing and is depicted in the schematic below. The allied pipework was constructed of 316 stainless steel $\frac{1}{4}$ " piping. The Bertly reactor vessel combined an integrated heater unit, with dual thermocouples positioned within the reactor vessel and an additional trip thermocouple placed on the exterior of the heater unit. WEST temperature

controllers were used for the integration of the reactor heater unit, the trace heated sections and the thermocouples and trips within the central control unit.

Gases were fed to the reactor via Brooks SMART 5805S mass flow controllers and at pressures of up to 50 barg, which were achieved within the reactor by use of a gas booster system and limited and controlled by a proportional relief valve. An acetic acid liquid feed was introduced into the system prior to the reactor via a Gynkotek High Precision HPLC pump, model 480. The feed was vapourised upon introduction to the inlet pipework that was trace heated to 150 °C. All post-reactor pipework was trace heated to 190 °C to prevent condensation of products in the exit stream prior to gas chromatographic (GC) analysis. Product analysis was achieved through the use of an online GC system with the GC sampling valves being heated within a purpose built oven.

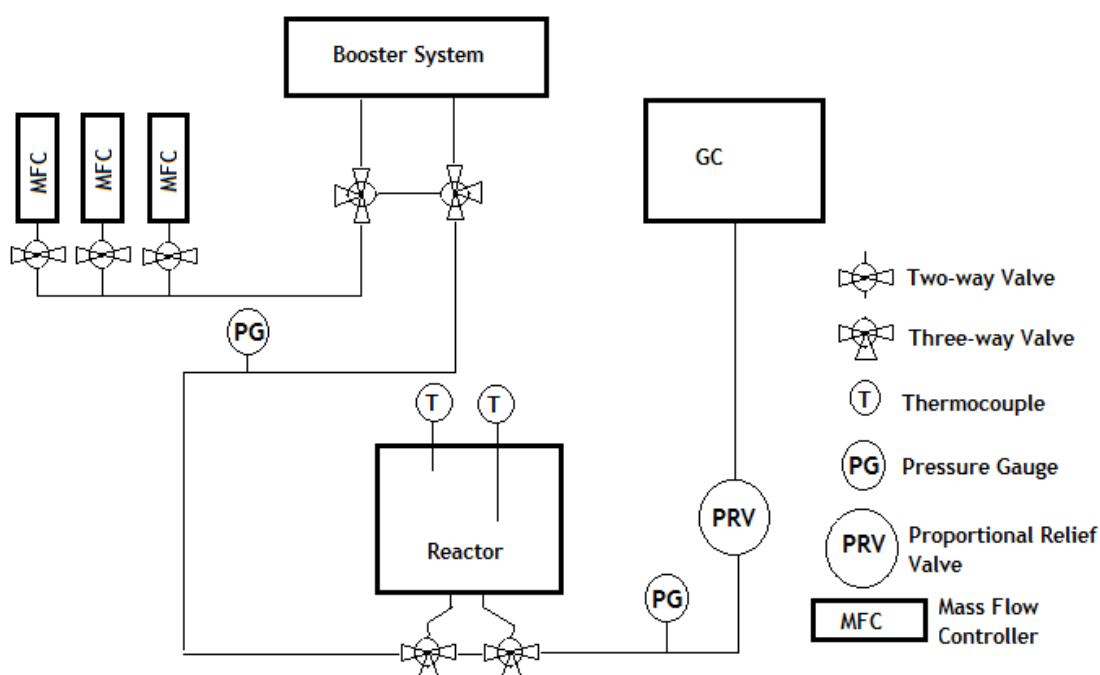


Figure 2-1 Schematic of BERTY reactor system

Safety features of the high pressure system included the integration of bursting discs with values of 100 barg within the system at various points. In addition, for the monitoring of gas leaks, there were CO monitors present under the workbench by the booster unit and within the vented cabinet. Safe shutdown of

the reactor system would occur upon activation of the CO monitors, any high temperature trip sensors and high or low gas flow trip sensors.

Catalyst (1.3 ml) was placed in the reactor basket, using a wire mesh base to hold the catalyst within the basket. The reactor lid was inserted and bolted down using a torque wrench to a pressure of 50 lb/in². The copper catalyst samples tested were reduced *in situ* at 250 °C for 3 hours under atmospheric pressure and at a flow of 50 ml min⁻¹ H₂. Once reduction was complete, the gas flow was changed to a N₂/H₂ mix of 190 ml min⁻¹ H₂ and 60 ml min⁻¹ N₂. The booster system was used to increase the reactor pressure to the desired level of up to 50 barg. The pressure in the reactor system was controlled throughout the reaction with the use of a proportional relief valve system.

Once stable at the desired pressure and temperature, the acetic acid feed was started and in turn the GC analysis. The HPLC was set to a flow of 10 µl min⁻¹. This relates to a 1.5 mol.% acid feed as a percentage of the total gas feed into the BERTY reactor.

2.3.1.2 Gas Chromatography

Online product analysis was carried out using a ThermoFinnigan ThermoQuest CE Instruments Trace GC fitted with a dual sampling, column and TCD detectors systems. The two columns used were:

1. Supelco Mol Sieve 5A Plot Fused Silica Cap column, 50 m x 0.53 mm used for methane, CO, nitrogen and ethane separation and identification.
2. HP Plot Q (Divinylbenzene/styrene porous polymer), 30 m x 0.53 mm x 40.0 µm Film thickness used for all other reaction product separation and identification.

The sample loop volume was 1 ml. The temperature profile for the GC is depicted below in figure 2-2.

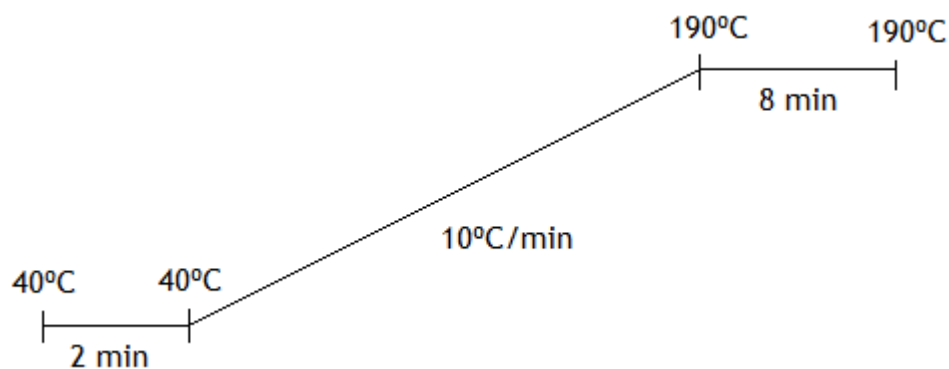


Figure 2-2: Method from BERTY GC

Prior to analysis the GC was calibrated for CO, CO₂, ethane, methane, nitrogen, acetaldehyde, acetic acid, acetone, ethanol, ethyl acetate, methanol, methyl acetate, n-octane and water. The calibration values for the major products and reactants are shown in figure 2-3.

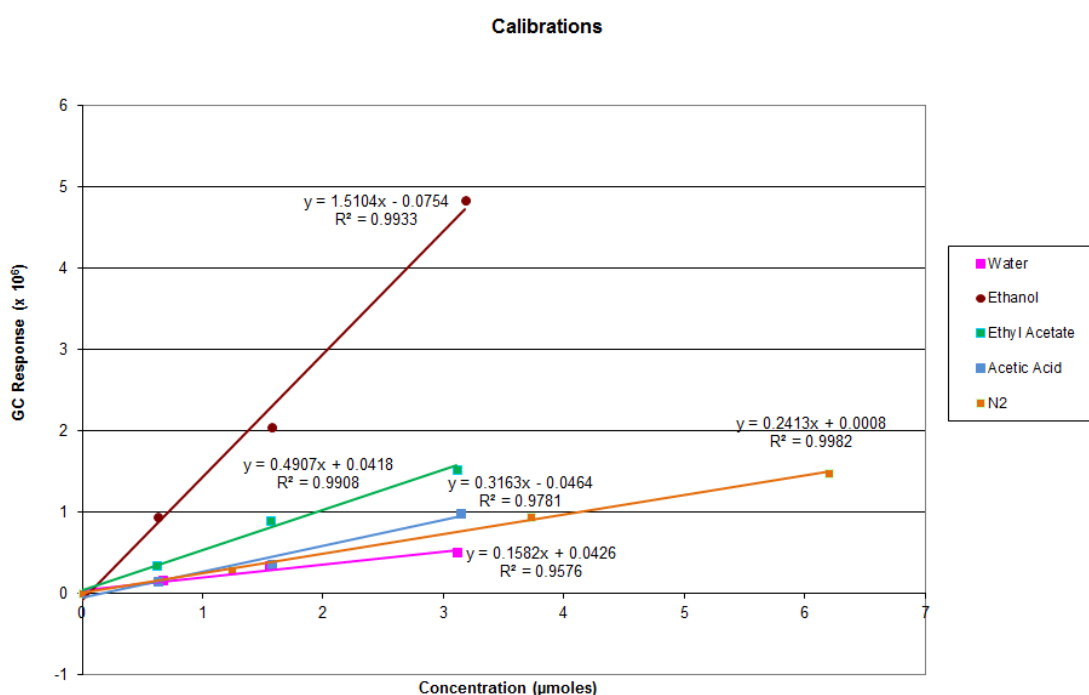


Figure 2-3: GC Calibration graph

2.3.2 Low Pressure Microreactor

2.3.2.1 Apparatus

The glassline pipework was made from Boro 3.3 Pyrex. The glassline microreactor itself was a combination of the same Boro 3.3 Pyrex, with a Quartz-boro transition just above the heated section of the reactor tube. The bottom section of the reactor tube was naturally fused quartz with a 0.52 expansion rating, with a quartz sinter. The reactor tube had an internal diameter of 22 mm.

Due to the nature of the reactor system, only the reactor itself was heated with the use of a LPC Elements 240V tube furnace. Control of the tube furnace was via WEST control box with a thermocouple placed within a central catalyst bed thermowell and a trip thermocouple positioned within the tube furnace. The exit glass tubing was connected to metal pipework link to a 6-way valve sample loop which connected to the GC. The metal pipe work was heated to 100 °C to help prevent condensation of the products prior to the GC sample loop. This trace heating temperature of 120 °C was maintained at all times.

A single gas flow of (usually) hydrogen controlled by a rotameter was fed into the reactor at atmospheric pressure. The H₂ flow for the reduction and reaction stages was checked each day with a digital flowmeter.

The system used a bubbler for temperature controlled introduction of the acetic acid starting material. The feed was situated in bubbler 2 in the schematic in figure 2-4 and the bubbler could be isolated from the rest of the system.

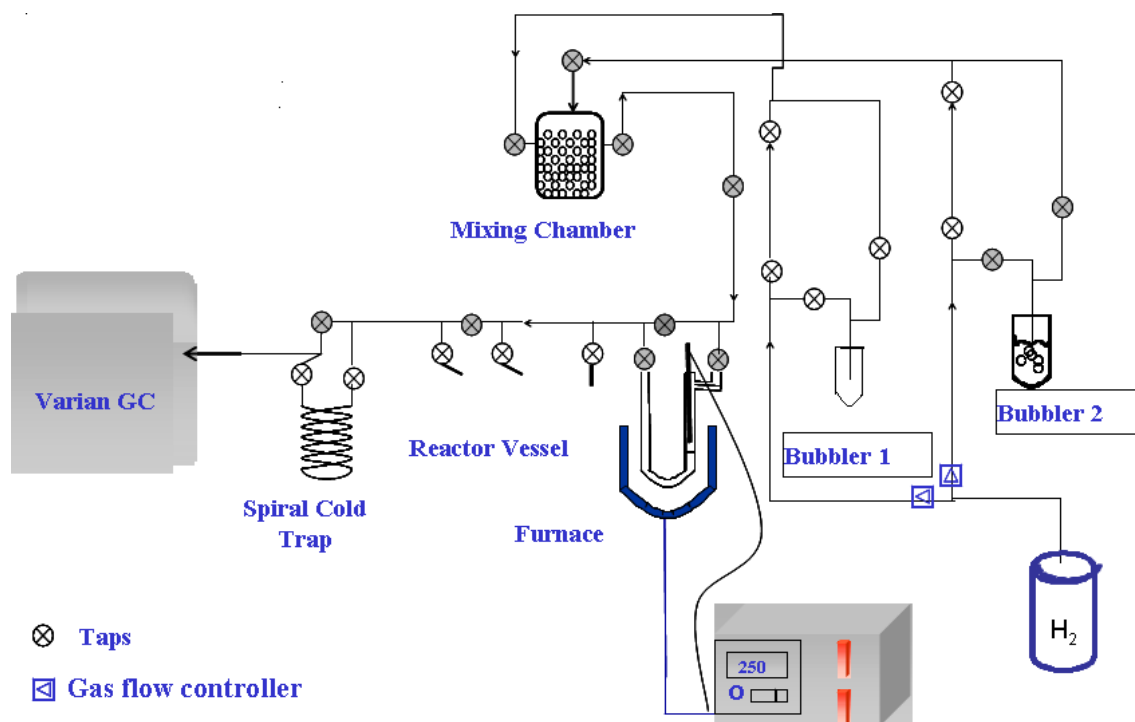


Figure 2-4: Schematic of low pressure microreactor system

The bubbler contained the liquid feed, through which the gas feed was sparged through at a rate of $60 \text{ ml min}^{-1} \text{ H}_2$. Control of the temperature to $\sim 20 \text{ }^\circ\text{C}$ was achieved and maintained through the use of a water bath. The temperature of the water bath was monitored throughout the reaction with the use of a digital thermometer.

2.3.2.2 Reaction Procedure

Crushed catalyst samples (1 mL) of the fraction 250-425 μm was used for each experiment. The catalyst sample was loaded on top of the quartz sinter, with the gas feed flowing up through the catalyst. The reactor tube was then sealed into the glassline with the use of black wax and the joints were leak tested to ensure complete sealing of the system. The tube furnace was then placed around the reactor tube and the top section insulated with glasswool.

Catalyst activation was carried out *in-situ* and standard reduction conditions are shown below in table 2-7. The catalyst reduction temperatures and holds were individually assessed for each catalyst from its TPR data. The temperatures and holds are discussed for each reaction within the results chapters.

Table 2-7: Standard reduction parameters for glassline reactions

Ramp Rate ($^{\circ}\text{C min}^{-1}$)	10.0
Gas Feed	H_2
Gas Flow (ml min^{-1})	30

Once activation was complete, the reactor temperature was changed to that of the reaction conditions, as listed in table 2-8, and left to stabilise. Mass spectrometer monitoring commenced once the reduction stage was complete. The reactor was then isolated whilst background GC flow was analysed and daily H_2 and acetic acid calibrations were completed. The H_2 calibrations on the GC were completed with the reactor and bubbler isolated. The gas flow was then introduced to the bubbler and calibrations for acetic acid were completed by GC analysis. Once stable values were achieved, the reaction was started by passing the H_2 and acetic acid flow over the catalyst bed. The first GC sample was taken after 5 minutes on stream (at T+5), with subsequent samples every 35 minutes.

Table 2-8: Standard reaction conditions for Glassline reactions

Temperature ($^{\circ}\text{C}$)	250
Pressure	Atmospheric
Gas	H_2
Flow (ml min^{-1})	60
GHSV (hr^{-1})	3,600

The reactor system was 'closed down' at the end of each experimental day, with the tube furnace switched off, MS monitoring and GC analysis ceased and the H_2 flow was decreased to 30 ml min^{-1} whilst the reactor was cooling and also overnight.

At the start of the following experimental day, the H_2 flow was increased back to 60 ml min^{-1} and MS monitoring recommenced. The sample daily calibration routine was then carried out. This repetition continued until four days of experimental work were completed.

2.3.2.3 Gas Chromatography

Analysis of reaction samples was carried out by gas chromatography, with samples taken at 35 minute intervals. The GC used was a Varian 330 with a TCD detector. The column used for analysis was a CB Wax 52 (capillary column) (30m, 0.53 mm). The chromatography data was integrated and printed out using a HP 3396 Series II Integrator. Calibrations were carried out daily for both the H₂ and acetic acid to demonstrate stability and have reference values for the reaction.

The calibrations for the reactants and products on the low pressure microreactor were achieved through the temperature control of the bubbler and the corresponding vapour pressure calculations.

Calculation of the vapour pressures of each reactant and product was completed using the Clausius - Clapeyron relationship seen below in equation 3.

$$\ln \frac{P2}{P1} = \frac{\Delta H_{vap}}{R} \left(\frac{1}{T1} \right) \left(\frac{1}{T2} \right)$$

Equation 3: Clausius – Clapeyron Equation

Where:

- R = Universal gas constant
- ΔH_{vap} = Enthalpy of vapourisation
- $P1$ = Known vapour pressure (kPa) at temperature $T1$
- $P2$ = Unknown vapour pressure (kPa)
- $T1$ = Known temperature (K) at vapour pressure $P1$
- $T2$ = Recorded temperature of bubbler (K)

The vapour pressures were calculated for each reactant and products at three different temperatures using literature data [46] and were included into the Clausius-Clapeyron equation. The ideal gas equation (equation 4) was then used to number of moles corresponding to that vapour pressure. All this data was combined for the calibration step on the low pressure microreactor.

$$PV = nRT$$

Equation 4: Ideal Gas Equation

Where: P = Vapour Pressure
 V = Volume of the GC sample loop
 n = Number of moles
 R = Universal gas constant
 T = Temperature of the sample loop (K)

2.3.2.4 Mass Spectroscopy

Connected to the vent line from the reactor system was a European Spectroscopy Systems (ESS) GeneSys Mass Spectrometer. The unit was portable and so was used to monitor the final reaction day (Day 4) for some reactions, whilst all four days were monitored in the later reactions. The M/Z values monitored were 2, 12, 14, 15, 16, 17, 18, 20, 28, 30, 32, 40, 42, 43, 44, 45, 46, 58, 59, 60, 87 and 88.

2.3.3 HRTC Atmospheric Fixed Bed Reactor**2.3.3.1 Apparatus**

At the BP Research Centre in Hull (HRTC), a glass quartz tube (1 m, 40 mm diameter) was used as a reactor tube within an atmospheric fixed bed system. This alternative low pressure fixed bed reactor was employed to test a range of copper based catalysts within an alternate but similar system to the low pressure glass microreactor. Use of this reactor system allowed for testing of the catalysts in pelletized/spherical form as well as testing of larger volumes of the catalysts.

10 ml of catalyst was centrally loaded into the reactor tube. To enable the central positioning, the catalyst bed was packed between two silicon carbide layers. The 'pre-bed' or top layer of silicon carbide was greater in depth and was additionally used as a volatilisation bed for the acetic acid feed. The silicon carbide layers and catalyst bed were separated by glasswool. The reactor tube was positioned within an encased heating block controlled by a WEST controller unit. The entire unit, including all sampling systems and rotameter, were used within a vented fume cupboard.

The acetic acid feed to the reaction was controlled by a syringe pump where the acetic acid was introduced into the reactor through a stainless steel needle at a rate of 4 ml hr^{-1} for the 20 mol.% acetic acid feed reactions. The tip of the syringe needle was positioned touching the silicon carbide 'pre-bed' so volatilisation occurred on silicon carbide. In this study, the silicon carbide was used as an inert packing material within the reactor system. Silicon carbide, or carborundum, is often labelled as a non-microporous 'inert' material [44]. Gas flow rates were controlled using a rotameter which was calibrated using a digital flow meter. The standard flow was 100 ml min^{-1} for the H_2 flow.

No online GC analysis was available with this reactor system, so alternatively a daily liquid sample was collected using a condenser at $19 \text{ }^\circ\text{C}$ and the exit gas flow was collected in a SKC Quality sample bag for offline analysis.

The syringes and gas bags were checked for compatibility with acetic acid and showed suitable viability within the system. A new syringe was used each day for the acetic acid to minimise degradation and the possibility of failure.

2.3.3.2 Reaction Procedure

Figure 2-8 shows a schematic diagram for the setup of the reactor apparatus. 10 ml of the catalyst was loaded into the reactor tube which was centrally positioned between two layers of silicon carbide packing material and glasswool, as shown in figure 2-5.

The syringe feed was positioned so that it touched the surface of the silicon carbide pre-bed to allow for complete volatilisation of the acetic acid feed.

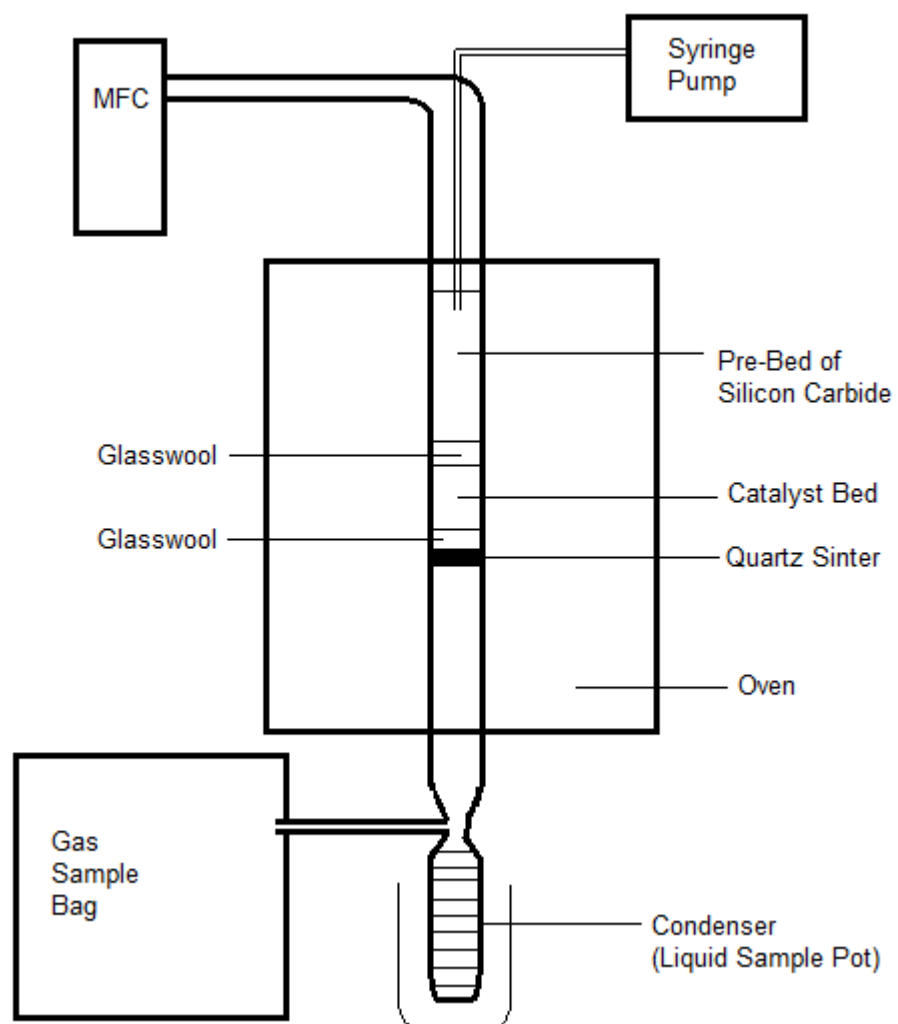


Figure 2-5: Schematic of HRTC glass atmospheric fixed bed reactor system

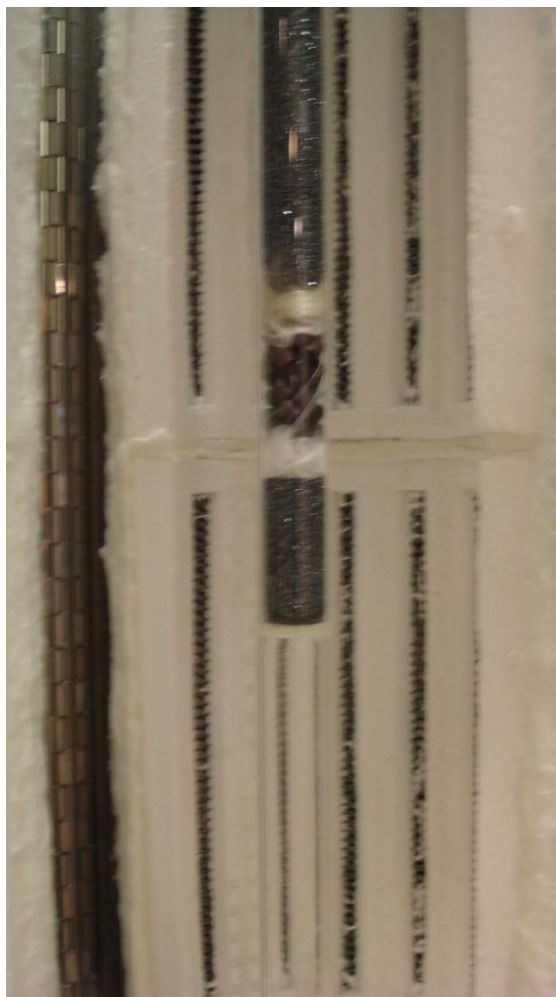


Figure 2-6: Photo of HRTC atmospheric fixed bed reactor (when loaded) (40 mm diameter, 1 m length quartz tube)

In-situ activation of the catalyst was carried out with a H₂ flow. The activation conditions for all the catalysts tested are shown in table 2-9. No sampling occurred during the reduction step, with the H₂ exit flow vented at the rear of the fume cupboard.

Table 2-9: Standard reduction conditions for HRTC atmospheric fixed bed reactions

Flow rate (ml min ⁻¹ H ₂)	100
Temperature (°C)	250
Ramp Rate (°C min ⁻¹)	10
Dwell (mins)	60

Once the activation stage was complete the reaction could be started immediately, as the temperature and gas flow rate were the same for the reduction and reaction stages. The gas sample bag was attached to the exit vent and the syringe pump was started to introduce acetic acid to the system. The reaction was then run for four hours under the conditions stated in table 2-10.

Table 2-10: Standard reaction conditions for Hull Glassware reactions

Temperature (°C)	250
Pressure	Atmospheric
Gas Flow (ml min ⁻¹ H ₂)	100
Volume of catalyst (ml)	10
GHSV (hr ⁻¹)	~ 750
Acetic Acid Feed (ml hr ⁻¹) (via syringe pump)	4 (20 mol.% acetic Acid) (Except for AL6, which was 10 mol.% acetic acid, so 2 ml hr ⁻¹)

Once the four hour reaction period was completed, the acetic acid feed was stopped. Subsequently, the gas flow was changed to 100 ml min⁻¹ N₂, the heating block was turned off and the reactor was left to cool overnight.

2.3.3.3 Product Analysis

Liquid Samples

The liquid samples were analysed by GC and ICP-MS at HRTC. GC analysis required two different methods for the major and minor component analysis. To determine the major components a polar column was utilised under temperature programmed conditions and detection was by TCD. Quantification for this method was by the addition of an internal standard and the limit of quantification was 0.1 % m/m. To determine minor and low level components, a more polar column was used under temperature programmed conditions, and

detection was by FID. Quantification for this method is by external standard with a typical limit of quantification of 10 ppm m/m.

Gas Samples

The gas samples from the sampling bags were also submitted for analysis. The GC compositional analysis included identification of various hydrocarbons at low percentage levels. The analysis was performed on two different GC systems incorporating a variety of columns capable of analysing vapour streams. Detection is by FID and TCD, and the limit of quantification for most components is 0.05 % v/v, but this is dependent on the particular method in question.

ICP-MS Analysis

Additionally the liquid samples were submitted for multi-element analysis by ICP-MS for quantification of the potential leaching of metals from the catalysts during the reactions.

Fully quantitative simultaneous multi-element quantification was performed by inductively coupled plasma mass spectrometry (ICP-MS 7500ce, Agilent Technologies). ICP-MS analysis was carried out using Octapole Reaction System (ORS) technology for the simple removal of spectral interferences. This is achieved by the introduction of hydrogen (reaction mode) and/or helium (collision mode). The ICP-MS was tuned prior to analysis using a certified tune solution to ensure satisfactory instrument performance.

Sample solutions (2 %) were prepared. Approximately 1 g sample was weighed directly into Sarstedt polypropylene sample tubes. Samples were made up to a known volume using 2 % nitric acid (Romil-SpA Super Purity Acid) in high purity water (Milli-Q, 18 MΩ.cm).

Calibration standards (0, 5, 10, 20 & 100 ppb) were prepared using traceable certified calibrations standards. Any instrumental drift occurring during the analysis was corrected for using a certified internal standard solution. Quality control samples of known concentration were analysed at regular intervals to assess ICP-MS performance. The results were reported in ppb. The high zinc

values observed with the ICP-MS analysis were confirmed by ICP-OES analysis (Thermo Scientific, iCAP 6500 Duo).

2.3.4 Materials

The table below displays the chemicals used in the reactions, for GC calibration standards and for catalyst preparation. In addition, it also lists the commercially available catalysts that were tested in this investigation. The chemicals listed were used without any additional purification.

Table 2-11: Gases used for the reactions, calibrations and characterisation techniques

Compound	Purity (%)	Supplier
2%O ₂ /Ar	---	BOC
2% CO/Ar	---	BOC
2% CO ₂ /Ar	---	BOC
5%H ₂ /N ₂	---	BOC
Air	---	BOC
Argon	99.998	BOC
Carbon Dioxide	99.99	BOC
Carbon Monoxide	99.99	BOC
Deuterium	>99.9 (99.8 isotopic)	BOC
Dimethyl Ether (DME)	99+	Sigma Aldrich
Ethane	100	BOC
Helium	100	BOC
Hydrogen	99.995 minimum	BOC
Methane	99.5	BOC
Nitrogen	100	BOC

Table 2-12: Reactants and products used for reactions and GC calibrations

Compound	Purity (%)	Supplier
Acetaldehyde	99	Aldrich
Acetic Acid	100	AnalaR NORMAPUR
Acetone	HPLC Grade	Fisher Scientific
Ethanol	99.99	Fisher Scientific
Ethyl Acetate	99.5 minimum	Sigma Aldrich
Methanol	99.99	Fisher Scientific
Methyl Acetate	99	Sigma Aldrich
Methyl Formate	99	Sigma Aldrich
Water	HPLC Gradient Grade	Fisher Scientific

Table 2-13: Materials used for the preparation of catalysts and the supplied catalyst supports used

Compound	Purity (%)	Supplier
Silica Q10	---	Fuji-Silysia
Silica Q30	---	Fuji-Silysia
Alumina SA6X75	---	Saint-Gobain Norpro
Alumina Al-3392E	---	Engelhard
Titania ST61120	---	Saint-Gobain Norpro
Copper(II) Acetate Tetrahydrate	98	Sigma Aldrich
Copper(II) Nitrate Hemipentahydrate	98	Sigma Aldrich
Nickel (II) Nitrate Hexahydrate	≥98	Fluka
Cobalt (II) Nitrate Hexahydrate	97.7	Alfa Aesar
Cobalt (II) Acetate Tetrahydrate	98	Alfa Aesar
Ammonium Hydroxide Solution	ca. 25 v/v % NH ₃ basis	Sigma Aldrich
Ammonium Carbonate	99.99	Alfa Aesar
Cobalt (II) Carbonate	99% metals basis	Alfa Aesar
Copper (II)Carbonate Basic	≥95	Sigma Aldrich
Nickel (II)Carbonate Hydroxide Tetrahydrate	99.5	Alfa Aesar

Table 2-14: Commercially available catalysts used within the project

Compound	Form	Supplier
Katalco 51-8 (ICI MeOH cat)	Pelletized	BP
Copper Chromite	Pelletized	Sud-Chemie
Copper Chromite (with 120ppm Na)	Powder	Sud-Chemie
Copper Chromite (with 1600ppm Na)	Powder	Sud-Chemie
Copper Chromite	Pelletized	
Cobalt on Zinc Oxide	Pelletized	BP

3 Results and Discussion

3.1 Copper Catalysts

Copper based catalysts were the first range of catalysts tested for use as acetic acid hydrogenation catalysts. Initial testing started with a commercially available methanol synthesis catalyst. Subsequent testing looked at other supported copper systems, at a variety of metal loadings by impregnation, and copper chromite catalysts. Each of these will be discussed within this chapter.

3.1.1 Methanol Synthesis Catalyst

The choice of a methanol synthesis catalyst followed on from research into the effect of acetic acid within a feed stream over a methanol synthesis catalyst [1].

The specific methanol synthesis industrial catalyst that was used for this study was Johnson Matthey's co-precipitated Katalco 51-8, and hereafter is referred to as MeOHSC. The methanol synthesis catalyst is a copper based catalyst using an alumina support and zinc oxide stabiliser/ promoter component.

3.1.1.1 Characterisation

X-Ray Diffraction (XRD)

The pelletized catalyst was received pre-calcined and subsequently was crushed for XRD analysis. This allowed for the determination of the composite compounds and the copper phase in the calcined catalyst form.

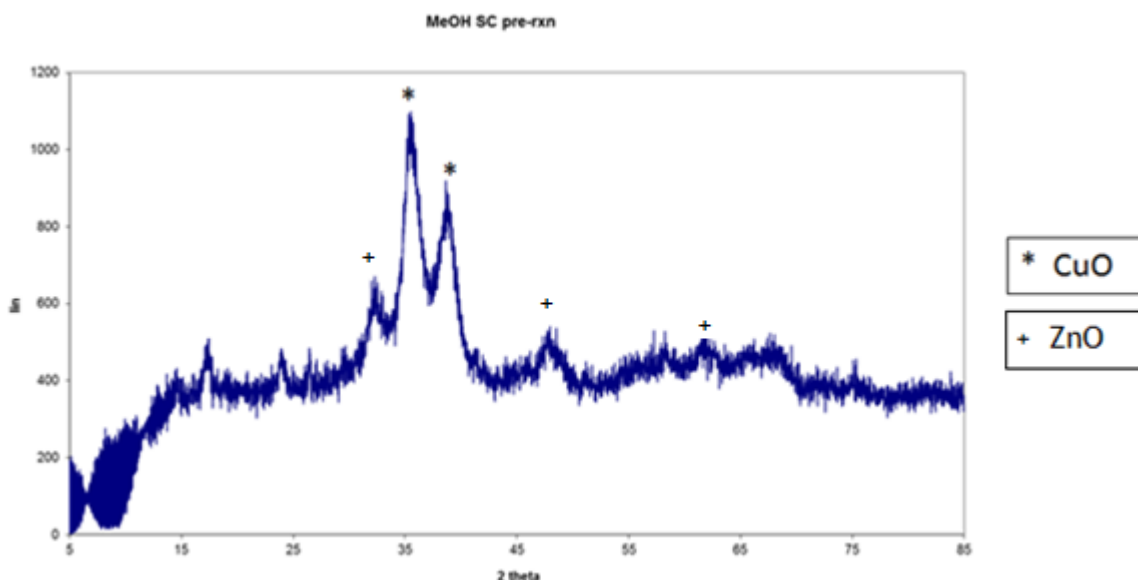


Figure 3-1: XRD pattern of commercial methanol synthesis catalyst

Features that were attributable to the presence of CuO and ZnO were visible within the XRD pattern in figure 3-1. The peaks at 35.5° and 38.8° are attributable to CuO. Using the Scherrer equation, the CuO average particle size was calculated to be 4.6 nm using the CuO peak at 35.5° . Other components of the Katalco 51-8 catalyst are aluminium oxide and zinc oxide. Features corresponding to zinc oxide were also identified in the XRD pattern in figure 3-1 with peaks seen at 31.8° , 47.6° and 62.8° .

BET Analysis

Surface area determination analysis was carried out on the methanol synthesis catalyst prior to reduction and is shown in table 3-1.

Table 3-1: BET analysis of commercial methanol synthesis catalyst

Catalyst	Surface Area (m^2/g)	Pore Volume (cm^3/g)	Pore Diameter (nm)
MeOHSC	86	0.25	11.7

Thermogravimetric Analysis

TPR analysis of the catalysts was used to determine the temperature range over which the copper oxide content of the catalyst was reduced to copper. The TPR profile in figure 3-2, of the Katalco 51-8 methanol synthesis catalyst shows a

large broad peak centred at 287 °C with a shoulder at 374 °C. With the peak spread between 200 °C and 400 °C. The weight loss in the TPR profile was calculated to be ~20 % of the total weight and was the only event seen within the 25 °C to 600 °C temperature range. This weight loss corresponds to the full reduction of the copper oxide content to metallic copper, assuming the highest copper value of the catalyst composition of 80 %, taken from table 2-5.

Reduction and reaction temperatures greater than 300 °C cannot be used with the methanol synthesis catalyst due to the sintering of copper content [47]. This temperature limitation is extended to all copper containing catalysts, if the integrity of the copper particle size is to be maintained.

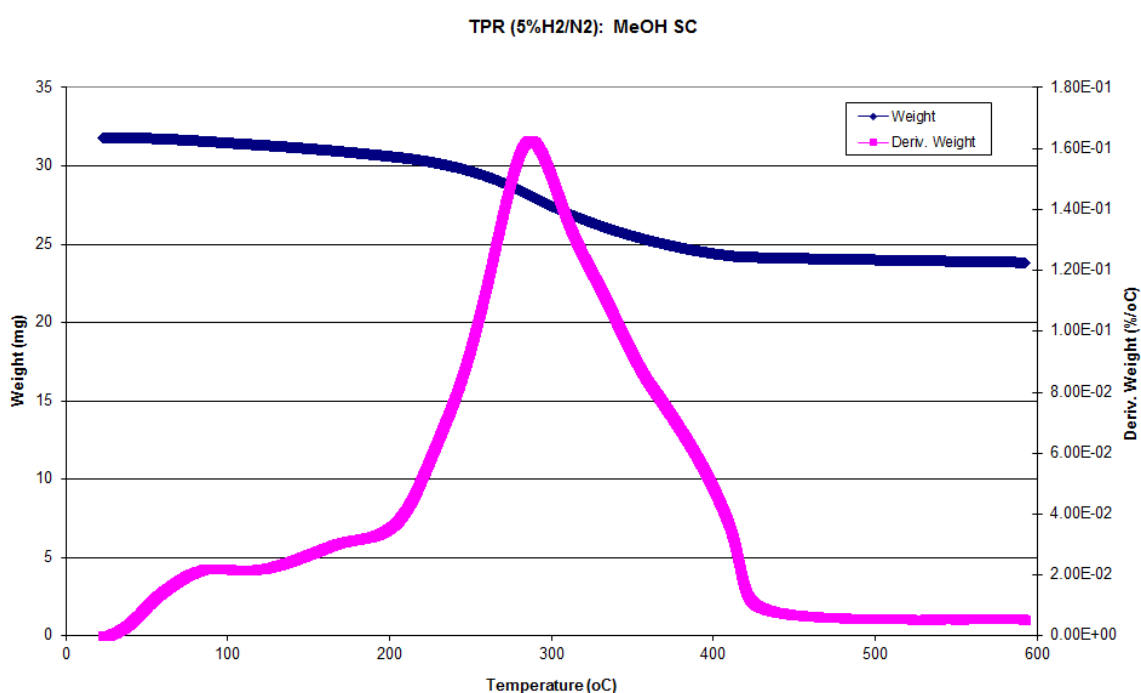


Figure 3-2: TPR of commercial methanol synthesis catalyst

DSC monitoring of the TPR profile shows that the event between 200-400 °C is actually two shouldering exothermic events. These shouldering events are also

seen in the mass spectrometry (MS) data in Figure 3-3.

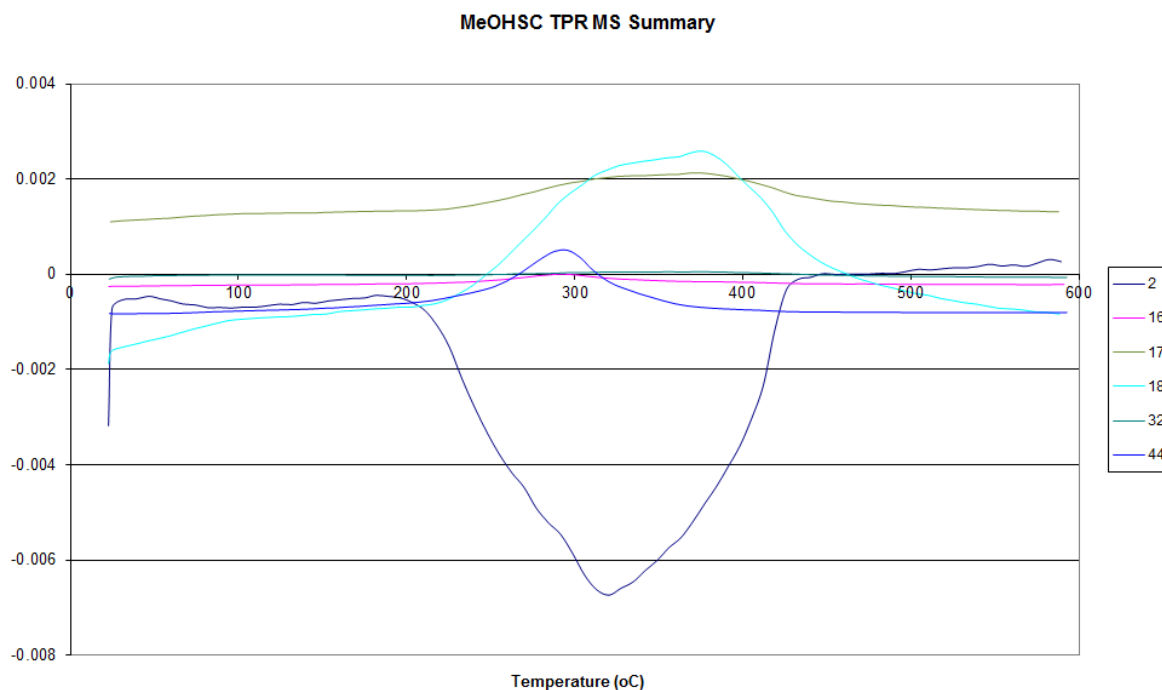


Figure 3-3: MS Summary for Methanol Synthesis catalyst TPR

Significant hydrogen (MS 2) uptake was observed across the 200 - 400 °C range in figure 3-3, with a corresponding evolution of water (MS 18). This is the expected profile for the reduction of the high copper content of the methanol synthesis catalyst from the copper oxide to the reduced copper metal species. From this TPR data within a 5 % H₂/N₂ atmosphere, reduction conditions for the methanol synthesis catalyst were established. The broad thermal event in the TPR is centred on 300 °C suggested this is the optimal range for the reduction process to occur at. However, the reduction temperature was lowered to 250 °C to minimise the amount of thermal sintering that would occur during the reduction step, as it is known that increased copper sintering is observed at temperatures of 300 °C and above [6]. This lowering of the reduction temperature within the reactor systems is compensated for by the increase in hydrogen concentration to 100 % H₂ within the reducing atmosphere compared to 5 % H₂ in the TGA. The differentiation between the availability of hydrogen in the two systems is important as an increased concentration of hydrogen will produce a more powerful reducing atmosphere. With a stronger reducing atmosphere, lower temperatures are often required to achieve the same reduction effect of lower hydrogen concentrations at higher temperatures.

Table 3-2: Conditions for the reduction of methanol synthesis catalyst

Ramp Rate ($^{\circ}\text{C min}^{-1}$)	Temperature ($^{\circ}\text{C}$)	Hold (mins)
10.0	250	240

3.1.1.2 Catalyst Testing: BERTY

The testing of the methanol synthesis catalyst Katalco 51-8 within the high temperature, high pressure non-differential BERTY reactor allowed for comparative work against the previous acetic acid feed study [1], which had comparable results to those observed within this project. This initial testing was important to establish the effect of acetic acid on the catalyst, including the support, stabiliser/promoter and active metal species.

Table 3-3: Reaction conditions for MeOHSC tested in BERTY reactor (B1)

Temperature ($^{\circ}\text{C}$)	250
Flow (ml min^{-1})	190 (H_2), 60 (N_2)
Feed	1.5 mol.% Acetic Acid via HPLC pump (9 $\mu\text{l/min}$)
Catalyst Weight (g)	1.3
Catalyst Volume (ml)	3.3
Pressure (barg)	50
GHSV (hr^{-1})	~11,000

The reaction profile in figure 3-4 shows that the methanol synthesis catalyst is selective to ethanol. The major product from the methanol synthesis catalyst was ethanol, with a selectivity of 34 %. A small amount of ethyl acetate is also seen to be produced during the reaction. The production of ethyl acetate can be viewed as a secondary reaction of the system and was expected given that an internal recycle reactor was used.

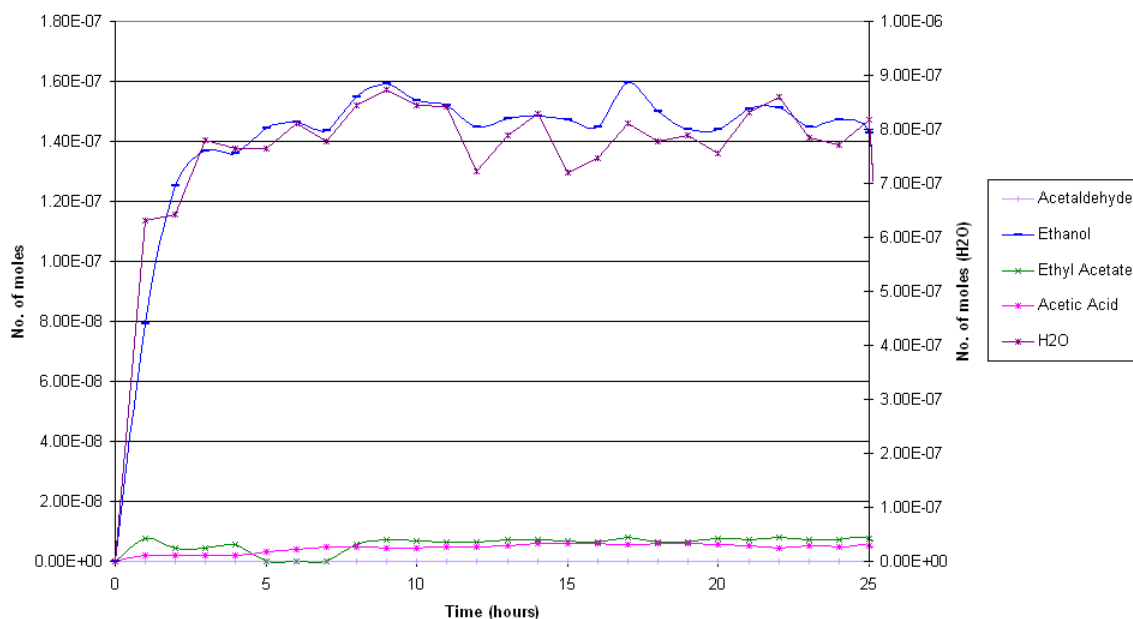


Figure 3-4: Reaction profile of B1

The averages taken from the results of the methanol synthesis catalyst over the 24 hour reaction period can be seen in table 3-4.

Table 3-4: Conversion and selectivities from reaction B1

Selectivities (%)	Ethanol	34.7
	Ethyl Acetate	3.5
	Acetaldehyde	0
Conversion(%)		98.8

The production of ethanol as the primary product and in high yield shows a positive start for the investigation into copper based catalysts for acetic acid hydrogenation. However, from the results in table 3-4, it is clear that there is a significant proportion of the acetic acid feed that is unaccounted for within the reaction. This observation is compounded by an average carbon balance value of 0.3 seen throughout the reaction. One possibility is that acid laydown is occurring on the catalyst surface, or decomposition leading to carbon laydown.

The oxygen balance, however, is centred on a value of 1 throughout the reaction. Therefore, the oxygen content within the system appears to be accounted by the production of water throughout the reaction.

3.1.1.3 Post-Reaction Characterisation

Post-reaction characterisation was performed on crushed catalyst samples. Prior to crushing the pellets, there was visible physical degradation of the catalyst with cracks observed on the pellet surfaces that were not visible pre-reaction. An additional observation was the increased ease with which the post-reaction pellets crushed compared to those analysed pre-reaction. An adverse effect of the acetic acid on any catalyst was to be expected given the corrosive nature of the reactant. However, the active phase stability and the integrity of the catalyst as a whole are important factors within a potential acetic acid hydrogenation catalyst.

TPO analysis of the methanol synthesis catalyst post-reaction in figure 3-5 shows the combustion of the organic species on the surface of the catalyst upon exposure to a 2 % O₂/Ar atmosphere with increasing temperature.

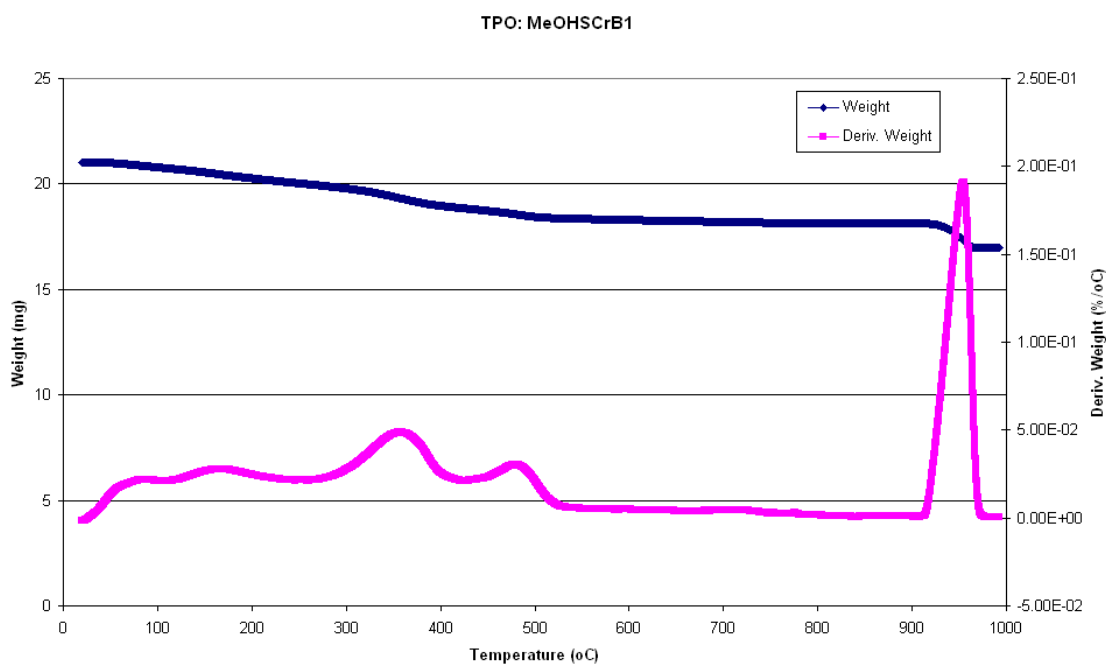


Figure 3-5: TPO of post-reaction MeOHSCrB1

The post-reaction catalyst was analysed by TPO and TPO-DSC. The TPO profile shown in figure 3-5 displays three separate events. The TPO-DSC analysis showed that the events at 300 °C and 420 °C were mildly exothermic. The three events identified on the TPO profile correspond to evolutions of CO₂ in the MS data, seen in figure 3-6, which is the full combustion product of organic species on the catalyst.

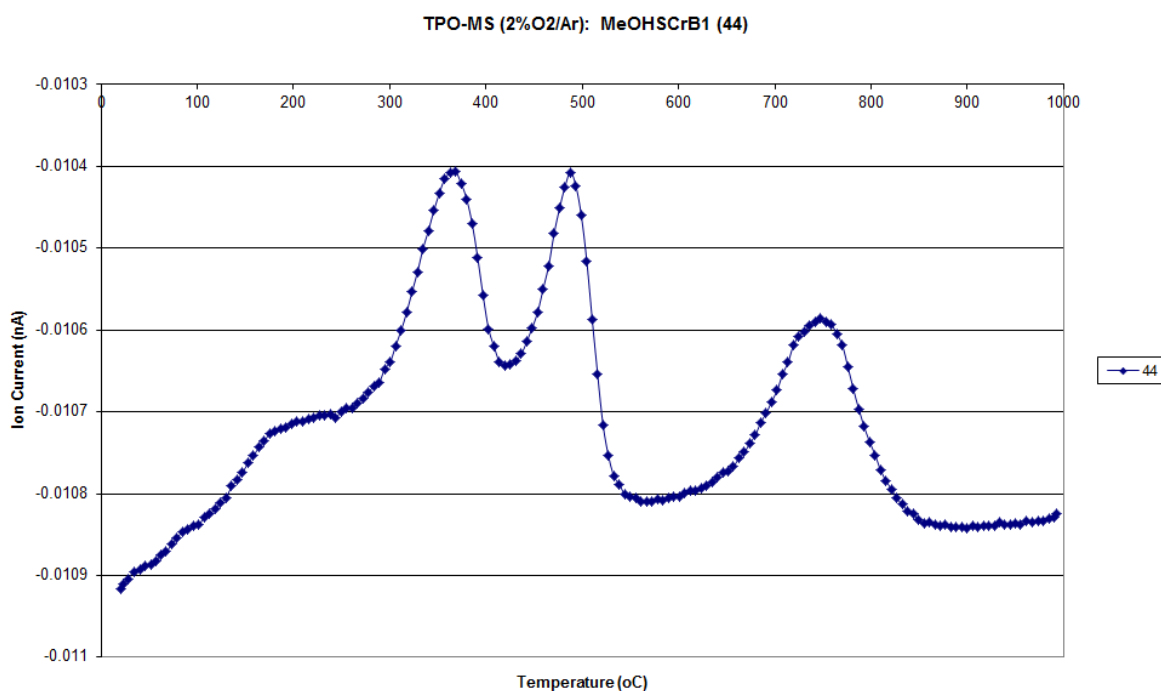


Figure 3-6: MS (44) for methanol synthesis catalyst post-reaction B1

The MS data and TPO profile show distinct groupings for the CO₂ evolutions: two lower and one higher temperature event. This difference in the temperature at which the carbon dioxide is evolved suggests separate types of carbonaceous species on the catalyst. The strength of their adsorption to the catalyst will determine the temperature at which combustion and subsequent CO₂ evolution occurs.

Further post-reaction characterisation of the catalyst included XRD analysis, the pattern of which is shown in figure 3-7.

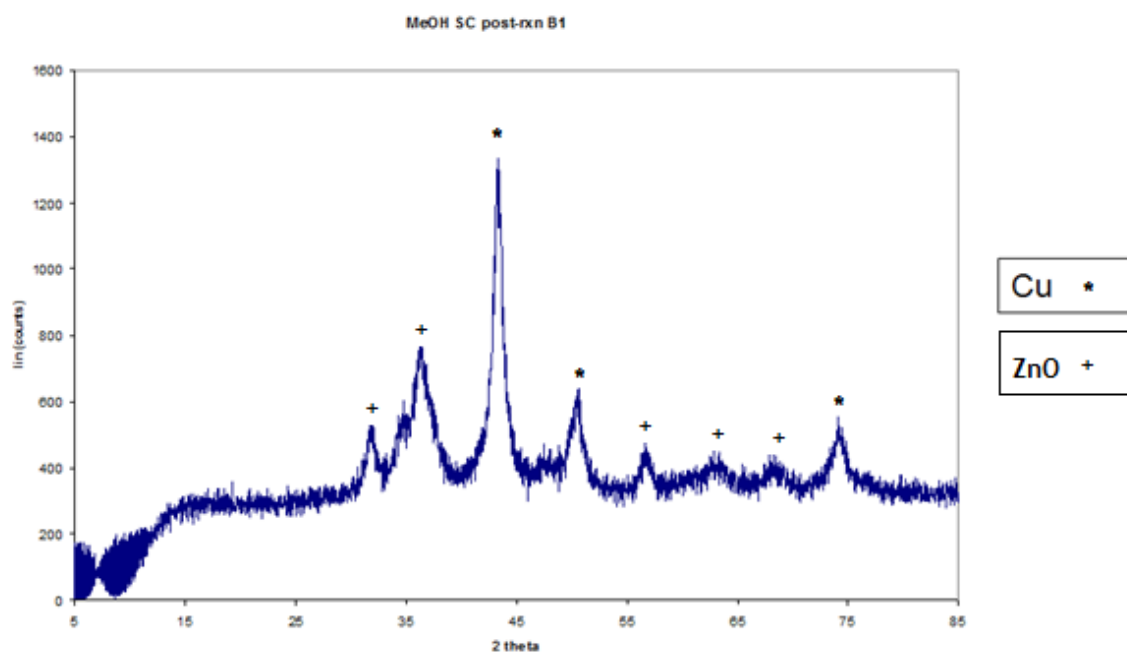


Figure 3-7: XRD pattern and assignment for post-reaction MeOHSCrB1

Peaks in the post-reaction XRD pattern in figure 3-7 were attributable to Cu and ZnO. Cu peaks were visible at 43.3° , 50.5° and 74.1° . The Scherrer equation was used to calculate an average Cu particle size of 9.5 nm. This is a significant increase when compared to the pre-reaction CuO particle size which was calculated as 3.9 nm. ZnO peaks are visible at 31.8° , 36.3° , 56.6° , 62.8° and 67.9° . The particle size calculations for ZnO particles using the peak at 36.3° give a value of 3.9 nm. The peaks attributable to zinc oxide display increased peak intensity compared to the pre-reaction sample, which indicates that increase in the crystal long range order has occurred during the reaction. Chemical deactivation of the catalyst through sintering was expected in the reaction given the reactivity of the acetic acid feed.

Table 3-5: BET data for comparison of pre- and post- reaction samples

	Surface Area (m^2/g)	Pore Volume (cm^3/g)	Av. Pore Diameter (nm)
Methanol synthesis catalyst	86	0.25	11.7
MeOHSCrB1	69	0.21	12.8

The characterisation data of the catalysts pre- and post-reaction by BET significant changes in the physical characteristics of the catalyst are seen, that may detrimentally affect the activity of the methanol synthesis catalyst. A loss of surface area and a growth in the metal particle size was observed within the catalyst through BET and XRD characterisation. However, these changes in the physical parameters of the catalyst do not appear to translate into a decrease in activity seen with the catalyst. This can be explained by the large quantity of copper within the methanol synthesis catalyst compared to the acetic acid feed within the system. The amount of copper that would need to be sintered or removed from the catalyst before deactivation was observed would be much larger than the amount currently affected by the low levels of acetic acid in the reactor system. The results in table 3-5 show a decrease surface area which would correspond to the collapse of the porous structure and a reduction in the catalyst surface area due to sintering of the copper metal particles and the anticipated reaction of the zinc oxide component with the acetic acid feed. A possible explanation for the poor mass balance within these reactions is that the acetic acid has reacted with the ZnO stabiliser component and produced alternative products, such as zinc acetate, within the catalyst pellets.

3.1.2 Impregnated Copper Catalysts

Following the testing of the methanol synthesis catalyst and data from the literature [2, 18], copper based catalysts have been identified as hydrogenators of acetic acid. Initially, the copper catalysts being tested contained low metal loadings to order minimise the metal content of the catalyst whilst trying to maximise the catalytic activity. The first impregnated copper catalysts were prepared with a nominal loading of 5 wt.% copper on a silica support (CARiACT Q10). Characterisation and testing of the silica Q10 support and impregnated 5 wt.% and 10 wt.% copper catalysts was completed and compared to the previously discussed methanol synthesis catalyst.

3.1.2.1 Silica Support

The silica support used was Fuji-Silysia CARiACT Q10, which was supplied as 1-2 mm spheres. XRD analysis of the silica Q10 support, shown in Figure 3-8, shows

a large broad peak attributable to amorphous silica. No other features are visible on the XRD pattern.

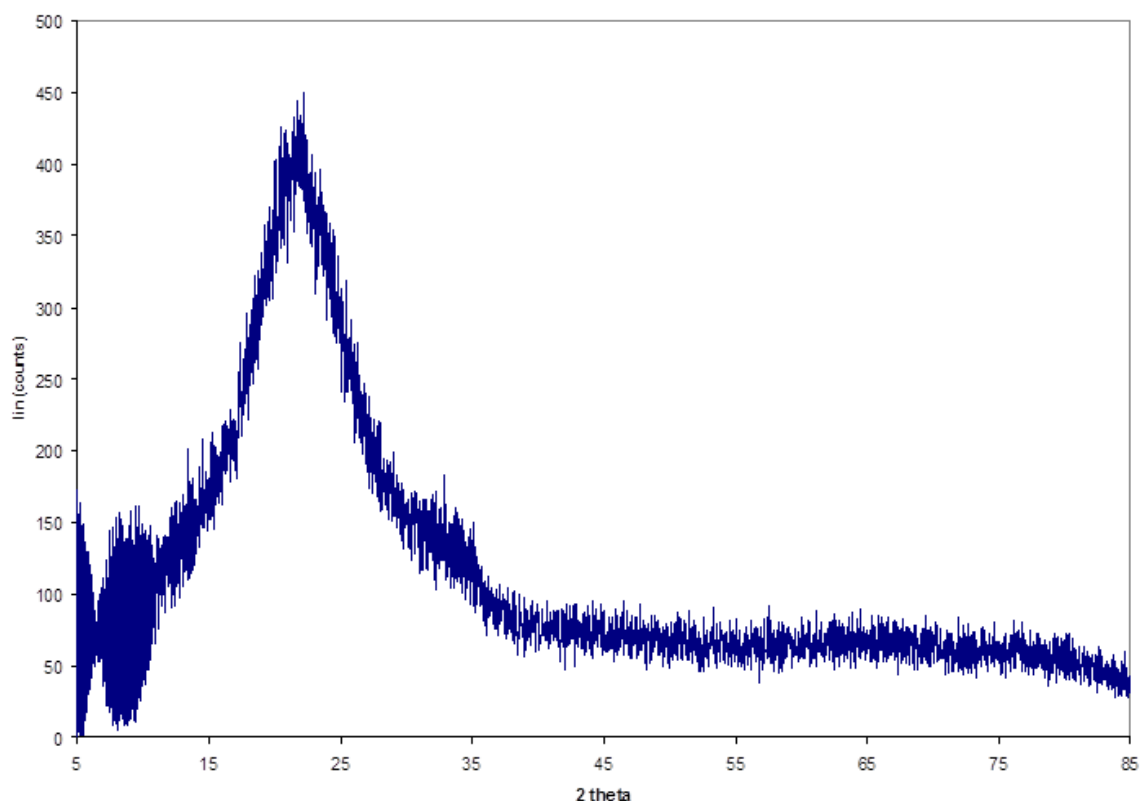


Figure 3-8: XRD pattern of uncalcined silica Q10

BET analysis data of the silica support is shown in table 3-6.

Table 3-6: Silica Q10 BET data

Catalyst	Surface Area (cm ² /g)	Pore Volume (cm ³ /g)	Average Pore Diameter (nm)
Q10	284	1.0	14

TPR analysis of the support was completed to identify any thermal events that were unique to the silica support and that may also have been observed in the impregnated catalysts.

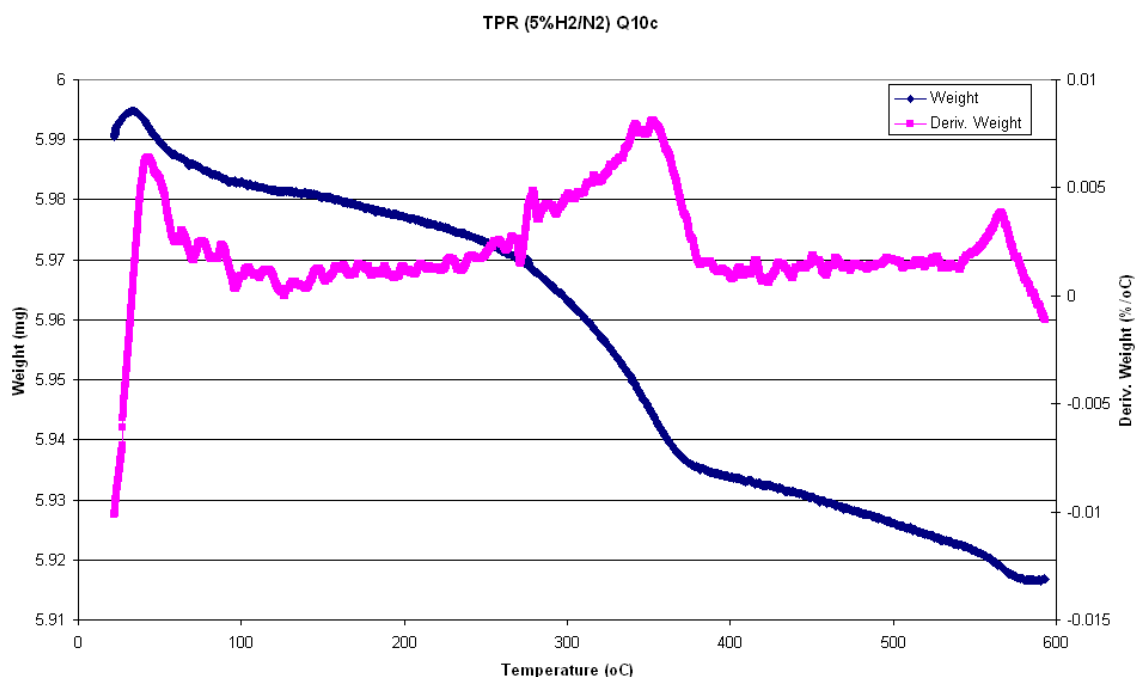


Figure 3-9: TPR profile of silica Q10

The TPR profile in figure 3-9 shows some small weight loss events around the expected values of 100 °C and further on at 367 °C, the corresponding MS data for the TPR analysis showed small peaks relating to the evolution of water (MS 17 and 18) and the uptake of hydrogen (MS 2). Importantly, the scale of the weight loss observed with the silica support at $<0.01\ \%/^{\circ}\text{C}$ is significantly lower than any observed with the supported metal catalysts.

XRD analysis of the calcined support gives an identical XRD pattern to that of the uncalcined support seen in figure 3-8.

3.1.2.2 5wt. % Copper Catalysts

5 wt.% copper catalysts were the first catalysts prepared for this study. Copper salts were impregnated on a preformed high surface area silica support. These were the first laboratory prepared catalysts of this project. The silica support used was Fuji-Silycia CARI^{ACT} Q10 with a surface area of around $300\ \text{m}^2\ \text{g}^{-1}$ and a pore volume of $1\ \text{ml}\ \text{g}^{-1}$, described in section 3.1.2.1. Two 5 wt.% copper catalysts were produced using two different copper salt precursors; one using the acetate salt and the other from the nitrate salt.

Characterisation

The two supported copper catalysts used were all prepared via the same method and exhibit similar profiles for characterisation, with variation for the different copper precursors used in the catalyst preparation step.

The initial TGA was to determine the temperature required for catalyst calcination; the process by which the catalyst is heated in air to convert the precursor to the metal oxide. Subsequent analysis in a reducing environment of 5 % H₂/N₂ for the TPR was to determine the temperature at which reduction and activation of the catalyst occurs. The two 5 wt.% copper supported on silica catalysts showed profiles for the TGA and TPR analysis that centre around similar temperature events.

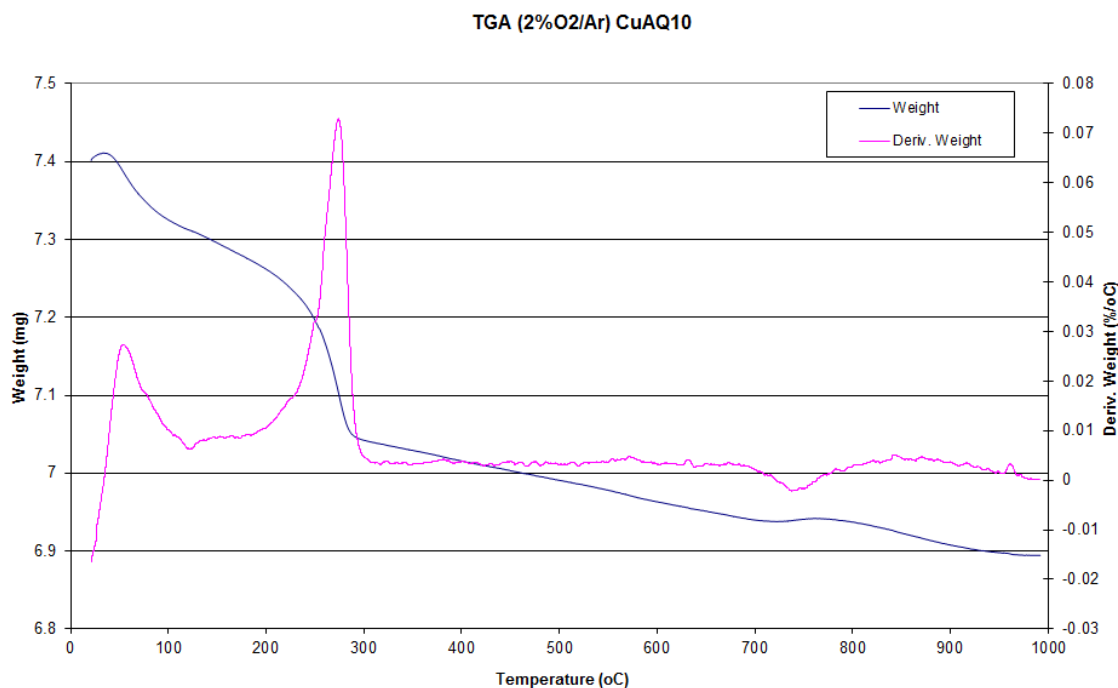


Figure 3-10: TGA profile of uncalcined CuAQ10

The TGA analysis of the 5 wt.% copper on silica catalyst from the acetate salt (CuAQ10) is shown in figure 3-10. A weight loss event at 273 °C, has an initial shoulder at ~240 °C which corresponds to the literature values for the decomposition event of Cu^{II} acetate [46]. The corresponding MS data from the TGA analysis is shown in figure 3-11. The decomposition of acetate groups has been extensively documented in the literature: for example, Bowker *et al.*

showed the autocatalytic decomposition of acetate groups in on oxidised surfaces and Rh (110) and Pd (110) crystals [16, 33, 48].

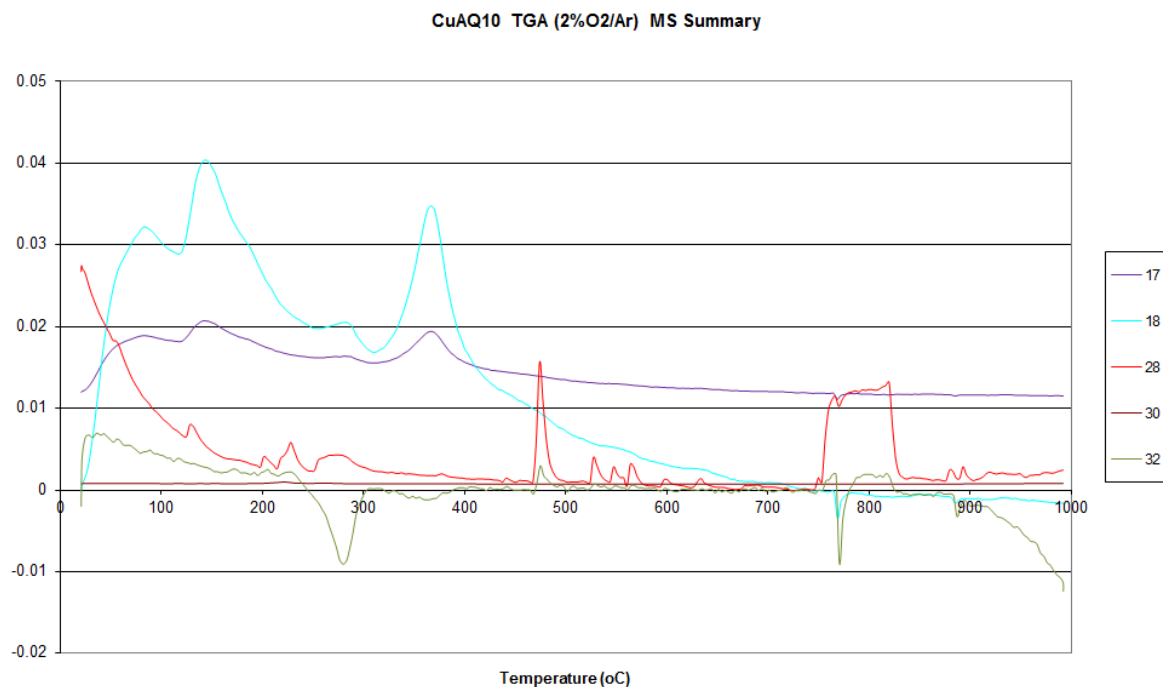


Figure 3-11: TGA-MS profile of uncalcined CuAQ10

The TGA event in figure 3-10, prior to 100 °C corresponds to the loss of H₂O from the catalyst. The shoulder at the start of the acetate decomposition profile correlates to the uptake of O₂ by the catalyst and the corresponding evolution of H₂O, CO₂ and the MS fraction 2. The same analysis was completed with the 5 wt.% copper on silica catalyst produced using the nitrate salt (CuNQ10) and can be observed in the figures 3-12 and 3-13.

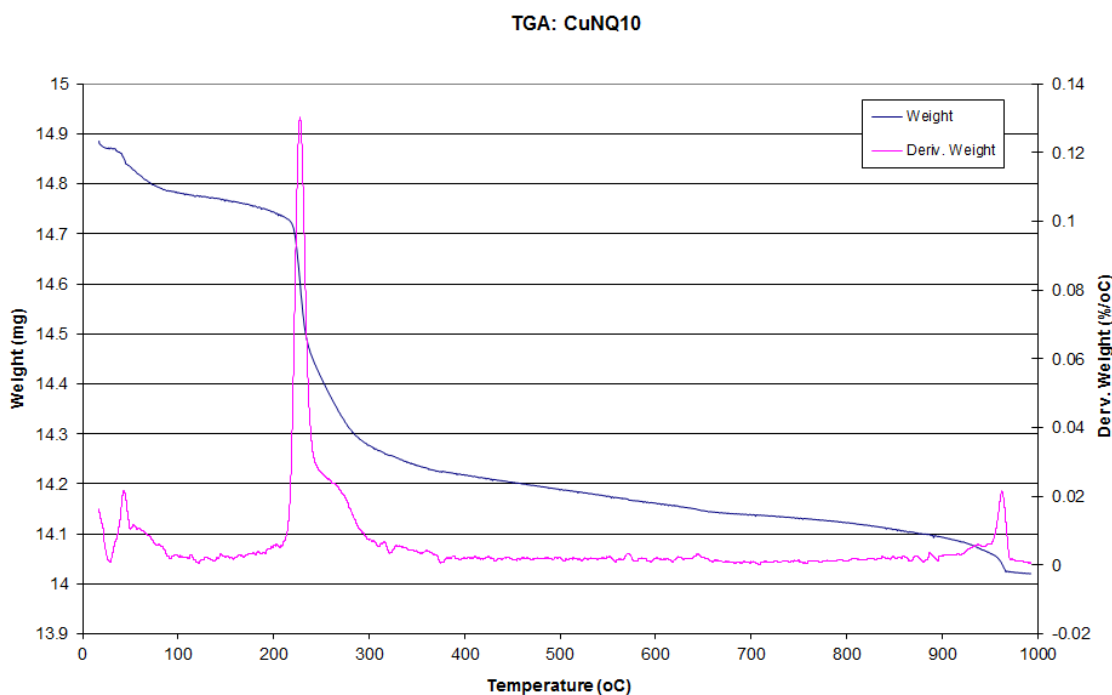


Figure 3-12: TGA profile of uncalcined CuNQ10

In figure 3-12, the TGA profile of CuNQ10 shows a sharp event at 227 °C. The corresponding MS data, in figure 3-12, shows that the small event prior to 100 °C is the evolution of water as would be expected. The sharp peak at 227 °C corresponds to peaks for the evolution of H₂, NO, N₂O and H₂O. A MS peak for NO (MS 30), seen in figure 3-13, is the predominant feature for the shoulder observed at 267 °C.

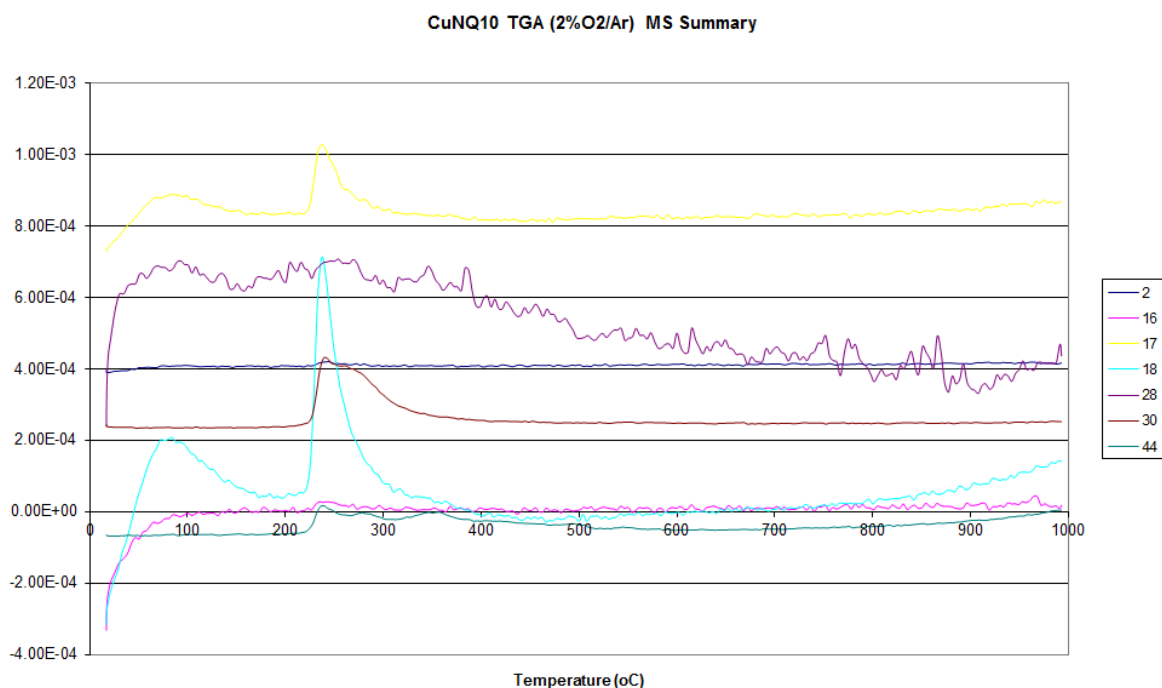


Figure 3-13: TGA-MS profile of uncalcined CuNQ10

Calcination of the catalysts was carried out in the tube furnace to a temperature of 250 °C as identified from the TGA profiles. The slightly different breakdown patterns are in line with the degradation observed for nitrates and acetates.

Temperature-Programmed Reduction

Analysis of the calcined catalysts via TPR on the TGA-DSC-MS was used to obtain appropriate reduction conditions for each of the catalysts. The two copper supported on silica catalysts showed similar TPR profiles as expected due to the reduction being the conversion of the copper oxide species to copper. TPR analysis of CuAQ10 is shown in figure 3-14.

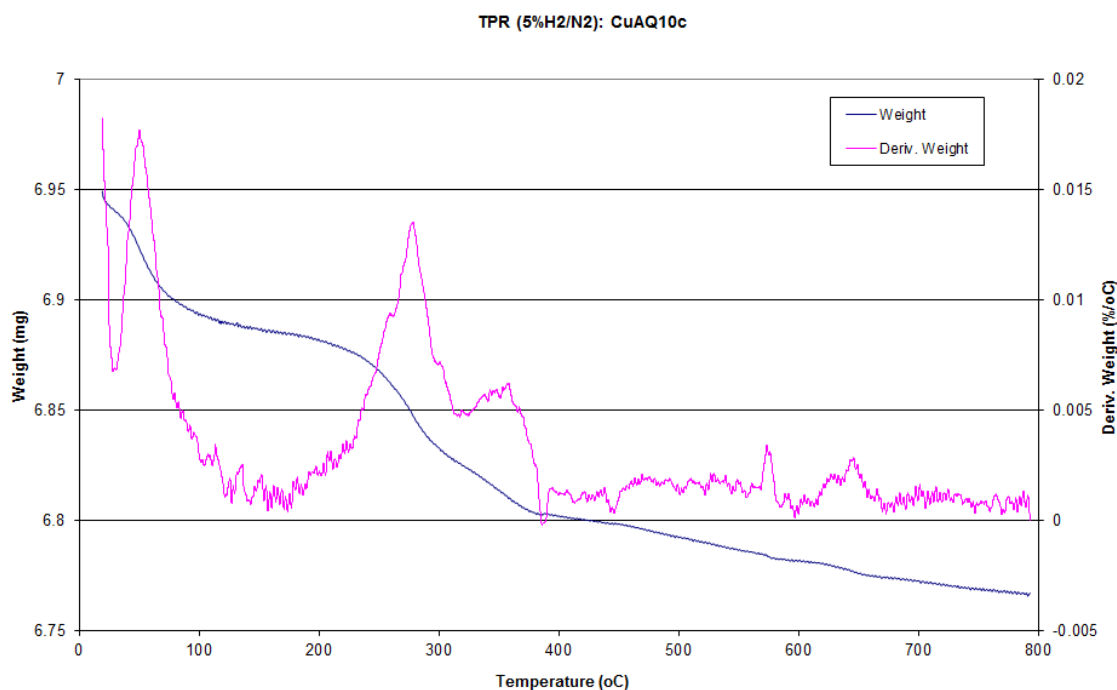


Figure 3-14: TPR profile of calcined CuAQ10

The corresponding MS profile only shows a small uptake of H₂ at the event at 278 °C and the evolution of H₂O (MS 17 and 18) for the two shouldering events around 300 °C. The expectation is that the events observed are the two stage reduction of Cu₂O and CuO on to metallic copper.

TPR analysis was also completed for CuNQ10. The profile showed a sharp weight loss event at 280 °C in figure 3-15.

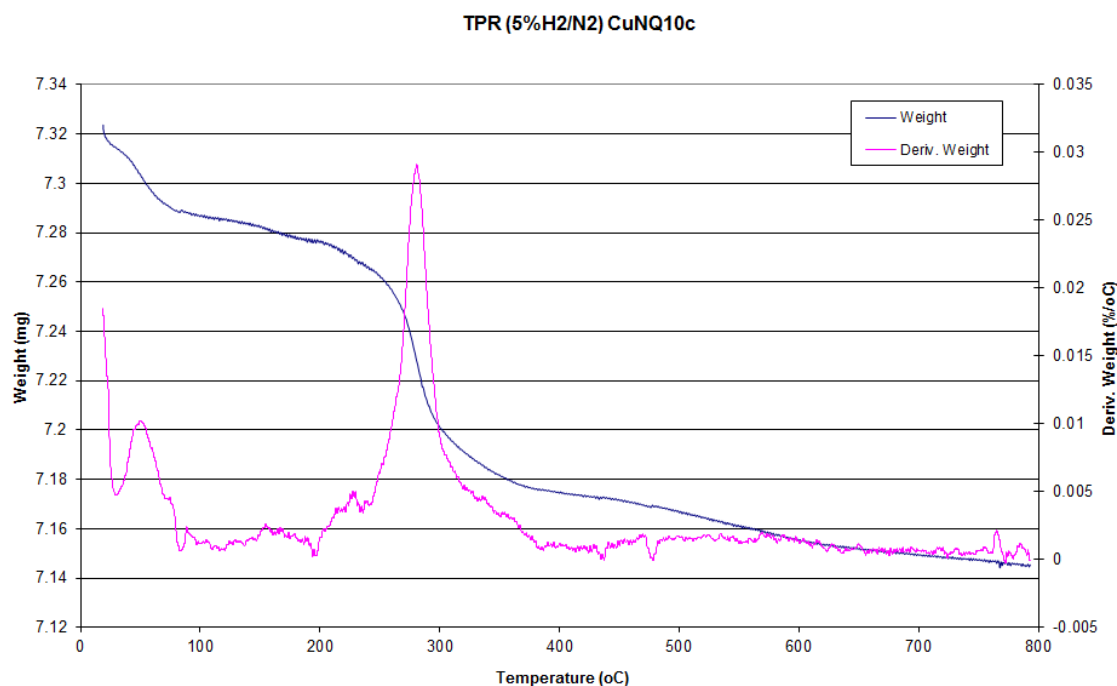


Figure 3-15: TPR of calcined CuNQ10

MS data showed that the small weight loss at around 100 °C had corresponding MS peaks for the evolution of H₂O (MS 17 and 18). The sharp weight loss event at 280°C corresponds with an exothermic event with an uptake of H₂ (MS 2). This uptake of hydrogen corresponds to the reduction of the copper oxide species to the metallic reduced copper species and the corresponding evolution of H₂O (MS 17 and 18) was observed. From the TPR profiles seen in figures 3-14 and 3-15, the reduction conditions were established for the two 5 wt.% copper on silica catalysts. The conditions are tabulated in table 3-7.

Table 3-7: Reduction conditions for CuAQ10c and CuNQ10c

Catalyst	Max Temp (°C)	Ramp Rate (°C/min)	Hold (mins)
CuAQ10c	250	10.0	180
CuNQ10c	250	10.0	180

In much of the TGA analysis described above, changes in the copper species in the catalyst were expected as a consequence of either the oxidising or reducing atmosphere that the catalyst is subjected to. XRD analysis was used to characterise the copper species present with the catalyst at the uncalcined and

calcined stages. XRD analysis of the CuNQ10 catalyst in figure 3-16 shows the presence of copper nitrate species within the uncalcined catalyst sample, as expected. This is because the nitrate salt was used for the preparation of this catalyst. The pattern in figure 3-16 of the calcined CuNQ10 sample shows a change in the copper species present in the catalyst. The features attributable to the copper nitrate salt are no longer visible, whilst features attributable to CuO are visible against the silica background post-calcination. This oxidation of the copper nitrate species to CuO corresponds to the transformation of the copper species upon calcination.

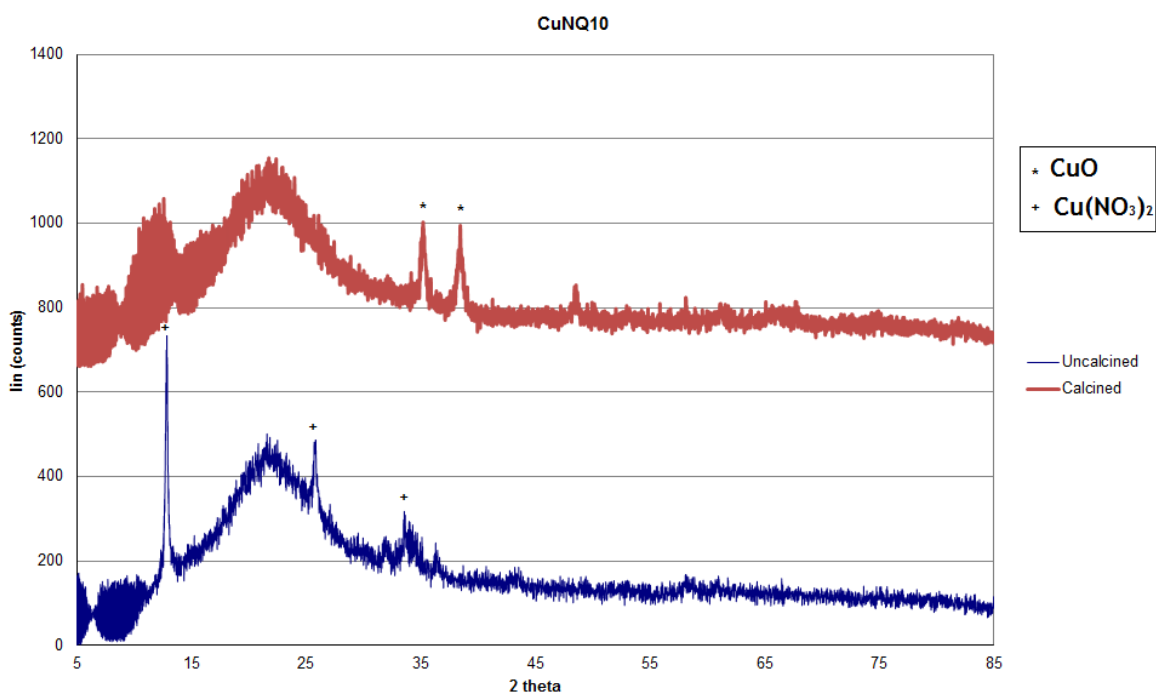


Figure 3-16: XRD pattern of uncalcined and calcined CuNQ10

Further analysis of the calcined CuNQ10 by hot-stage XRD under a 5 % H₂/N₂ atmosphere, which was used to determine the phases present in the catalyst after reduction. The profiles are shown in figure 3-17.

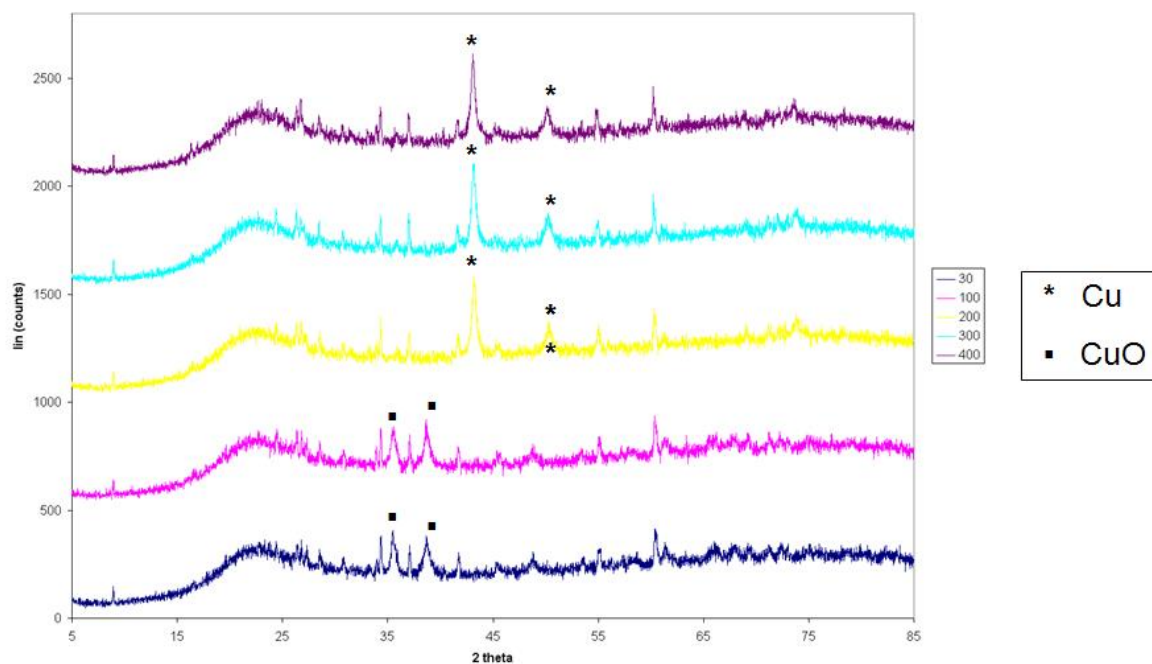


Figure 3-17: Hot-Stage XRD patterns of CuNQ10c at 25°C, 100°C, 200°C, 300°C and 400°C

The hot-stage XRD patterns show the temperature dependent reduction of the copper oxide species (CuO) in CuNQ10 to metallic copper (Cu). A large broad peak centring around 22°, which was previously assigned to the amorphous silica support, is the other consistent peak within each temperature scan. The analysis was completed with the CuAQ10 catalyst at both the uncalcined and calcined stages and is shown in figure 3-18.

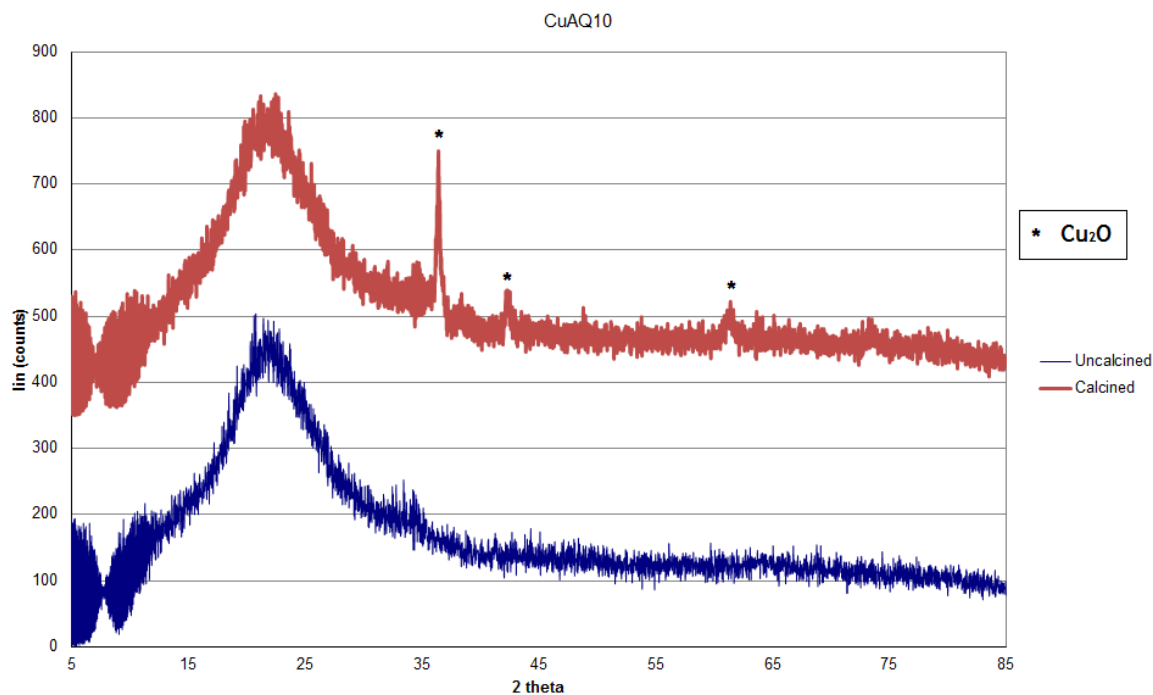


Figure 3-18: XRD patterns of uncalcined and calcined CuAQ10 samples

The XRD pattern of the uncalcined CuAQ10 catalyst sample had no observable peaks, possibly due to their amorphous nature or the small crystallite size of the copper species. Post calcination features, attributable to Cu_2O , became visible demonstrating the expected oxidation of the copper content. Subsequent hot-stage analysis of the CuAQ10 sample, shown in figure 3-19, shows the reduction of the Cu_2O species to Cu metal under a heated reducing atmosphere.

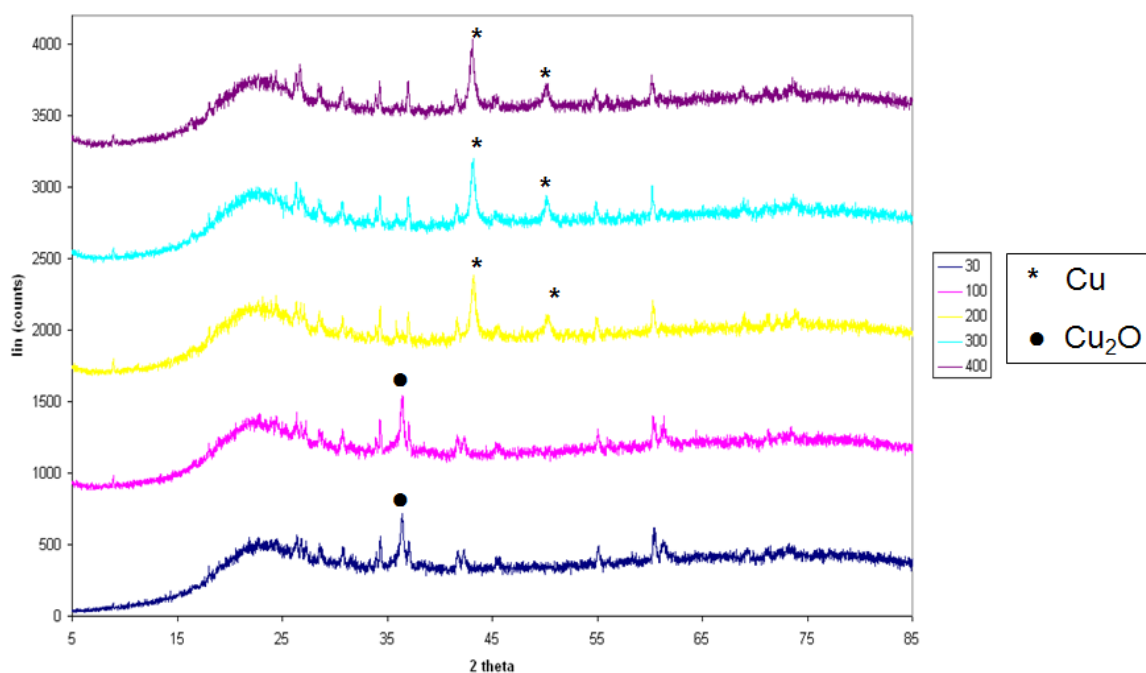


Figure 3-19: Hot-stage XRD patterns of CuAQ10c at 25 °C, 100 °C, 200 °C, 300 °C and 400 °C

By looking at the two different precursor salts used in the preparation of the 5 wt.% copper catalysts, two separate thermal decomposition routes producing two different copper oxides at the post-calcination stage are visible. These different copper oxides (Cu_2O and CuO) reduce at slightly different temperatures, as can be seen previously in the TPR profiles in figures 3-14 and 3-15. The copper species observed, dependent upon the precursor used, are shown below in figure 3-20.

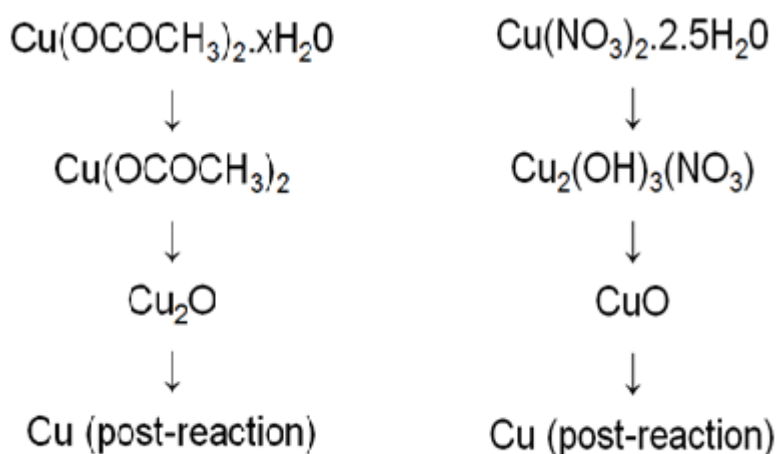


Figure 3-20: Copper reduction routes

3.1.3 Catalytic Testing: BERTY reactor

After identifying that the 5 wt.% impregnated copper catalysts would be active due to the presence of copper within the catalyst, an initial check was made on the activity of the silica support within the reactor system too. The catalyst support, Q10, underwent the same calcination and reduction conditions as the copper based catalysts to ensure consistency in experimental parameters. The standard reaction conditions, shown in table 3-8, are the same conditions as those used for testing of the methanol synthesis catalyst in section 3.1.1.2.

Table 3-8: Standard reaction conditions for testing in the BERTY reactor

Temperature (°C)	250
Flow (ml min ⁻¹)	190 (H ₂), 60 (N ₂)
Feed	1.5 mol.% Acetic Acid via HPLC pump (9 µl/min)
Catalyst Weight (g)	1.3
Catalyst Volume (ml)	3.3
Pressure (barg)	50
GHSV (hr ⁻¹)	~4,500

It can be observed from the reaction profile in figure 3-21, that the major product for the CuNQ10c catalyst within the BERTY reactor was ethyl acetate. The product of ethyl acetate is considered as a secondary reaction within this system, given the need for the initial hydrogenation of acetic acid to ethanol before the ‘secondary’ esterification reaction can occur. Clearly visible within the reaction profile is variance in the product concentration that appears almost cyclical. A reaction profile including the nitrogen marker is seen in figure 3-22.

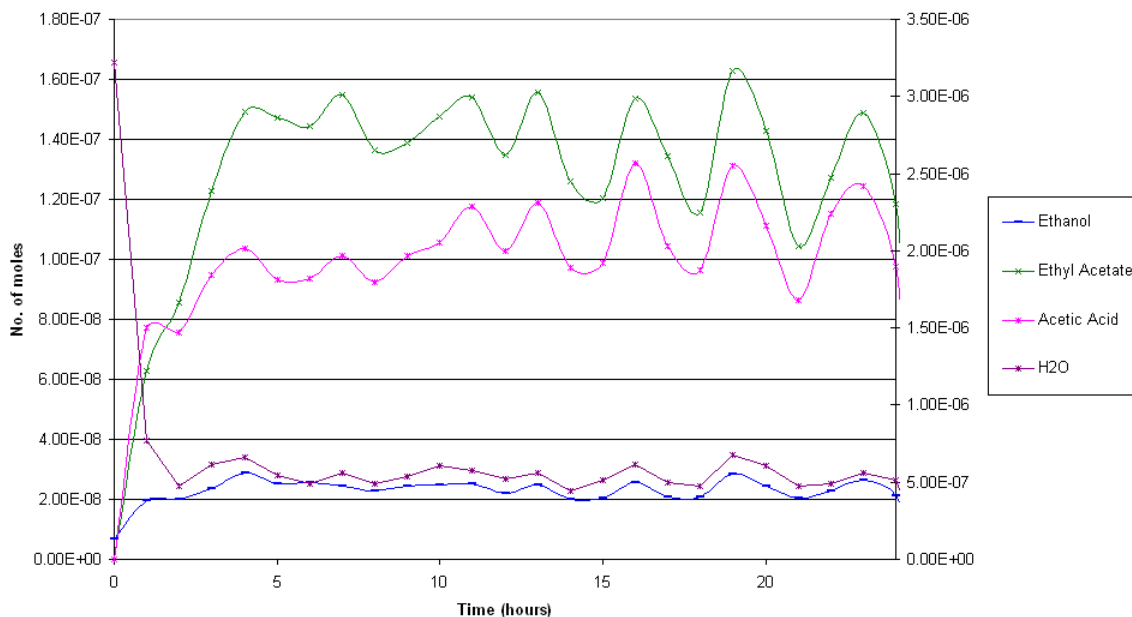


Figure 3-21: Reaction profile for CuNQ10 BERTY reaction

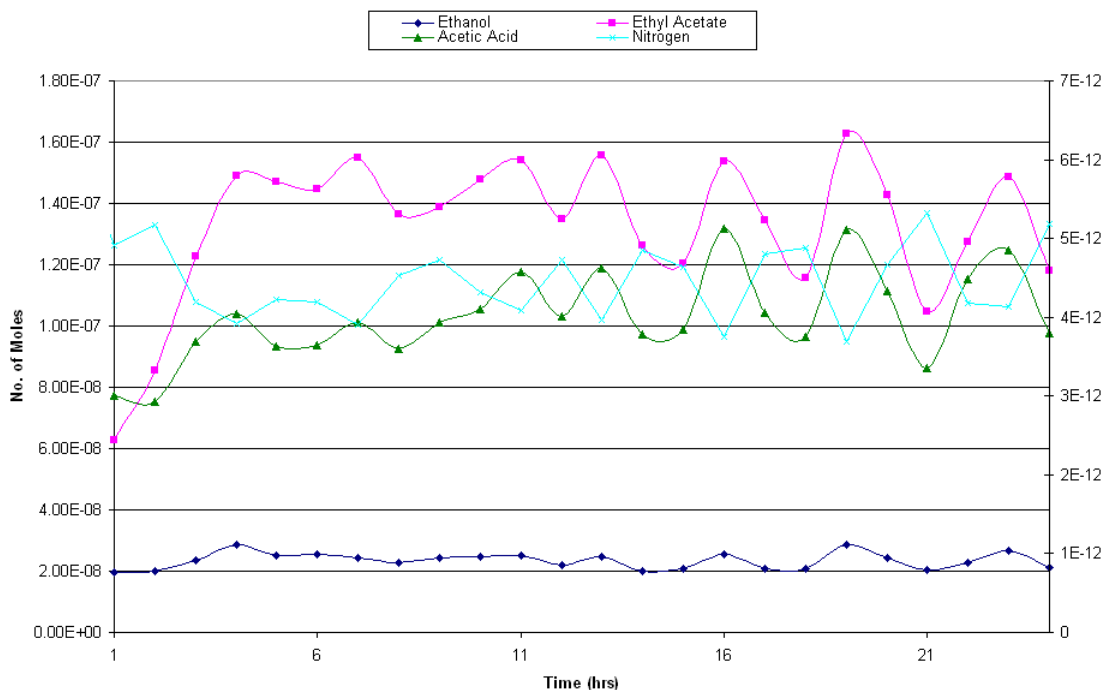


Figure 3-22: Reaction profile for CuNQ10 BERTY reaction, normalised to nitrogen feed marker

The use of nitrogen as an ‘inert’ marker within the system was used to explain the cyclical variance seen within the reaction profile, over the 24 hour reaction period. Upon analysis of the nitrogen marker, the nitrogen values mirrored those of the organic products. The combination of the moles of products and

nitrogen gave stable samples sizes throughout the reactions. The CuNQ10 catalyst was selective to ethyl acetate and the level of ethanol that was not esterified appeared to remain relatively steady throughout the reaction. The carbon and oxygen balance for the reaction again follows the oscillations of the reaction profile, but varies within the range of 0.6 - 1.

The same reaction profile approach was employed with the CuAQ10 catalyst. It was observed that for both 5 wt.% copper catalysts, tested in the BERTY reactor, ethyl acetate was the major product. The rate of product of ethanol and the subsequent conversion to ethyl acetate remain relatively consistent through the reaction. Additionally, it was observed that the 5 wt.% copper catalysts gave significantly lower conversions of acetic acid than the methanol synthesis catalyst.

Table 3-9: Selectivities and conversions of the 5 wt.% Cu catalysts

		CuNQ10rB2	CuAQ10rB3
Selectivities (%)	Ethanol	5.7	3.3
	Ethyl Acetate	67.8	63.3
	Acetaldehyde	0	0
Conversion (%)		90.6	88.6

For both reactions, fluctuations were seen in the product stream. One possible explanation for this oscillation pattern could be linked to the orientation of the vapouriser. The orientation was top loading, leading to possible dripping of the feed into the vapourising section rather than a consistent feed rate. The pulsation of the acetic acid from the HPLC pump or the flash volatilisation of the acetic acid dripping into the vapourising tube could explain the cyclical results. To address these issues, the inlet to the feed inlet was orientated at 90° to the pipe direction, at the side. In addition, *n*-octane was inserted into the acetic acid feed as a liquid marker: an additional internal reference within the system.

3.1.3.1 Post-reaction characterisation

Post-reaction characterisation of the catalysts was carried out to establish the effect of the reaction system upon the catalyst. Samples of the post-reaction CuAQ10 and CuNQ10 catalysts underwent TPO analysis. The TPO profiles can be seen in figure 3-23 and 3-25.

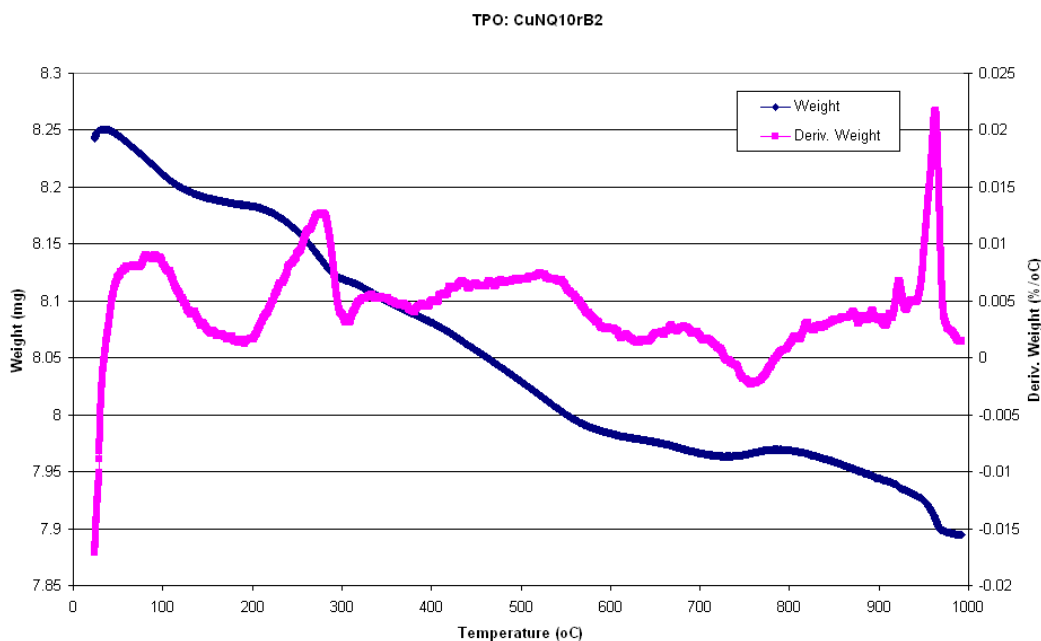


Figure 3-23: TPO analysis of post reaction CuNQ10

TPO analysis of the CuNQ10 catalyst sample showed a small exothermic event at 281 °C, although the weight loss seen is around 0.01 %/°C in figure 3-23. MS analysis during the TPO showed that the weight loss at <100 °C corresponded to MS peaks for 18 and 17. The weight loss at 281 °C in figure 3-22 corresponded to MS peaks for the evolution of 44, 18, 17 and 2 and the uptake of O₂ (MS 32). The weight loss between 400-550 °C corresponds to a broad evolution of CO₂ (MS 44). Figure 3-24 shows the XRD analysis of the CuNQ10 post-reaction catalyst sample, with features attributable to metallic copper. This reduced form of the copper was expected in the post-reaction sample, as the reducing reaction atmosphere was expected to maintain the copper in reduced form throughout the reaction, following the catalyst activation step.

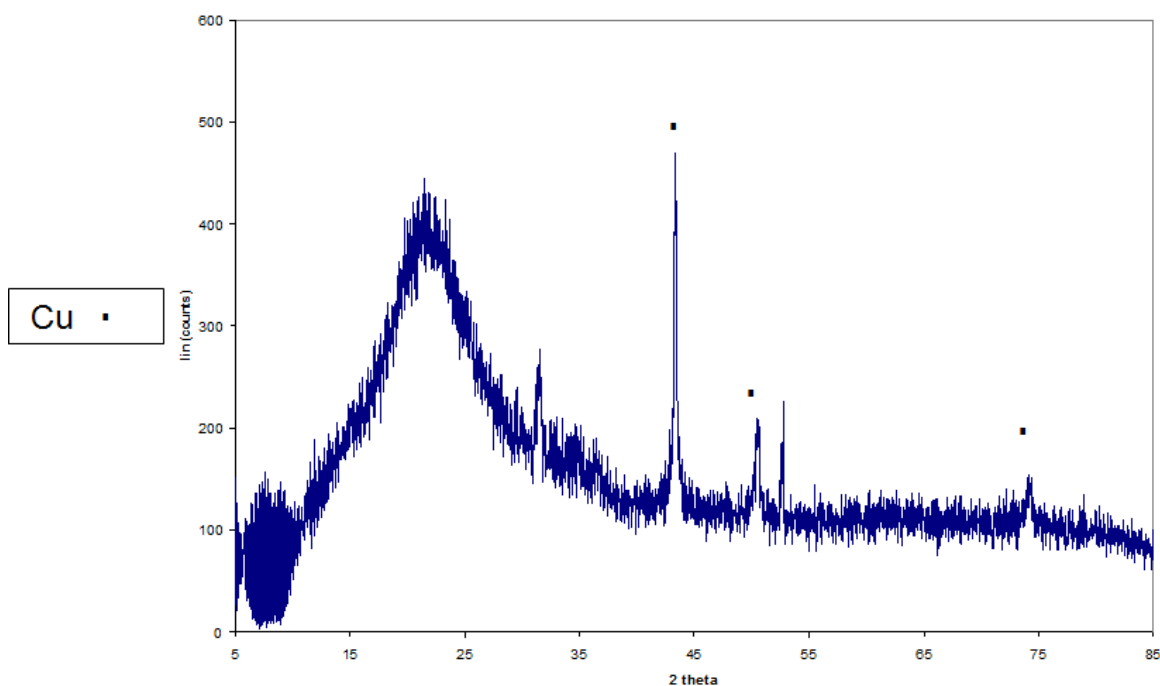


Figure 3-24: XRD pattern of post-reaction CuNQ10

The same analytical techniques were employed for the post-reaction sample of the CuAQ10 catalyst. The TPO profile in figure 3-25 from the TGA-DSC data shows a small exothermic event corresponding to the peak at 257 °C. MS analysis showed that the weight loss at < 100 °C had peaks corresponding to the evolution of H₂O (MS 17 and 18). The weight loss event at peak at 257 °C is an exothermic event and the MS data showed the evolution of CO₂ (MS 44) and H₂O (MS 17 and 18). Similarities in the post-reaction characterisation of the two 5 wt.% copper catalysts, suggests that similar acetate species are present on the surface of the catalyst which are then oxidised during the TPO temperature ramp.

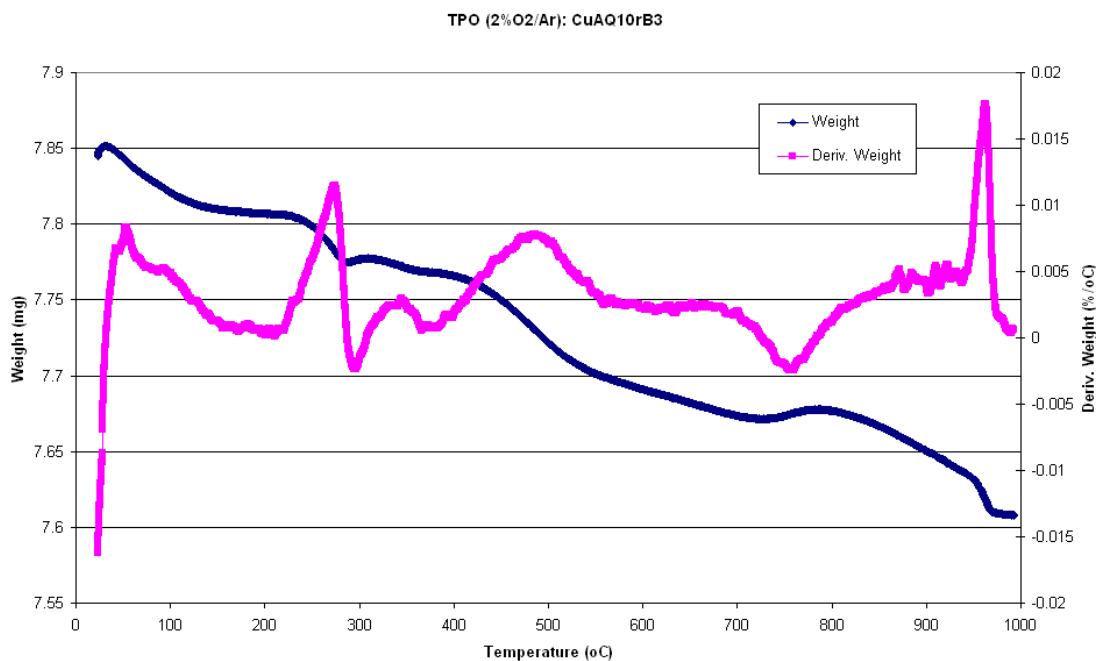


Figure 3-25: TPO analysis of post-reaction CuAQ10

Mirroring the transformation seen in the hot-stage XRD analysis of both 5 wt.% copper catalysts, the CuAQ10 catalyst post-reaction contained reduced copper as features for Cu were clearly visible in figure 3-26, above the silica background.

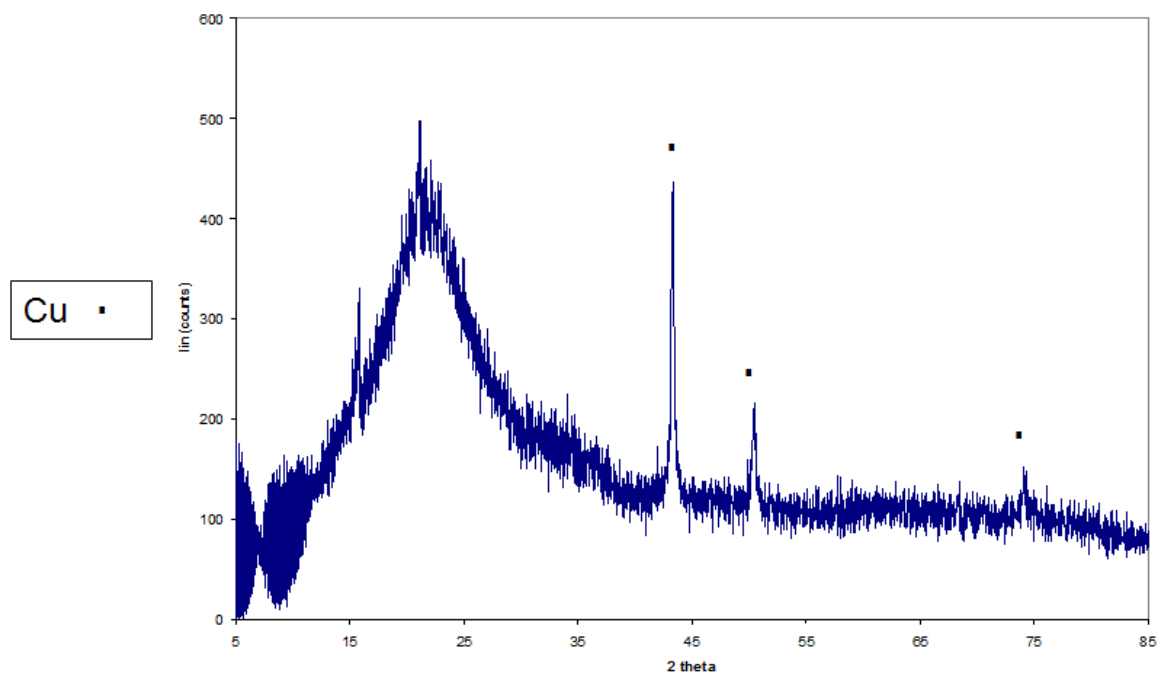


Figure 3-26: XRD pattern of post-reaction CuAQ10

3.1.3.2 Addition of a liquid marker in the feed

The activity of the CuNQ10c catalyst was also investigated with the system modified to include the liquid marker, *n*-octane, in the feed. The results from the 70 hour reaction are shown below in figure 3-27. Clearly visible from the product profile is the effect of the introduction of *n*-octane, which is a decrease in the production of ethanol, and subsequently ethyl acetate, over the same catalyst system.

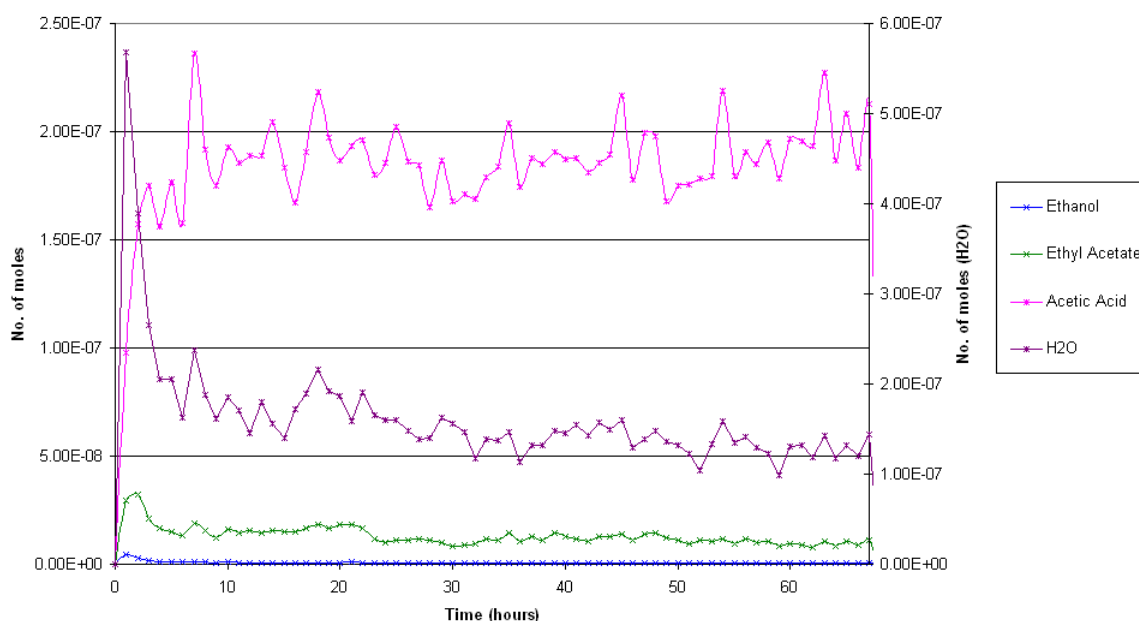


Figure 3-27: Reaction profile for CuNQ10 with *n*-octane (B6)

Although the inclusion of the *n*-octane marker in the acetic acid appears to decrease the activity of the catalyst with respect to ethanol and ethyl acetate, the variance in the results appears smaller than previously seen with this catalyst. Stabilisation of the values for ethanol, ethyl acetate and acetic acid are observed when normalised against the internal standard. The same reaction conditions were investigated using the CuAQ10. Its major product remained ethyl acetate as was previously seen, but in diminished levels which mirrored the effect of the addition of *n*-octane to the system in the CuNQ10 reaction. Silica Q10 was also tested and the results are shown in table 3-10 with the use of the *n*-octane internal standard. The carbon and oxygen balance for these reactions remained steady at ~0.5 for the duration of the reactions.

Table 3-10: Selectivities

CATALYST		MeOH SC (B1)	Q10 (B5)	CuNQ10 (B2)	CuNQ10 (B6) (with n-octane)	CuAQ10 (B3)	CuAQ10 (B8) (with n-octane)
Selectivities (%)	Ethanol	34.7	0	5.7	0.3	3.3	0.3
	Ethyl Acetate	3.5	6.4	67.8	12.2	63.3	7.4
	Acetaldehyde	0	0	0	0	0	0
Conversion (%)		98.8	59.3	90.6	58.9	88.6	68.5

The selectivities of the catalysts, seen in table 3-10, showed that the methanol synthesis catalyst was the better catalyst for the production of ethanol. However, the 75 % selectivity and 68.5 % conversion are the averages from day one of the four day reaction period. Over the course of the four days, the catalyst deactivated significantly losing nearly half of its activity for ethanol production. Lower conversions of acetic acid were observed with the 5 wt.% copper catalysts than for the methanol synthesis catalyst. What is clearly visible from the comparison of data above is that the addition of the n-octane to the feed, impacts upon the conversion. A significantly increased amount of acetic acid was seen in the product stream at the end of the reaction.

Post-reaction characterisation of the catalyst, including TPO analysis, was completed for each of the catalysts tested with the n-octane marker. The TPO profiles, such as for CuNQ10 in figure 3-28, all show the same sharp weight loss event at ~287 °C, mirroring what was seen for the reactions completed without the presence of *n*-octane.

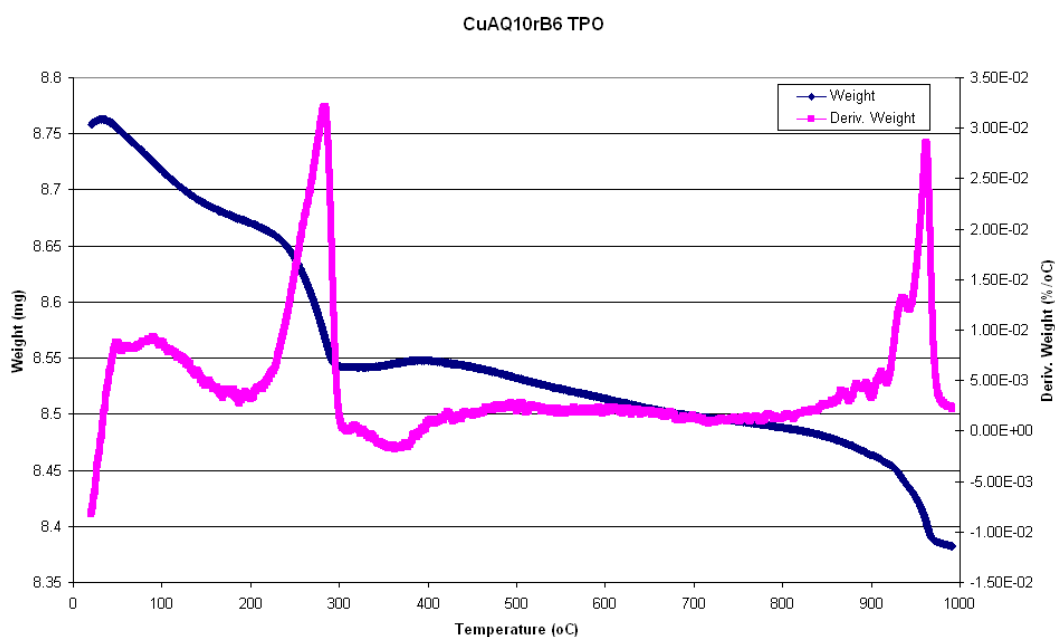


Figure 3-28: TPO analysis of post-reaction CuAQ10

The corresponding DSC analysis showed that the sharp weight loss event at 287 °C seen in figure 3-28 was an exothermic event. The weight loss event was accompanied by the evolution of CO₂. This is visible within the MS data as peaks for MS 44 and an uptake peak of O₂ to facilitate the combustion. The small weight loss at < 100 °C has corresponding peaks for H₂O (MS 18 and 17). The same peak around 300 °C was observed, suggesting that acetate species are also bound to the surface of the silica support during the reaction with their combustion is observed in the TPO. Once more, XRD analysis in figure 3-29 displays features identifying Cu as the copper species present within the catalyst post-reaction. Analysis of the silica Q10 support samples was completed post-reaction.

Again, XRD analysis of each of the catalyst samples post-reaction was completed. Each of the XRD patterns for the post-reaction 5wt% copper catalysts show features that are attributable to metallic copper.

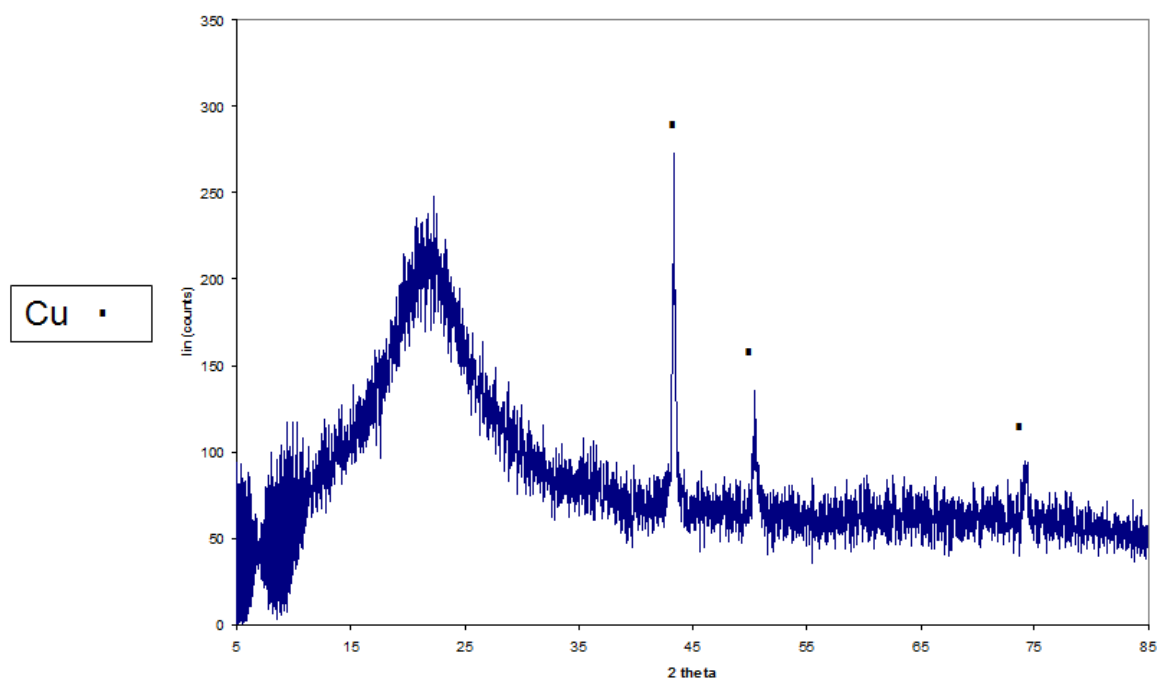


Figure 3-29: XRD analysis of post-reaction CuAQ10

3.1.3.3 Change in operating conditions: Lower pressure

A profound effect on the activity of the catalyst was observed with the addition of *n*-octane, an ‘inert’ marker into the liquid feed. In another attempt to minimise the variance seen in the reaction profiles, a lower operating pressure of 30 barg was investigated with the BERTY reactor. All other reaction parameters were maintained. The reaction profile in figure 3-30, shows an observable decrease in the amount of acetic acid converted within the system. This observation is reinforced with the selectivity and conversion values tabulated in table 3-11.

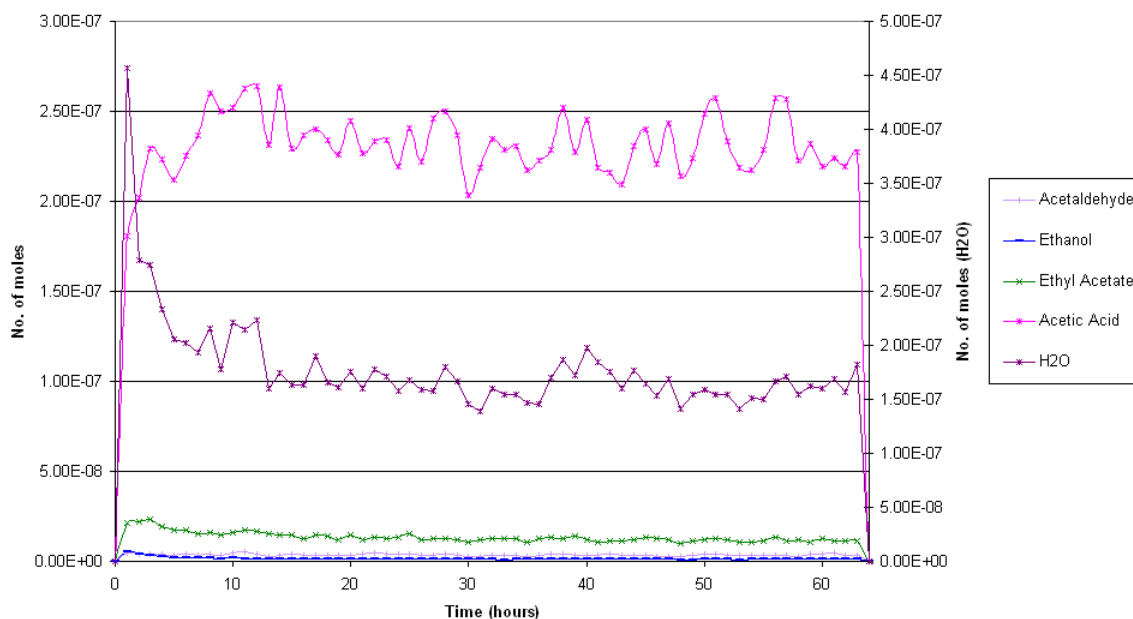


Figure 3-30: Reaction profile for CuNQ10 at 30 barg.

Table 3-11: Selectivities for CuNQ10rB9 (CuNQ10 at 30 barg)

CATALYST	CuNQ10 (B9) (with <i>n</i> -octane)
Conversion (%)	43.2
Acetaldehyde Selectivity (%)	1.8
Ethanol selectivity (%)	0.7
Ethyl Acetate Selectivity (%)	16.8

The testing at a reduced operating pressure of 30 barg appears to give a more stable reaction. The decreased pressure used in the CuNQ10 reaction means that ethyl acetate is seen as the major product, but the system also produces acetaldehyde.

The same post-reaction analysis was completed on the catalysts, as before. And the results are comparable. TPO analysis in figure 3-31 shows a sharp peak at 287 °C replicating the post-reaction analysis that was seen with the catalyst when previously tested using this reactor system.

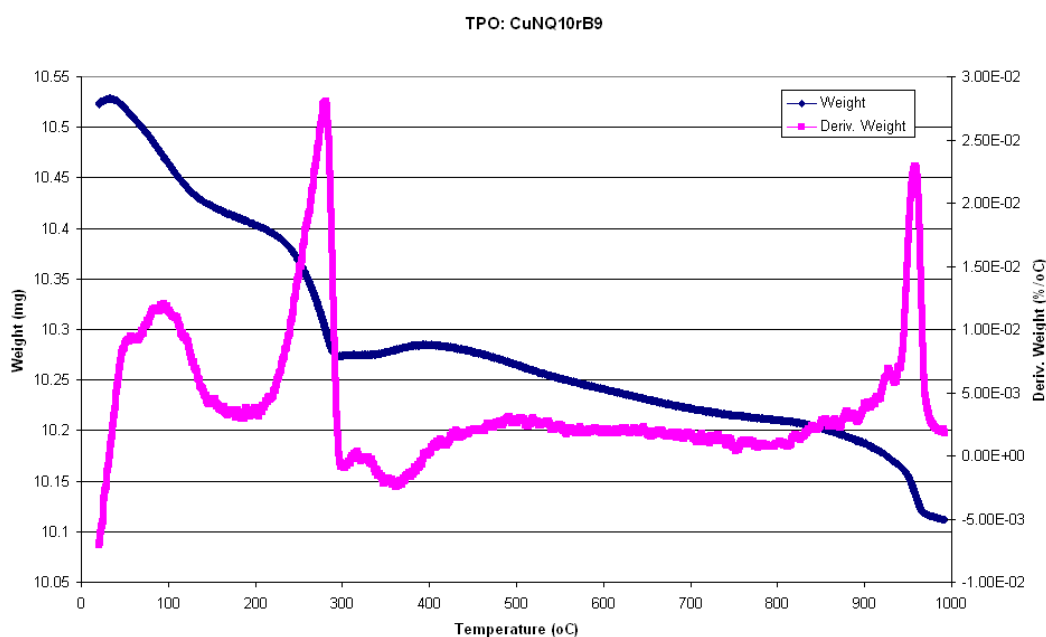


Figure 3-31: TPO analysis of CuNQ10 (reaction at 30 barg)

The MS analysis shows a weight loss peak at < 100 °C with a corresponding evolution of H₂O. In figure 3-31, the peak at 276 °C is an exothermic event and has corresponding MS events for the evolution of CO₂, CO and the uptake of O₂. Additionally, the same Cu features were observed within the XRD pattern. The same three peaks as were seen in figure 3-31 are observed in the post-reaction catalyst of this lower pressure reaction.

3.1.3.4 BERTY Summary

After identifying that the copper catalysts were active, it was important to compare the activity and the selectivity of the 5 wt.% copper catalysts to that of the methanol synthesis catalyst which contained about 40 % copper. The expectation was that the methanol synthesis catalyst would be markedly more active, if only due to the significantly greater amount of the active metal phase in the catalyst. Two 5 wt.% copper catalysts, a silica support and a commercial methanol synthesis catalyst were all tested in a BERTY reactor. Of the catalysts tested within this system, the methanol synthesis catalyst was the only catalyst with majority selectivity towards ethanol.

Variance in the reaction profiles for the 5 wt.% copper catalysts lead to the inclusion of an 'inert' liquid marker into the system. When the system was normalised to the n-octane liquid marker, an effect of the octane is observed

where the system appears to lose conversion towards ethanol and ethyl acetate. This observation shows how the conversion and subsequent selectivities of a catalytic system can be affected by the presence of additional 'reactive' species.

The post-reaction XRDs identify metallic Cu species within each of the catalysts post-reaction as well as a large peak appropriate for amorphous silica. The Q10 silica support was selective to ethyl acetate. The silica support has acid sites that may facilitate the conversion of the ethanol produced to ethyl acetate.

3.1.4 10 wt.% Copper Catalyst

Upon seeing the marked increase in activity with the methanol synthesis catalyst, compared to the 5 wt.% impregnated copper catalysts, an increase in activity was desired. Increasing the catalyst's copper content was a route by which the activity of a catalyst may be increased. As such a 10 wt.% copper catalyst was prepared via the same impregnation route. The nitrate salt was used for the impregnation and the same characterisation, calcination and analysis was completed as for the 5 wt.% copper catalysts.

Decomposition of the nitrate salt precursor in the TGA analysis mirrored that observed with the CuNQ10 catalyst (seen in figure 3-12). The TPR analysis also followed the TPR for the CuNQ10 catalyst. The mirroring of the characterisation profiles between the CuNQ10 and CuN(10)Q10 catalysts was to be expected. The catalysts were prepared using the same metal precursor and impregnation technique. The only difference was the metal loading, as the 10 wt.% copper on silica catalyst had double the quantity of copper deposited on the support as the 5 wt.% copper catalyst.

3.1.5 Catalyst Testing: Low pressure microreactor

The hydrogenation of acetic acid to ethanol over copper based catalysts was investigated using a low pressure microreactor. The testing procedure is described in chapter 2.3.2 and the reaction conditions detailed in table 3-12 were maintained for all the catalysts compared in this section.

The stability of the system was checked through the completion of comparative reactions with either a blank reactor vessel or a loading of silicon carbide (1 ml). In addition, the reaction process was also conducted for both a blank reactor and silicon carbide loading (1 ml), at room temperature. This was to account for the acetic acid being fed into the system.

3.1.5.1 Silicon Carbide/ Blank reactions

The experimental method used for catalyst testing was followed but with an empty reactor chamber to test the integrity of the system in terms of carbon and oxygen balance, and to show that the system was not autocatalytic. The blank reactions were completed at both standard reaction temperature (250 °C) and room temperature (20 °C). In addition, the system was tested using the 'inert' packing material: silicon carbide.

Reaction profiles for the blank reactions and those with a loading of silicon carbide (1 ml) showed accountability for acetic acid introduced to the reactor system, whilst showing no products with the GC exit stream analysis.

3.1.5.2 Copper Catalysts

The same two 5 wt.% copper on silica catalysts (CuNQ10 and CuAQ10) were tested on the low pressure microreactor. Additional catalysts with a 5 wt.% copper loading prepared via the same impregnation techniques were prepared and tested within this system. One new 5 wt.% copper catalyst was prepared using copper acetate as a precursor (CuA3Q10), whilst the other used copper nitrate (CuN2Q10). Characterisation of these catalysts was completed using the same techniques as CuNQ10 and CuAQ10 and mirrored the results seen with the catalysts prepared with the same precursors.

The standard reaction conditions used with each of the copper based catalysts in the low pressure microreactor are shown below in table 3-12.

Table 3-12: Standard reaction conditions for microreactor reactions with copper catalysts

Reaction Temperature (°C)	250
Catalyst Volume (ml)	1
Gas Flow Rate (ml min ⁻¹)	60 (H ₂)
GHSV (hr ⁻¹)	3,600

The results for the copper based catalysts within the low pressure microreactor are shown in table 3-13. It includes acetic acid conversion and selectivity for each of the products seen.

Table 3-13: Selectivities and conversions of copper catalysts in low pressure microreactor

	Catalyst	Q10	CuNQ10	CuAQ10	CuN2Q10	CuA3Q10	MeOHSC
Selectivities	Ethanol	0	0	0.4	0.9	0.3	75
	Ethyl Acetate	0	1.3	0	0	0	0
	Acetaldehyde	0	0	0	0	0	14.8
Conversion (%)		82.4	77.9	81.4	80.4	81.8	100

The loss of acetic acid within the system, given the initial experimentation completed with the blank reactions, can confidently be attributed to adsorption of acetic acid onto the silica support. This conclusion is strengthened by a similar conversion level of 82 % observed with the silica support reaction but without any ethanol, acetaldehyde and ethyl acetate observed within the GC traces.

Catalytic testing of the silica support within the low pressure microreactor gave a conversion of 82.4 %. No products, however, were observed on the GC traces, including ethanol and ethyl acetate. The low pressure Q10 reaction yielded no

products, whilst the reaction at 50 barg pressure did see the product of ethyl acetate.

In the reaction using CuN2Q10 catalyst, there was minimal ethanol production (0.9 %) observed even though it was the singular product in the reaction system and the conversion of acetic acid within the system was 80.4 %, as shown in table 3-13. No ethyl acetate or other expected products were observed on the GC traces. This was a trend observed for all four of the 5 wt.% copper on silica catalysts.

The data observed for the methanol synthesis catalyst is an average of the four day reaction given that there is deactivation of the catalyst observed during the reaction period. The methanol synthesis catalyst displays a much higher conversion to ethanol than the other catalysts tested, but unlike the others demonstrates deactivation.

Post-reaction characterisation of the catalyst samples was completed using TPO, BET and XRD analysis. TPO analysis was of particular interest given that the majority of the acetic acid being fed into the system was unaccounted for with the silica based catalysts. Identification of the presence of carbon species on the catalyst was confirmed by the presence of oxidation products, CO and CO₂, within the MS profile.

3.1.5.3 Silica Support

Post-reaction analysis of the silica support produced a TPO profile with a large event around 100 °C in figure 3-32. The corresponding MS data is shown in figure 3-33.

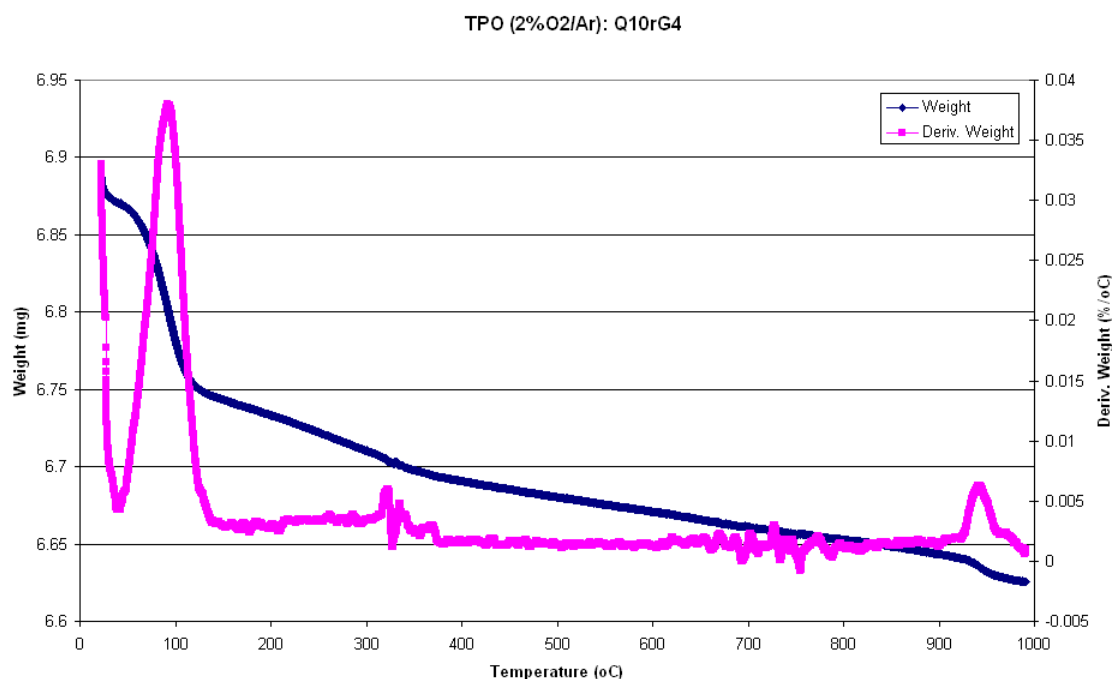


Figure 3-32: TPO profile of post-reaction silica Q10

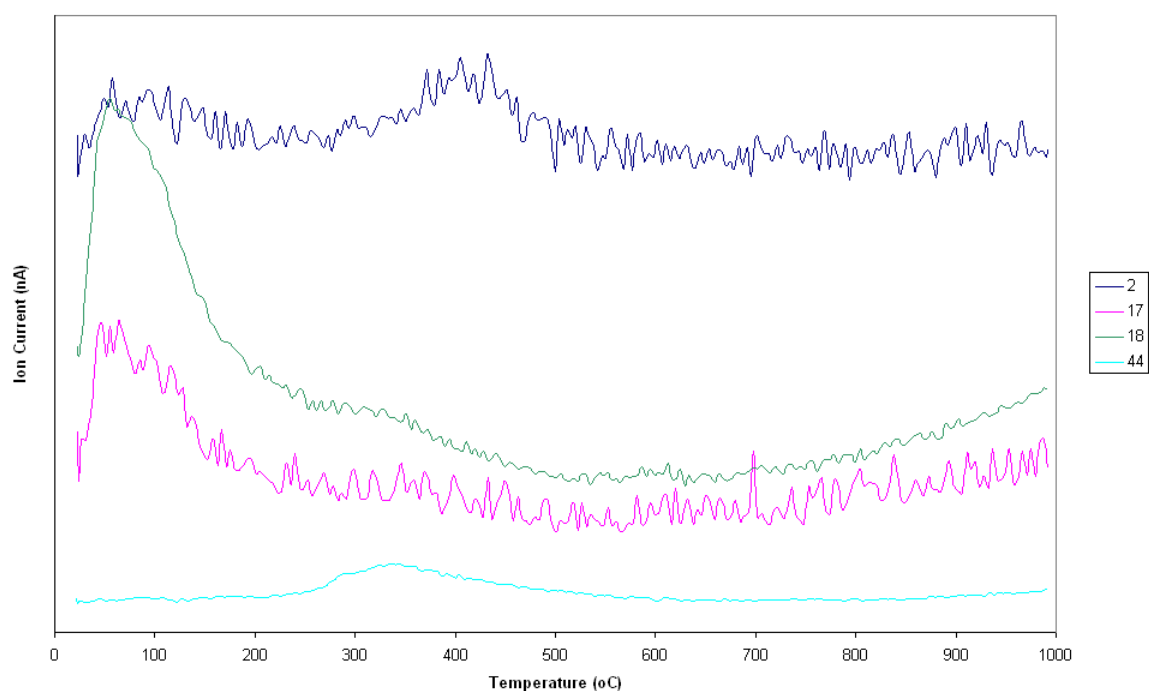


Figure 3-33: MS data for Q10rG4

The MS data shows that the event at 100 °C relates to the evolution of H₂O (MS 17 and 18). Additionally observed within the MS data, is that the small multipeak event between 300 - 350 °C corresponds to an evolution of CO₂ (MS 44). This further consolidates the idea of the presence of the unaccounted acetic acid being on the silica support, which is then combusted when the catalyst is heated in the presence of an oxidising atmosphere.

The XRD pattern for the post-reaction Q10 catalyst shows only the large broad peak assignable for amorphous silica. No other species were expected to be present within the post-reaction silica sample.

3.1.5.4 5 wt.% Copper Catalysts

The four 5 wt.% copper catalysts investigated were all characterised individually but showed the same post-reaction profiles. As such, the post-reaction characterisation data for CuN2Q10 is shown as an exemplar of the four 5 wt.% catalysts. The TPO analysis yielded the profile shown below in figure 3-34.

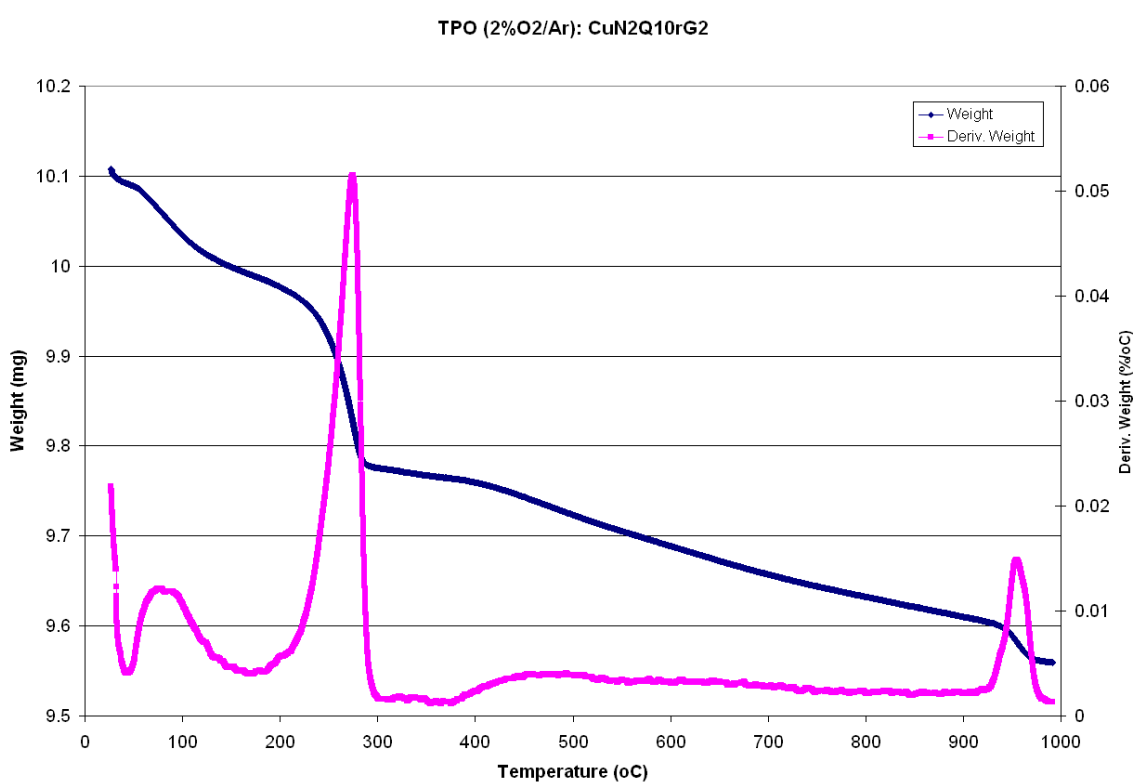


Figure 3-34: TPO profile of CuN2Q10rG2

The TPO analysis of CuN2Q10 post-reaction shows the initial peak at 100 °C in figure 3-34 with a corresponding evolution of H₂O. Additionally, a single sharp peak was observed at 278 °C. This peak has corresponding features in the MS data in figure 3-35 for the evolution of CO₂, H₂O and a MS fragment (2).

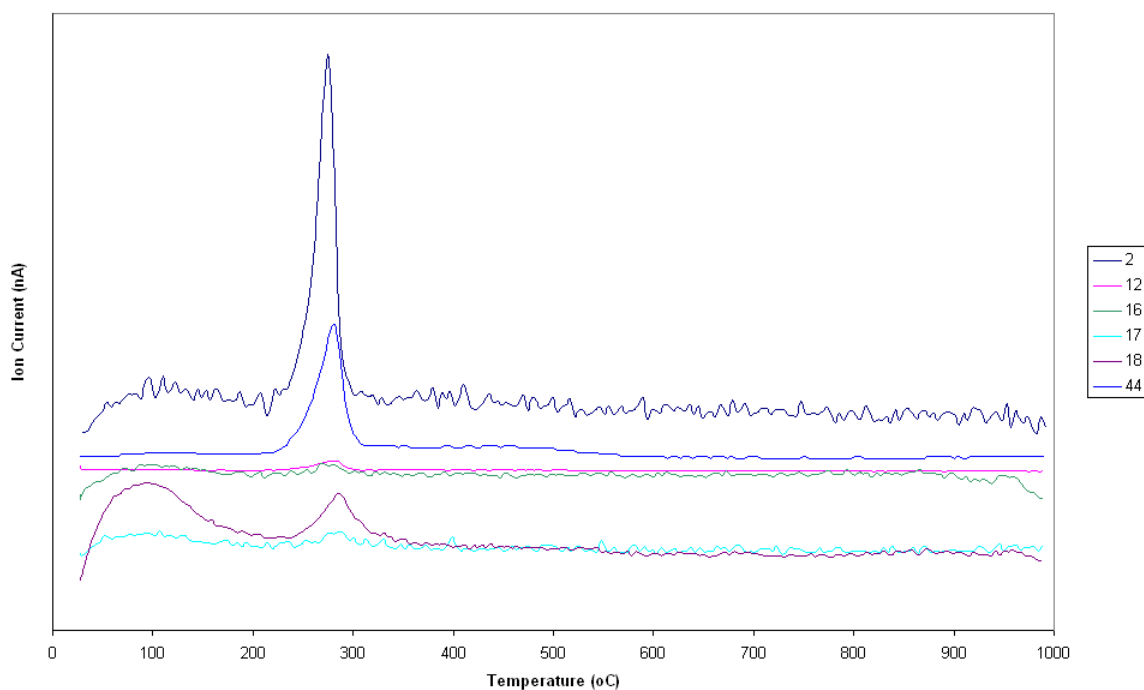


Figure 3-35: MS data of CuN2Q10rG2

The XRD pattern shown in figure 3-36 identifies the post-reaction copper species as metallic copper. This is the same XRD pattern observed for the four 5 wt.% copper catalysts analysed.

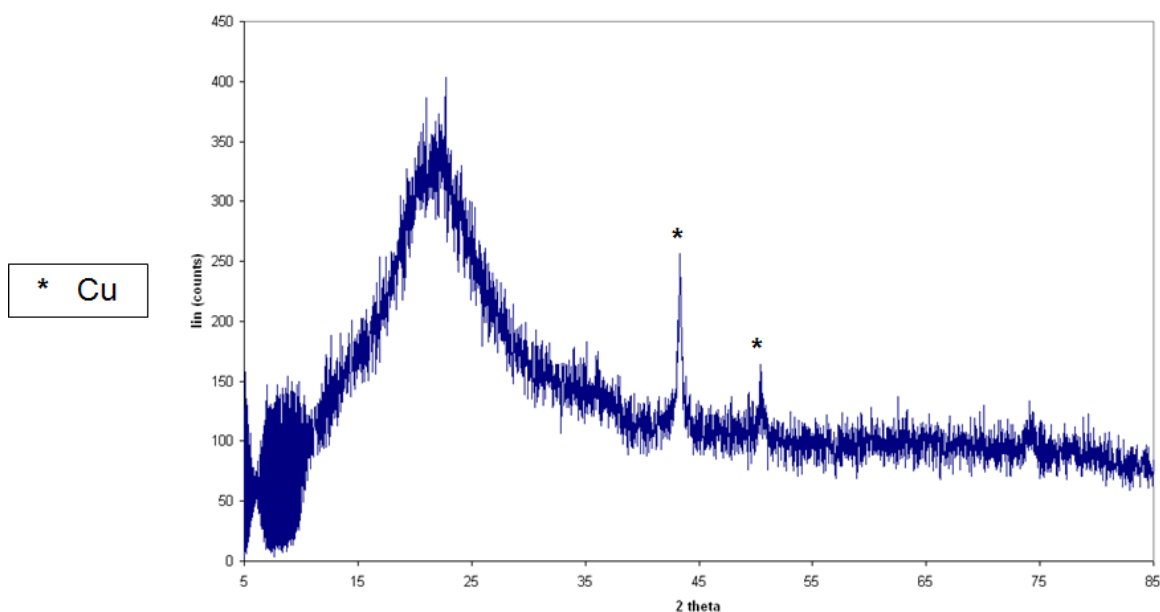


Figure 3-36: XRD pattern of CuN2Q10rG2

BET analysis was carried out on the silica Q10 support and the 5 wt.% copper catalysts post-reaction with the data presented below in table 3-14. All the

silica-based samples start with surface areas around the same values. Analysis of the silica support shows minimal change in the surface area and pore volume, whilst the silica supported copper catalysts show a decrease in the silica surface area post-reaction. This difference between the support only reaction and copper based catalysts suggests that the change in the surface area is a result of the presence of copper in the catalysts.

Table 3-14: BET data of copper catalyst, pre and post reaction

Sample	Surface Area (m ² /g)	Av. Pore Diameter (nm)	Surface Area (m ² /g)	Av. Pore Diameter (nm)
	<i>Pre-reaction</i>		<i>Post-reaction</i>	
Q10c	286	13.8	287	13.4
CuNQ10c	272	14.2	248	14.6
CuAQ10c	272	14.6	246	15.0
CuN2Q10c	271	14.9	260	14.8
CuA3Q10c	274	15.0	268	14.9

3.1.5.5 MeOHSC

TGA analysis post-reaction shown in figure 3-37 shows a significant weight gain in the profile linked to a characteristic re-oxidation of the copper content of the catalyst [1].

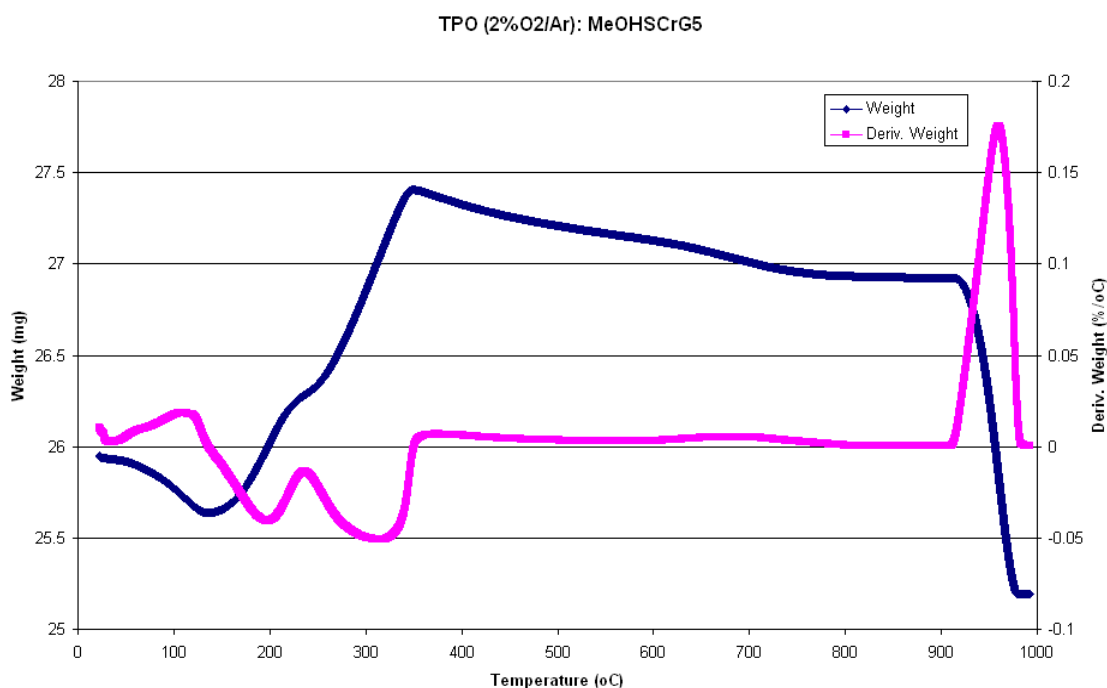


Figure 3-37: TPO profile of MeOHSCrG5

A significant weight gain is an unusual feature in TPO analysis. The explanation for this weight gain is the reoxidation of the high levels of copper present in the catalyst which are in metallic form post-reaction. The corresponding large uptake of O₂ links with copper reoxidation step.

The XRD pattern in figure 3-38 shows post-reaction characterization of the methanol synthesis catalyst. Features within the pattern are assignable to metallic copper as would be expected post-reaction, given the reducing reaction atmosphere.

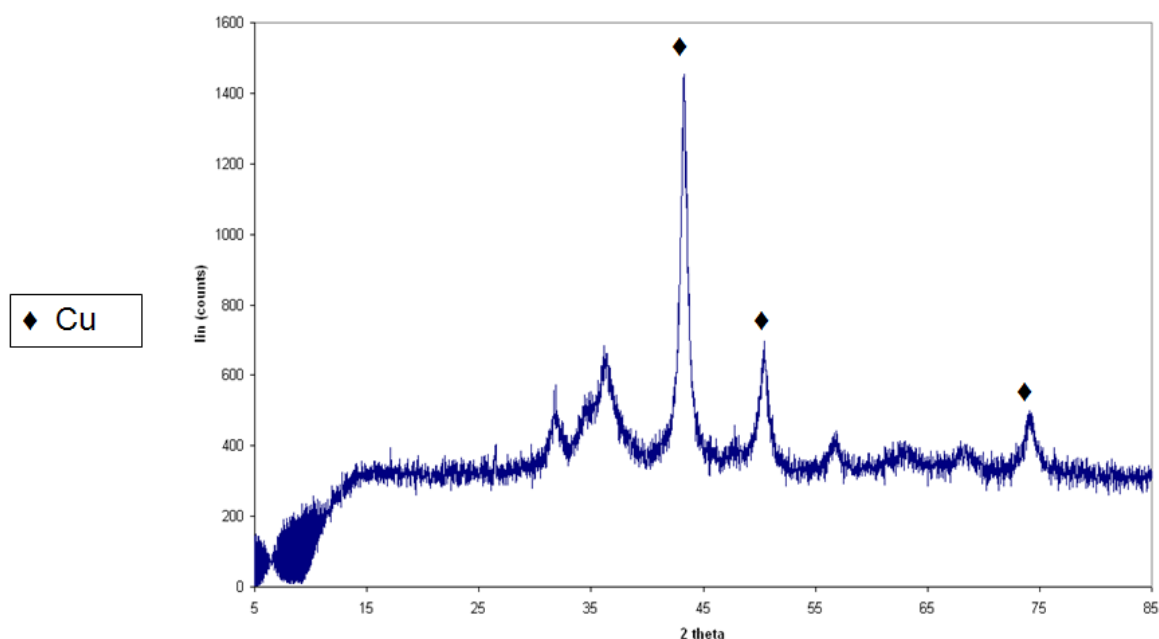


Figure 3-38: XRD pattern of MeOHSCrG5

3.1.5.6 10 wt.% copper catalyst

The 10 wt.% copper catalyst was additionally tested within the low pressure microreactor. The conversion and selectivities of this catalyst are shown in table 3-15.

Table 3-15: Conversion and selectivities of 10 wt.% copper on silica catalyst

Conversion (%)	6.0
Acetaldehyde Selectivity (%)	0
Ethanol selectivity (%)	5
Ethyl Acetate Selectivity (%)	8.3

The higher copper loading catalyst appears not to be the same ‘sink’ for acetic acid as that of the 5 wt.% copper catalysts and the silica support itself. It is, unsurprisingly, more active for the hydrogenation of acetic acid to ethanol, although the esterification to ethyl acetate is also facilitated. This similar to

the 5 wt.% copper on silica catalysts where the esterification activity can be attributed to the silica support rather than the copper species.

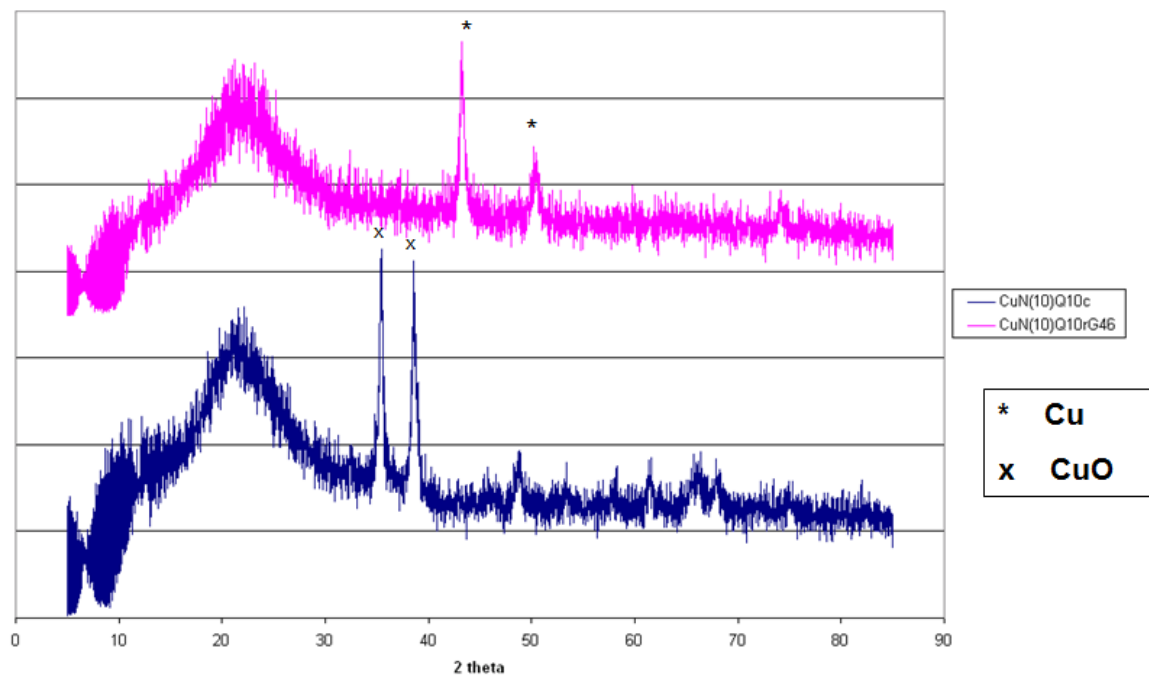


Figure 3-39: XRD pattern for 10 wt.% copper on silica catalyst

Table 3-16: BET analysis of pre- and post-reaction 10 wt.% copper catalyst

Sample	Surface Area (m ² /g)	Av. Pore Diameter (nm)	Surface Area (m ² /g)	Av. Pore Diameter (nm)
	<i>Pre-reaction</i>		<i>Post-reaction</i>	
CuN(10)Q10rG19	247	14.1	223	14.1

The largest decrease in catalyst surface area was seen for CuN(10)Q10, which contained the largest amount of copper of the impregnated copper on silica catalysts. The large amount of copper has the propensity to sinter throughout the catalyst, causing large changes to the attributes of the catalyst.

3.1.5.7 Summary

The testing completed using the low pressure microreactor encompassed 5 wt.% and 10 wt.% copper on silica catalysts and a commercial methanol synthesis

catalyst. It also included the silica support upon which the copper /silica catalysts were prepared. The higher copper content of the methanol synthesis catalyst has shown superior activity for ethanol production, and the link between copper content and activity is further proven by the increased activity of the 10 wt.% copper catalyst over that of its 5 wt.% counterparts. Despite this observed increase in activity, the 10wt% copper on silica catalyst also facilitates the secondary esterification reaction through to ethyl acetate. Optimisation of the behaviour would limit its esterification abilities, as well as increasing activity to the levels of the methanol synthesis catalyst and above. Other copper based systems that were qualified with respect to higher copper content were copper chromite systems. These are discussed below.

3.1.6 Copper Chromite catalysts

It was clear from the activities displayed by the 5 wt.% copper catalysts, and the subsequent increase in activity upon doubling of the metal loading, that there was a correlation between activity and copper content, as was previously predicted. Following this trend, another high copper content catalyst was tested, in addition to the methanol synthesis catalyst, Katalco 51-8. Copper chromite catalysts were commercially available options that fulfilled the required criteria of high copper content.

Four different copper chromite catalysts were tested. This included two sodium doped copper chromite catalysts, as mentioned in section 2.1.3.2. The best activities were seen with the undoped copper chromite catalyst (CuChr) and the pelletized copper chromite catalyst (CuCr). The conversions and selectivities of the copper chromite catalysts, compared to the other copper catalysts, are shown in table 3-17.

Table 3-17: Copper catalysts conversions and selectivities

	Catalyst	Q10	CuNQ10	CuAQ10	CuN2Q10	CuA3Q10	MeOHSC	CuChr	CuCr
Selectivities (%)	Acid to Ethanol (%)	0	0	0.4	0.9	0.2	0	6.6	10.5
	Acid to Ethyl Acetate (%)	0	1.3	0	0	0	75	0	0
	Acid to Acetaldehyde (%)	0	0	0	0	0	14.8	0	0
Conversion (%)		82.4	77.9	81.4	80.4	81.8	100	76.9	72.6

The copper chromite and methanol synthesis catalysts are the most active of the copper catalysts tested, although different product profiles are achieved dependent upon the catalyst used. The copper chromite catalyst produces ethanol as its major product, whilst the methanol synthesis further esterifies the ethanol produced to ethyl acetate.

The copper chromite catalysts displayed significant increases in activity relative to the impregnated copper catalysts. However, they were not viewed as a viable option due to issues related to use of chromium compounds within catalytic systems (CuChr and CuCr contained CuCr_2O_4), and due to the pyrophoric nature of the catalysts. Despite not continuing to test these systems further, the results from the low pressure microreactor further confirmed the correlation between copper content and activity. Post-reaction analysis of the copper chromite catalysts was not performed, as the catalysts were re-oxidised *in-situ* due to their pyrophoric nature when in the reduced form.

3.1.7 Summary

A range of copper based catalysts were investigated and confirmed the literature results [2, 18] that copper is catalytically active for the hydrogenation

of acetic acid to ethanol. The catalysts were tested in both an integral BERTY reactor and a differential low pressure fixed bed system. And different reactor designs influenced the propensity of a catalyst to facilitate the 'secondary' esterification reaction to ethyl acetate.

The most interesting result for ethanol production was observed with a standard industrial methanol synthesis catalyst, Katalco 51-8. Within the BERTY system, the methanol synthesis catalyst was active for the production of ethanol with a sustained selectivity of 34 %. When comparing this to testing in the microreactor, the selectivity of 75 % towards ethanol remained but the catalyst experienced significant deactivation over the duration of the four day reaction period.

Despite this interesting result, the pivotal issue of catalyst stability was problematic with copper sintering and pellet cracking being visible signs of the degradation of the catalyst. Other indications from the characterisation techniques such as BET confirmed that changes were seen, with severe decreases observed in the surface area of the catalyst post-reaction.

The other commercial copper catalyst investigated was in the form of copper chromite. Initial testing identified that the copper chromite catalysts did not display an activity for ethanol synthesis that superseded the drawbacks of using a highly toxic and pyrophoric catalytic system.

A range of 5 wt.% copper catalysts and a 10 wt.% copper catalyst, all supported on silica Q10 were also investigated. The activity of these impregnated catalysts remained far below that observed for the methanol synthesis catalyst; a simple linear relationship was observed between the copper metal content and the catalyst activity. This is a link that was to be expected, and one that will be expanded upon in chapter 3.4.

3.2 High Acetic Acid Concentration Reactions

A low pressure reactor system at the BP Saltend Hull Research & Technology Centre (HRTC) site was used to test a variety of copper containing catalysts. The catalysts tested were the laboratory prepared 5 wt. % and 10 wt.% copper on silica Q10 catalysts, industrial methanol synthesis catalyst Katalco 51-8 and comparative tests using the silica support Q10 and silicon carbide packing material.

As described in the experimental section, the fixed bed reactor tube was packed with silicon carbide above and below the catalyst bed (10 ml) to aid the central positioning of the catalyst within the reactor tube, all of which sat upon a quartz sinter. The zones of silicon carbide packing and catalyst were separated by plugs of glass wool. The silicon carbide was also tested to rule out any catalytic activity attributable to the packing material.

3.2.1 Reduction Conditions

Previous TPR analysis of the catalysts, described in chapter 3.1, identified the required reduction conditions for each of the catalysts in the low pressure fixed bed reactor. Similarities were visible in the TPR profiles of the copper containing catalysts, giving a set of universal reduction conditions, seen in table 3-18. These conditions took into account the temperature limitations of using a copper catalyst (maximum 300 °C) to avoid sintering of the metal. The reduction ramp rate was maintained at 10 °C min⁻¹, in line with the rate used for the TGA-DSC-MS analysis and all other catalyst testing. The silicon carbide and the silica Q10 support reactions also went through the reduction procedure to allow standardisation of the reduction and reaction method.

Table 3-18: Universal reduction conditions for all copper catalyst in the low pressure fixed bed reactor

Ramp Rate ($^{\circ}\text{C min}^{-1}$)	10.0
Temperature ($^{\circ}\text{C}$)	250
Hold (mins)	60
Reduction Gas	H_2
Flow rate (ml min^{-1})	100

3.2.2 Reactions

The 5 wt.% copper catalysts (both from the acetate and nitrate precursors), a 10 wt.% copper catalyst and the Q10 support were all tested. As a comparative reaction, the commercial methanol synthesis catalyst was also tested. Standard reaction conditions were also used for all the copper catalysts tested and are described in table 3-19.

Table 3-19: Reaction conditions for all materials tested in low pressure HRTC reactor

Temperature ($^{\circ}\text{C}$)	250
Pressure	Atmospheric
Gas Flow ($\text{ml min}^{-1} \text{H}_2$)	100
Volume of Catalyst (ml)	10
GHSV (hr^{-1})	~ 750
Feed	20 mol% Acetic Acid via syringe pump (4 ml/hr) (except for AL6 which was 10% Acetic Acid (2 ml/hr) with a maintained GHSV)

3.2.3 Liquid Samples

A single liquid sample was collected from each reaction, which was collected in a condensing coil within a water bath at 19°C . The liquid samples were analysed by GC on site at HRTC.

Table 3-20: GC analysis high level results (% m/m)

Sample	Acetaldehyde (% m/m)	Ethyl Acetate (% m/m)	Ethanol (% m/m)	Water (% m/m)	Acetic Acid (% m/m)
Acetic Acid Reference	--	--	--	0.14	Balance
SiC (AL1)	--	--	--	0.32	Balance
CuN2Q10c (AL2)	--	--	--	0.60	Balance
CuN(10)Q10c (AL3)	--	--	--	0.88	Balance
MeOHSC (AL4)	0.97	10.4	6.6	13.9	Balance
Q10c (AL5)	--	--	--	0.30	Balance
MeOHSC (AL6)	1.6	3.0	29.2	25.4	Balance
CuA3Q10c (AL7)	--	--	--	0.56	Balance

The GC analysis results in table 3-20 identify that the methanol synthesis catalyst was the only catalyst of those tested within this system that produced any products in quantities greater than ‘parts per million’ (ppm) levels. The ppm GC results in table 3-21 account for the results for the rest of the catalysts tested.

Table 3-21: GC analysis low level results (ppm m/m)

Sample	Acetaldehyde (ppm m/m)	Acetone (ppm m/m)	Ethanol (ppm m/m)	Water (ppm m/m)
Acetic Acid Reference	<10	<10	<10	<10
SiC (AL1)	<10	15	<10	<10
CuN2Q10c (AL2)	390	20	1340	645
CuN(10)Q10c (AL3)	655	20	2690	1605
MeOHSC(1) (AL4)	--	4605	--	--
Q10c (AL5)	<10	20	35	20
MeOHSC(2) (AL6)	--	2840	--	--
CuA3Q10c (AL7)	375	30	1230	620

Combining the results from tables 3-20 and 3-21 in figure 3-40 shows the distinctive difference between the methanol synthesis catalyst and the rest of the copper catalysts tested. The methanol synthesis catalyst displayed significantly greater activity for the production of the reduction products, ethanol, acetone and acetaldehyde and also for the ethanol esterification product, ethyl acetate.

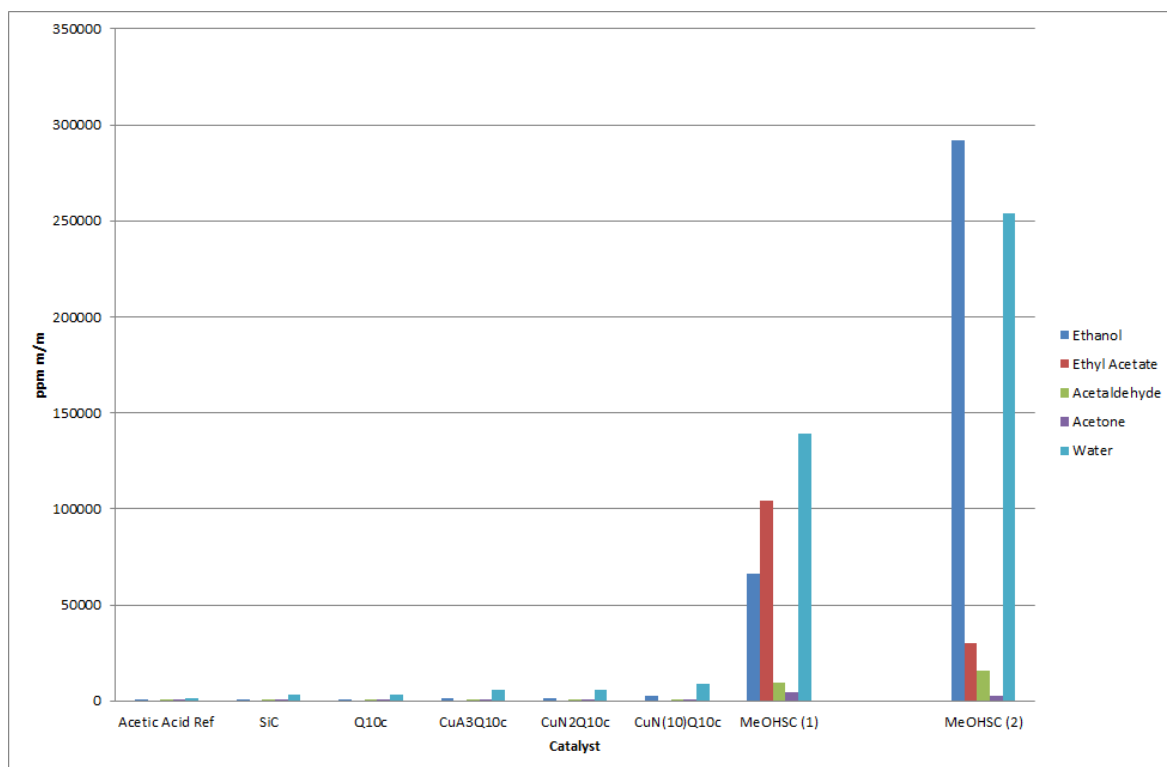


Figure 3-40: GC analysis results for all materials tested and acetic acid reference

The difference between the product values observed with the methanol synthesis catalyst and the supported copper catalysts means that the results for these two groupings are best addressed separately. The GC results for the supported metal catalysts are shown below in figure 3-41 and will be discussed first. The methanol synthesis catalysts results are shown in figure 3-42, and will be discussed later.

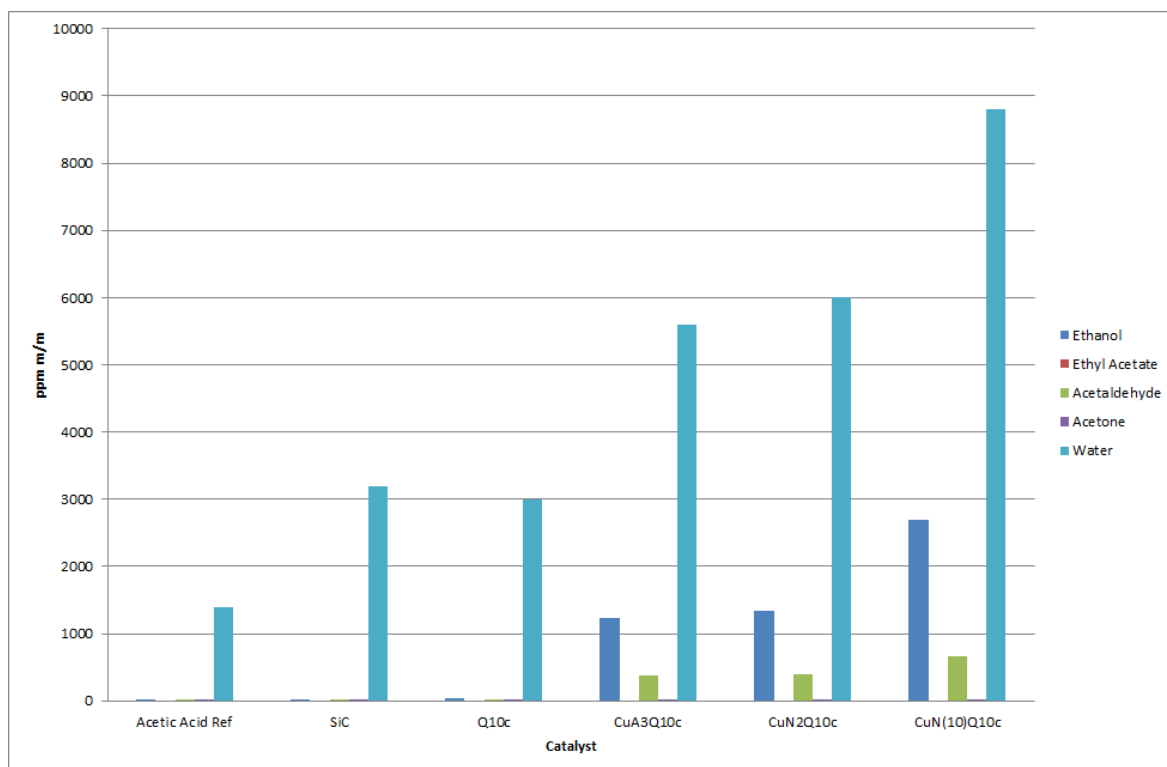


Figure 3-41: GC analysis results for supports and lab prepped copper catalysts

The analysis of an acetic acid reference sample provided a base line for the feed composition. The levels of ethanol produced during the silicon carbide and silica Q10 reactions were not above those seen in the acetic acid reference as expected, showing that no activity was observed for either of these materials.

Ethanol production was observed upon use of copper containing catalysts. The two 5 wt.% Cu catalysts (reactions AL2 & AL7) showed very similar activities and selectivities, showing no difference between the two catalysts. These similarities demonstrates that although the catalysts were prepared using two different metal salt precursors and produced different copper species post-calcination, the presence of Cu metal species post-reduction on the same silica support produces a comparable catalyst.

Most striking from these results is the doubling of the ethanol production with the doubling of the copper content between the 5 wt.% and 10 wt.% copper catalysts. This observation was not unexpected given the lack of activity due to the silica Q10 support meaning that the catalytic activities of the 5 wt.% copper catalysts were attributable entirely to the metal content. A direct linear

relationship was seen between the copper content and the amount of ethanol and acetaldehyde produced during the reaction. The water content of the liquid samples also reflects this linear relationship, although it was to be expected as it is also a product of the two reduction reactions.

There was no ethyl acetate observed within the product stream for any of the copper supported metal catalysts within this system. Although the esterification product is not desired, this confirms the difference seen between the differential and integral reactor product profiles for impregnated copper catalysts, as discussed in chapter 3.1.

Following this, the difference in the product profiles of the methanol synthesis catalyst reactions, with varying acetic acid amounts in the feed, was of particular interest. The reduction and reaction conditions of the two reactions were the same apart from the amount of acetic acid being fed into the system. For MeOHSC(2), the rate of addition of acetic acid was halved for the duration of the reaction, with the reaction time being kept the same. The product profiles for the liquids samples are seen below in figure 3-42.

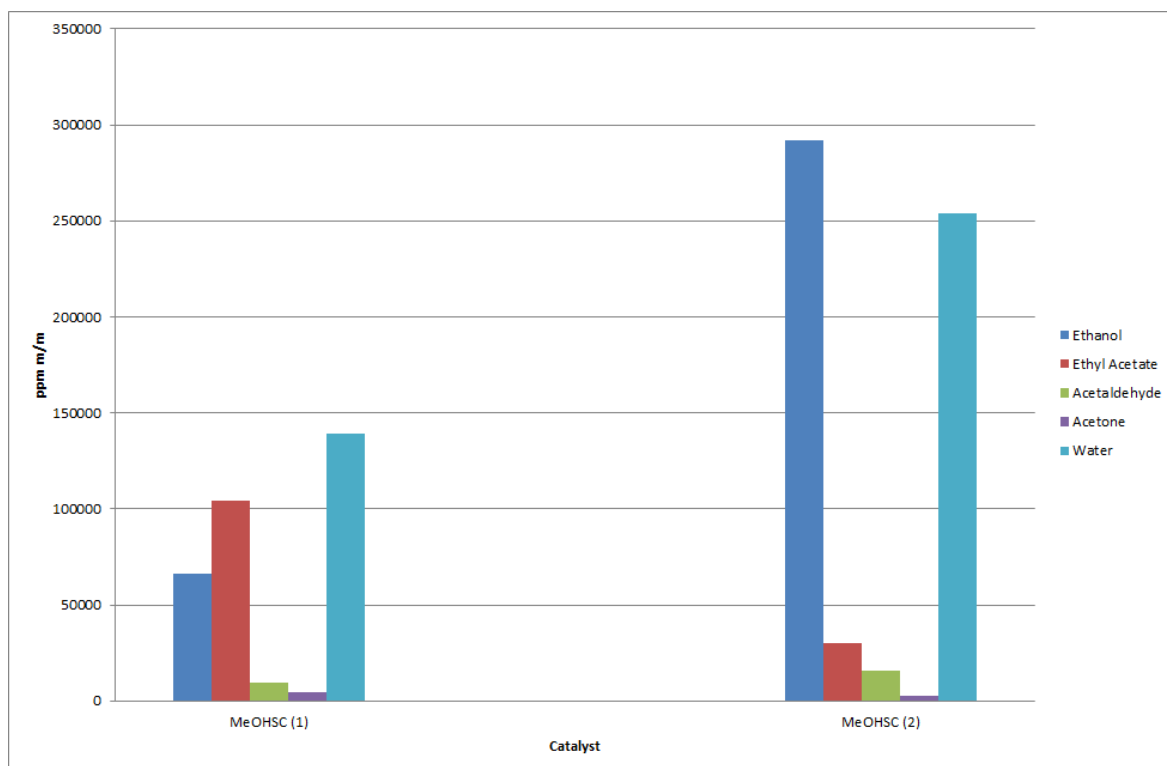


Figure 3-42: Liquid sample data for two methanol synthesis catalyst reactions

In the reaction using MeOHSC(1), a feed stream with 20 mol.% acetic acid was passed over the catalyst, whereas in the reaction using MeOHSC(2), the feed stream contained 10 mol.% acetic acid. Intuitively, an increase in the amount of feed passed over a catalyst would increase the amount of product seen. Such a simple linear relationship, however, does not take into account limitations in the activity of a catalyst due to the number of active sites available for reaction. It also assumes that the catalyst is not affected by the reactants, products or reaction itself. In fact, as seen in figure 3-42, an increase in the amount of acetic acid passed over the methanol synthesis catalyst has a detrimental effect on the amount of ethanol produced.

As ethanol is required for the esterification reaction, the amount of ethanol produced within the system can also be indicated by a combination of the amount of ethyl acetate and ethanol within the liquid sample. The combined values for ethyl acetate and ethanol are seen below in table 3-22. These combined ethyl acetate and ethanol values show a clear difference between the two methanol synthesis catalyst reactions, confirming the earlier observation of doubling in catalyst activity upon reduction, by half, of the acetic acid feed.

Table 3-22: Numerical comparison of the ethanol production values between the methanol synthesis catalyst reactions

	Ethyl Acetate (ppm) Ethanol (ppm)	Ethyl Acetate and Ethanol (ppm)	Water (ppm)
MeOHSC (1)	104,000 60,000	170,000	139,000
MeOHSC (2)	30,000 292,000	322,000	254,000

This observation indicates a change in the ability of the catalyst as a consequence of the acetic acid hydrogenation reaction. Copper sintering and pellet degradation were to be expected with the catalyst in this reaction, following observations post-reaction with the same catalyst in chapter 3-1. The expected sintering would decrease the copper surface area within the catalyst and subsequently decrease the number of metal active sites available for

reaction. This in turn would limit the catalyst's activity, and account for the reduced ethanol production.

Ethyl acetate production values for these two reactions suggests that the esterification reaction is enhanced by the increased availability of both acetic acid and ethanol in the catalyst bed with the higher acetic acid content in the feed.

3.2.4 Gas Samples

Gas sample bags collected the reaction gas effluent stream for the duration of the reaction. The gas samples collected were then analysed using GC at the HRTC site. Analysis of the gas products from the reactions was to ensure the identification of any highly volatile products that may not be seen in the liquid sampling.

The GC results for the gas samples are shown below in table 3-23. The lower quantification limit for methane, ethane and ethylene was 0.001 % v/v, whilst the limit for nitrogen, carbon monoxide, carbon dioxide, ethanol, acetaldehyde and ethyl acetate was 0.1 mol %. Acetic acid was not analysed for within the gas samples. Additional C₂, C₃, C₄ and C₅ compounds were analysed for although no quantifiable peaks were observed for any of those components.

Table 3-23: Gas sample GC results

	Methane (% v/v)	Ethane (% v/v)	Ethene (% v/v)	CO (mol %)	N ₂ (mol %)	CO ₂ (mol %)	Ethanol	Acetaldehyde	Ethyl Acetate
AL1	<0.001	<0.001	<0.001	<0.1	1.7	<0.1	<0.1	<0.1	<0.1
AL2	0.001	<0.001	<0.001	<0.1	0.8	<0.1	<0.1	<0.1	<0.1
AL3	0.033	0.003	<0.001	<0.1	1.1	<0.1	<0.1	<0.1	<0.1
AL4	0.003	<0.001	<0.001	<0.1	1.8	0.3	0.4	1.2	0.5
AL5	<0.001	<0.001	<0.001	<0.1	0.5	<0.1	<0.1	<0.1	<0.1
AL6	0.021	0.015	0.002	<0.1	19.7	<0.1	0.5	0.4	<0.1
AL7	0.002	<0.001	<0.001	<0.1	1.3	<0.1	<0.1	<0.1	<0.1

The GHSV within the reactor system during the 10 wt.% acetic acid feed reaction (AL6) was maintained using an additional supplementary nitrogen feed. The presence of this small amount of nitrogen feed within the system accounts for the elevated nitrogen values (19.7 mol %) observed for the AL6 results. The 20 mol.% acetic acid feed reactions did not use nitrogen, although there were small amounts identified in each of the gas samples. This can be explained as nitrogen was used to clean the gas sampling bags prior to use and the amounts seen may be residual from this cleaning process.

The two detected values for ethanol were both from the methanol synthesis catalyst reactions. The highest value for ethanol was 0.5 % v/v detected in AL6 (methanol synthesis reaction with a 10 mol.% acetic acid feed) and is in line with that being the highest ethanol value within the liquid samples. The gas sample values are reflective of the liquid sample with respect to ethanol, acetaldehyde and ethyl acetate.

The highest methane value was for AL3 (CuN2Q10) with a value of 0.033 % v/v. Although this is above the threshold value and was the highest observed for the methane and ethane values, the quantity observed was severely limited.

3.2.5 ICP-MS Results

ICP-MS analysis was carried out on each of the post-reaction liquid samples submitted for GC analysis as well as the acetic acid reference sample. No values above the threshold values of 25 ppb (parts per billion) were found for Ag, As, Be, Cd, Co, Cs, Ga, Mo, Pb, Rb, Se, Sr and U for any of the samples. These elements were not expected to be identified by the ICP-MS analysis as they should not be present within the catalysts, the reactor system and the reactant feed, and as such should not be present within the product stream. Table 3-24 below shows the results for the elemental analysis where values were observed above their threshold limits.

Table 3-24: ICP-MS values

	Al	Ba	Cr	Cu	Fe	Mg	Mn	Ni	V	Zn
AL1	<250	<25	<25	90	980	130	<25	50	65	1100
AL2	<250	<25	<25	170	200	85	<25	<25	<25	1700
AL3	<250	<25	<25	60	250	60	<25	100	<25	800
AL4	2500	60	35	45	1300	5700	<25	35	40	550000
AL5	<250	<25	<25	35	200	7800	<25	<25	<25	3300
AL6	280	<25	<25	160	4400	720	55	55	40	750000
AL7	<250	30	<25	190	310	4000	<25	<25	<25	10000
AA ref	<250	<25	<25	<25	<25	30	<25	<25	<25	<250

Figure 3-43 shows the data for the values above the ICP-MS methodology 25 ppb threshold. The only exceptions to this are zinc and aluminium which had a higher threshold of 250 ppb. Any results below those threshold values are indicated as zero.

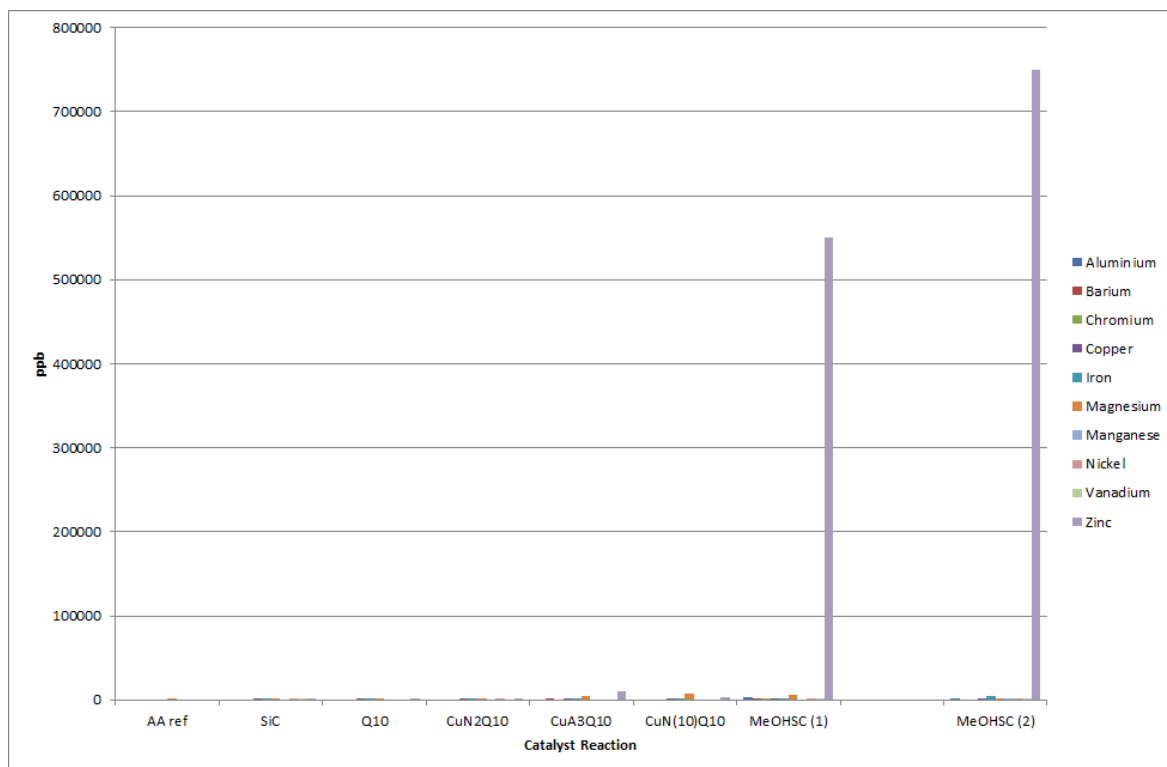


Figure 3-43: All ICP-MS data (ppb) above the standard <25 ppb threshold for all elements analysed.

In figure 3-43, the zinc ppb values for the two methanol synthesis catalyst reactions are significantly higher than the values seen for any of the other elements, and dwarf any trends that may be visible on a smaller scale. As such, the zinc values were removed and the rest of the data is presented below in figure 3-44. The zinc ICP-MS data will be addressed later when the methanol synthesis catalyst is directly discussed.

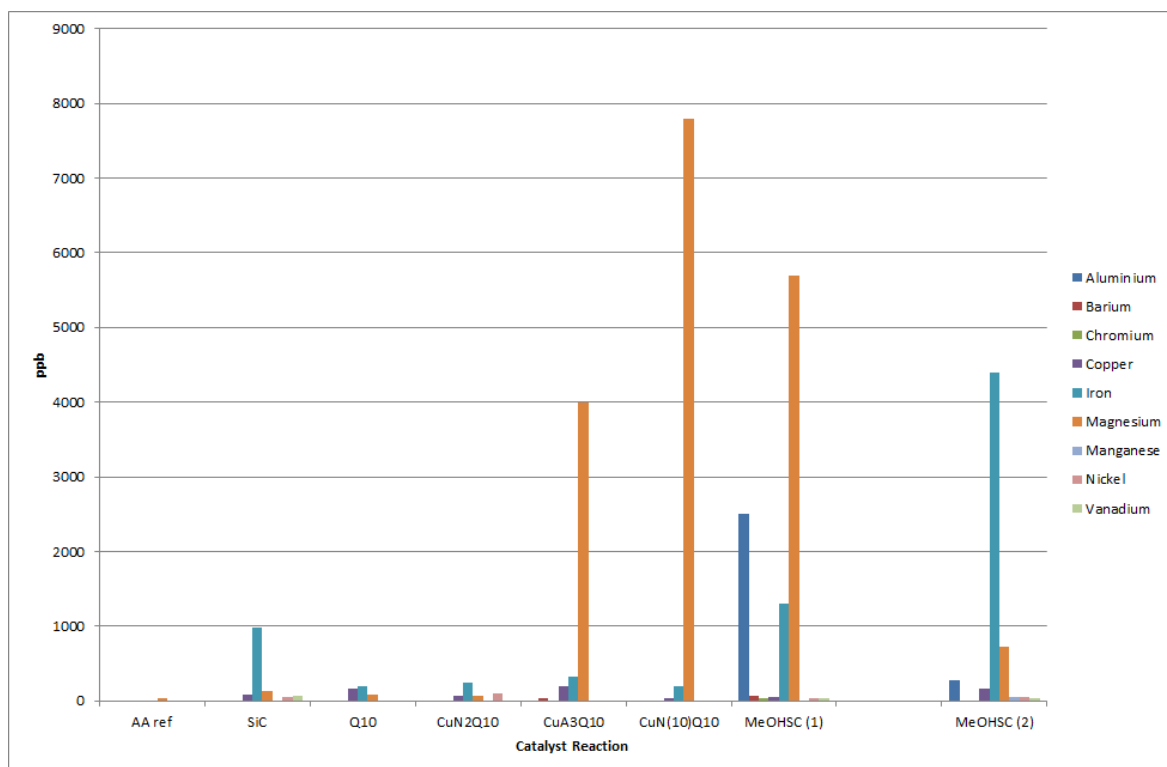


Figure 3-44: ICP-MS data (ppb)(zinc removed)

ICP-MS analysis of the acetic acid reference liquid sample clearly demonstrates that the liquid feed of acetic acid is not the source of many of the elemental components detected. Its only quantified elemental contribution was magnesium with a value of 30 ppb, just above the 25 ppb threshold. The analysis of the liquid samples from the reactions over the silicon carbide packing material and silica support, Q10, helped determine if there was a significant elemental contribution from the packing material or catalyst support. The values for the silica Q10 reaction are low across the board with no obvious spikes. From the results gained, the SiC reaction shows a relatively high value of Fe not seen in the Q10 reaction. This suggests that there is iron extraction occurring from the silicon carbide when it is the only material in the reactor. This shows that the sources of the major elemental contributions in the liquid samples are the catalysts themselves and not the reactor or associated glassware.

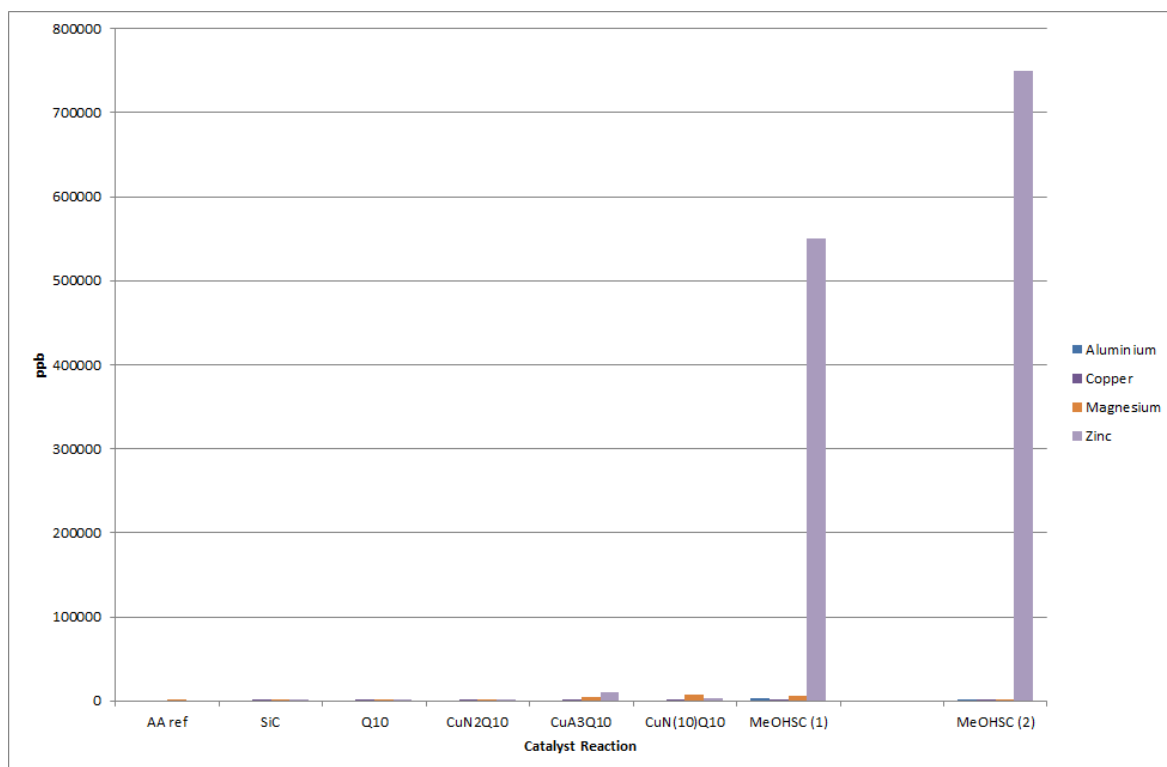


Figure 3-45: ICP-MS data for expected elemental contributions from the catalysts

Figure 3-45 focuses on the four elemental contributions that were expected in the methanol synthesis catalyst reactions, due to the catalyst composition. Referring back to the catalyst composition as described in section 2.1.4.1, we know that the methanol synthesis catalyst is mainly copper oxide on an alumina support and zinc oxide framework with a magnesium oxide stabiliser. Each of those components can be seen in figure 3-44 in the methanol synthesis catalyst reaction liquid samples. The zinc ICP-MS values were removed in figure 3-45 for an easier comparison between the aluminium, copper and magnesium values.

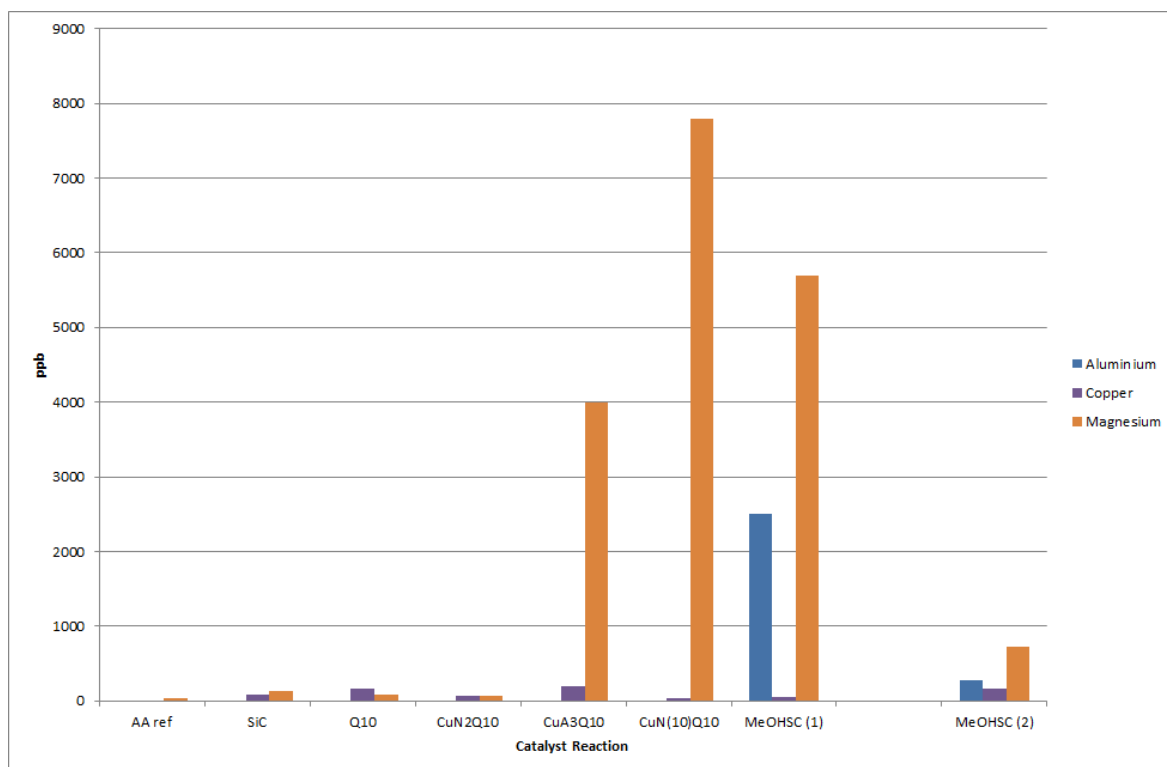


Figure 3-46: ICP-MS for Al, Cu and Mg contributions

The three elements that are being analysed here are those that were expected from the methanol synthesis catalyst reactions given the catalyst's composition.

The presence of aluminium on the methanol synthesis catalysts shows extraction of the alumina support from the catalyst as well as the other components.

The high value for magnesium in the MeOHSC (1) (AL4) reaction was expected as the reaction used a 20 mol.% acetic acid feed which was also seen to extract zinc from the catalyst framework. A lower magnesium value was observed for the MeOHSC(2) (AL6) reaction which used a decreased acetic acid feed of 10 mol.%. The presence of magnesium and the amounts observed link to the amount of acetic acid used and the catalyst composition. The unexpected magnesium results appear in the CuA3Q10 and CuN(10)Q10 reactions where the results are high and the presence of magnesium is unexpected. An explanation for the magnesium contents in the CuN(10)Q10 and CuA3Q10 reactions is that they are in fact residues within the system from the previous methanol synthesis reactions. The reactions were not carried out in the order that they were described in the above graphs, but the CuA3Q10 and CuN(10)Q10 catalysts were both tested after the methanol synthesis catalyst. Removal of the Mg ICP-

MS values leaves comparison between the aluminium and copper values below in the figure 3-47.

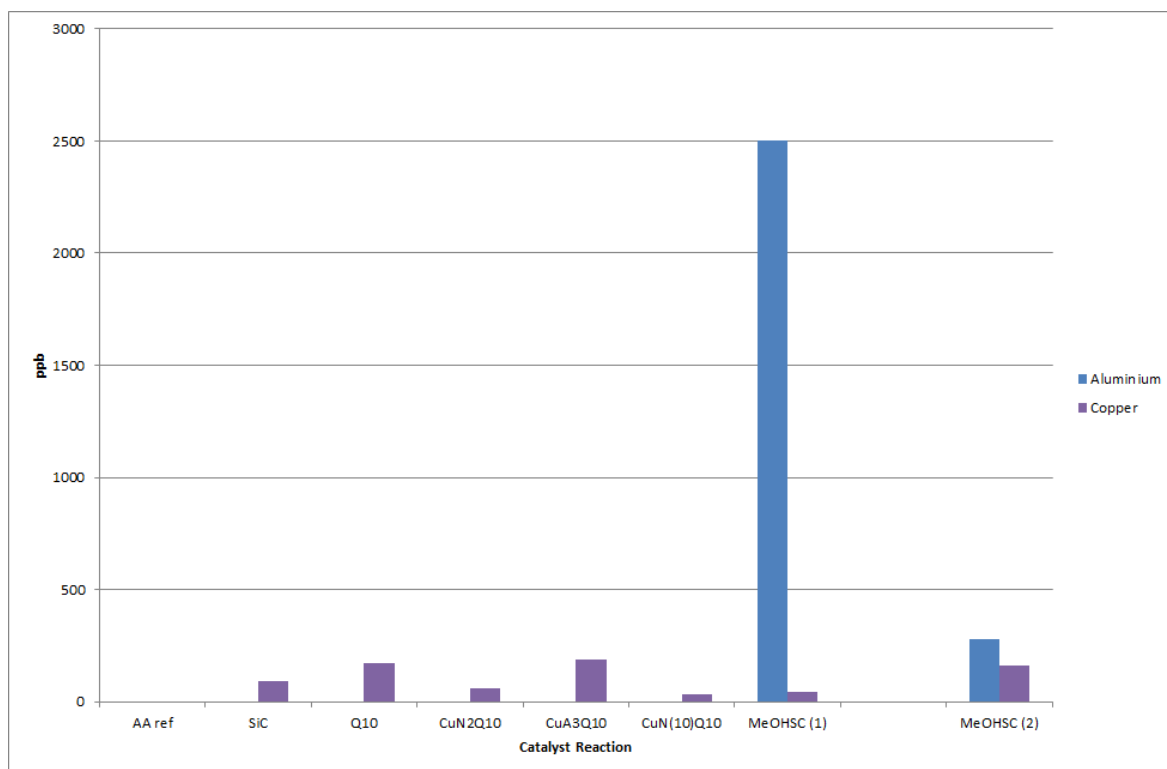


Figure 3-47: ICP-MS data for aluminium and copper

No elemental analysis for silicon removed the possibility of determining if the dissolution of the support material is occurring. Visual inspection of the silica spheres used in the Q10 only reaction (AL2) did not show any discernible degradation of the support surface or the sphere as a whole.

3.2.6 Post reaction characterisation: MeOHSC

The two reactions completed using the methanol synthesis catalyst, showed a decrease in the activity of the catalyst with a higher acetic acid feed. One explanation for this decrease in activity was changes to the methanol synthesis catalyst were more severe with a higher acetic acid feed due to the corrosive nature of acetic acid. Sintering of the copper content and degradation of the methanol synthesis catalyst pellets was expected as it had previously been seen after testing on the low pressure microreactor and BERTY systems.

Post-reaction there were various visible changes to the methanol synthesis pellets. The production of a white crystalline product on the exterior of the catalyst pellets and some degradation of the pellets themselves was observed. This had been seen to a much lesser extent with the methanol synthesis catalyst in the BERTY reactor, although there only a 1.5 mol.% acid feed was used and much greater degradation of the pellets was observed but was attributed to the reactor design. In addition, within the HRTC glass tube reactor, the formation of a white crystalline product was seen at the temperature junction at the base of the reactor tube. This white crystalline product, seen in figure 3-48, was only visible post-reaction once the reactor system had cooled and that part of the reactor was accessible.



Figure 3-48: Photograph of cooled inverted HRTC glass reactor tube (40 mm diameter, 1 m length quartz tube)

White crystalline product deposition was also observed for the methanol synthesis catalyst reaction repeated at a lower acetic acid feed of 10 mol.%, although the quantity deposited was less. It was postulated that the crystalline product was zinc acetate produced from the reaction of acetic acid and the zinc oxide stabiliser within the methanol synthesis catalyst.

As previously stated, the white crystalline substance was thought to be zinc acetate which is described as a monoclinic and colourless compound that is soluble in cold water and decomposes at 200 °C [46]. The visual indicators of the deposited substance agree with the description given for zinc acetate. The literature describes the route for the production of zinc acetate dihydrate, also known as E650, as the reaction of acetic acid on zinc carbonate or zinc metal

[49] This supports our hypothesis that it was zinc acetate produced from the reaction of the acetic acid with the zinc oxide stabiliser within the methanol synthesis catalyst. The hydrated form is zinc acetate dihydrate ($\text{Zn}(\text{C}_2\text{H}_3\text{O}_2)_2 \cdot 2\text{H}_2\text{O}$) and could also be a possibility for the product as it is also colourless and monoclinic [46] with a melting point of 237 °C. Presence of the hydrated species would be expected, at least to some extent given the presence of water within the system. Various identification techniques were carried out to ascertain the composition of the crystalline deposits.

Initially melting point analysis was employed. The sample from the reactor tube had a melting point range of 243-249 °C. The zinc acetate dihydrate reference had a melting point of 237 °C. This was a value from literature [46] and was confirmed with analysis of a reference sample on the same melting point kit apparatus. This variation reference compound could be attributed to impurities within the crystalline substance. As the reaction with acetic acid extracts the zinc oxide from the catalyst framework, other components of the catalyst composition may also be extracted. Previous ICP-MS data shows significant extraction of magnesium from the methanol synthesis catalysts, which may account for impurities in the postulated hydrated zinc acetate deposits.

Further attempts to confirm the chemical composition of the crystalline residue included elemental analysis for carbon, nitrogen and oxygen content. The CHN data (C: 22.29 %, H: 4.28 %, N: nil) for the crystalline residue produces a C: H ratio of 1: 2.3. A comparison of the crystalline residue data to the calculated empirical values for both zinc acetate and zinc acetate dihydrate shows that the CHN composition and C: H ratio is similar to that of the hydrated zinc acetate compound. The calculated values for the carbon and hydrogen ratio for $\text{Zn}(\text{CH}_3\text{COO})_2$ is a C: H ratio of 1: 1.5. with calculated empirical percentages of C: 26.19 %, H: 3.30 % and N: nil. Falling closer to the observed values, zinc acetate dihydrate has a calculated C: H ratio of 1: 2.5 and calculated empirical percentages of C: 21.89 %, H: 4.59 % and N: nil. The similarity in the composition proportions indicates that the compound could be zinc acetate dihydrate, as suspected.

XRD analysis of the crystalline residue was not appropriate on the powder X-Ray diffractometer used for the analysis of the bulk catalyst samples. Alternatively,

the Xpert Diffractometer was used in capillary configuration to elucidate a sharper and clearer XRD pattern, seen in figure 3-49.

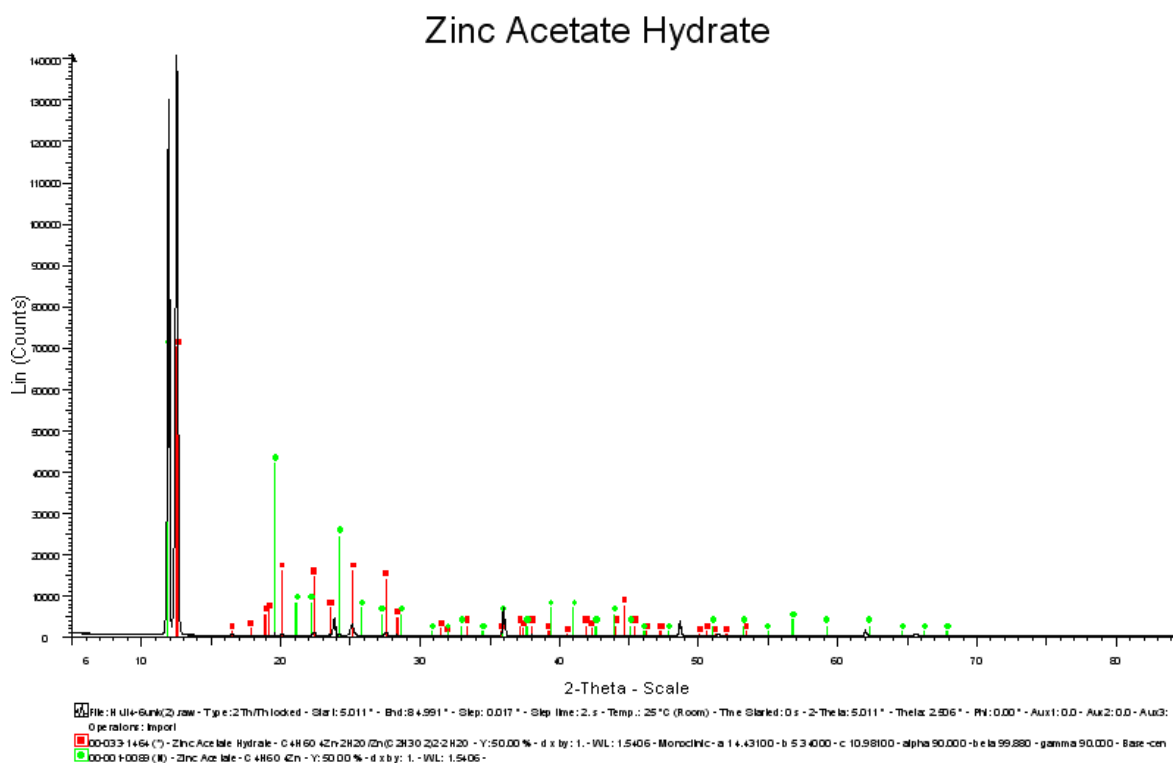


Figure 3-49: XRD pattern of zinc acetate hydrate sample

The XRD analysis was completed but clear identification remained elusive. Further analysis by NMR was completed using a 400 MHz spectrometer in DMSO. The results were as follows; ^1H NMR (δH) = 1.81 (3H, CH_3). Solvent peaks; DMSO = 2.50 ppm, H_2O = 3.46 ppm. ^{13}C NMR (δC) = 198.8 (C=O), 22.43 (CH_3). Solvent peak; DMSO = 39.58 ppm. The NMR spectra confirmed the presence of acetate groups within the sample and also showed that there were no other organic impurities present.

Following analysis of the crystalline product by XRD, microanalysis and NMR, its identification was still postulated as zinc acetate dihydrate although no conclusive characterisation data was collated.

3.2.7 Post-reaction characterisation

Analysis of the catalyst samples post-reaction was completed to indicate any changes in the catalysts as a result of the catalyst testing.

Table 3-25: BET data for post reaction samples from HRTC

Sample	BET Surface Area (m ² /g)	Average Pore Diameter (nm)
SiC (AL1)	n/a	n/a
CuN2Q10c (AL2)	257	15.4
CuN(10)Q10c (AL3)	265	13.4
MeOHSC (AL4)	24	14.5
Q10c (AL5)	299	14.2
MeOHSC (AL6)	49	23.8
CuA3Q10c (AL7)	258	15.3

BET data in table 3-25 shows that surface area and pore diameter values for the silica based catalysts remained similar pre and post-reaction. However, the methanol synthesis catalyst support did not maintain its structural integrity which is clear when comparing the post-reaction BET data to that of the pre-reaction methanol synthesis catalyst. Pre-reaction, the catalyst had a surface area of 86 m²/g and an average pore diameter of 11.7 nm. Post-reaction, the surface area values were halved for the 10 mol.% acid feed reaction and were a quarter of the pre-reaction value for the 20 mol.% acid reaction. It is clear that there was a significant impact on the structural and dispersion properties of the catalyst after reaction with acetic acid.

XRD analysis was completed with each of the catalyst samples post reaction. As expected, there was no change in the amorphous silica peak seen for silica Q10 or the corborundum spectrum attributable to silicon carbide reaction. Figure 3-50, below, shows a typical impregnated copper catalyst spectrum post-reaction where peaks assignable to copper metal are clearly visible against the wide amorphous silica peak background.

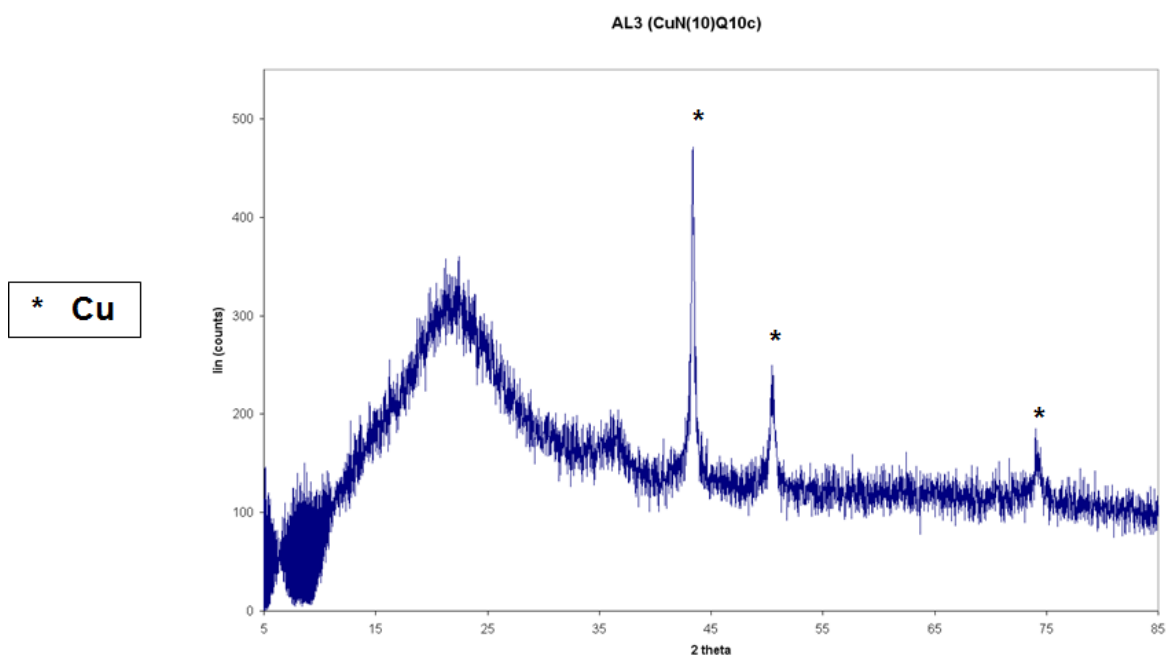


Figure 3-50: XRD pattern of post-reaction CuN(10)Q10

The spectrums for the two methanol synthesis catalyst samples post-reactions display clear and defined peaks attributable to copper metal and zinc oxide.

Figure 3-51, below, shows the XRD pattern for reaction AL4.

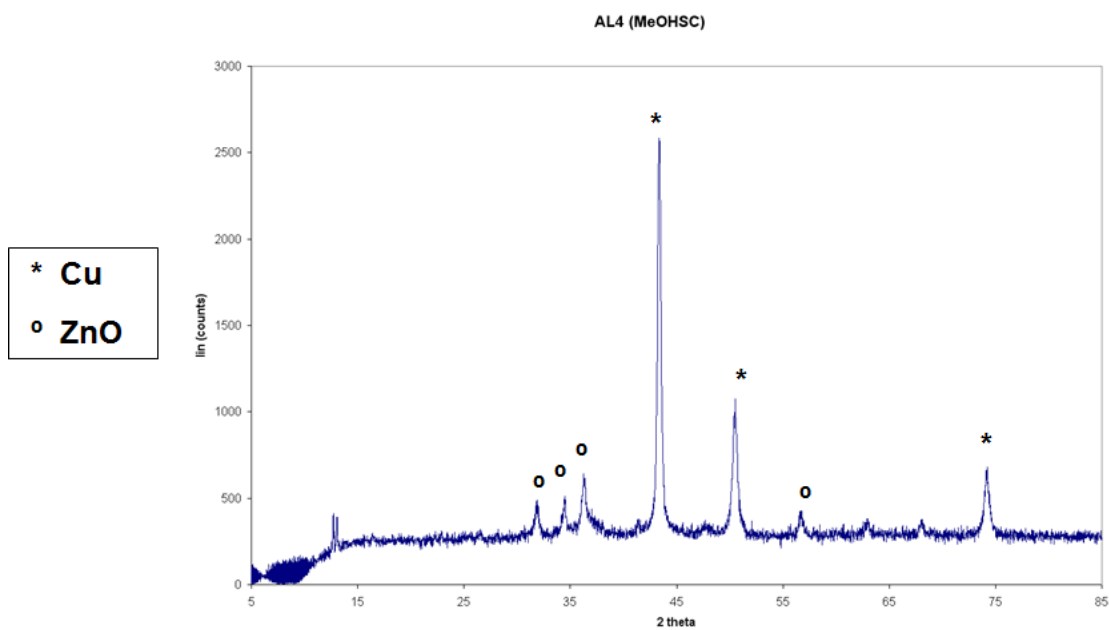


Figure 3-51: XRD pattern of post-reaction methanol synthesis catalyst

The copper particle sizes post-reaction, calculated using the Scherrer equation using the Cu peak at 43.3° , range from 21 to 30 nm in size across the copper catalysts investigated. The particle size calculations pre and post reaction may be used to give an indication of the level of sintering of the copper metal particles during the reactions. Increases in the copper particle size will also have an effect on the stability of the catalyst. Sintering, either by thermal or in this case more likely by chemical means, will have a distinctive impact upon the support's structure and integrity. Degradation of the support structure with the large scale migration and coalescence of copper particles to the catalyst surface is not the result of the acid on the silica but by virtue of the metal's behaviour.

3.2.8 Conclusions

Copper catalysts were seen to be unsuitable for the hydrogenation of acetic acid. The impregnated copper catalysts displayed low conversions at low metal loadings where additionally, the copper active phase was leached from the catalyst support as well as well as sintering of the copper content, through both chemical and thermal routes. Despite the low activity, the two 5 wt.% Cu catalysts (from two different precursors) gave similar results whilst the 10 wt.% Cu catalyst doubled the 5 wt.% Cu catalyst activity, displaying a linearity between the activity of a impregnated copper catalyst and its metal loading.

The methanol synthesis catalyst outperformed the laboratory prepared catalysts in terms of activity and selectivity, as it was the only catalyst to produce high levels of ethanol and any other products. Ethanol was not the only product, with acetaldehyde and ethyl acetate also being produced. It is clearly visible from the ethyl acetate quantities that the activity of the catalyst is affected by the amount of acetic acid being passed over the catalyst (20 mol.% vs. 10 mol.%). Despite its higher activity, the methanol synthesis catalyst was severely affected by the presence of acetic acid with copper particle sintering, zinc oxide extraction and pellet degradation all visible post-reaction.

The effects of the higher levels of acetic acid used within this reactor system were visible on the post-reaction catalysts, which displayed a significant level of degradation. The methanol synthesis catalyst had some of its zinc oxide and magnesium oxide content extracted from the catalyst framework, depositing a

white crystalline substance, suspected to be hydrated zinc acetate, at the base of the reactor. The sintering of the copper particles into visible particles on the catalyst surface was especially prominent on the CuN(10)Q10rAL3 catalyst sample.

The copper catalysts were seen to be unsuitable because of three distinctive areas that were hoped to be improved upon;

- (i) Low conversion at low metal loading
- (ii) Leaching of copper from the catalyst
- (iii) Sintering of copper on the catalyst surface

In order to address issues (ii) and (iii), an another active phase may be used i.e an alternative base metal loading or use an alternative loading such as bimetallic catalysts. A potential answer to this is to increase the metal loading. For a change to higher metal loadings and for bimetallic catalyst preparation, a change in the preparation method was necessary. For (iii), acetic acid degradation of the catalyst support therefore change the support, i.e. $\text{Al}_2\text{O}_3/\text{SiO}_2$, ZrO_2 , TiO_2 .

3.3 Alternative Base Metal Catalysts

Given the observed propensity of copper based catalysts in chapters 3.1 and 3.2 to undergo significant sintering in the presence of acetic acid, especially at temperature, the scope of experimentation was expanded to include the preparation and testing of nickel and cobalt based catalysts. The aim was to investigate alternative active phases for the acetic acid hydrogenation reaction.

Initially, nickel and cobalt catalysts were prepared using the same impregnation technique used for the 5 and 10 wt.% copper catalysts. For the nickel and cobalt alternatives, however, only catalysts with a 10 wt.% metal loading were prepared and tested.

3.3.1 10 wt.% Nickel catalyst

Nickel catalysts are often used in steam reforming [50-52] and have been also been used as hydrogenation catalysts [53], although their limited selectivity means that fully hydrogenated alkane product is often achieved.

Characterisation of the nickel and cobalt catalysts was completed in the same pattern as the impregnated copper catalysts. The initial TGA was to determine the temperature required for catalyst calcination. This was followed by TPR analysis to determine the temperature required for reduction. XRD analysis was also completed at the uncalcined and calcined stages to ascertain the metal species present within the catalyst at that particular stage of life.

TPR analysis showed the temperature at which the nickel oxide was reduced to nickel.

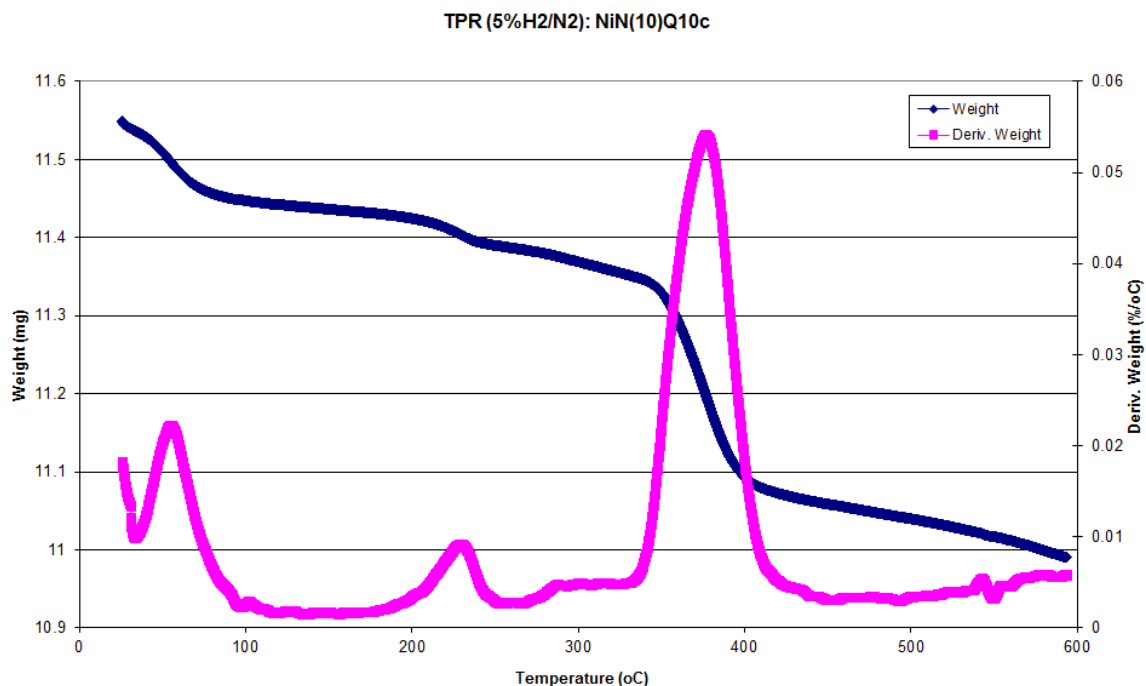


Figure 3-52: TPR analysis of 10 wt.% nickel on silica catalyst

The large event at 373 °C in figure 3-52 was identified as the reduction step for nickel oxide to metallic nickel on the catalyst. Mass spectrometer results show that the species evolved at 62 °C corresponded to water. Therefore, the reduction temperature used for this catalyst was 375 °C.

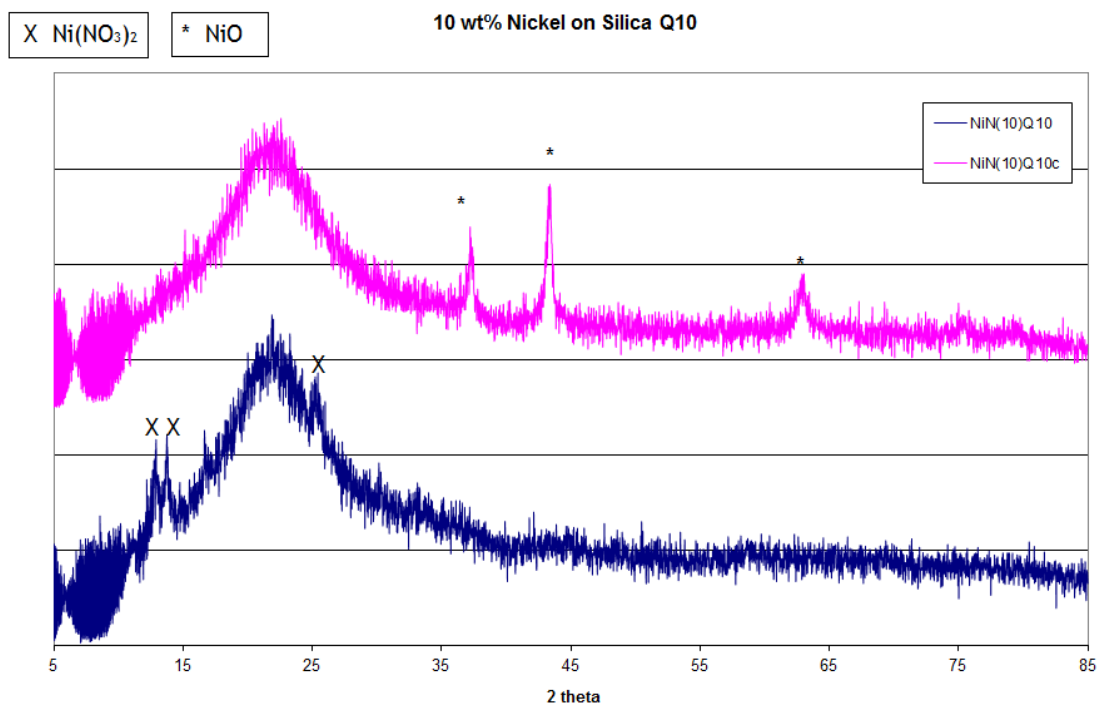


Figure 3-53: XRD patterns of 10 wt.% nickel on silica catalysts

The XRD data in figure 3-53, shows several features for the uncalcined and calcined samples. The uncalcined nickel catalyst displays features corresponding to the nickel nitrate species used in the impregnation technique. Calcination of the catalyst removes these features and new peaks relating to the nickel oxide species become visible.

3.3.2 10 wt.% Cobalt catalyst

The third catalyst with a 10 wt.% metal loading contained cobalt, prepared via impregnation using the metal acetate salt on a silica Q10 support. Cobalt based catalysts are documented as active hydrogenation catalysts for acetic acid [2, 18], although they are used significantly in the Fischer-Tropsch synthesis sector.

TPR analysis of the catalysts was used to determine that for the reduction of cobalt oxide to metallic cobalt, a reduction temperature of 350 °C was required.

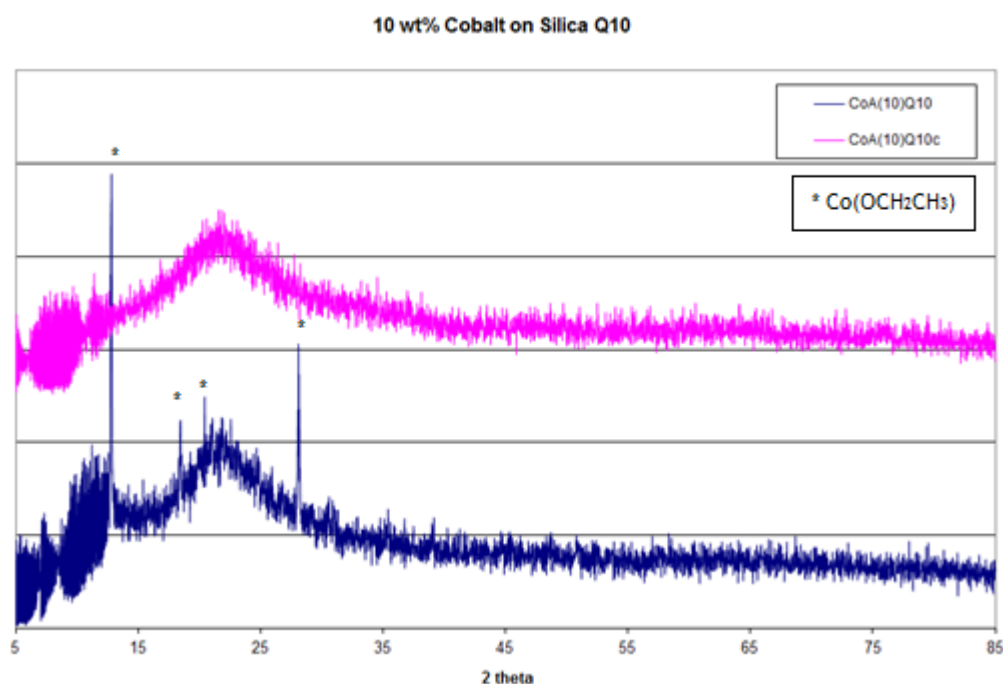


Figure 3-54: XRD analysis of uncalcined and calcined 10 wt.% cobalt on silica catalyst

The XRD patterns in figure 3-54 of the uncalcined 10 wt.% cobalt catalyst has features corresponding to cobalt acetate, as would be expected given its use in the catalyst preparation technique. Calcination of the cobalt catalyst removed the features attributable to cobalt acetate. The resulting catalyst XRD pattern post-calcination showed only one feature; a broad band attributed to the

amorphous silica support. The lack of features assignable to cobalt species suggests that the cobalt oxide was amorphous in nature.

3.3.3 Comparing 10 wt.% catalysts

The three 10 wt.% metal catalysts were tested using the low pressure microreactor. The rates of ethanol production for each catalyst are shown in figure 3-55.

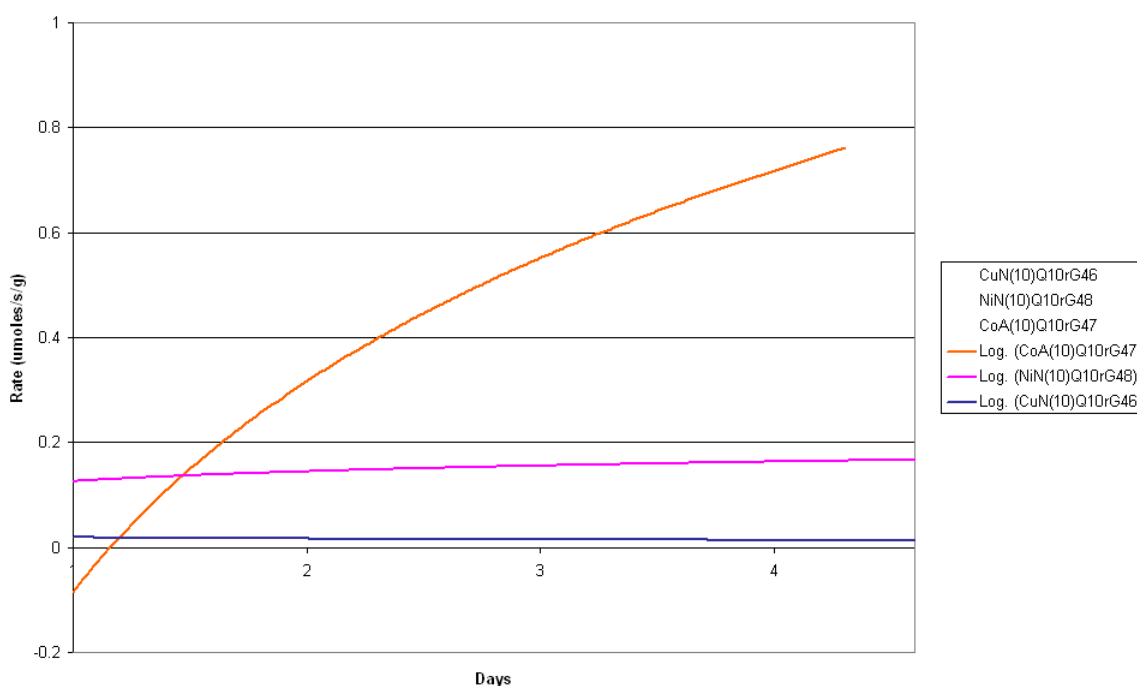


Figure 3-55: Rates of ethanol production for 10 wt.% catalysts

The rates observed for ethanol production vary significantly between the three metal catalysts being investigated. In order to understand fully the activity profile of each catalyst, the selectivities of each catalyst for other products such as acetaldehyde and ethyl acetate also need to be taken into account. These are shown in table 3-26.

Table 3-26: Reaction data for 10 wt.% catalysts

	Catalyst	CuN(10)Q10c	NiN(10)Q10c	CoA(10)Q10c	
	Reaction Day	(4 Day Average)	(4 Day Average)	1	4
Selectivities (%)	Ethanol	5	15	57.2	86.5
	Ethyl Acetate	2.5	0	22.2	8.0
	Acetaldehyde	0	0	0	0
Conversion (%)		6	14	1.8	8.9

The copper catalyst, a previously discussed catalyst, displays the lowest rate of ethanol production of the three catalysts with a value of $\sim 0.03 \mu\text{moles/s/g}$. Additionally, the copper catalyst was active for the esterification of ethanol and acetic acid through to ethyl acetate. Even accounting for the amount of ethanol esterified to ethyl acetate, the copper catalyst activity for hydrogenation of acetic acid to ethanol is still lower than the values observed for the alternative nickel and cobalt catalysts.

The nickel catalyst was seen to be more active for ethanol production than the 10 wt.% copper catalyst, and was not active for esterification through to the ethyl acetate product. Conversion of acetic acid through to methane/ethane was suspected, but these products were not identifiable via the GC method and were not quantified by the mass spectrometry analysis.

The copper and nickel catalysts, despite having limited activity for the ethanol production reaction, did produce rates that remained relatively steady throughout the four day reaction period. The 10 wt.% cobalt catalyst appears to continue to activate during the course of the reaction, increasing from a zero rate to a value of $0.8 \mu\text{moles/s/g}$ by the end of day four. This far exceeds the rate observed for the nickel and copper catalysts. The data in table 3-26

reflects an increase over time in the amount of ethanol and ethyl acetate produced. The cobalt catalyst, therefore, was observed as the most active catalyst for ethanol production of the prepared catalysts discussed thus far. The increasing yield pattern seen with the 10 wt.% cobalt on silica suggests that the catalyst becomes more active as the reaction progresses. One explanation for this could be an initial incomplete reduction of the cobalt oxide to cobalt metal during the reduction stage, and instead the catalyst continues to reduce during the reaction under the hydrogen atmosphere. Alternatively, the activity could also be increasing with an increase in the cobalt particle size during the course of the reaction.

Identification of the metal species in the nickel and cobalt catalysts post-reaction was completed using XRD analysis. The patterns for both catalysts are shown in figures 3-56 and 3-57.

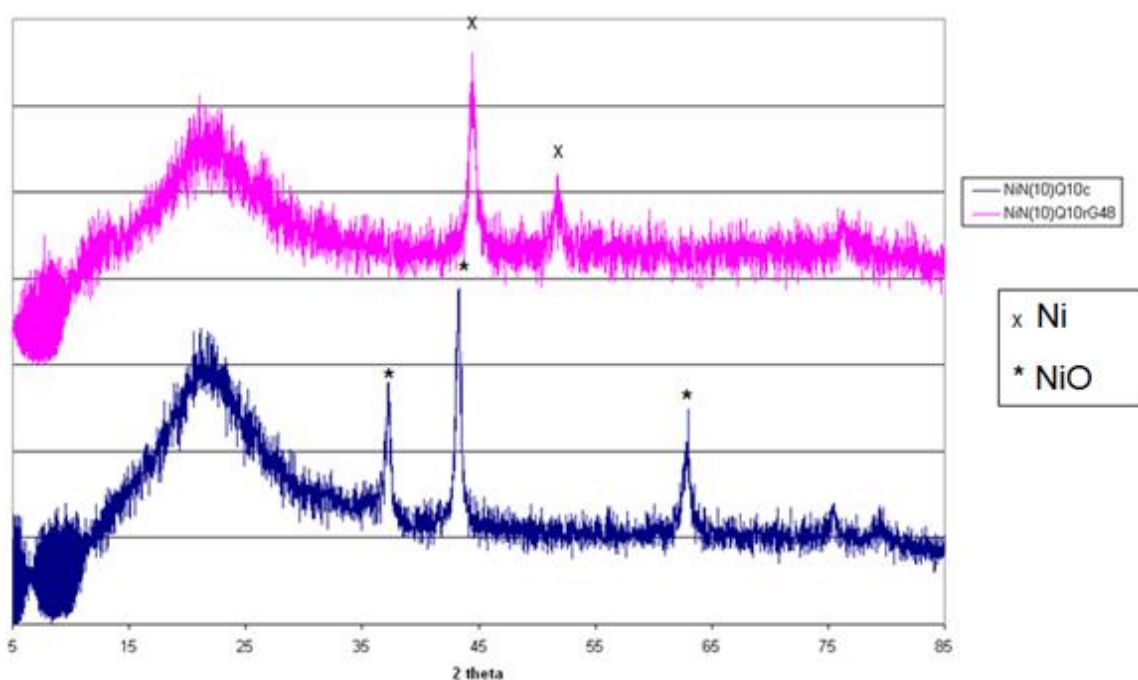


Figure 3-56: XRD patterns for pre and post reaction 10 wt.% nickel on silica catalyst

The XRD patterns in figure 3-56 show the calcined and post-reaction samples of the 10 wt.% nickel on silica catalyst. Features in the XRD pattern of the calcined sample indicate the presence of NiO. Post reaction, the NiO features had disappeared and had been replaced with peaks relating to Ni metal. The disappearance of all peaks relating to nickel oxide shows that the catalyst was

fully reduced during the reaction. This reduction to the active metallic phase was as expected, and mirrors the reduction pattern seen with the copper catalysts.

A similar trend was observed with the cobalt species in the XRD patterns, calcined and post-reaction, for the 10 wt.% cobalt on silica catalyst in figure 3-57. However, the pre-reaction or calcined sample XRD pattern was featureless, with the exception of the broad peak attributed to the amorphous silica support. The lack of features on the calcined cobalt catalyst XRD pattern does not allow for identification of the cobalt species.

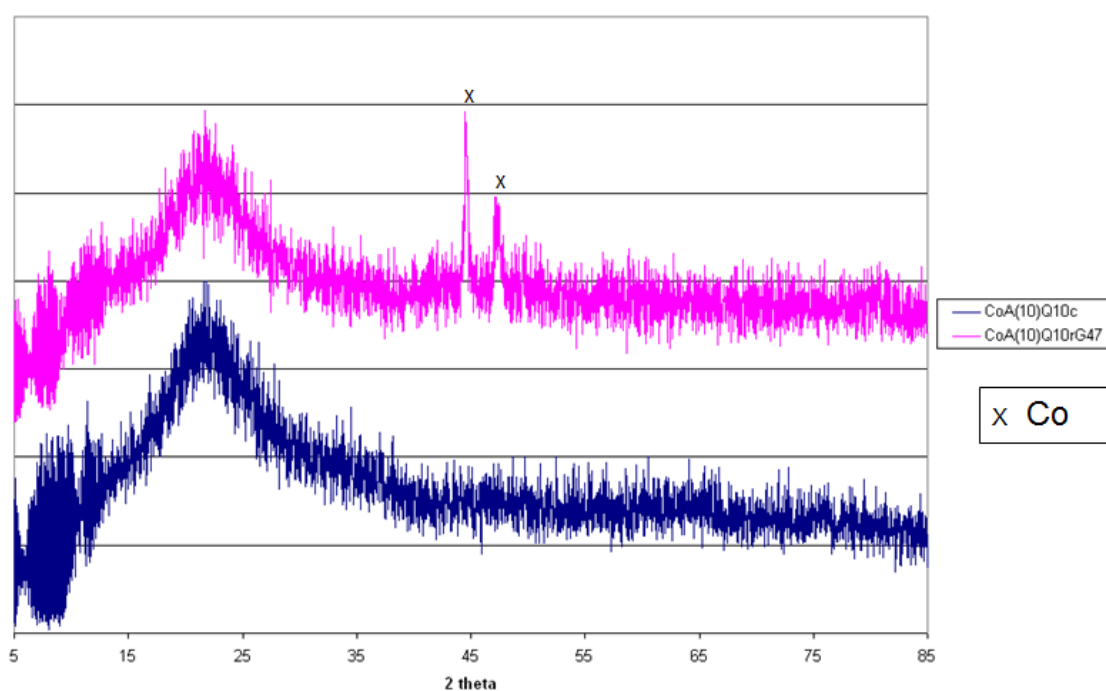


Figure 3-57: XRD patterns of calcined and post-reaction 10 wt.% cobalt on silica

3.3.4 Conclusions

An investigation of alternative base metal catalysts in the form of 10 wt.% cobalt and nickel catalysts shows that both metals are active for the hydrogenation of acetic acid, with ethanol being the major product. However, the activities of these catalysts is not significantly greater than that of the 10 wt.% copper catalyst as can be seen from the ethanol production rates in figure 3-55. This suggests that the change to an alternative base metal is not sufficient to

produce a catalyst that can equal the activity of the methanol synthesis catalyst, but that an increase in metal content may also be required.

The 10 wt.% cobalt catalyst shows an increasing ethanol yield over time, a pattern not observed with any other catalysts tested. Two explanations are hypothesised; (i) the reduction of the cobalt oxide to cobalt metal was incomplete in the initial reduction step and is instead occurring throughout the duration of the reaction and (ii) the increase in activity of the cobalt catalyst is related to an increase in cobalt particle size observed over the course of the reaction. With either of these explanations, the activity of the cobalt catalyst far exceeds that of its base metal counterparts.

None of the 10 wt.% catalysts demonstrate a deactivation profile as was seen with the methanol synthesis catalyst and all show activity towards the production of ethanol. The lack of deactivation with these catalysts suggested viability for testing with increased metal contents to yield higher ethanol activities.

3.4 20 wt.% Metal Catalysts

Increasing the catalyst metal loading was a suggestion at the close of chapter 3.2 as a possible route to increase the activity for ethanol production seen with 5 and 10 wt.% copper catalysts. In chapter 3.3, other base metals in the form of cobalt and nickel catalysts were also investigated and again increased metal contents were suggested as a possibility to increase ethanol yields. In this chapter, increased metal loadings to the amount of 20 wt.% were investigated for copper, nickel and cobalt catalysts.

With an increase in metal content to 20 wt.%, the simple incipient wetness impregnation technique for catalyst preparation was not seen to be an appropriate technique, due to the lack of control of crystallite size and dispersion on the support surface. An alternative preparation technique (HDC) was employed using an alumina support, the details of which are given in section 2.1.2.2.

3.4.1 Alumina SA6X75

The alumina support used was Saint-Gobain Norpro SA6X75. The alumina was supplied as 5mm pellets, which was a same size as the Methanol Synthesis catalyst pellets previously tested.

XRD analysis, shown in figure 3-58, identified Θ -alumina peaks within the alumina support.

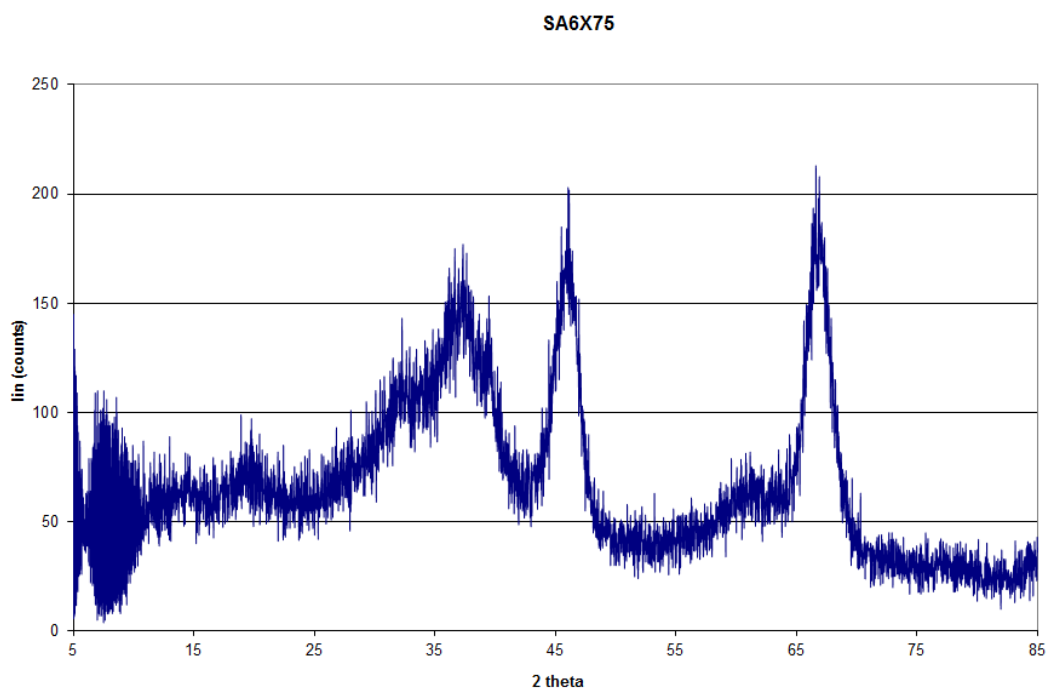


Figure 3-58: XRD pattern of SA6X75 alumina

BET analysis data of the alumina support is displayed in table 3-27, with a high surface area comparable to that of the silica Q10 previously used as a support.

Table 3-27: BET data for Alumina SA6X75

	Pore Volume (cm ³ /g)	Surface Area (m ² /g)	Average Pore Diameter (nm)
SA6X75	0.89	251	9

3.4.2 20 wt.% Nickel Catalyst

A 20 wt.% nickel catalyst was prepared on alumina using the HDC preparation method. Maintenance of the small particle size (<5 nm) appears to have worked as no nickel species could be identified in the hot stage XRD patterns in figure 3-59 from room temperature through to 500 °C.

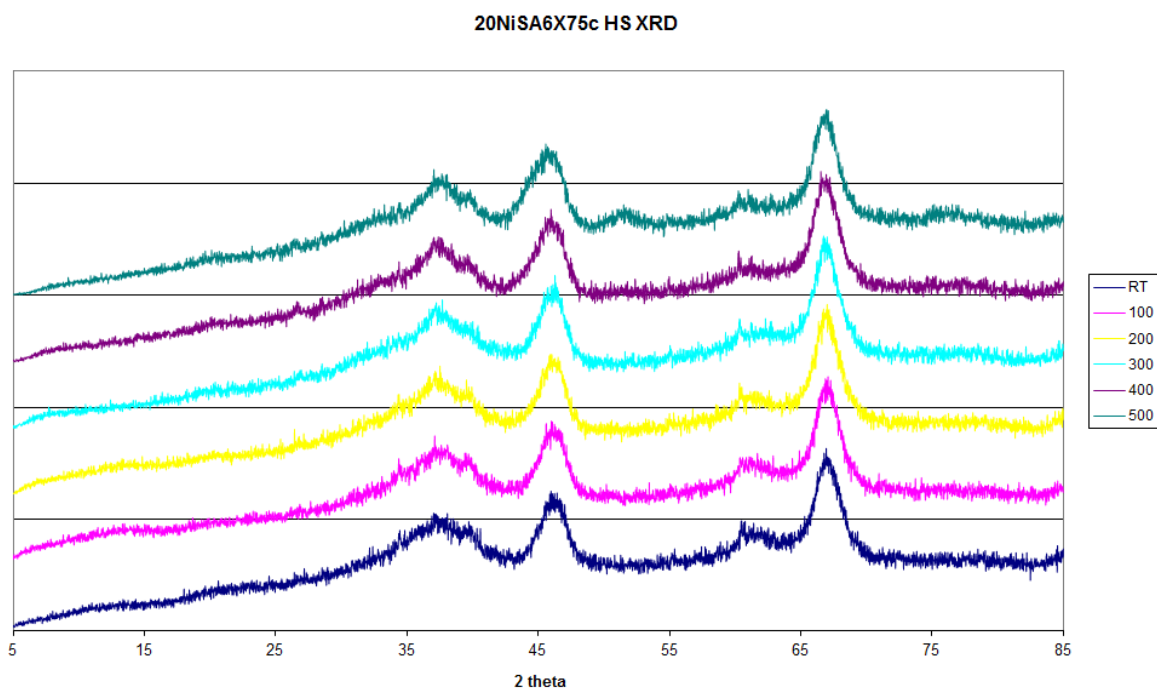


Figure 3-59: HS XRD patterns for 20 wt.% Ni catalyst

TPR analysis of the calcined 20NiSA6X75 catalyst was used to investigate an appropriate reduction temperature for the catalyst.

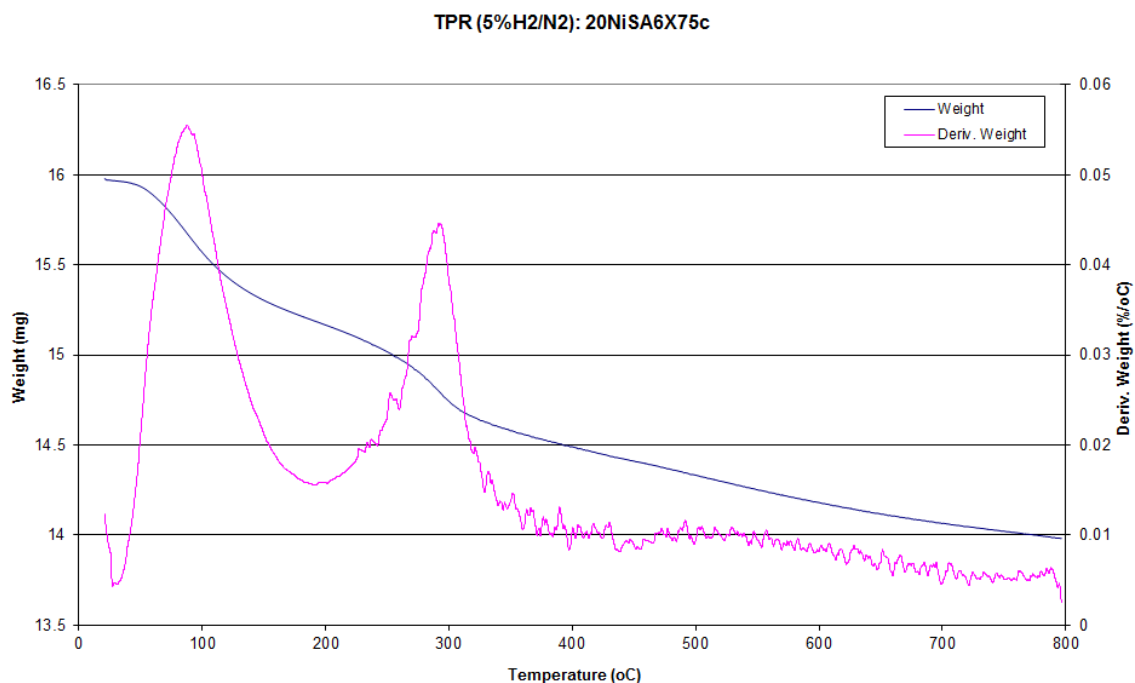


Figure 3-60: TPR profile of 20NiSA6X75c

Mass spectrometry data for the TPR analysis shows that the weight loss at 100 °C corresponds to the loss of water, which is most likely in the form of physisorbed

water on the catalyst surface. The second weight loss at 297 °C can be attributed to the reduction of the nickel oxide to the metallic species. A reduction programme with a temperature of 375 °C with a six hour hold was identified from this TPR profile. The extension of the hold time at the reduction temperature compared to the cobalt and copper catalyst is caused by the difficulty in ensuring complete reduction of nickel.

3.4.3 20 wt.% Cobalt Catalyst

A 20 wt.% cobalt on alumina catalyst was also prepared via the HDC preparation method. TPR analysis of the catalyst produced a two event profile similar to the TPR profile observed for 20NiSA6X75c. A reduction temperature of 350 °C with a four hour hold was used for reduction of the 20 wt.% cobalt on alumina catalyst.

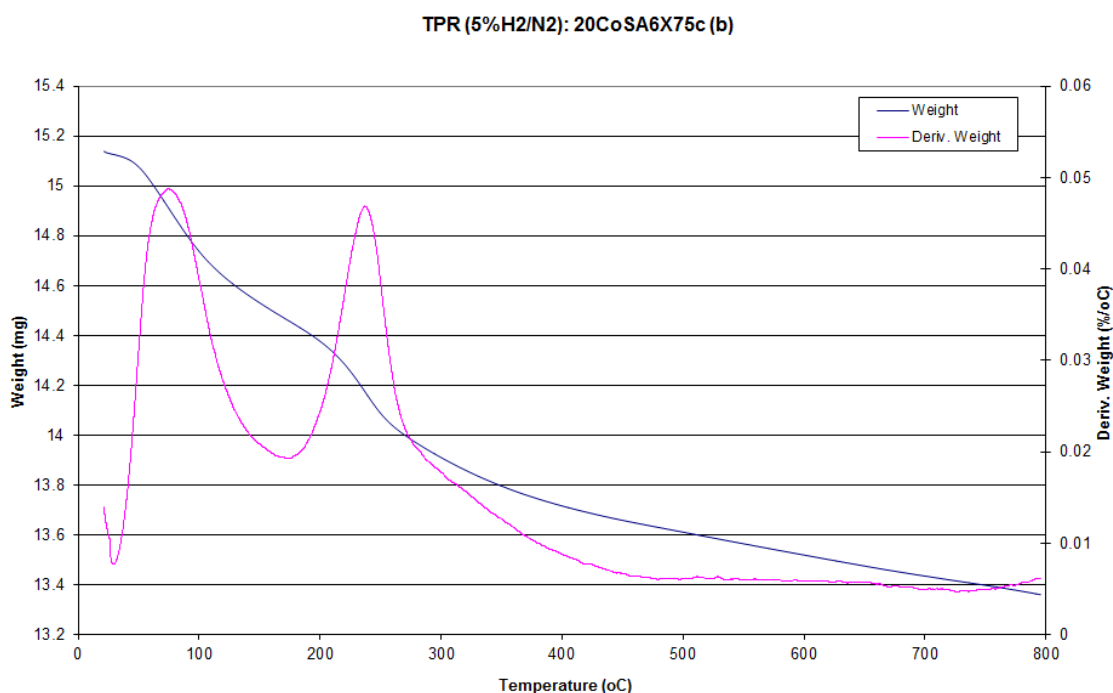


Figure 3-61: TPR analysis of 20 wt.% Co catalyst

The XRD pattern for the calcined 20CoSA6X75c catalyst was as expected with an alumina background, showing no features relating to the presence of cobalt species. This is in line with the patterns observed for the 20 wt.% nickel on alumina catalyst and the preparation technique particle size control.

3.4.4 20 wt.% Copper Catalyst

The third 20 wt.% HDC catalyst contained a 20 wt.% copper loading on alumina. Like the two 20 wt.% catalysts, the 20 wt.% copper catalyst was also analysed by XRD and TPR. A reduction temperature of 250 °C was maintained for all copper catalysts, given copper's propensity for sintering at temperatures above 300 °C. A hold of four hours was employed for the reduction step.

The XRD pattern for 20CuSA6X75c mirrored the alumina background observed for both the cobalt and nickel catalysts and was also expected with the copper option.

3.4.5 Comparing 20 wt.% catalysts

The three metal 20 wt.% catalysts were each tested using standard conditions on the low pressure glass microreactor with a catalyst loading of 1 ml.

As with the 10 wt%. monometallic catalysts, the rate of ethanol production was used as the main comparative tool whilst looking at the 20 wt.% catalysts. The rates of ethanol production for the three 20 wt.% catalysts over the four day reactions are shown below in figure 3-62.

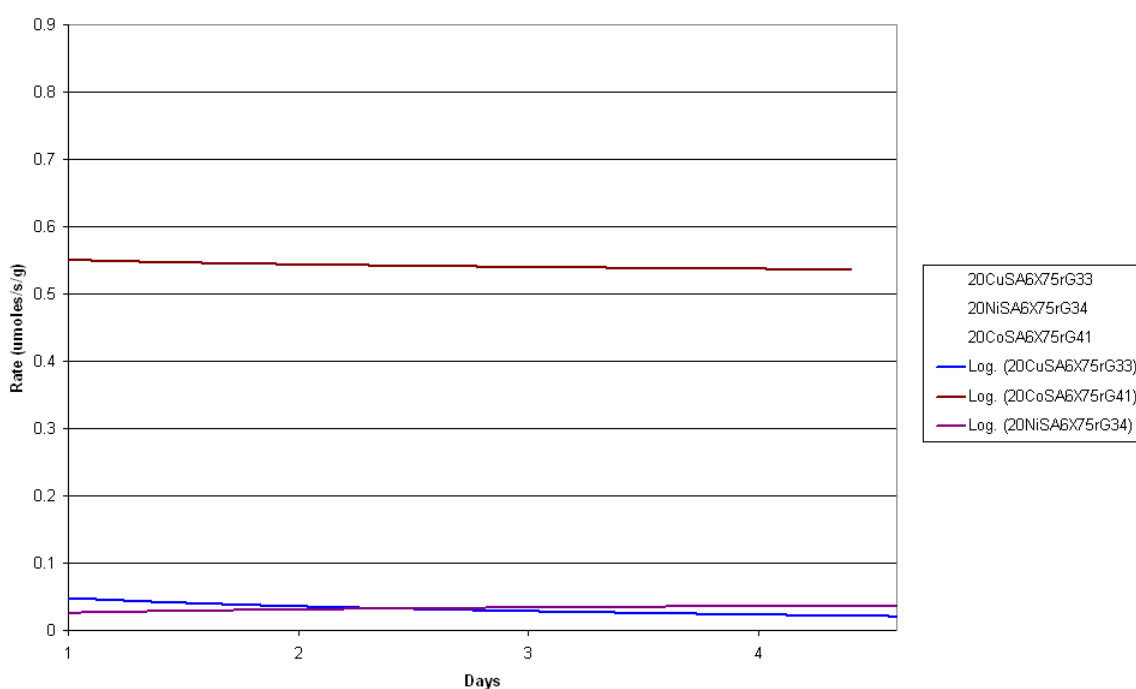


Figure 3-62: Rates of ethanol production for 20 wt.% catalysts

The rate of ethanol production for the 20 wt.% cobalt catalyst is at a steady level of $\sim 0.55 \mu\text{moles/s/g}$ for the duration of the four day reaction. The rate value is significantly higher than the copper and nickel based counterparts.

Cobalt appears to be the best metal of the three base metals investigated for ethanol formation. This ties in with the 2009 Celanese patent [12] which uses Co with Pd/C or Pt/SiO₂. The use of cobalt as a catalyst for steam reforming, including from acetic acid, has been also investigated [52, 54, 55]. Metal catalyst activity follows the order: Co > Ni > Cu, as has been seen in aqueous - phase hydrogenation research [18].

3.4.5.1 Post-reaction characterisation

Comparison of the XRD patterns from the pre- and post-reaction stages was conducted in an attempt to identify any changes in crystallite sizes. Copper sintering was clearly visible in post reaction samples discussed in chapters 3.1 and 3.2, and the 20 wt.% copper catalyst also displays a significant increase in the metal particle size post-reaction. The XRD patterns in figure 3-63 show a comparison of the pre and post reaction 20CuSA6X75 samples.

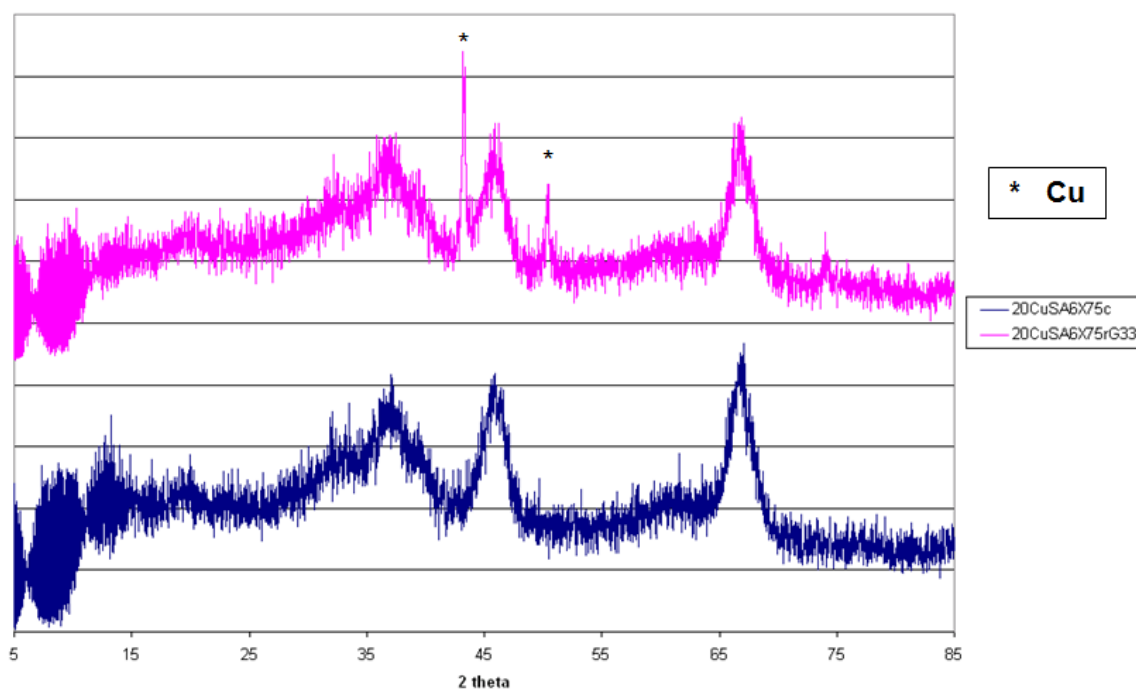


Figure 3-63: XRD patterns of calcined and post reaction 20CuSA6X75

Of the post-reaction samples, only the copper catalyst shows any peaks in addition to those attributed to the alumina support. All post-reaction XRD patterns for the 20 wt.% catalysts are shown in figure 3-64. The lack of additional features demonstrates the small crystallite size produced with the HDC method is maintained in the cobalt and nickel catalysts throughout the reaction. The observation of copper peaks within the XRD pattern post-reaction was not unexpected given copper catalyst's propensity to sinter both at temperature and in the presence of acetic acid.

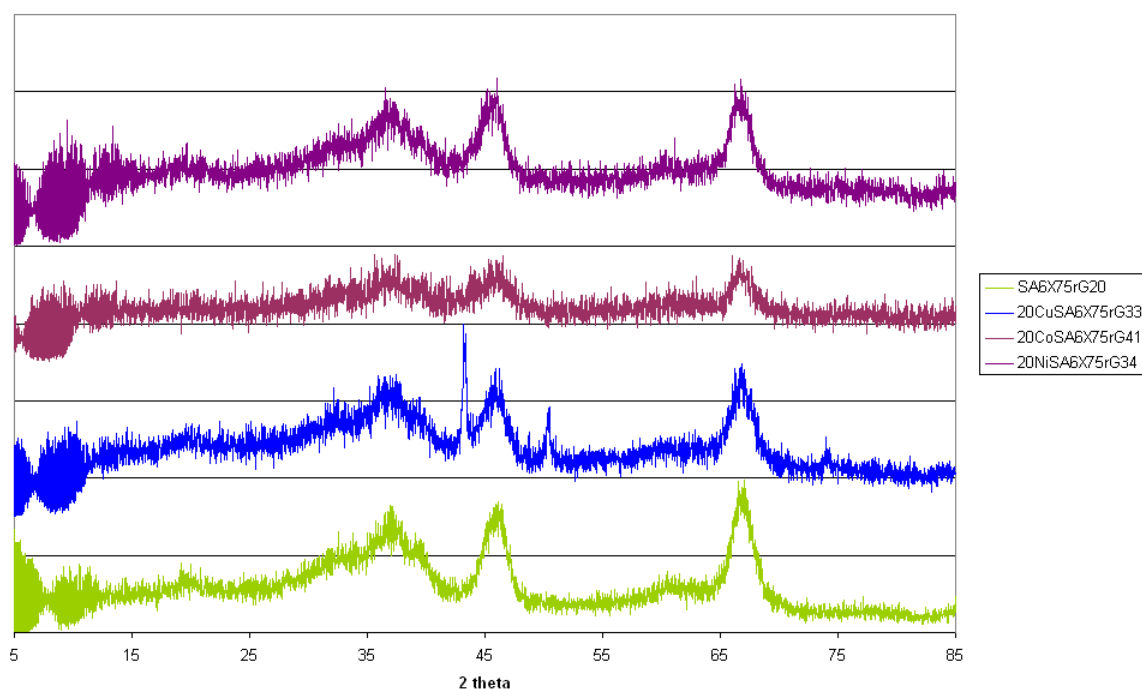


Figure 3-64: XRD patterns for post reaction 20 wt.% alumina catalysts

The results for the TPO analysis of the post-reaction 20 wt.% catalyst samples showed a consistency in the profiles produced. Below, in figures 3-65, 3-66 and 3-67, are the TPO profiles for each of the 20 wt.% catalysts.

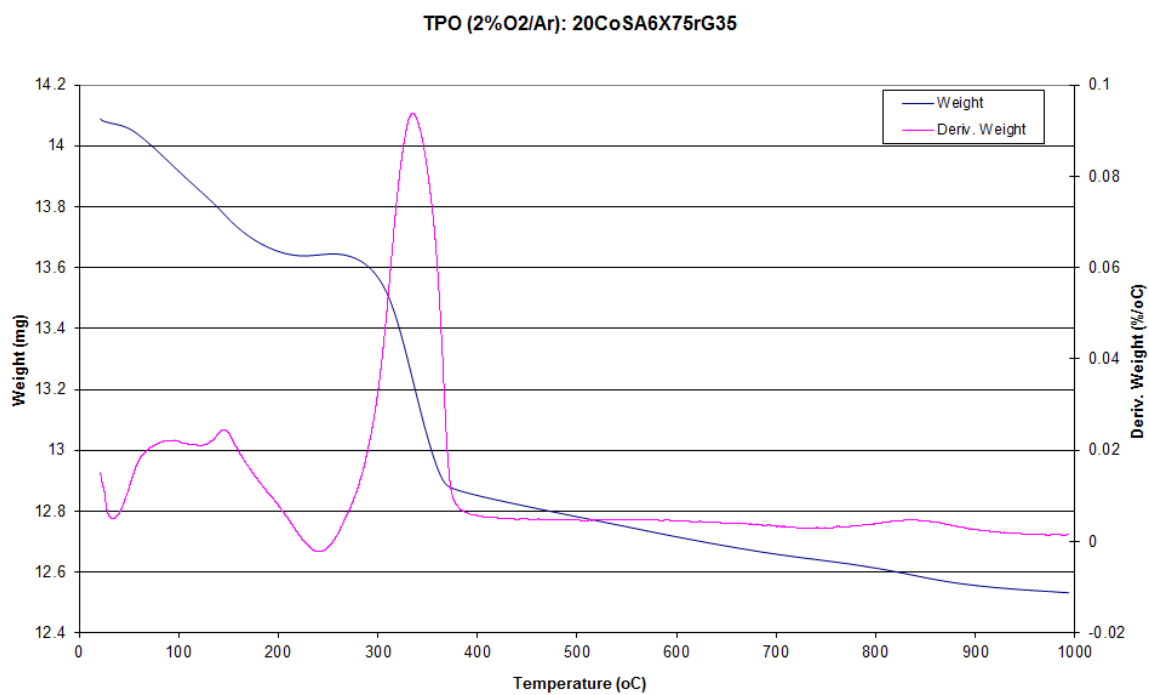


Figure 3-65: TPO analysis of 20 wt.% Co catalyst

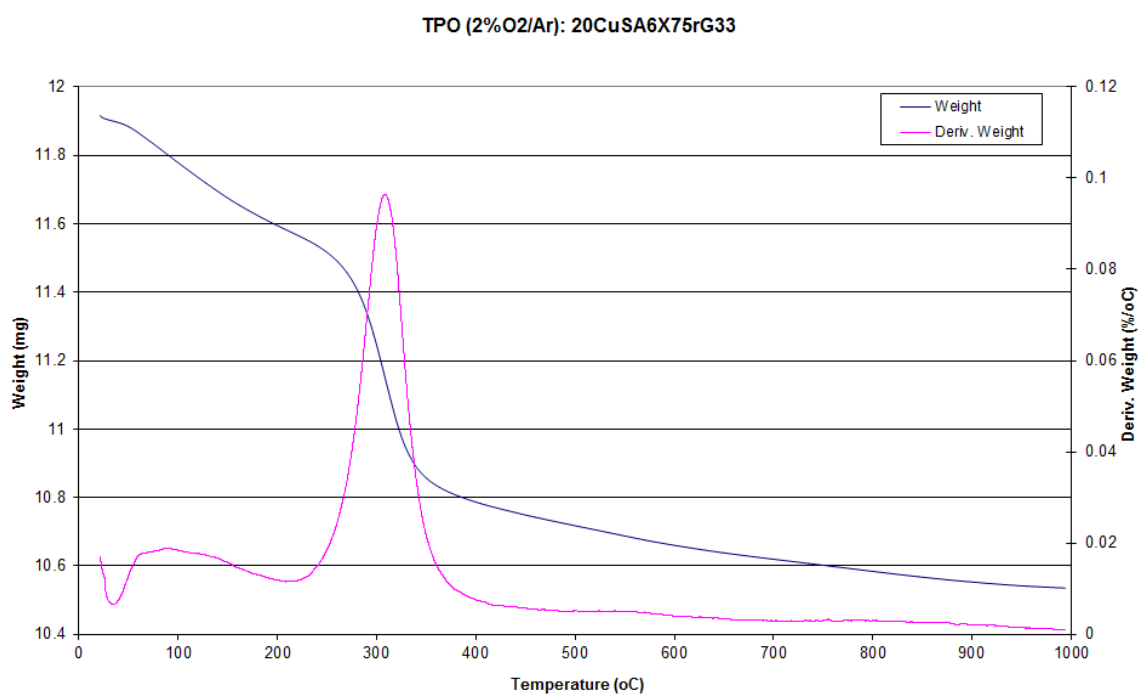


Figure 3-66: TPO analysis of 20 wt.% Cu catalyst

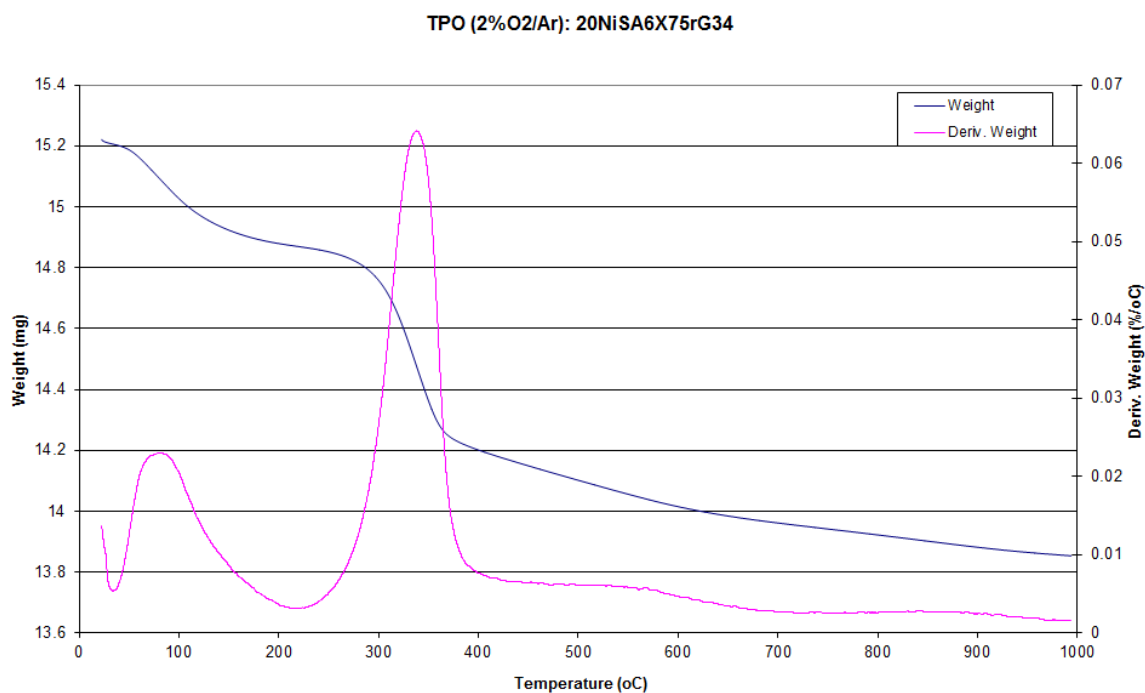


Figure 3-67: TPO analysis of 20 wt.% Ni catalyst

The first event in each TPO profile corresponds to the loss of water, as identified from the MS pattern. The second events, at ~300 °C for 20CuSA6X75 and ~350 °C for 20CoSA6X75 and 20NiSA6X75, all correspond to weight loss events of 5.8 %, 5.6 % and 4.6 % respectively. The MS profile shows an evolution of CO₂ corresponding to each of these events.

3.4.6 Bimetallic catalysts

Following the appreciable increase in the ability of the individual metal 20 wt.% HDC catalysts to produce ethanol compared to their lower metal loading counterparts, the next area of interest was bimetallic catalysts. The investigation into bi-metallic base metal catalysts was to identify any synergistic effects of the bimetallic options compared to the mono-metallic catalysts. Bimetallic catalysts were then prepared using combinations of nickel, copper and cobalt with a 10 wt.% metal loading of each metal to an overall total of 20 wt.%. Preparation of the bimetallic catalysts achieved through co-precipitation of the metals using the HDC method.

The bimetallic catalysts were characterised in the same way as the mono-metallic catalysts. The results of the XRD patterns of the calcined catalysts followed the trend seen with the mono metallic HDC catalysts; where there

were no peaks attributable to the metallic species and only the XRD pattern for the alumina support was observed.

The rates of ethanol production for the three bimetallic catalysts over the four day reaction period can be seen in figure 3-68. In addition the selectivities of each of the bimetallic catalysts to ethanol, acetaldehyde and ethyl acetate are shown in table 3-28.

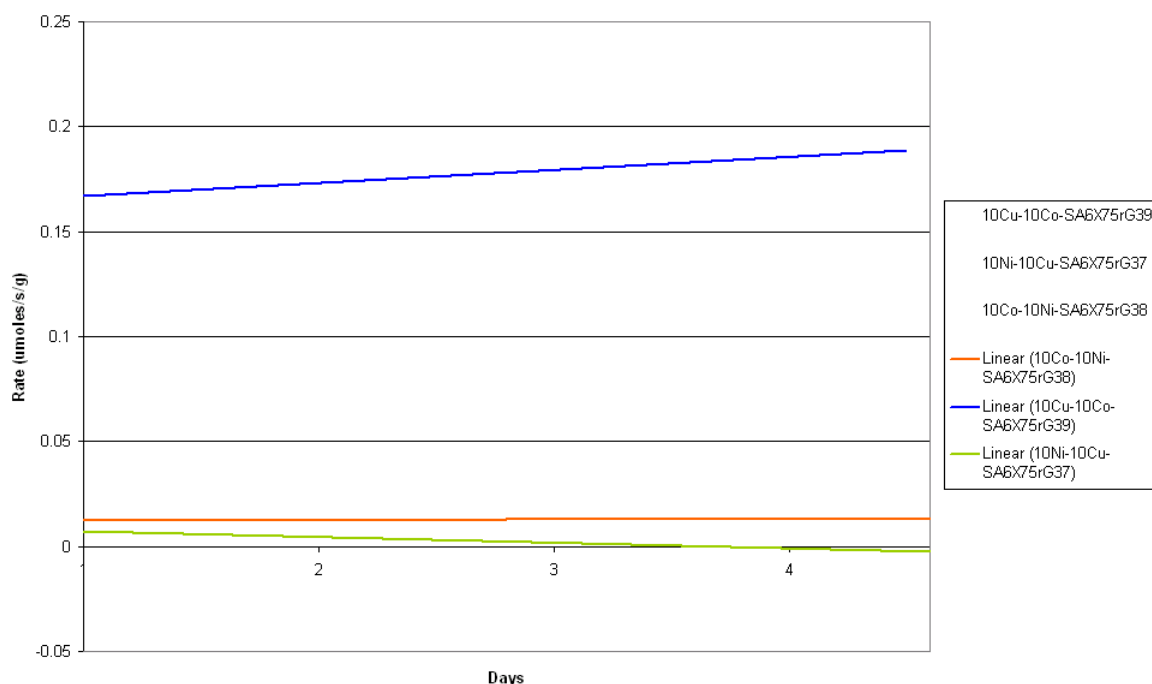


Figure 3-68: Rates of ethanol production for bimetallic catalysts

Table 3-28: Conversions and selectivities for bimetallic catalysts

	Catalyst	10Cu-10Co-SA6X75c	10Ni-10Cu-SA6X75c	10Co-10Ni-SA6X75c
Selectivities (%)	Ethanol	26.2	0.4	0.4
	Ethyl Acetate	0	0	0.3
	Acetaldehyde	0	0	0
Conversion (%)		8	46	54

A comparison of the rates of ethanol production for the bimetallic catalysts was assessed in conjunction with the overall selectivities of the catalyst. The Co-Ni

bimetallic catalyst not only makes ethanol, but further esterifies the ethanol produced with acetic acid to ethyl acetate. Neither of the other two bimetallic catalysts display any activity towards the esterification reaction.

With comparison of the bimetallic catalysts to the mono-metallics, the expectation would be that with 10 wt.% of two metals, the activity of the bimetallic catalyst would be positioned between the activities of the two monometallic catalysts that form its composite. However, there was no synergistic effect observed for any of them and the monometallic 20 wt.% cobalt on alumina (20CoSA6X75c) continued to be the best performer of the prepared catalysts. The rates of ethanol production for the mono-metallic and bi-metallic catalysts are all compared in figure 3-69.

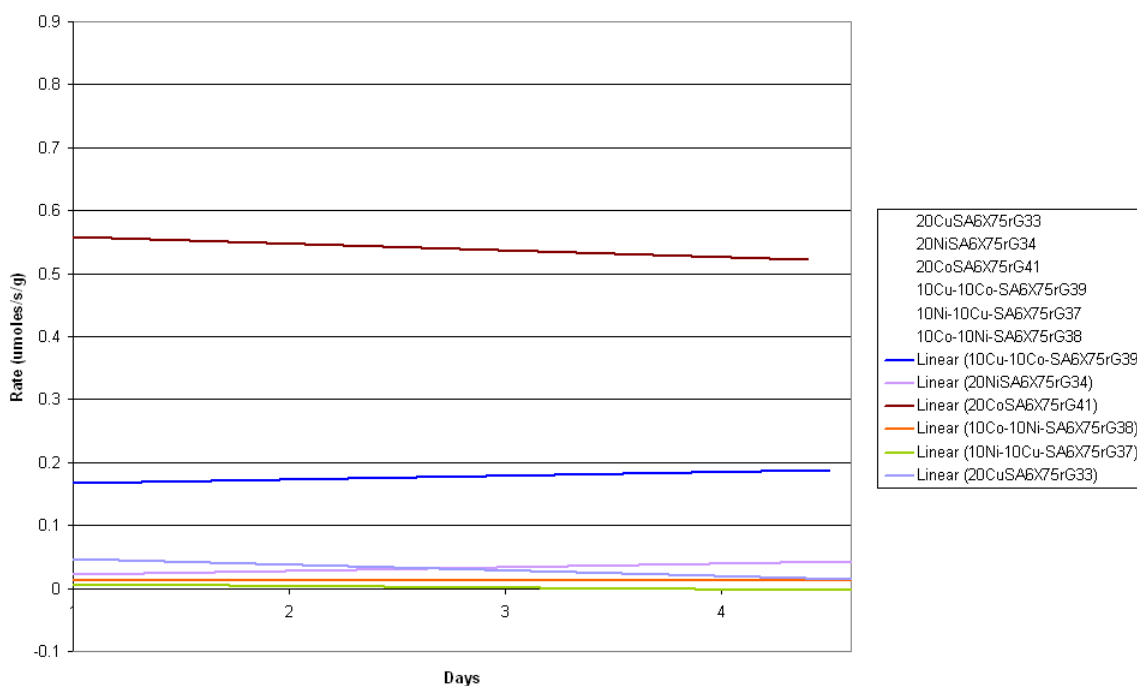


Figure 3-69: Lines of best fit for all 20 wt.% mono and bimetallic catalysts

3.4.7 Conclusions

Comparisons of the prepared monometallic and bimetallic 20 wt.% catalysts showed that the highest rate of ethanol production was observed with the 20 wt.% cobalt on alumina catalyst (20CoSA6X75c). The comparison is further expanded in Figure 3-70, which shows the catalyst with the highest ethanol production rate from each of the following categories; copper catalysts, 10 wt.% catalysts, 20 wt.% mono-metallic catalysts and 20wt% bimetallic catalysts.

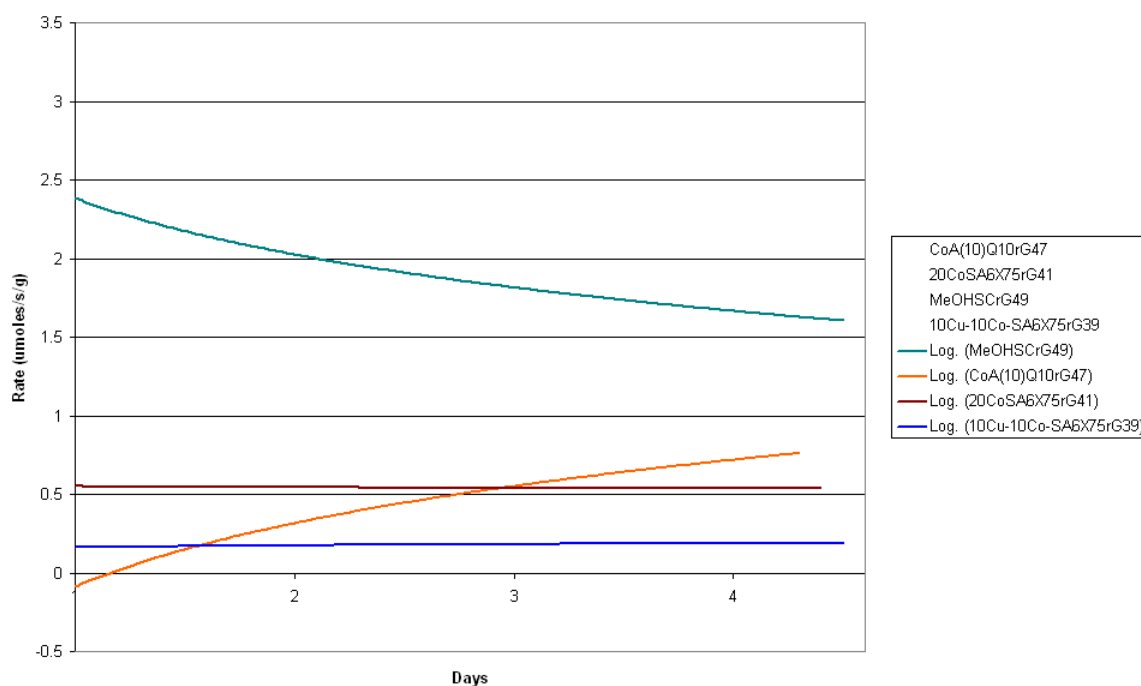


Figure 3-70: Best of each category for rates of ethanol production

The rates of ethanol production in figure 3-70 show a range of processes occurring. The methanol synthesis catalyst, despite having the highest rate of ethanol production, observes a rate decrease by a third over the course of the reaction period. The activity of the 10 wt.% cobalt on silica catalyst conversely increases over the four day reaction period. Rate stability is observed for the mono-metallic 20 wt.% cobalt on alumina and the bimetallic copper/cobalt on alumina catalyst. The bimetallic catalyst compared to the 20 wt.% monometallic only exhibits a third of the rate of ethanol production.

Of the cobalt containing catalysts, on day 1 and 2, the 20 wt.% cobalt on alumina is the most active catalyst for ethanol production. By days 3 and 4, the 10 wt.% cobalt on silica increases its ethanol production rate above that of the 20 wt.% cobalt on alumina and continues to increase. As previously mentioned, this may be due to incomplete reduction of the catalyst during the initial reduction stage or the increase in activity may be observed with an increase in metal particle size during the course of the reaction.

With the exception of the methanol synthesis catalyst and the copper chromite catalysts, all of which are industrially manufactured, the catalysts containing cobalt display the greatest activity for ethanol production. The selectivities and

conversions for the 10 wt.% cobalt on silica, 20 wt.% cobalt on alumina and methanol synthesis catalysts are tabulated below in table 3-29.

Table 3-29: Conversions and selectivities of the most active catalysts

	Catalyst	CoA(10)Q10c		20CoSA6X75c		MeOHSC	
	DAY	1	4	1	4	1	4
Selectivities (%)	Ethanol	57.2	86.5	82.2	19.9	59.3	41.0
	Ethyl Acetate	22.2	7.9	---	---	---	0.44
	Acetaldehyde	---	---	---	---	6.5	10.7
Conversion (%)		1.8	8.9	7.9	30.7	100	80.8

Although ethanol production is the primary objective in this project, there is also interest in the other components produced as side products from the reaction. Of particular interest is a catalyst with a low selectivity towards ethyl acetate due to separation challenges. Relatively low conversions to ethyl acetate are seen with each of the catalysts when tested in the low pressure microreactor. Of the three catalysts mentioned above, the cobalt supported on alumina catalyst is the only catalyst not to show any activity towards the production of ethyl acetate.

3.5 Optimisation Studies

This chapter incorporates a number of studies that were completed. These included investigations into the impact of changes to the reaction temperature or the impact of using different catalyst supports. Each study was completed using a cobalt based catalyst.

3.5.1 Temperature Dependence

Following determination of the superior performance of the 20 wt.% cobalt on alumina catalyst compared to other cobalt, nickel and copper catalysts for the hydrogenation to ethanol, temperature dependence was investigated using this catalyst.

The temperature dependence of the catalyst in terms of activity and stability were of particular interest, especially as a single reaction temperature of 250 °C had previously been used throughout the investigation. Particle size variation pre and post-reaction seen with the copper based catalysts was not observed with the 20CoSA6X75c reaction at 250 °C. An investigation at a higher temperature of 300 °C was completed to see if there was any thermal sintering occurring at this elevated temperature.

The same reaction parameters that were used for previous low pressure microreactor testwork were employed, with the reactor temperature being the variable which was tested at 200, 250 and 300 °C. The 20CoSA6X75c catalyst was used for this study because it showed superior activity to its 20 wt.% metal counterparts, its carbon and acid balances were good compared to other reactions and for a reaction at 250 °C and it appeared to be stable for the duration of the four day reaction period.

Figure 3-71 shows the rates of ethanol production for the three temperatures investigated with 20CoSA6X75c under a reducing atmosphere.

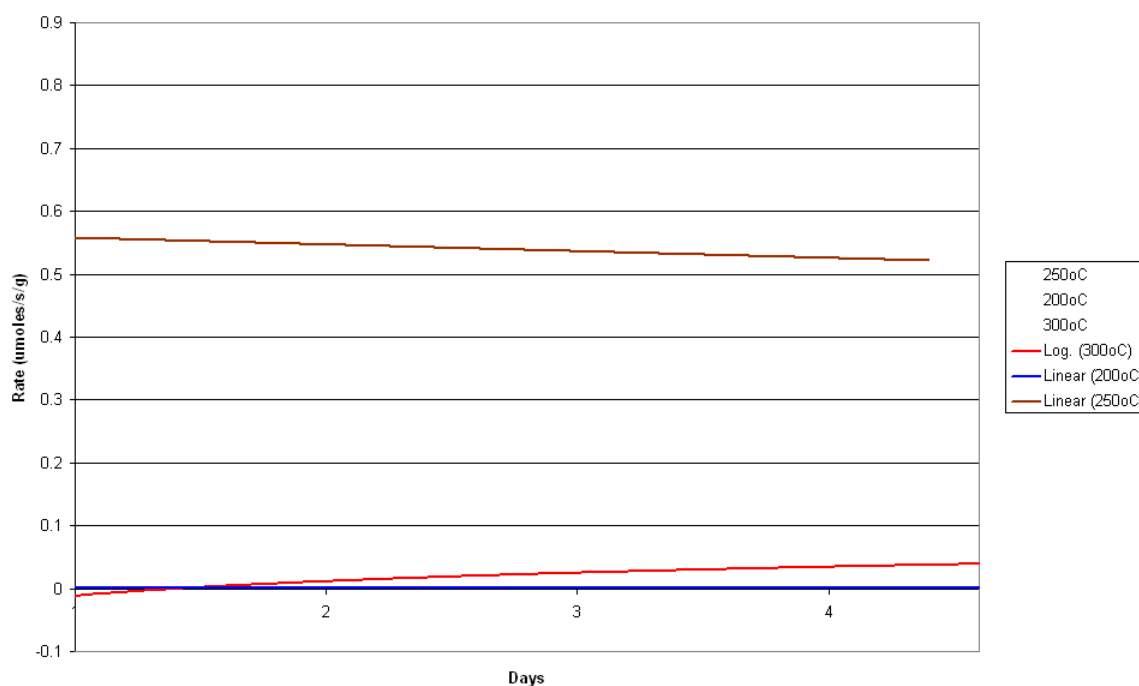


Figure 3-71: Best fits for temperature study for rates of ethanol production

Ethanol production is seen to be severely limited at the 200 °C and 300 °C reactions, especially in comparison to the 250 °C reaction, and does not appear to produce anywhere near the same levels of ethanol at these temperatures. Although the graph in figure 3-71 only shows ethanol production, other potential products from were also monitored for each of these reactions. Table 3-30 shows the selectivity averages for days one and four of the reaction for each of the temperatures investigated. GC analysis of the product stream did not show the presence of products such as acetaldehyde and ethyl acetate. Online MS monitoring of the product stream was continued in this study, although as the MS was not calibrated, the species are not quantifiable.

Table 3-30: Selectivities on day averages at end and start of reaction

	Reaction Temperature	200 °C		250 °C		300 °C	
		<i>1</i>	<i>4</i>	<i>1</i>	<i>4</i>	<i>1</i>	<i>4</i>
Selectivities (%)	Ethanol	1.8	0.3	82.2	19.8	0.1	0.9
	Ethyl Acetate	0	0	0	0	0	0
	Acetaldehyde	0	0	0	0	0	0
Conversion (%)		13.7	35.5	7.9	30.7	98.4	98.7

The MS profiles, in figures 3-72, 3-73 and 3-74, show the trends for comparison of the three different temperature reactions completed. Previous investigations into acetic acid hydrogenation using cobalt catalysts [2] identified the instability of acetate species on a cobalt surface and the subsequent decomposition through an acetic anhydride intermediate route. The systems tested there were bulk cobalt, or supported on silica. Cressely's results [2] for cobalt on silica show conversion of acetic acid to ethanol, but also the decomposition to CH₄ and CO₂. These decomposition products were also monitored during the course of our reaction, with the profiles shown in the figures 3-72 to 3-74.

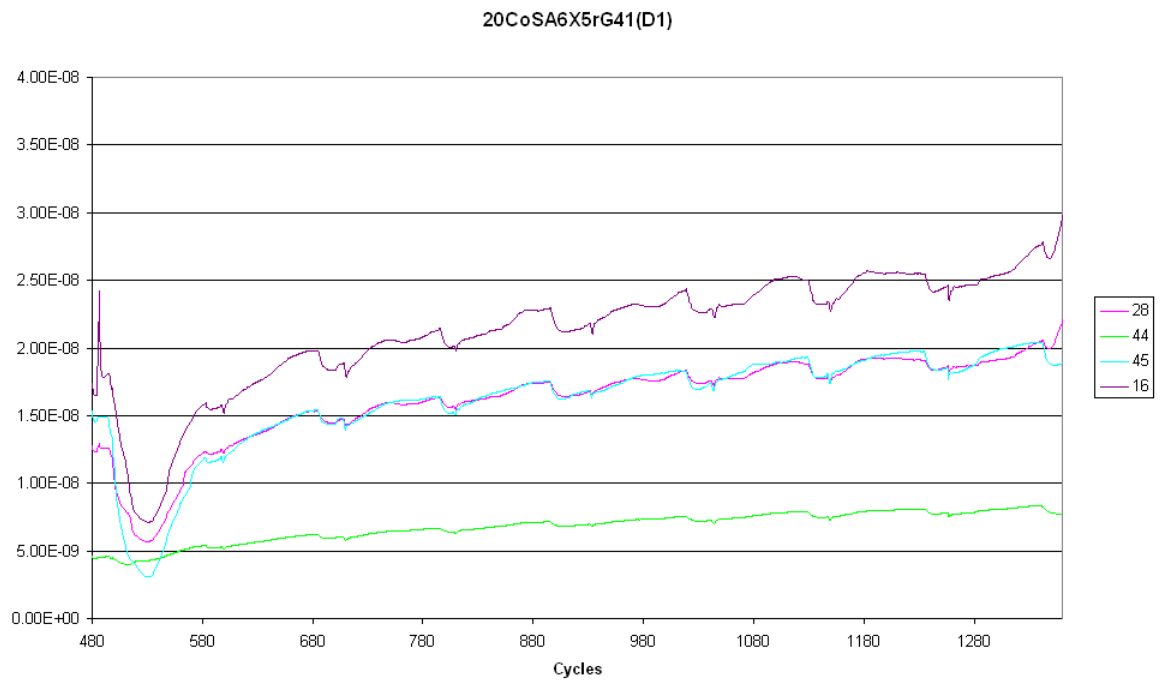


Figure 3-72: MS data for day one of 20CoSA6X75c 250 °C reaction

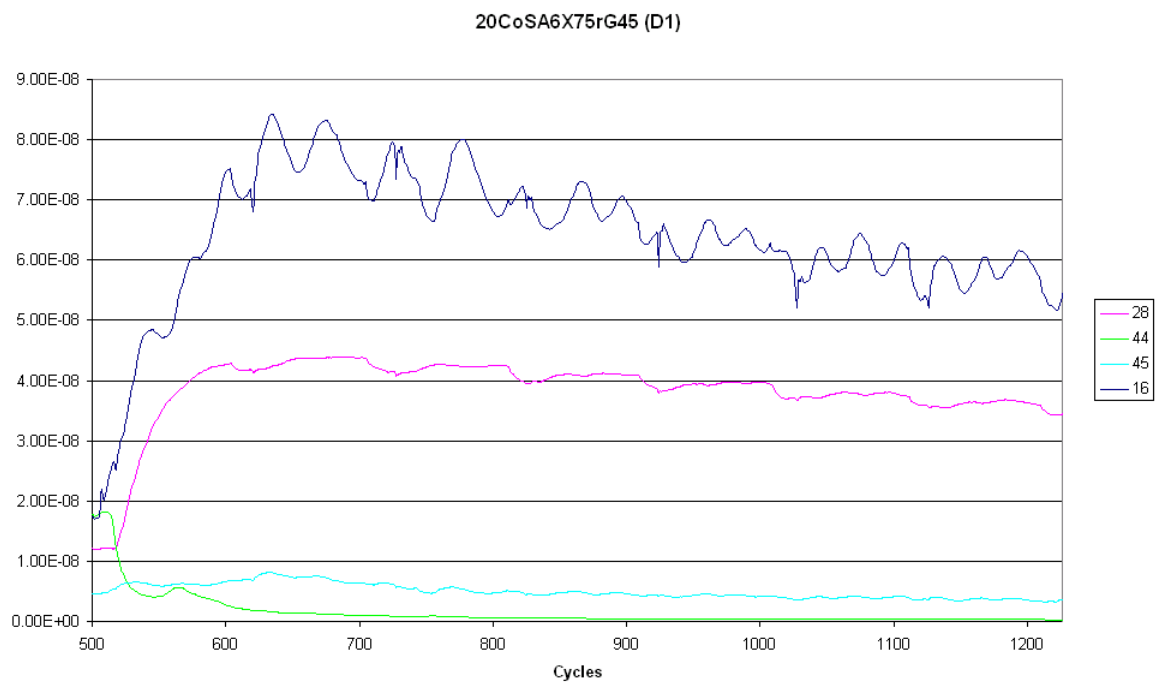


Figure 3-73: MS data for day one of 20CoSA6X75c 300 °C reaction

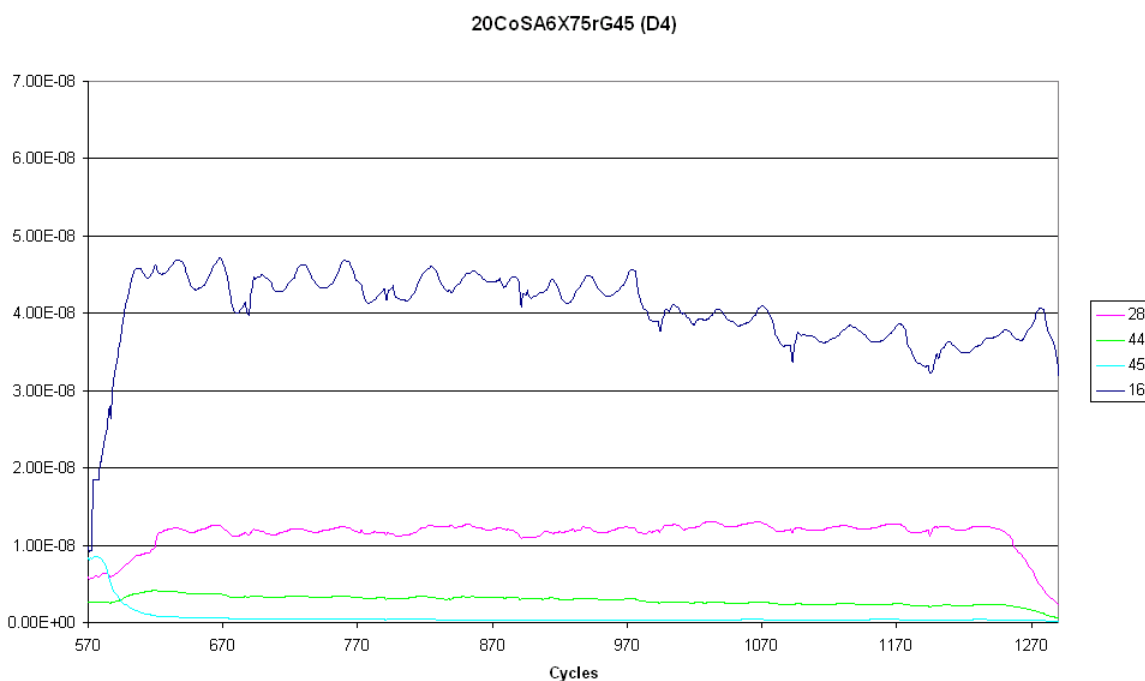


Figure 3-74: MS data for day four of 20CoSA6X75c 300 °C reaction

The MS data, seen in the above three figures, shows two distinct profiles; with a seemingly increased CH_4 make for the reaction at 300 °C, across the four day reaction period, compared to the 250 °C reaction. This reflects the pattern seen with Cressely's cobalt catalysts [2] where an increase in temperature equated to an increase in the methane make for his highest loading catalyst.

3.5.1.1 Post-reaction analysis

Post-reaction XRD analysis was carried out on the catalysts from the three temperatures investigated. Figure 3-75 shows no difference between the patterns.

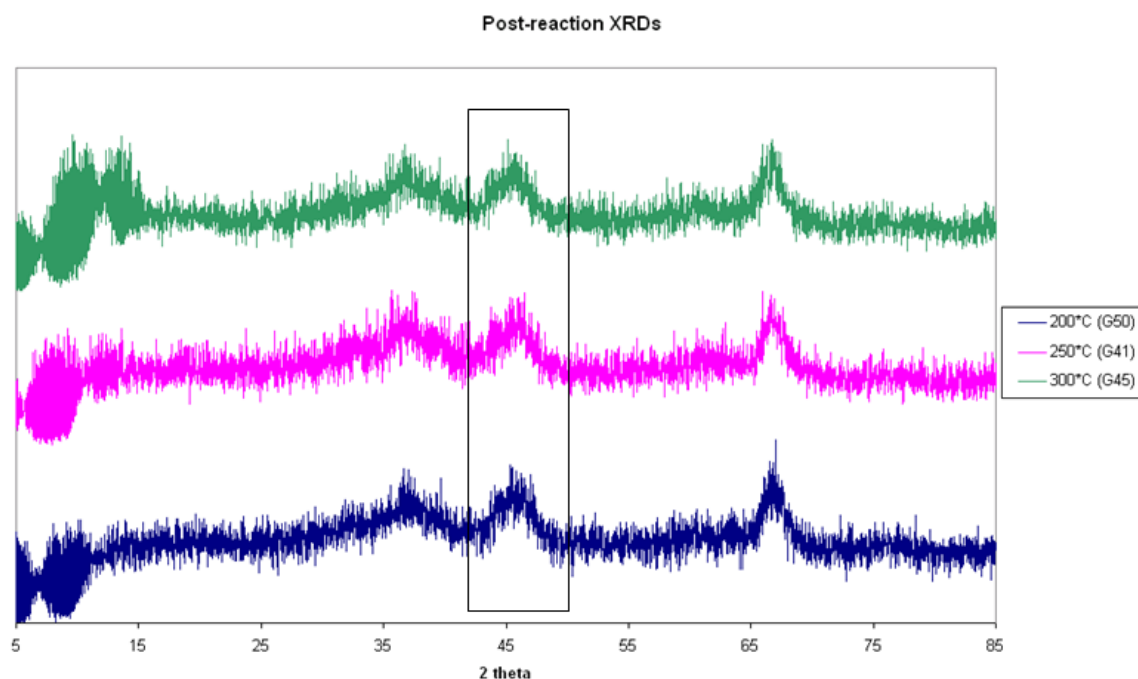


Figure 3-75: XRD patterns of the various temperature samples post-reaction

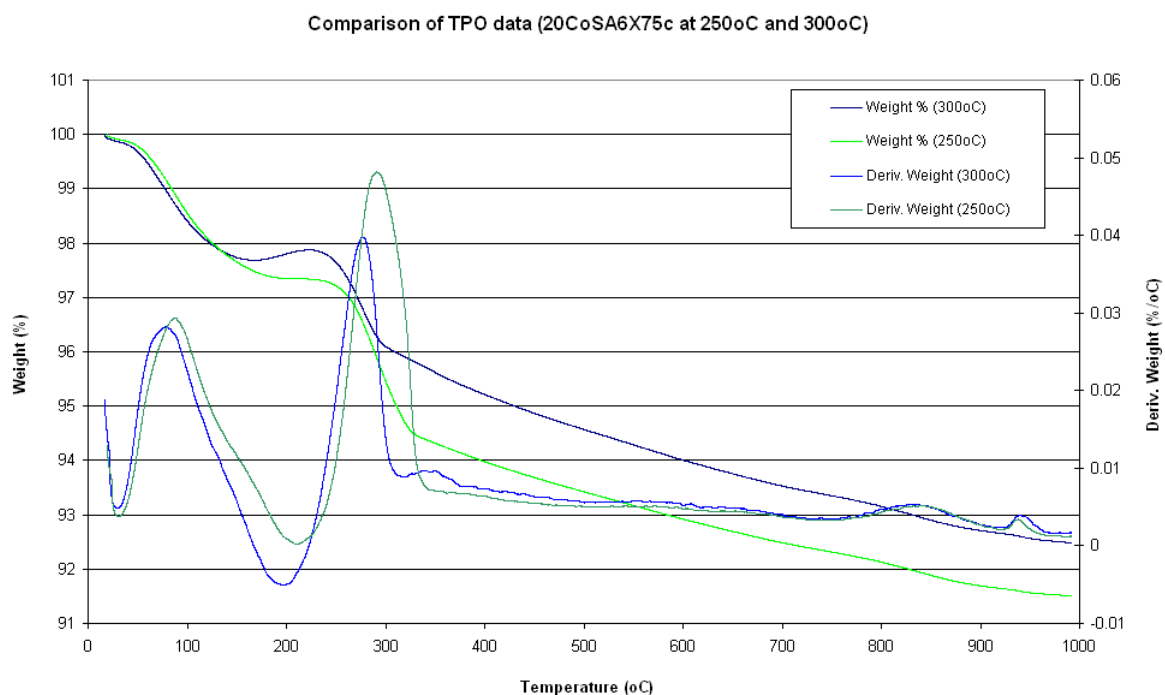
The highlighted section shows on the area of the diffraction pattern where peaks corresponding to cobalt metal or cobalt oxide would be expected. As is clear from the XRD patterns, there are peaks visible against the alumina background that are attributable to cobalt at any of the temperatures investigated. Compared to the copper catalyst patterns seen in chapter 3.4, where the copper peaks post-reaction are clearly visible, it demonstrates once more that the amount of metal sintering for cobalt is lower than for copper even at slightly elevated temperatures.

BET analysis on the post-reaction sample was also employed to help ascertain any changes in the catalyst as a result of the temperature variance. A consistent decrease is visible in the BET surface area in the catalyst's post-reaction, compared to that of the calcined catalyst. The apparent temperature independence of the decrease in surface area suggests that the temperatures tested were not diverse or extreme enough, but also that the decrease in surface area may be an artefact of acetic acid in the system rather than an effect of temperature.

Table 3-31: BET data for 20CoSA6X75c tested at a range of temperatures

Reaction Temperature	Calcined catalyst	200 °C	250 °C	300 °C
BET Surface Area (m ² /g)	237	179	165	188
Pore Volume (cm ³ /g)	0.64	0.58	0.55	0.63
Av. Pore Diameter (nm)	11	13	13	13

TPOs were performed on the catalysts post-reaction. The usual decrease of the catalyst sample upon exposure to the oxidising gas was observed for the three TPO profiles. Comparison of the 250 °C and 300 °C TPO profiles in figure 3-76 shows the same low temperature evolution corresponding to H₂O for both samples. Additionally a mass decrease event was seen in both profiles centring around 300 °C.

**Figure 3-76: TPO data of post-reaction 20CoSA6X75 for 250 and 300 °C reactions**

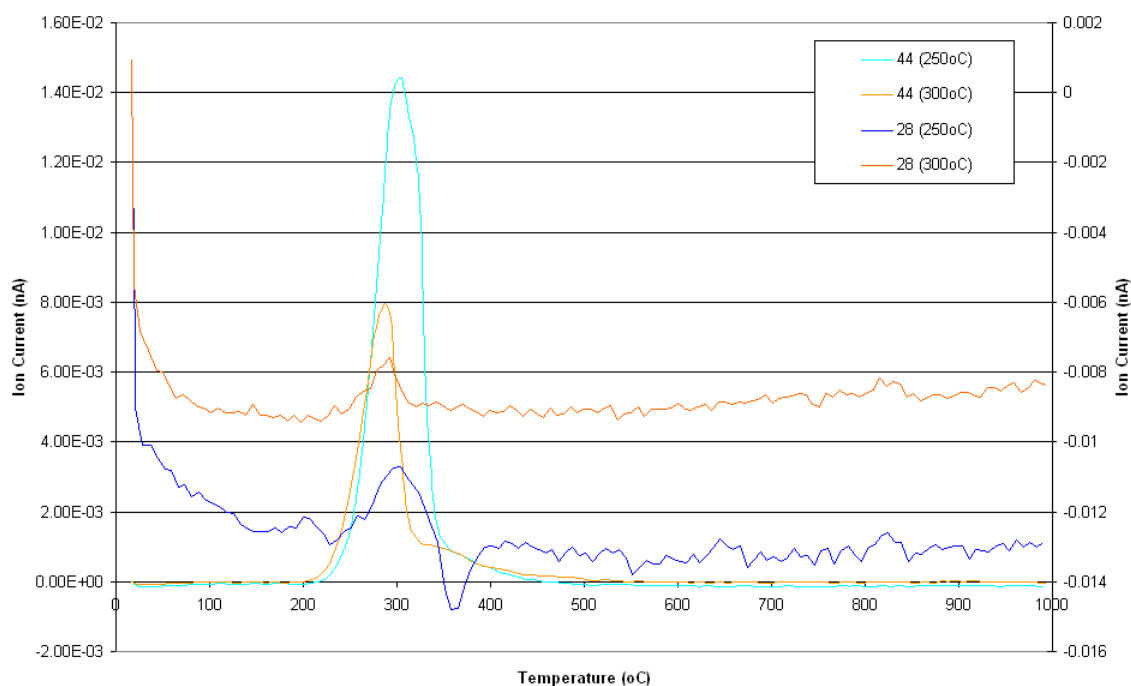


Figure 3-77: MS data of post-reaction 20CoSA6X75 for 250 and 300 °C reactions

The mass decreases seen in both profiles in figure 3-76 centring on 300 °C have corresponding evolutions of CO₂ and CO in figure 3-77 in the same region, indicative of the combustion of surface carbonaceous species. The TPO and MS profiles for the 300 °C reaction show a single event for both CO and CO₂ at 278 °C. The profiles for the 250 °C reaction also show this sharp event but it appears to be shouldered by a secondary event with the same combustion products at a slightly higher temperature. This slight variance in the TPO profiles suggests a difference in the species on the catalyst surface and that different surface reactions taking place. This combined with the MS monitoring during the reaction, shows that there is a difference in the surface reactions, the product profile and the residual surface species between the reactions completed at 250 and 300 °C on samples of the same catalyst.

No high temperature evolutions were seen, suggesting that the carbon present on the surface of the catalyst post-reaction was in the form of surface acetate species rather than carbonaceous residues which would combust at a higher temperature than 300 °C.

3.5.1.2 Argon only reactions

Comparative reactions to those described above (catalyst 20CoSA6X75c at a range of three temperatures) were completed under an inert atmosphere using a flow of 60 ml min⁻¹ Ar.

The reactions under argon where the same acetic acid feed was used show, unsurprisingly, no conversion to ethanol or any other reduction product. The corresponding MS monitoring does however show the presence of decomposition products: CO, CO₂ and CH₄ in the exit stream.

Comparing the MS profiles for the two reactions at 300 °C, one under an inert atmosphere and the other under a reducing atmosphere, seen in figures 3-73 and 3-74, a similarity in the profiles is observed.

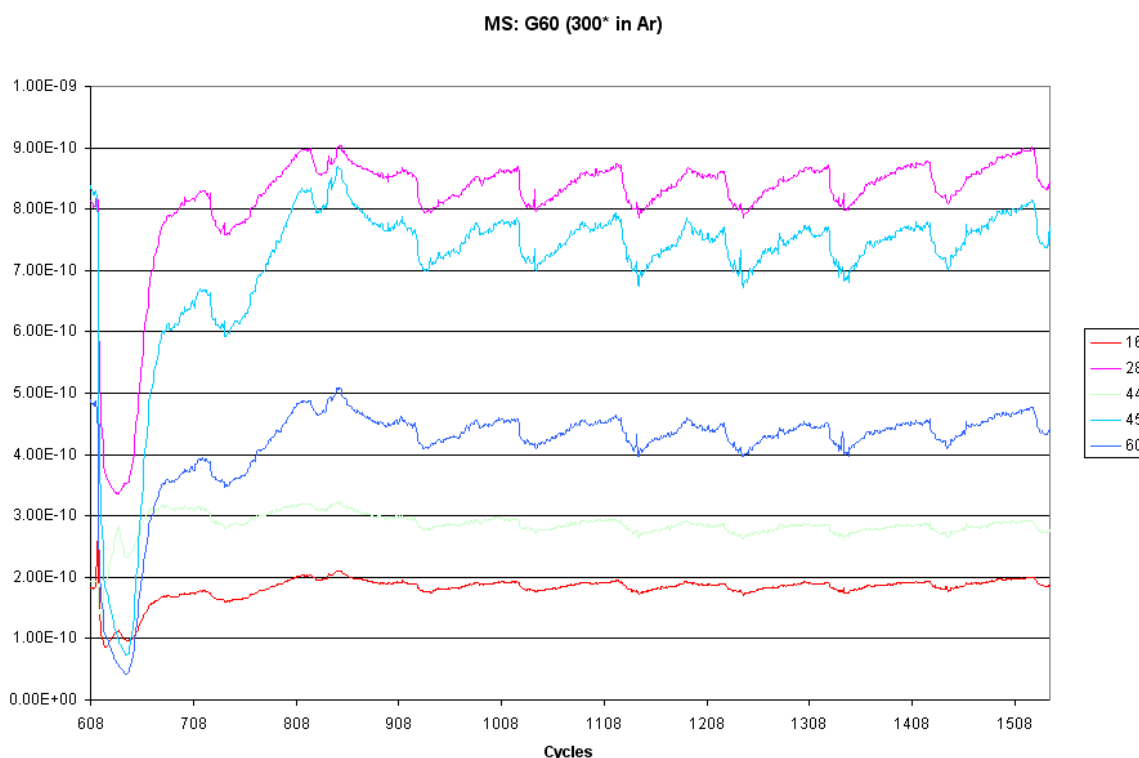


Figure 3-78: MS data of 20CoSA6X75 reaction at 300 °C

Once more, the post-reaction catalyst samples were analysed by XRD, and as previously seen with the samples from the reducing atmosphere, there was no identification of peaks attributable to cobalt metal or cobalt oxide against the alumina background. The highlighted box in figure 3-79 shows the degree range

in which it would have been expected to observe peaks, if they had been present.

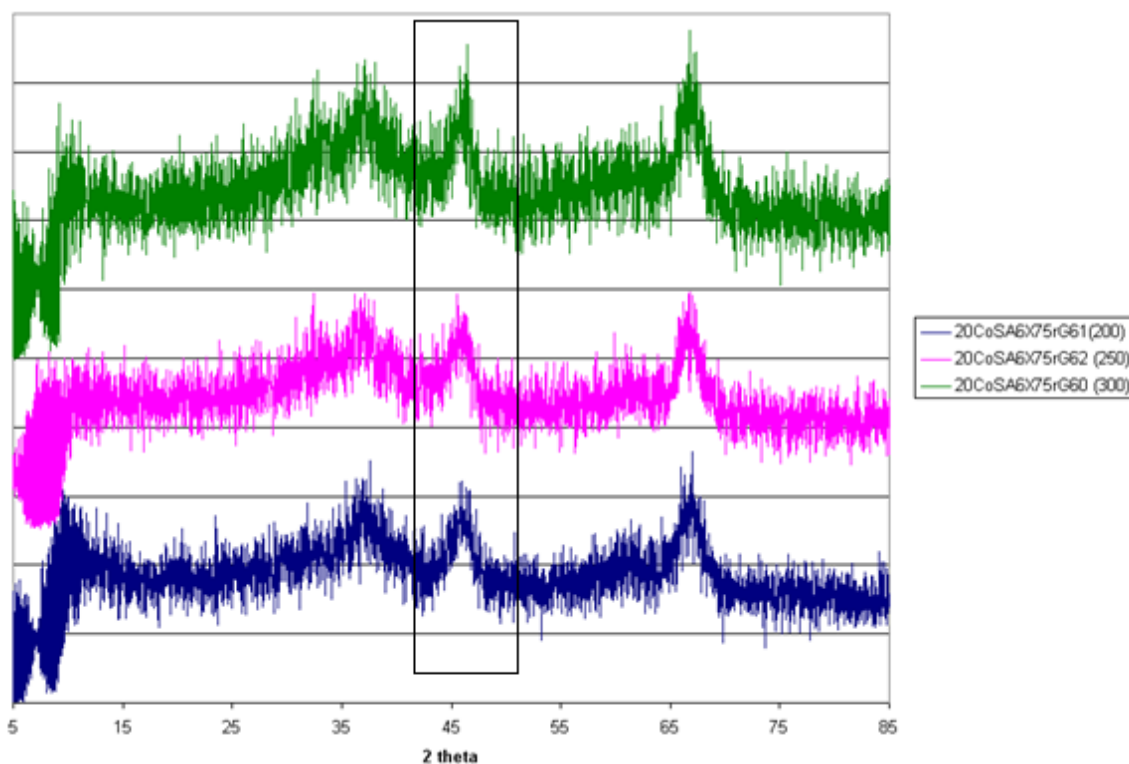


Figure 3-79: XRD patterns of post-reaction 20CoSA6X75, reactions at varying temperatures

TPO analysis was completed for the three catalyst samples. Similar profiles were obtained for the three samples and the 300 °C reaction sample is displayed in figure 3-80 to show a direct comparison to the 300 °C reaction under a reducing atmosphere in figure 3-77.

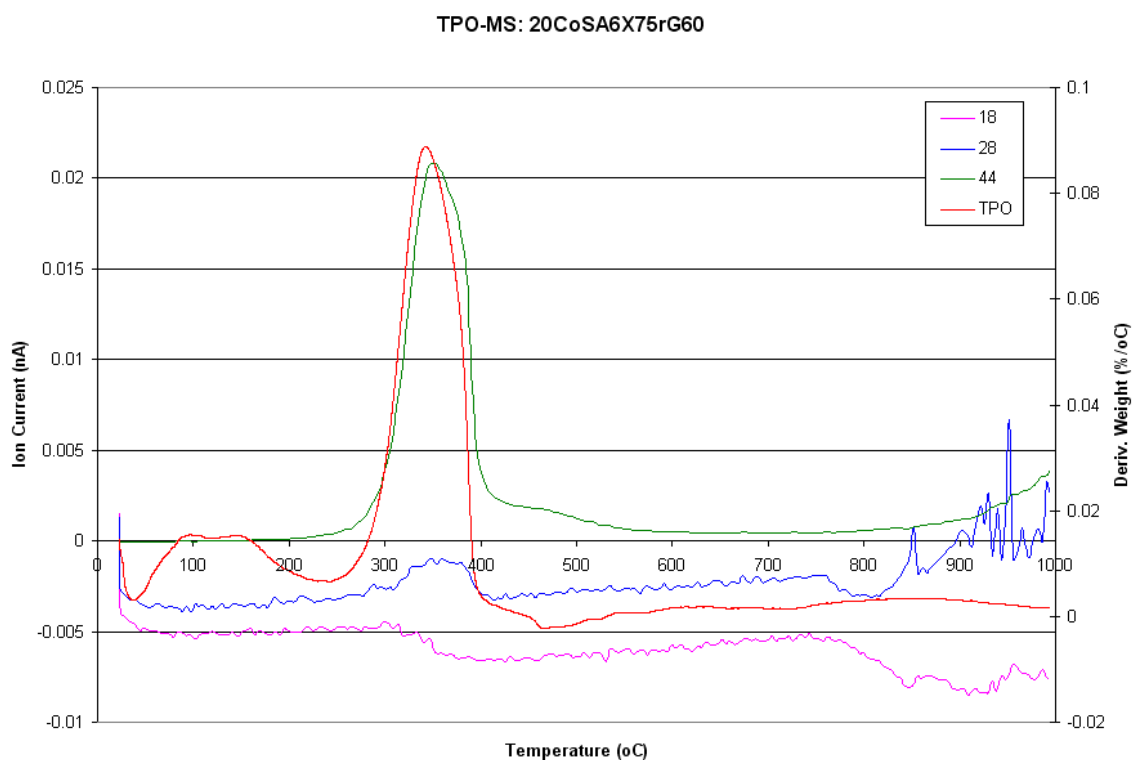


Figure 3-80: TPO profile of post 300 °C reaction 20CoSA6X75

The TPO profile in figure 3-80 for the 300 °C argon reaction is reminiscent of the 300 °C reducing atmosphere TPO profile, where the major reaction that occurred was the decomposition of the acetic acid feed. The similarities in the TPO profiles, in combination with the reaction MS profile, show that acetic acid decomposition is the reaction occurring under the inert atmospheres.

BET measurements of the post-reaction samples, shown in table 3-32, were carried out. Here the same post-reaction decrease in surface area was observed to a similar extent as with the reaction completed under a reducing environment.

Table 3-32: BET data of post-reaction 20CoSA6X75, reactions at varying temperatures

Reaction Temperature	Calcined catalyst	200 °C	250 °C	300 °C
BET Surface Area (m ² /g)	236.8	145.9	158.9	166.8
Pore Volume (cm ³ /g)	0.64	0.51	0.55	0.54
Av. Pore Diameter (nm)	11	14	13	13

3.5.1.3 Summary

From the temperature dependence study using 20 wt.% cobalt catalyst, 20CoSA6X75c, a reaction temperature of 250 °C appears to be the optimum temperature for ethanol production of the three temperatures tested. The reaction temperature used with the 20 wt.% cobalt on alumina catalyst has a profound impact on the activity of the catalyst and also the product profile resulting from the reaction.

The optimal temperature was seen to be 250 °C which gave a major selectivity to ethanol. The 200 °C and 300 °C reactions do not produce similar levels of ethanol to the 250 °C reaction. The 300 °C reaction showed a much higher conversion value than the 200 °C and 250 °C. This is not reflected with an increase in the amount of C₂ oxygenate compounds produced, but instead results in a visible increase in the methane profile in the online MS analysis. With an increase in temperature, an increase in further hydrogenation to the alkane products is observed.

A repeat of the reactions under an inert atmosphere of argon, as opposed to the reducing hydrogen atmosphere, shows decomposition is the primary reaction for the three temperatures. This is confirmed by the TPO and MS profiles.

3.5.2 Sintering

An increase in temperature to 300 °C did not appear to enhance sintering of the metal content in the 20 wt.% cobalt on alumina catalyst, 20CoSA6X75c. This was concluded as there was no effect on the metal particle size, as calculated from the XRD peaks attributed to the cobalt metal phase. This statement is complicated by the fact that no cobalt peaks were able to be assigned against the alumina support background. The HDC preparation method [43] produces a high dispersion catalyst with Co crystalline sizes of between 3-5 nm. This small crystallite size is at the base of the detection limits for the XRD method employed.

Therefore, it is important to ask: what effects are observed for the cobalt catalysts that are not the same as those seen with the copper and nickel catalysts. The question posed: is the sintering mainly occurring as a result of temperature or as an effect of the presence of acid within the system?

XRD analysis was carried out on the pre and post reaction catalyst samples in order to identify changes in the metal species. However, as a clearer indicator of particle size changes, or sintering, hot-stage XRD analysis was employed, with subsequent metal particle size determination by Scherrer equation calculations.

The patterns for the hot-stage XRD analysis completed under a reducing atmosphere of 5 % H₂/N₂ are below in figure 3-80 for the 10 wt.% copper on silica. A distinctive metal species change was observed from CuO and to Cu between 100-200 °C. The corresponding metal particle size changes are detailed in table 3-33.

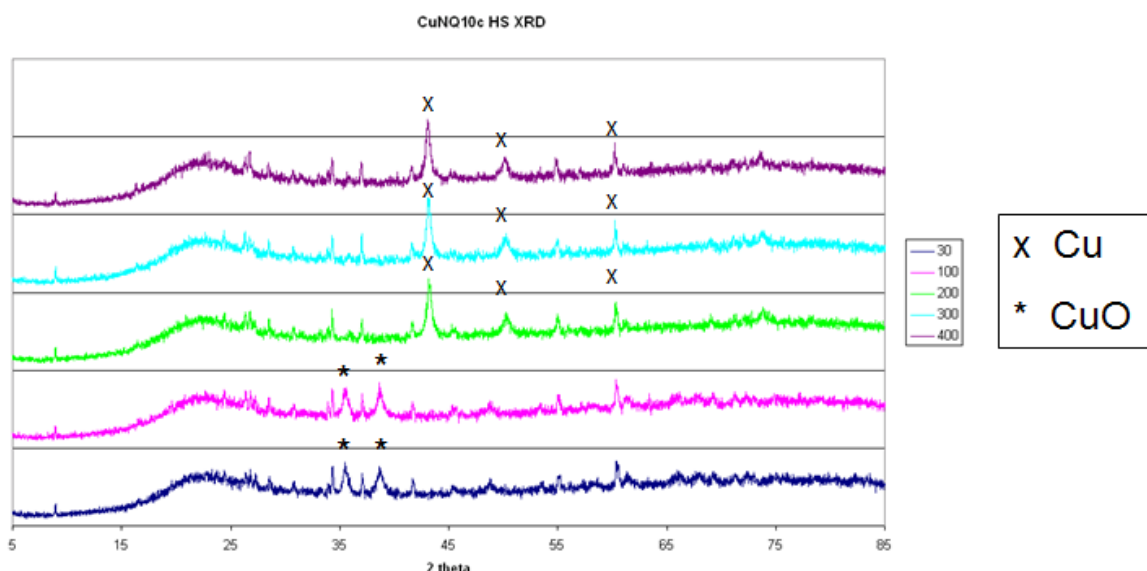


Figure 3-81: HS XRD patterns for CuNQ10c

Table 3-33: HS XRD particle sizes for CuNQ10

Temperature (°C)	Species	Particle Size (nm)
400	Cu	21.6
300	Cu	18.8
200	Cu	17
100	CuO	16.7

The hot-stage XRD patterns show a steady increase in metal particle size with temperature increase, with the largest increase seen between 300 and 400 °C. This distinction is to be expected given the temperature limitations of using copper which has an increased propensity for sintering at temperatures above 300 °C.

Similar hot-stage XRD analysis was carried out for the 10wt% nickel on silica catalyst. In figure 3-82, there is distinctive change in metal species from the nickel oxide to nickel metal. Although this reduction mirrors that observed with the 10 wt.% copper on silica catalyst, the temperature range at which this

occurs is 100 °C higher than for the copper catalyst.

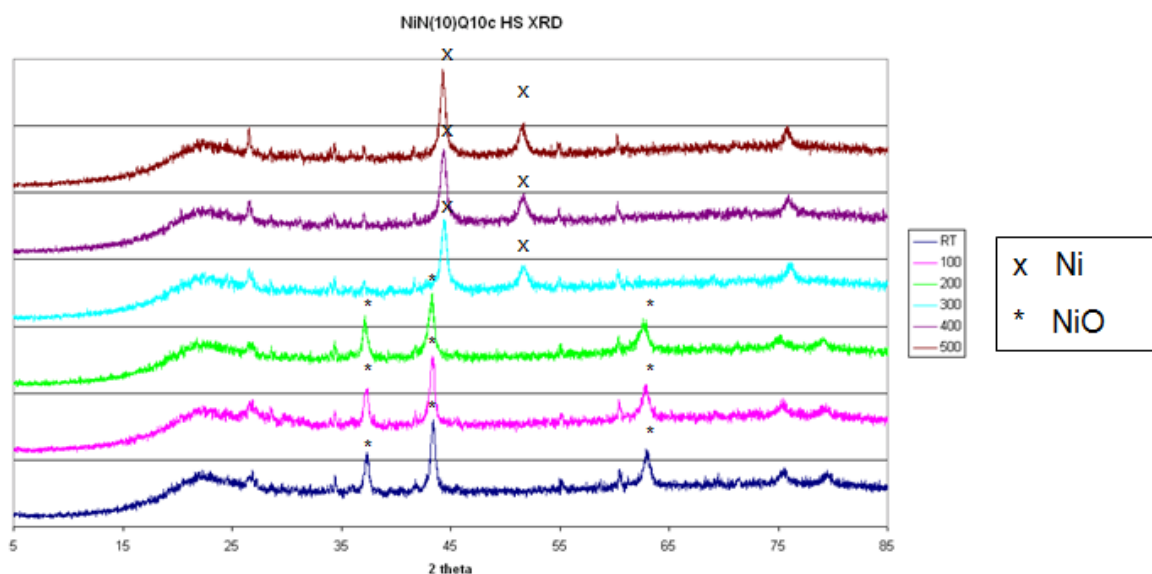


Figure 3-82: HS XRD patterns for 10 wt.% Ni on silica catalyst

Table 3-34: HS XRD particle sizes for 10 wt.% Ni on silica catalyst

Temperature (°C)	Species	Particle Size (nm)
500	Ni	14.0
400	Ni	13.2
300	Ni	13.2
200	NiO	14.0
100	NiO	15.8
RT	NiO	16.3

Metal particle sizes were also calculated from the XRD patterns. Despite some variance, the particle sizes did not appear to increase with temperature for the nickel catalyst under the hot-stage XRD conditions as opposed to the increase observed under the same parameters for the 10 wt.% copper on silica catalyst.

The impregnated supported metal catalysts were prepared via a technique that is not known for strict particle size control. Conversely, the HDC preparation technique produces catalysts with a strict metal particle size range of 3-5 nm.

Hot-stage analysis of the HDC copper catalyst in figure 3-83 gives patterns that are dominated by the alumina background. The highlighted area is the degree range in which peaks attributable to copper metal would be observed. However, no peaks are distinct above the alumina background even at the higher temperatures of 400 and 500 °C.

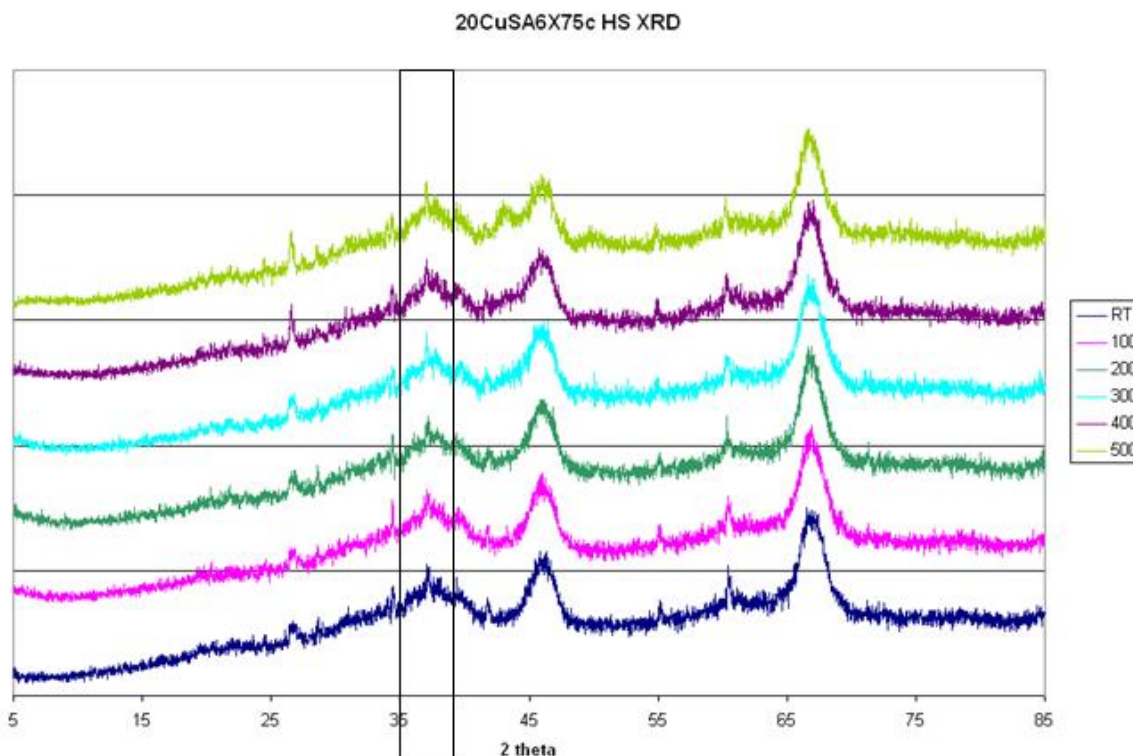


Figure 3-83: Hot-Stage XRD patterns for 20CuSA6X75

3.5.2.1 Summary

Metal particle size increases were seen in the 10 wt.% copper on silica catalyst post reaction samples. The copper catalysts post reaction was subject to high levels of sintering, which was not seen with the cobalt catalysts.

No peaks attributable to the metal components were visible on the HDC catalysts on SA6X75 due to the large alumina peaks as a background. In addition, the preparation method produces particle sizes that should be in the range of 3-5 nm, which is around the low threshold for visibility on a XRD pattern.

3.5.3 Bed Profiling

Profiling of the 20 wt.% cobalt on alumina catalyst bed was conducted by changing the bed depth, and in turn, investigating the activity of the bed profile.

Unlike traditional bed profiling, the standard bed of 1 ml of catalyst was halved to $\frac{1}{2}$ ml, and also doubled to 2 ml, to produce a range of catalyst bed depths. This was done to ensure that the thermocouple probe was situated centrally within the catalyst bed. Reduction to a quarter of the standard depth ($\frac{1}{4}$ ml) would not have allowed for this central thermocouple positioning and would not have given sufficient temperature indication of the catalyst bed.

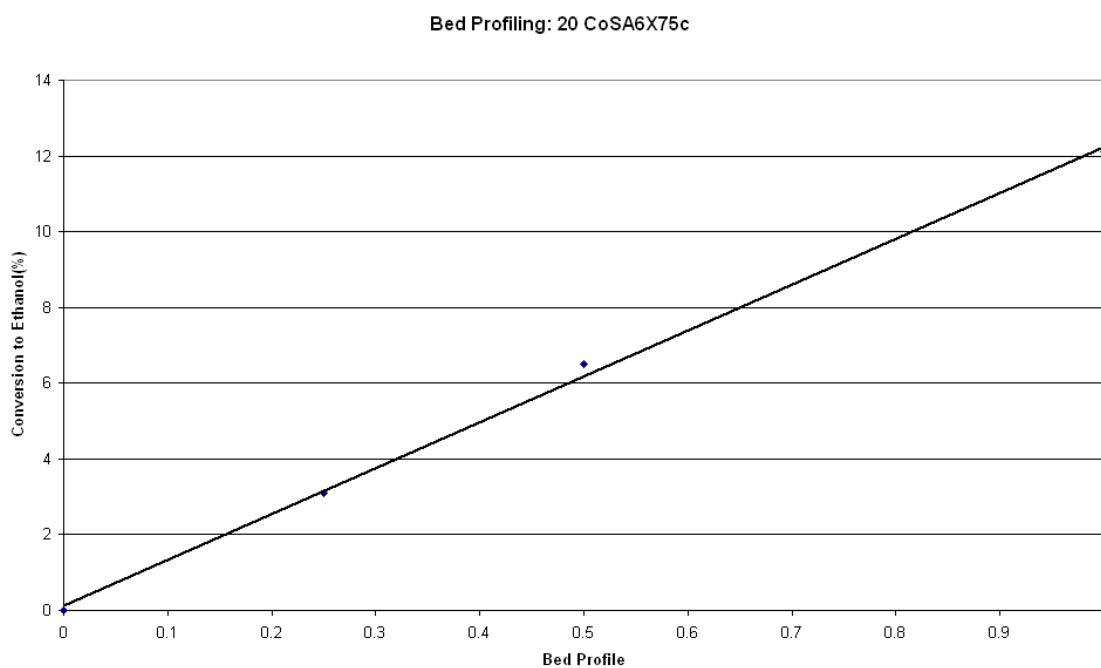


Figure 3-84: Bed profile relating bed depth to conversion to ethanol using 20CoSA6X75 catalyst

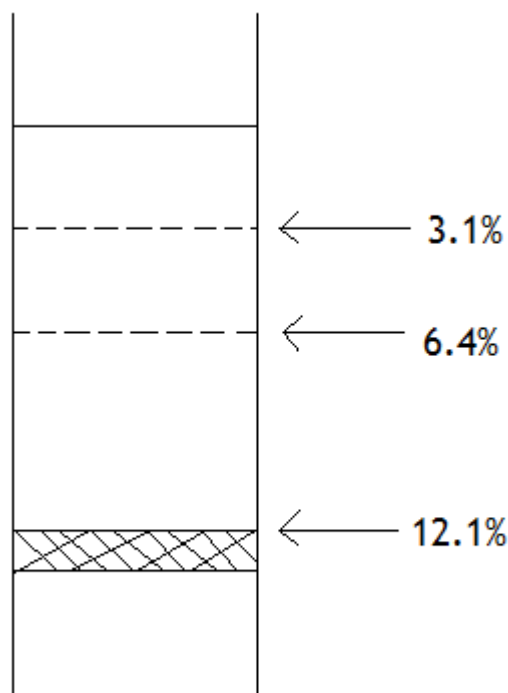


Figure 3-85: Bed profile summary using 20CoSA6X75

As can be seen from both profiling summaries in figures 3-84 and 3-85, there is a clear linear relationship between catalyst bed depth and the conversion of acetic acid to ethanol. The relationship between rate and the catalyst quantity are as would be expected, given that an increase in catalyst quantity and bed depth increases the amount of catalytic sites available for reaction. Additionally an increase in the bed depth would increase the residence time of the acetic acid over the catalyst bed, increasing the reactant- catalyst contact time.

3.5.4 Effect of Support Study

The effect of the support study ties in directly to the fundamental aims and objectives of this project. It asks the pertinent question: “Does a particular support have an increased activity and selectivity, even when using the same metal and at the same loading levels?” Given the catalysts examined throughout this research, the activity and stability of the cobalt based catalysts present cobalt as the best option of the three base metals investigated.

Impregnation catalysts with a 10 wt.% cobalt metal loading were produced on each of the following supports: silica Q10, alumina SA6X75 and titania ST61120. Additionally, a BP commercial 10 % Co/ZnO catalyst was also tested. Each of the

catalysts (excluding CoZnO) were prepared in the laboratory via an impregnation technique to a 10 wt.% cobalt loading. Each catalyst was tested in the same low pressure fixed bed reactor and under the same conditions as in chapter 3.6, for direct comparison between the supports.

Table 3-35: 10 wt.% cobalt catalysts with different supports

Support	Catalyst
Silica	CoA(10)Q10c
Alumina	CoN(10)SA6X75c
Titania	CoN(10)ST61120c
Zinc Oxide	CoZnO (BP catalyst)

Each catalyst was prepared onto a pelletized support or was supplied in that form. Prior to characterization and testing, all catalysts were crushed with the 250-425 μm particle size fraction used.

3.5.5 Supports

As part of the study into the effect of the support on the activity of the catalyst, it was important to be able to test the supports individually without the presence of the metal active phase.

3.5.5.1 Silica and Alumina Catalysts (CoN(10)Q10c and CoN(10)SA6X75c)

Of the four supports mentioned in this study, the silica Q10 and alumina SA6X75 have already been described in previous chapters. When previously mentioned within the context of testing on the low pressure glassline reactor system, the silica Q10 support displayed no activity for the hydrogenation of acetic acid to ethanol or to any other products. Following the on-line analysis of the product stream showed no hydrogenation products or otherwise. Similarly the alumina SA6X75 support was also tested on the low pressure reactor and also did not show any activity for the hydrogenation process. And, no individual support testing was carried out on either the titania or zinc oxide.

3.5.5.2 CoN(10)ST61120

The titania support used for the 10 wt.% cobalt on titania catalyst was Saint-Gobain Norpro ST61120, which was supplied in the form of 3 mm pellets. The XRD pattern showed sharp defined peaks that corresponded to the anatase form of titania. BET analysis of the titania support showed a slightly lower surface area value to that of the silica and alumina supports investigated.

3.5.5.3 CoZnO

The 10 wt.% cobalt on zinc oxide tested was a commercial BP catalyst, primarily used as in Fischer-Tropsch catalysis. The catalyst was pre-calcined upon receipt and was subsequently crushed from its pelletised form into the 250-425 μm fraction. XRD analysis of the CoZnO was completed pre-reaction and is seen in figure 3-96. The assignable features correspond to the presence of zinc oxide, as expected. The catalyst had a low surface area calculated by BET measurements of $11.6 \text{ m}^2/\text{g}$. This value is significantly lower than that observed for the alumina, silica and titania support systems also investigated.

3.5.5.4 Summary of Reduction Conditions

Reduction temperatures were identified from the TPR profiles of the calcined catalysts. A standard set of reduction conditions were employed for the 10 wt.% cobalt catalysts shown in table 3-36.

Table 3-36: Reduction conditions for cobalt based catalysts in catalyst support study

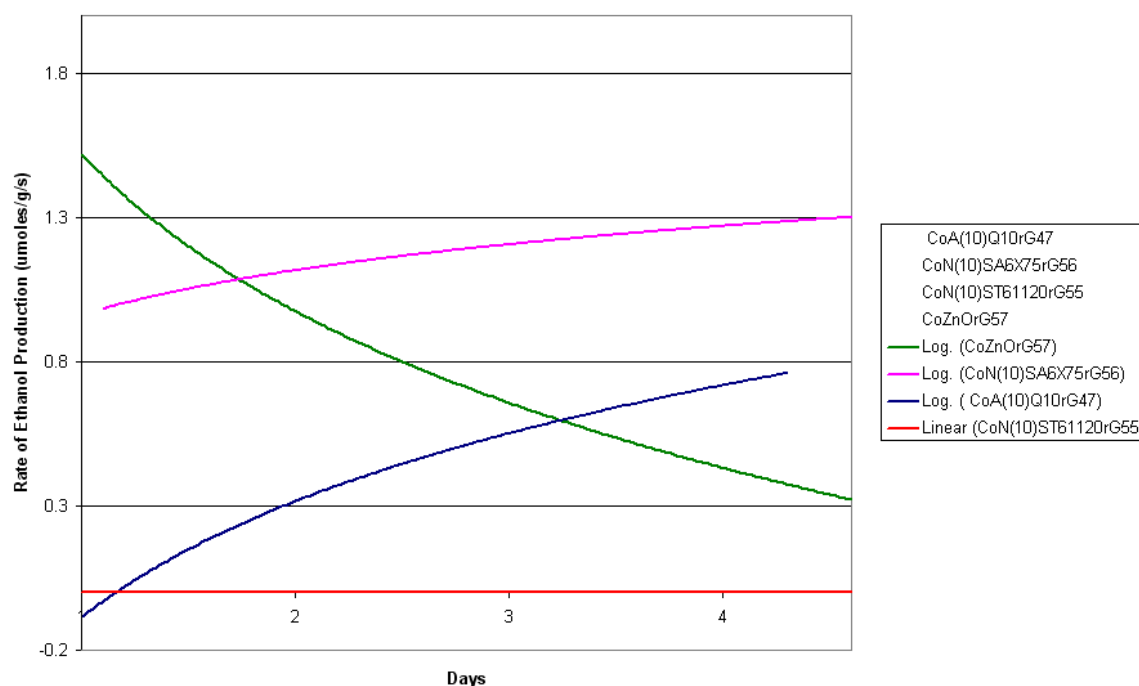
Temperature ($^{\circ}\text{C}$)	350
Ramp Rate ($^{\circ}\text{C}/\text{min}$)	10.0
Hold (mins)	240

3.5.6 Comparison of 10 wt.% cobalt catalysts

Each 10 wt.% cobalt catalyst was tested under the same conditions and using the same volume of catalyst (1 ml). The reaction conditions, shown in table 3-37, were the same as for all standard catalyst testing on the low pressure glass microreactor system.

Table 3-37: Table of reaction conditions for 10 wt.% cobalt catalysts

Temperature (°C)	Ramp Rate (°C min ⁻¹)	H ₂ Gas Flow (ml min ⁻¹)
250	10.0	60

Support Study: 10 wt. % Cobalt catalysts**Figure 3-86: Trend lines for the rates of ethanol production for 10 wt.% cobalt catalysts**

There is significant variance in the rates of ethanol production between the catalysts but the trend for each catalyst is quite distinctive. Apart from ST61220, which has a maintained ethanol production rate registering zero, the other trends vary quite a lot. Both Q10 and SA6X75 have increasing activity with time, although there is a large disparity between the activities.

The initial high activity of CoZnO is followed by a rapid deactivation of the catalyst which continues over the four day reaction period. This deactivation was seen to be a possibility due to the reactivity of the zinc oxide support with the acetic acid feed. A similar issue had been encountered with acetic acid and zinc oxide when using the commercial methanol synthesis catalyst, as discussed in chapter 3.2.

A surprising trend was observed with the 10 wt.% cobalt on silica, whose rate of ethanol production continued to increase throughout the reaction time. This trend is suggestive of a lack of complete activation of the catalyst post-reduction. An alternative explanation would be that a change in the catalyst or specifically changes to the metal active sites which make the catalyst more active for ethanol production as the reaction progresses. These trends are observed with the conversions and selectivity values shown in table 3-38.

Table 3-38: Table of results for each 10 wt.% Co catalyst on days one and four

Catalyst	CoA(10)Q10c		CoN(10)SA6X75c		CoN(10)ST61120c		CoZnO	
	1	4	1	4	1	4	1	4
Acid to EtOH(%)	1.1	7.7	12.9	17.4	0.3	--	51.8	25.3
Acid to Ethyl Acetate (%)	0.4	0.7	--	--	<0.1	--	--	--
Acid to Acetaldehyde (%)	--	--	--	--	--	--	--	--
Acid (%)	98.2	91.8	58.4	48.8	69.0	79.0	39.5	48.6
Conversion (%)	1.8	8.2	41.6	51.2	31.0	21.0	60.5	51.4

Online mass spectroscopy was monitored throughout the reactions. Despite this online system having no quantification of the results, we are still able to compare between samples and investigate the ratios. Looking at the MS data in figures 3-89 to 3-90 for day one for each of the 10 wt.% Co catalysts tested, we can see similarities between SA6X75, Q10 and ST61120 catalysts.

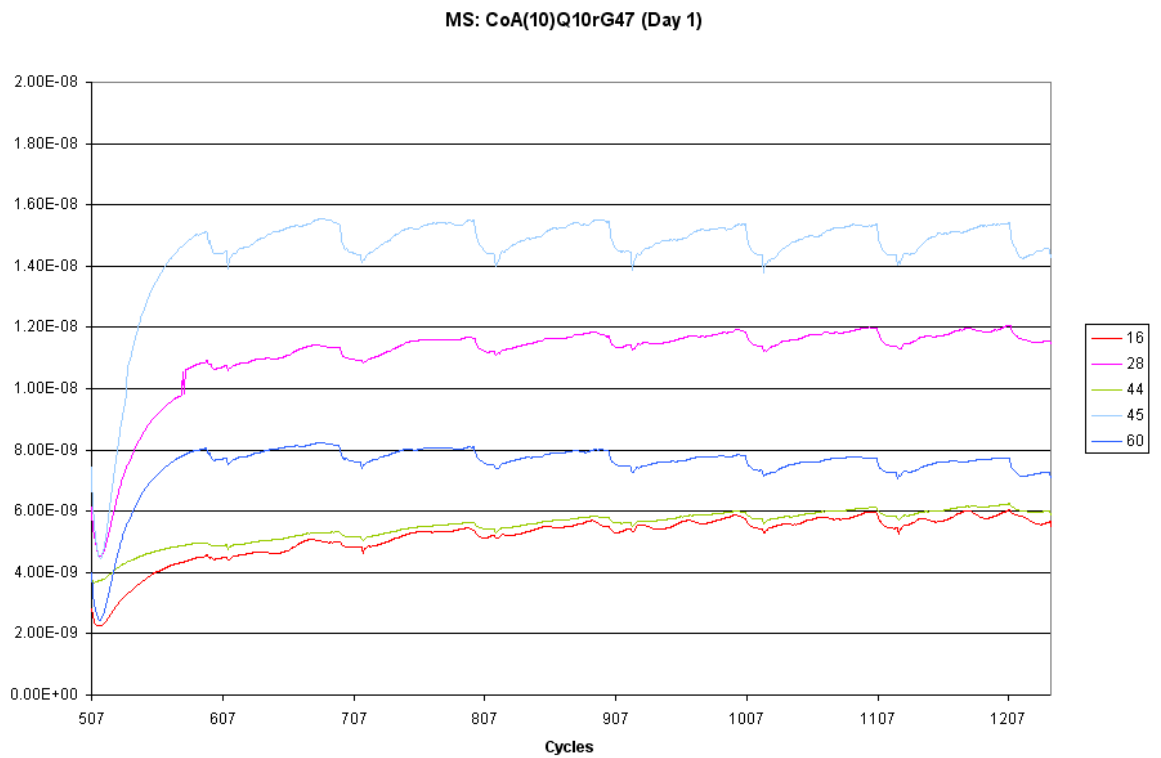


Figure 3-87: Day one of reaction MS data for CoA(10)Q10c

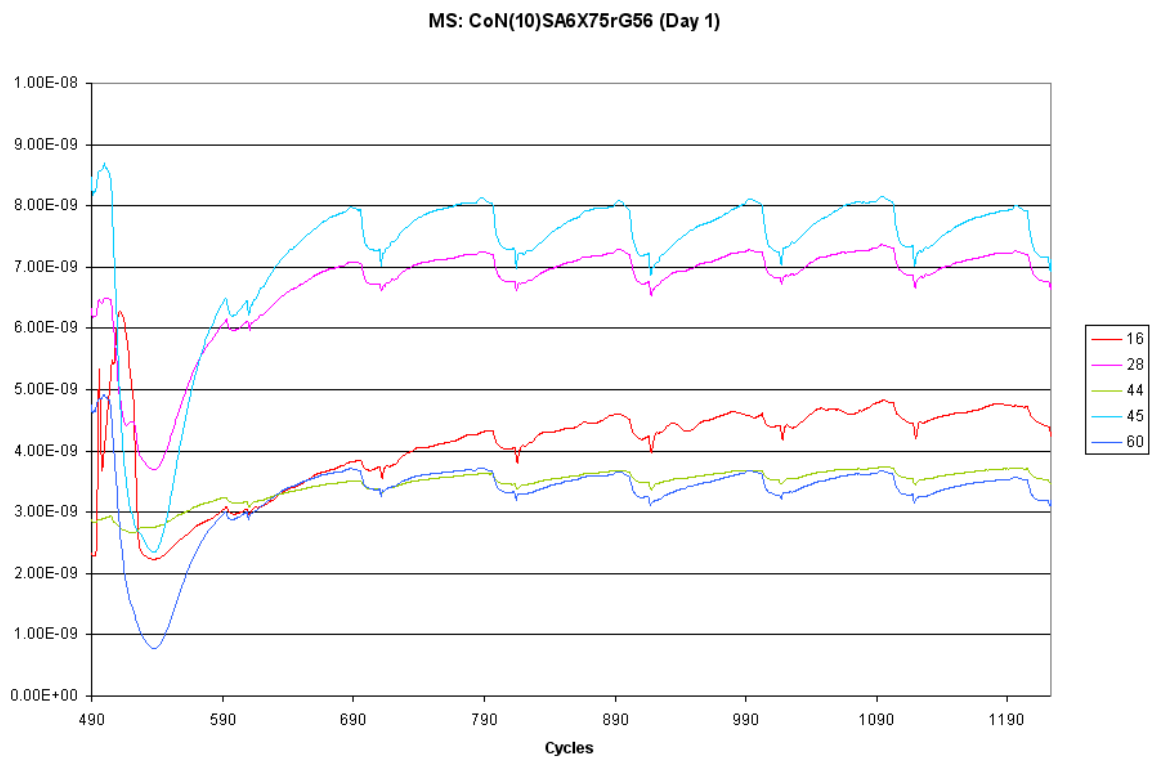


Figure 3-88: Day one of reaction MS data for CoN(10)SA6X75c

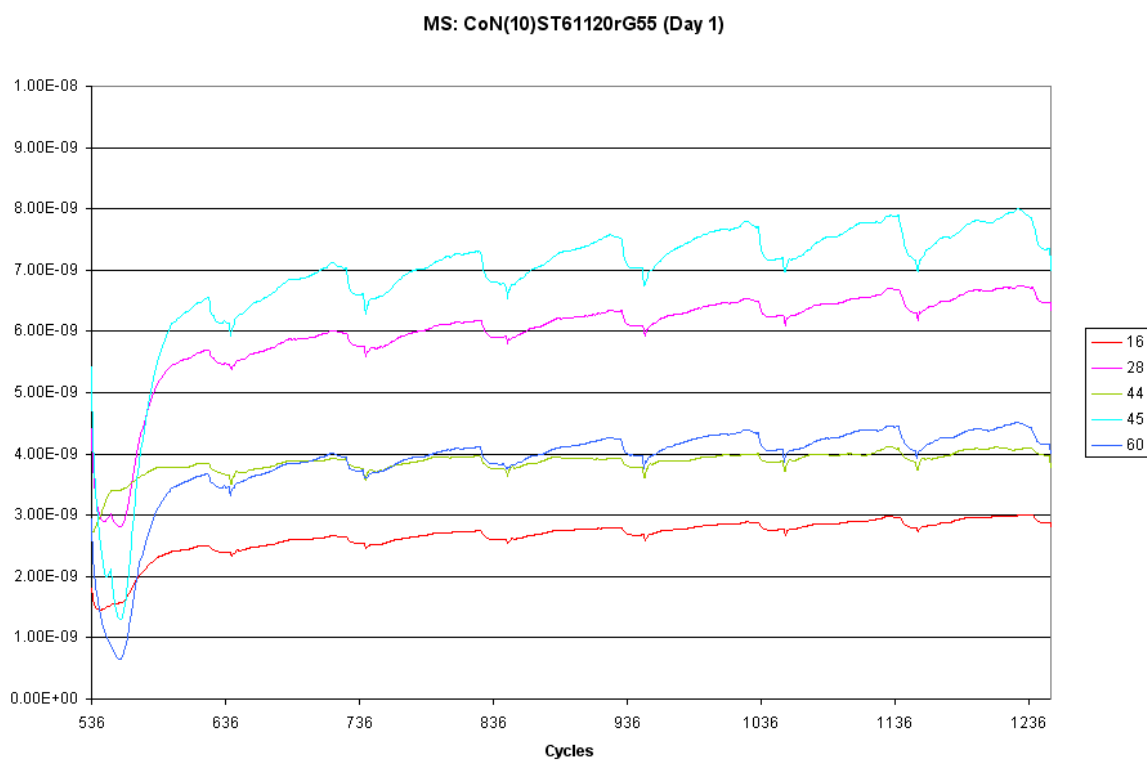


Figure 3-89: Day one of reaction MS data for CoN(10)ST61120c

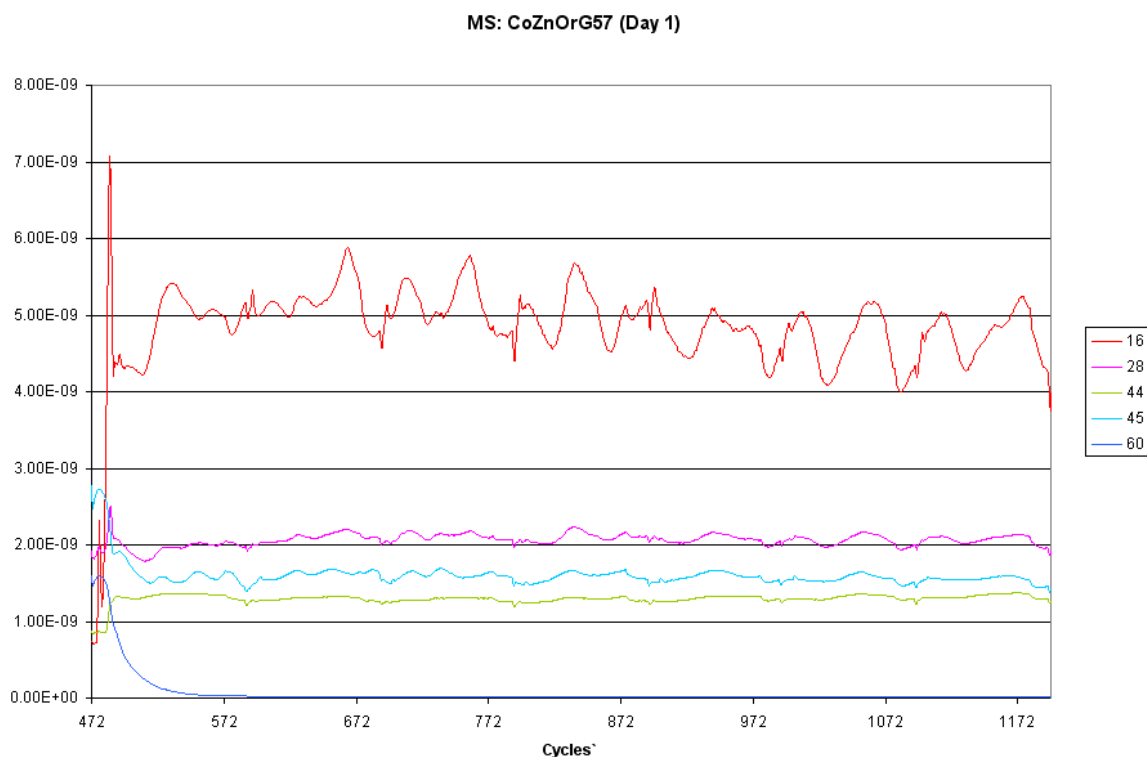


Figure 3-90: Day one of reaction MS data for CoZnO

CoZnO has a distinctly different MS pattern, seen in figure 3-90, from the other catalyst reactions with CH₄ product being much more pronounced.

3.5.7 Post-reaction characterisation

3.5.7.1 CoA(10)SA6X75

XRD analysis of the 10 wt.% cobalt on alumina catalyst showed no discernable difference in the patterns between the calcined and post-reaction samples. No distinctive peaks attributable to cobalt oxide or metallic cobalt were visible against the alumina background. The same inability to observe metal species features against the SA6X75 alumina XRD pattern was also encountered in the 20 wt.% base metal catalysts investigated in chapter 3.4.

The post-reaction TPO in figure 3-91 shows an initial loss around 100 °C for H₂O and then an additional single decomposition event.

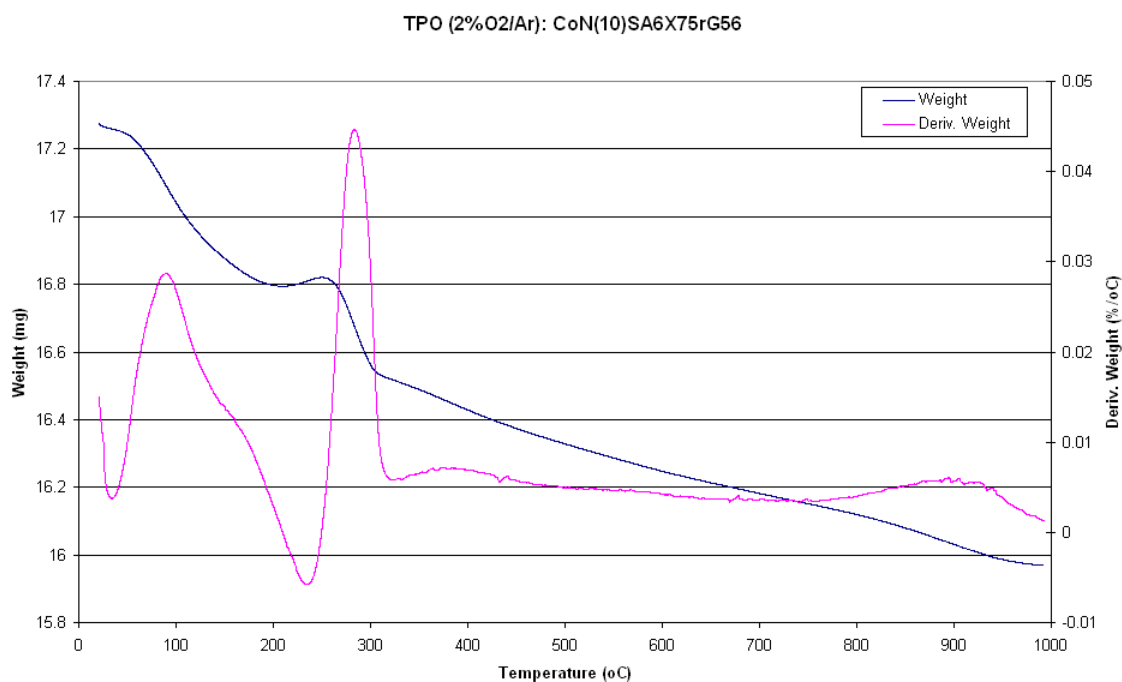


Figure 3-91: TPO of post-reaction 10 wt.% Co on SA6X75

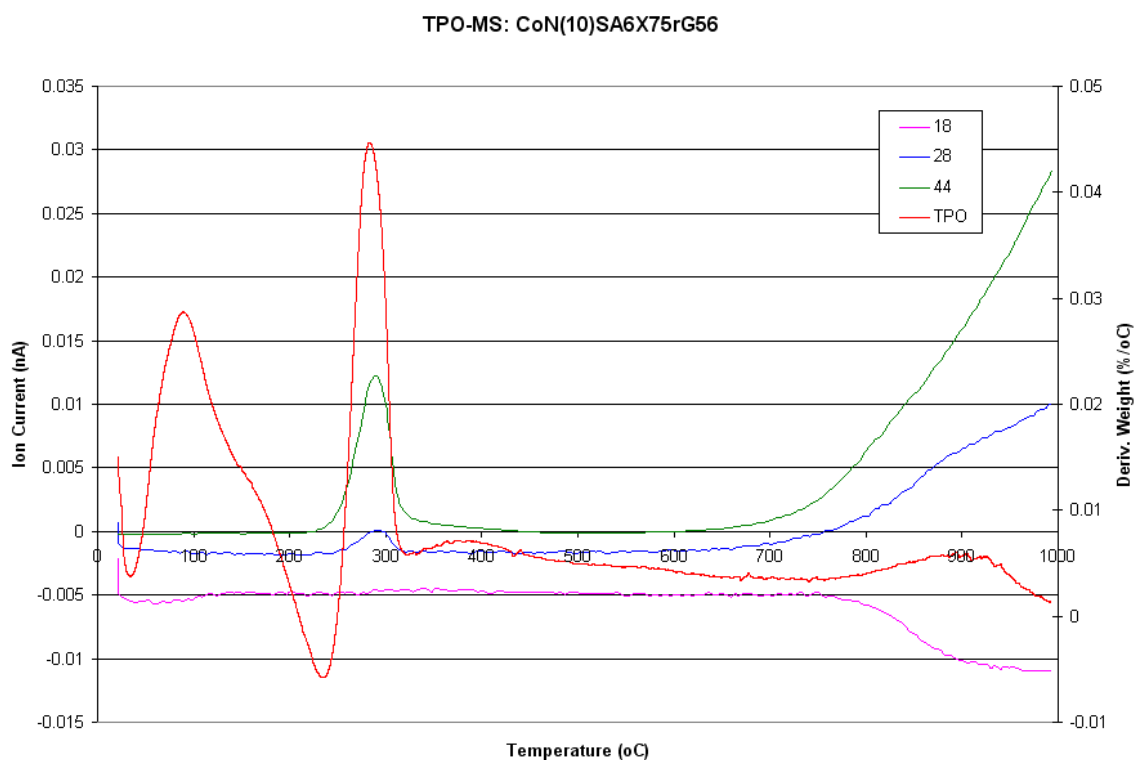


Figure 3-92: TPO-MS of post-reaction 10 wt.% Co on SA6X75

The large singular exothermic event at 287 °C in figure 3-92 has corresponding evolution events for CO₂ and CO. There is also a small corresponding peak for H₂O at the same event.

BET analysis shows no dramatic change in the surface area and pore volume measurements between the calcined catalyst and a post-reaction sample.

Table 3-39: BET results pre- and post-reaction for 10 wt.% Co on alumina SA6X75

Catalyst	Surface Area (m ² /g)	Pore Volume (ml/g)	Av. Pore Diameter (nm)
CoN(10)SA6X75c	179.6	0.53	12
CoN(10)SA6X75rG56	186	0.62	13

3.5.7.2 CoA(10)Q10c

XRD analysis of the cobalt on silica catalyst shows growth in the cobalt crystallite size between the calcined catalyst and the post-reaction sample. In the calcined sample, there are no peaks assignable to cobalt oxide against the amorphous silica background. Post-reaction, the presence of Co peaks confirms that the cobalt oxide was fully reduced and remained so throughout the reaction.

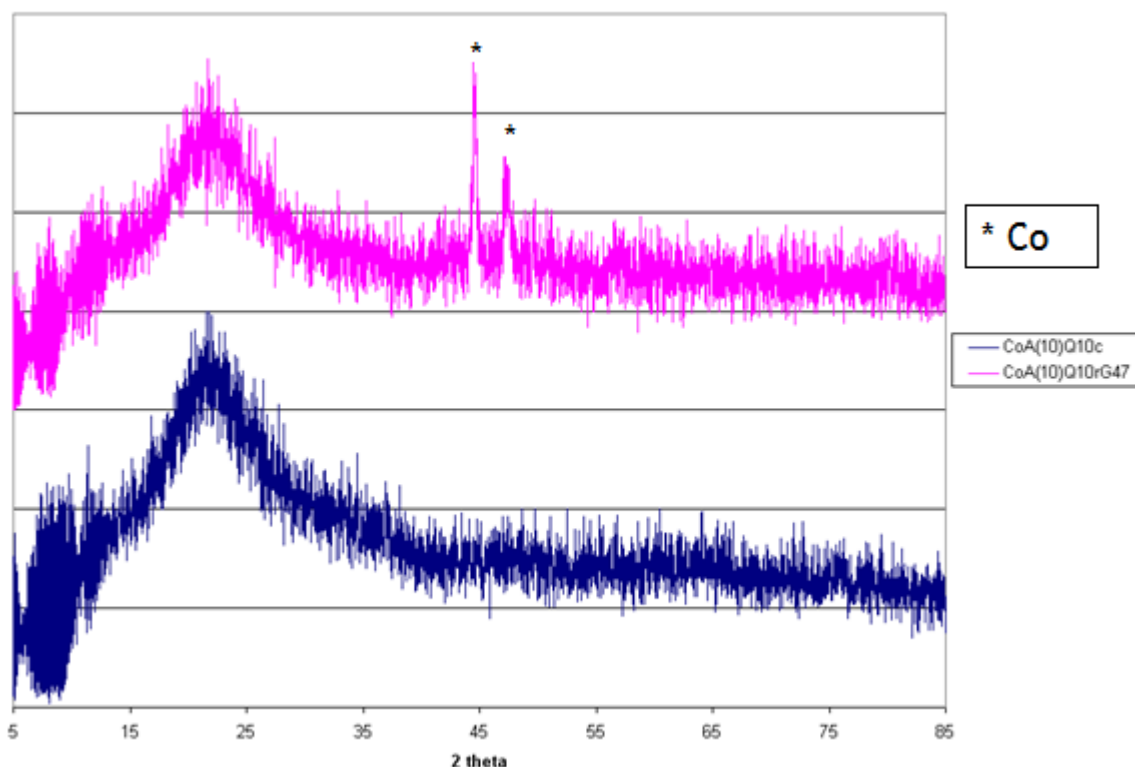


Figure 3-93: XRD patterns of calcined and post-reaction 10 wt.%Co on silica catalyst samples

The post reaction TPO of the catalyst revealed a low temperature evolution of CO_2 at 323 °C in figure 3-93, at a similar temperature to that seen in the TPO for 10 wt.% cobalt on alumina, suggesting similar species decomposition.

BET analysis of the catalyst in table 3-40, shows additional changes to the catalyst during the reaction with a decrease in surface area, a slight decrease in pore volume and an increase in the average pore diameter.

Table 3-40: BET results pre- and post-reaction for 10 wt.% Co on silica Q10

Catalyst	Surface Area (m ² /g)	Pore Volume (ml/g)	Av. Pore Diameter (nm)
CoA(10)Q10c	255.2	0.98	13
CoA(10)Q10rG47	201.2	0.81	16

3.5.7.3 CoN(10)ST61120

The 10 wt.% Co on titania showed severely limited activity towards the production of ethanol when tested on the low pressure glass microreactor. Despite not showing activity for ethanol, ethyl acetate or acetaldehyde production, the MS profile in figure 3-89 was not dissimilar to that of the alumina and silica based 10 wt.% cobalt catalysts.

XRD analysis of the catalyst does not show any significant change in the patterns between the calcined and post-reaction samples. The highlighted area in figure 3-93, around a value of 45°, would be the area in which peaks corresponding to metallic cobalt would be observed.

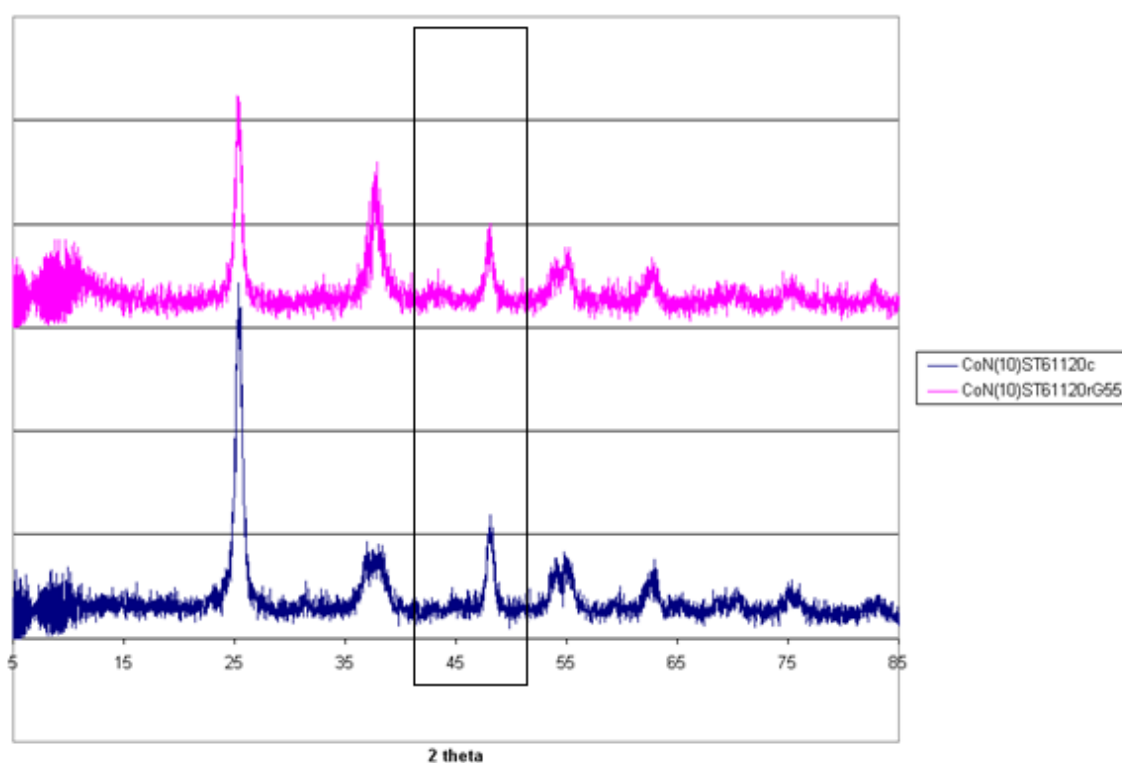


Figure 3-94: XRD patterns of 10 wt.% Co on titania; calcined and post-reaction

Post-reaction TPO analysis reveals a decomposition event at 323 °C in figure 3-95.

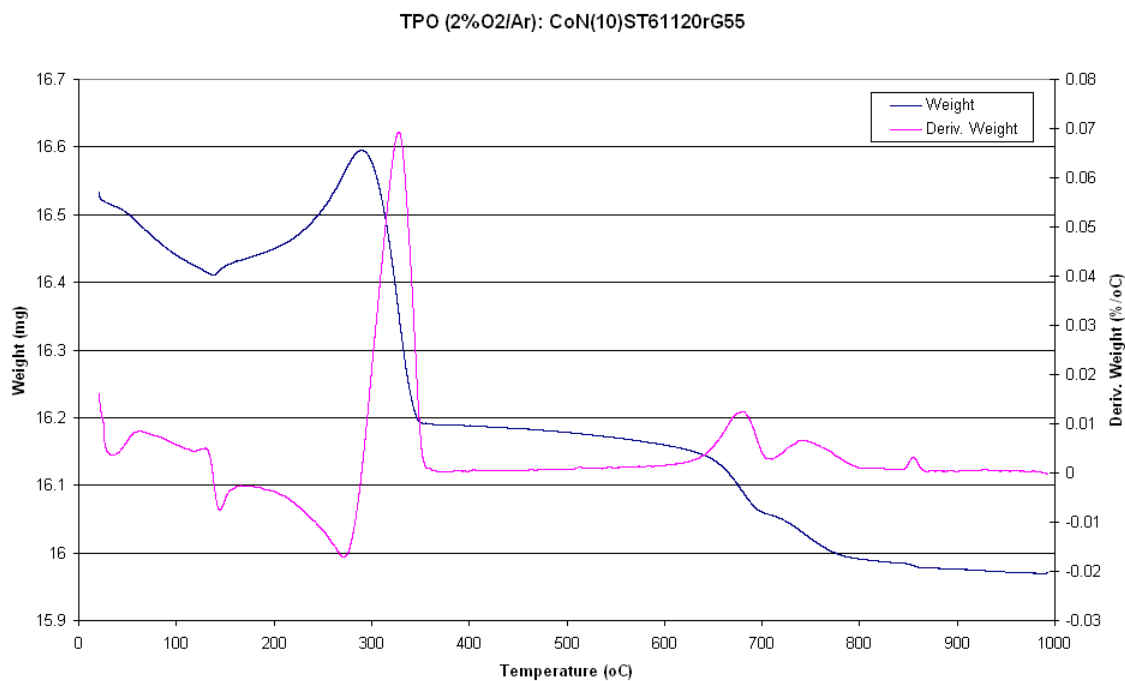


Figure 3-95: TPO for post-reaction 10 wt.% Co on ST61120

The evolution event at 323 °C, seen in figure 3-96, corresponds to an evolution of CO₂ and to a much lesser extent CO. This evolution is at a similar temperature to that the other 10 wt.% cobalt catalysts and would suggest that combustion products of similar species are evolving from the catalyst surface.

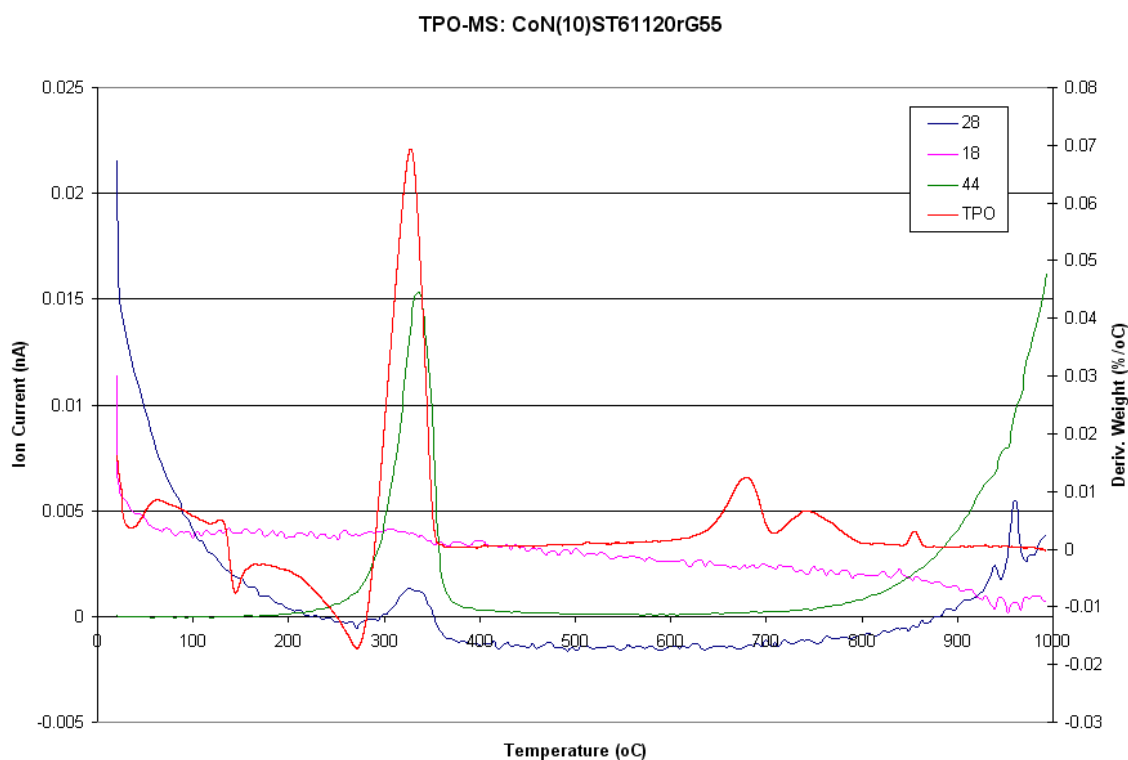


Figure 3-96: TPO-MS for post-reaction 10 wt.% Co on ST61120

BET analysis, shown in table 3-41, of the 10 wt.% cobalt on titania shows a slight decrease in surface area post-reaction. This decrease is observed even though the initial surface area of the titania support is lower than that of the alumina and silica alternatives.

Table 3-41: BET results for pre- and post-reaction 10 wt.% Co on titania ST61120 catalyst

Catalyst	Surface Area (m ² /g)	Pore Volume (ml/g)	Av. Pore Diameter (nm)
CoN(10)ST61120c	116.5	0.29	10
CoN(10)ST61120rG55	90.1	0.26	12

The amphoteric nature of titania could suggest an explanation for the lack of activity of the titania based catalyst. We can see that cobalt as a metal is active for the hydrogenation of acetic acid to ethanol, however this reduction is severely limited on the titania catalyst, suggesting that the acetic acid reacts

with the basic sites on the titania support rather than being hydrogenated through to the alcohol product.

3.5.7.4 CoZnO

The cobalt on zinc oxide catalyst was seen to deactivate rapidly over the duration of the hydrogenation reaction and as such changes in the physical properties of the catalyst would be expected.

XRD analysis in figure 3-97 of the CoZnO catalyst shows a decrease in crystallinity between the pre- and post- reaction samples, although no peaks are identifiable as cobalt species.

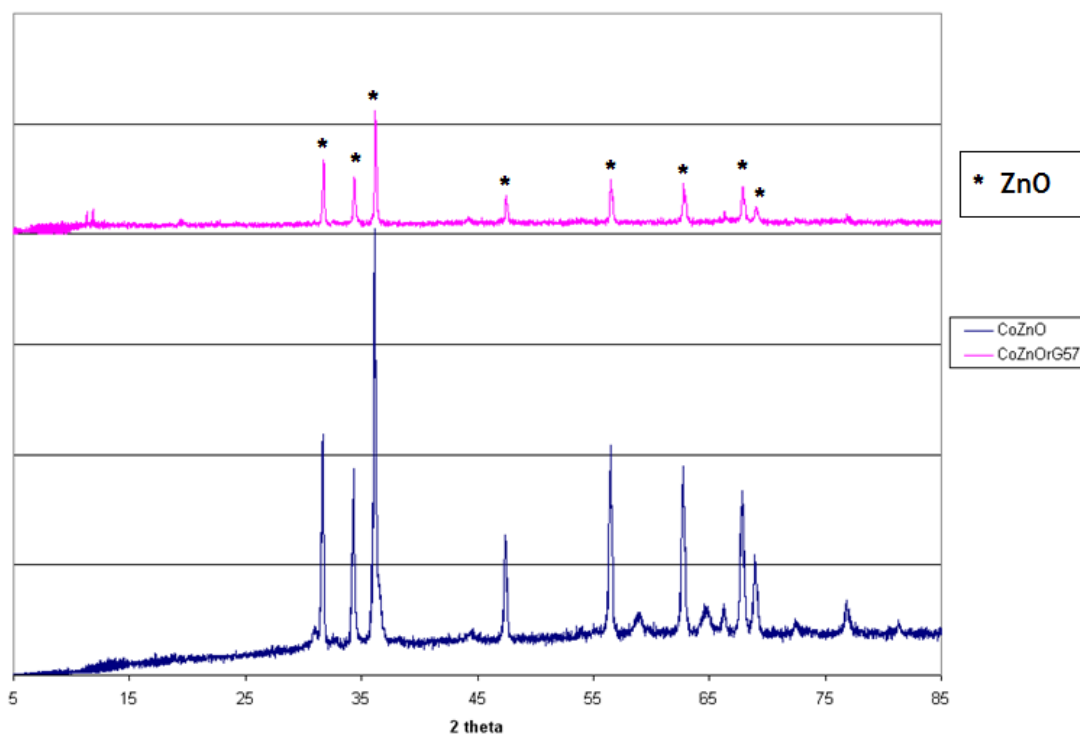


Figure 3-97: XRD patterns for 10% Co on Zinc Oxide; calcined and post-reaction

The post reaction TPO of the catalyst in figure 3-98 revealed a weight gain around 300 °C, as opposed to the traditional weight loss seen in the other TPOs for the alternative 10 wt.% cobalt catalysts.

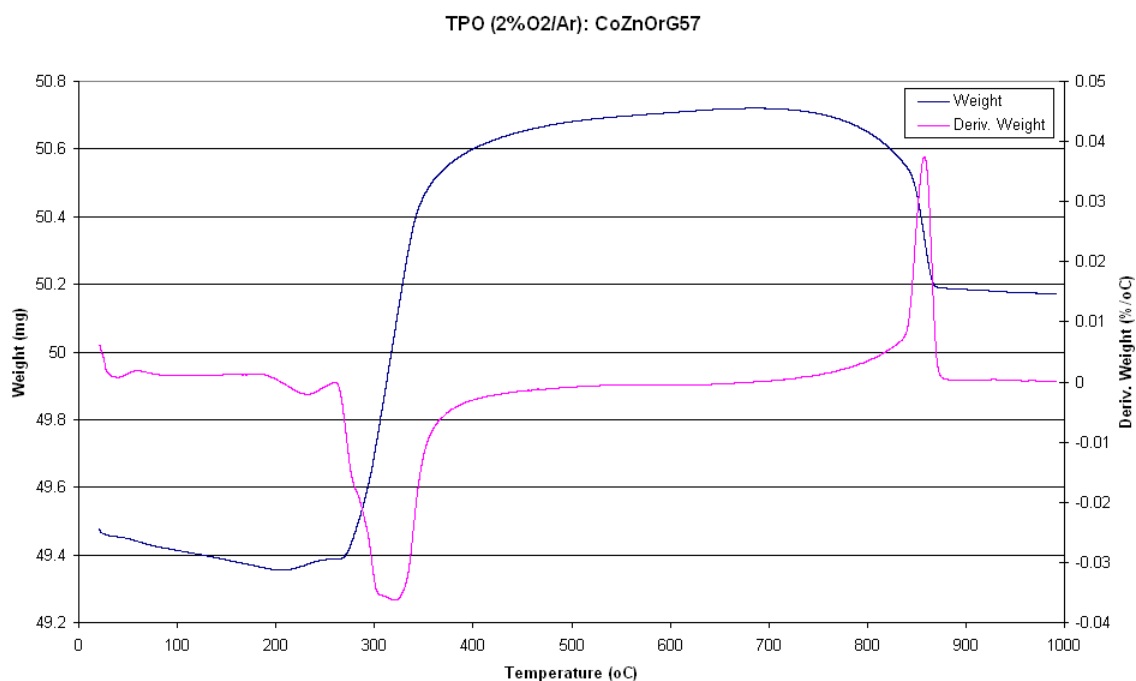


Figure 3-98: TPO of post-reaction 10% Co on ZnO

Interestingly, the uptake of O₂ during this 2 % weight gain produces a small evolution of CO₂. No CO evolution was observed within MS data.

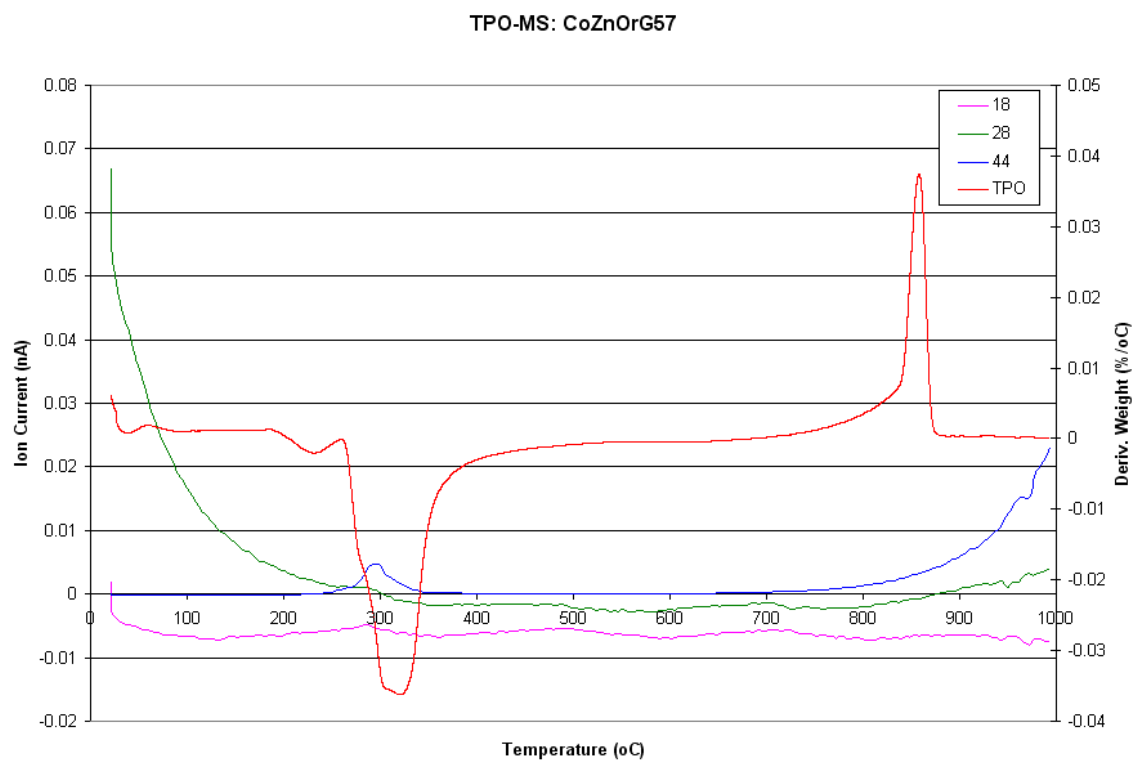


Figure 3-99: TPO-MS of post-reaction 10 wt.% Co on ZnO

BET analysis of the catalyst gives a clear indication of severe changes in the catalyst over the course of the reaction, as clear in table 3-42. The 90 % decrease in the pore volume of the catalyst along with diminished values for surface area and pore diameter are indicative of a sharp drop in crystallinity of the zinc oxide support. This is in agreement with the loss of crystallinity also observed in the XRD patterns in figure 3-97.

Table 3-42: BET results for pre-and post-reactions for 10 wt.% Co on ZnO

Catalyst	Surface Area (m ² /g)	Pore Volume (ml/g)	Av. Pore Diameter (nm)
CoZnO	11.6	0.1	35
CoZnOrG57	8.8	0.01	13

Significant decreases in the surface area, pore volume and average pore diameter of the CoZnO catalyst is in line with the activity decrease seen in the ethanol production rates in figure 3-86. This is in agreement with observations seen with the methanol synthesis catalyst. As the methanol synthesis catalyst also contains a zinc oxide component, the removal of ZnO from the catalyst particle via the reaction of acetic acid and ZnO to produce zinc acetate was observed. In addition, in the case of CoZnO, we saw the presence of lilac coloured crystals in the reactor tube post-reaction. The crystals were deposited around the temperature junction at the edge of the heated section of the reactor tube, mirroring the crystal deposits observed when using the methanol synthesis catalyst at HRTC which are discussed in chapter 3.2.

Analysis of the lilac crystals proved difficult due to the small quantity of crystals formed from the samples, but the colour of the crystals suggests that it is a cobalt containing complex. The small amount of crystals available, even in a capillary tube, was not enough for a distinctive diffraction pattern to be gained. Alternatively the sample was analysed via both ¹³C and ¹H NMR. The results listed below identify that the product contains acetate groups.

NMR analysis was completed using a 400 MHz spectrometer with DMSO as the solvent. ^1H NMR (δH) = 1.80 (3H, CH_3). Solvent peaks DMSO = 2.50 ppm, H_2O = 3.46 ppm. ^{13}C NMR (δC) = 200.3 (C=O), 22.43 (CH_3). Solvent peaks DMSO = 39.58 ppm.

3.5.8 Summary

This direct comparison of catalysts with the same metal loading of 10 wt.% cobalt but with varying catalyst supports allowed an investigation into the impact of the support on the activity of the catalyst. The alumina catalyst is seen to be the best performer for the hydrogenation of acetic acid to ethanol.

The four 10 wt.% cobalt catalysts all produce ethanol as their major or only product, so the activity of the catalysts can be represented solely by the rates of ethanol production. The CoA(10)Q10 catalyst shows an encouraging increase in activity over time, although there was a question about the possibility of an incomplete reduction of Co during the reduction process. A gradual reduction of the Co species to the active Co metal species over time might explain the gradual increase in activity but given that all the catalysts, except CoZnO, gave similar TPR profiles, this would be unexpected. However, the 10 wt.% Co on alumina and titania were prepared from the nitrate precursor whilst the 10 wt.% Co on silica was prepared from the acetate precursor.

There is research [43, 56] that attributes definitive differences in metal particle size control, metal reduction and intermediate species production differences dependent on the precursor species used in the preparation techniques, especially with regard to cobalt catalysts used in Fischer-Tropsch chemistry. This may be something unique to cobalt, as the studies with the acetate and nitrate precursors for copper, although they give different intermediates, appear to display the same end activity.

The titania based catalyst displayed limited activity which may be attributable to the amphoteric nature of the titania support. CoZnO's initial rate of ethanol production is encouraging although its rapid deactivation was not unexpected due to the reactivity of ZnO and acetic acid. Its rapid and continuing decrease in rate, below its silica and alumina counterparts, demonstrates the required

stability and inertness of a catalyst support, especially in this reaction with a corrosive reactant.

4 Conclusions

Previous literature on the hydrogenation of acetic acid [2] showed activity for copper based catalysts, which outperformed their base metal counterparts for the production of ethanol. However, the activity of the copper catalysts was low in comparison to the precious metal alternatives [18]. The activity of a copper based catalyst was again observed when acetic acid was hydrogenated to ethanol over a methanol synthesis catalyst [1] whilst investigating the possible effects of acetic acid in a carbonylation recycle stream. Following these observations, this research project aimed to investigate if base metal catalysts could produce ethanol at the same rates and selectivities as seen with precious metals. In doing so, it looked to identify potential acid -tolerant base-metal catalysts for the selective hydrogenation of acetic acid to ethanol.

The first base metal catalyst investigated was the methanol synthesis catalyst which was highly active for the hydrogenation of acetic acid to ethanol. It also deactivated rapidly. This deactivation combined with a lack of stability made it a non-viable option as an acetic acid hydrogenation catalyst. However, the high initial activity for the methanol synthesis catalyst is attributable to its high copper content. A linear relationship observed with the low copper loaded catalysts confirms the link between increased catalyst copper content and increased activity.

Aside from the catalyst composition, the design of the reactor used for testing also plays an important role in the product profiles seen. The differential reactor with its internal recycle increased the opportunities for esterification to ethyl acetate compared to fixed bed reactors; a trend which was observed amongst the copper based catalysts. Reactor design impact was observed with copper on silica catalysts which were much more active for the esterification reaction in the integral reactor than in the comparative fixed bed system.

Further investigations into reaction variables explored the use of higher acetic acid feed rates. A consequence of using high acetic acid concentrations was increased degradation of copper based catalysts. This was observed through sintering of the copper component into visible metal flakes exterior to the catalyst. Zinc oxide extraction from the catalyst pellets was observed with the

methanol synthesis catalyst. These physical catalyst degradations show why copper based catalysts are inappropriate for use with acetic acid.

Following this, alternative catalysts using cobalt and nickel were tested against a copper based system. Of the three base metals, cobalt was the most active. However, the activity of the cobalt catalyst increased over time. A possible explanation for this is the initial incomplete reduction of the catalyst. A gradual reduction in the cobalt species to the active Co metal species over time may explain the gradual increase in activity. Alternatively, the activity increase may be a result of increases in metal particle size due to sintering during the reaction. This observation demonstrated that either the reduction profile employed was not appropriate or that stricter control over the cobalt particle size was necessary to optimise activity.

The data for the 5 wt.% and 10 wt.% copper catalysts clearly shows a link between activity and metal loading on the catalyst. When the metal loading was increased to 20 wt.% for each of the base metal investigated, the cobalt catalyst was again superior. It gave the highest conversion with the highest selectivity to ethanol, whilst remaining stable over the four day reaction period. The 20 wt.% cobalt on alumina was the best catalyst investigated for this process.

Optimisation of the conditions for a cobalt catalyst included investigations into the reaction temperature. It was observed that 200 °C was too low with minimal activity observed, whilst 300 °C was too high with methane produced. An optimal temperature of 250 °C yielded the highest ethanol production.

Additional optimisation investigated the impact of supports on the activity of a cobalt based catalyst. Four supports were tested with a 10 wt.% cobalt loading, of which alumina was observed as the optimal support. The silica based catalyst was also active for ethanol production, but like the other silica systems tested also facilitated the secondary esterification reaction. The titania supported catalyst exhibited no activity towards the production of ethanol. The amphoteric nature of titania could be an explanation for the lack of activity, as the acetic acid would react with the basic sites on the support rather than be converted to ethanol. CoZnO's initial rate of ethanol production is encouraging although its rapid deactivation was not unexpected due to the reactivity of ZnO

and acetic acid. Its rapid and continuing decrease in rate, below its silica and alumina counterparts, demonstrates the required stability and inertness of a catalyst support, especially in this reaction with a corrosive reactant.

Comparison of all the base metal catalysts investigated in this project showed that cobalt based systems gave the most desirable results. The 20 wt.% cobalt on alumina, specifically, demonstrated the highest stable activity towards ethanol for the duration of the reaction period at an optimum reaction temperature of 250 °C. Despite the high metal loading, which is not desirable, the catalyst still does not achieve the activity expected from an ideal catalyst for hydrogenation of acetic acid to ethanol. Its stability, however, both in terms of ethanol production and catalyst integrity offers hope for further research.

References

1. Blain, S., Ditzel, E., and Jackson, S. D., *A mechanistic study into the effect of acetic acid on methanol synthesis*. *Catal. Sci.*, 2012. **2**(4): p. 778-783.
2. Cressely, J., Farkhani, D., Deluzarche, A., and Kiennemann, A., *The Evolution of Carboxylate Species in the Framework of CO-H₂ Synthesis - Reduction of Acetic-Acid on the Co,Cu,Fe System*. *Mat. Chem. Phys.*, 1984. **11**(5): p. 413-431.
3. Yokoyama, T., Setoyama, T., *Fine Chemicals through Heterogenous Catalysis*. 2001: Wiley-VCH.
4. Licht, F. O., *Renewable Fuels Association, Ethanol Industry Outlook 2008-2013 reports*.
5. Monick, J. A., *ALCOHOLS: Their Chemistry, Properties and Manufacture*. 1968: Reinhold Book Corporation.
6. Surisetty, V. R., Dalai, A. K., and Kozinski, J., *Alcohols as alternative fuels: an overview*. *Appl. Catal., A*, 2011. **404**(1-2): p. 1-11.
7. Berg, C., *World Fuel Ethanol Analysis and Outlook*. 2004.
8. *Directive 2009/30/EC*, in L140/88. 5 June 2009: Official Journal of the European Union.
9. *Energy Policy Act (EPAct) in Public Law 109-58*. 2005
http://www.afdc.energy.gov/laws/epact_2005: USA.
10. *Ineos Enterprises Ethanol Portfolio*. 16 Sep 2013]; Available from:
<http://www.ineos.com/en/businesses/INEOS-Enterprises/Portfolio/>.
11. Sakuth, M., Lohrengel, G., Maschmeyer, D., and Stochniol, G., *US 09/701054: Method for producing a dealuminized catalyst support*. 2005, Sasol Germany GmbH (Hamburg, DE): United States.
12. Johnston, V. J., Chen, L., Kimmich, B. F., Chapman, D. J., and Zink, D., *US 2010/0197485 A1: Catalysts for making ethanol from acetic acid (Celanese International Corporation)*, Office, U. S. P., Editor. 2010, Celanese International Corporation: US.
13. Kitson, M. and Williams, P. S., *EPO 86302692.8: Alcohols production by hydrogenation of carboxylic acids (BP Chemicals Ltd)*, Office, E. P., Editor. 1986: GB.
14. Kitson, M. and Williams, P. S., *EPO 86302691.0: Alcohols production by hydrogenation of carboxylic acids (BP Chemicals Ltd)*, Office, E. P., Editor. 1986: GB.
15. Kitson, M. and Williams, P. S., *EPO 88302891.2: The catalysed hydrogenation of carboxylic acids and their anhydrides to alcohols and/or esters*, Office, E. P., Editor. 1988: GB.
16. Bowker, M. and Cassidy, T. J., *Decomposition of Acetate Groups on an Alumina-Supported Rhodium Catalyst*. *J. Catal.*, 1998. **174**(1): p. 65-71.
17. Bowker, M., Morgan, C., and Couves, J., *Acetic acid adsorption and decomposition on Pd(110)*. *Surf. Sci.*, 2004. **555**(1-3): p. 145-156.
18. Olcay, H., Xu, L. J., Xu, Y., and Huber, G. W., *Aqueous-Phase Hydrogenation of Acetic Acid over Transition Metal Catalysts*. *Chemcatchem*. **2**(11): p. 1420-1424.
19. Alcalá, R., Shabaker, J. W., Huber, G. W., Sanchez-Castillo, M. A., and Dumesic, J. A., *Experimental and DFT Studies of the Conversion of Ethanol and Acetic Acid on PtSn-Based Catalysts*. *J. Phys. Chem. B*, 2004. **109**(6): p. 2074-2085.

20. Ferrin, P., Simonetti, D., Kandoi, S., Kunkes, E., Dumesic, J. A., Nørskov, J. K., and Mavrikakis, M., *Modeling Ethanol Decomposition on Transition Metals: A Combined Application of Scaling and Brønsted–Evans–Polanyi Relations*. *J. Am. Chem. Soc.*, 2009. **131**(16): p. 5809-5815.
21. Kiennemann, A., Farkhani, D., Deluzarche, A., and Cressely, J., *Evolution des especes carboxylates dans le cadre des synthèses CO-H₂. II. Promotion de la formation d'especes acetates par le choix de supports, de l'alcalinisation et de combinaisons bimetalliques sur systemes Co, Cu, Fe*. *Mater. Chem. Phys.*, 1985. **12**(5): p. 449-459.
22. *US 2011/0282109: Ethanol Production from Acetic Acid Utilizing a Cobalt Catalyst*. 2011, Celanese International Corporation: USA.
23. *US 2011/0263911: Direct and Selective Production of Ethanol from Acetic Acid Utilizing a Platinum/Tin Catalyst*. 2011, Celanese International Corporation: USA.
24. *US 2011/0245546: Ethanol Production from Acetic Acid Utilizing a Cobalt Catalyst*. 2011, Celanese International Corporation: USA.
25. *US 2012/0149949: Process For Producing Ethanol Using A Stacked Bed Reactor*. 2012, Celanese International Corporation: USA.
26. *US 2012/0178975: Process for Production of Ethanol Using a Mixed Feed Using Copper Containing Catalyst*. 2012, Celanese International Corporation: USA.
27. *US 2012/0238785: Process For The Production of Ethanol From An Acetic Acid Feed and A Recycled Ethyl Acetate Feed*. 2012, Celanese International Corporation: USA.
28. Onyestyák, G., Harnos, S., Klébert, S., Štolcová, M., Kaszonyi, A., and Kalló, D., *Selective reduction of acetic acid to ethanol over novel Cu₂In/Al₂O₃ catalyst*. *Appl. Catal., A*, 2013. **464-465**(0): p. 313-321.
29. *US 2012/0253085: Ethanol Production from Acetic Acid Utilizing a Molybdenum Carbide Catalyst*. 2012, Celanese International Corporation: USA.
30. Yoneda, N., Kusano, S., Yasui, M., Pujado, P., and Wilcher, S., *Recent advances in processes and catalysts for the production of acetic acid*. *Appl. Catal., A*, 2001. **221**(1-2): p. 253-265.
31. Vannice, M. A. and Rachmady, W., *Acetic acid hydrogenation over Pt and Fe catalysts*. Abstracts of Papers of the American Chemical Society, 2002. **223**: p. C7-C8.
32. Rachmady, W. and Vannice, M. A., *Acetic acid hydrogenation over supported platinum catalysts*. *J. Catal.*, 2000. **192**(2): p. 322-334.
33. Bowker, M., *On the Mechanism of Ethanol Synthesis on Rhodium*. *Catal. Today*, 1992. **15**(1): p. 77-100.
34. Waugh, K. C., *Methanol Synthesis*. *Catal. Lett.*, 2012. **142**: p. 1153-1166.
35. Behrens, M., Kasatkin, I., Kuhl, S., and Weinberg, G., *Phase-Pure Cu,Zn,Al Hydrotalcite-like Materials as Precursors for Copper rich Cu/ZnO/Al₂O₃ Catalysts*. *Chem. Mater.* **22**(2): p. 386-397.
36. Sofianos, A. C., Heveling, J., Scurrall, M. S., Armbruster, A., Gucci, L., Solymosi, F., and TÉTÉNYi, P., *Methanol Synthesis Over Copper Based Catalysts: Comparison of Co-Precipitated, Raney-Type and Catalysts Derived from Amorphous Alloy Precursors*, in *Studies in Surface Science and Catalysis*. 1993, Elsevier. p. 2721-2724.
37. Subramanian, N. D., Balaji, G., Kumar, C., and Spivey, J. J., *Development of cobalt-copper nanoparticles as catalysts for higher alcohol synthesis from syngas*. *Catal. Today*, 2009. **147**(2): p. 100-106.

38. Shabaker, J. W., Simonetti, D. A., Cortright, R. D., and Dumesic, J. A., *Sn-modified Ni catalysts for aqueous-phase reforming: Characterization and deactivation studies*. J. Catal., 2005. **231**(1): p. 67-76.
39. Rachmady, W. and Vannice, M. A., *Acetic acid reduction to acetaldehyde over iron catalysts I. Kinetic behavior*. J. Catal., 2002. **208**(1): p. 158-169.
40. Rachmady, W. and Vannice, M. A., *Acetic acid reduction to acetaldehyde over iron catalysts II. Characterization by Mossbauer spectroscopy, DRIFTS, TPD, and TPR*. J. Catal., 2002. **208**(1): p. 170-179.
41. Drossbach, O. and Johannsen, A., *U.S. Patent 2018350*. 1935.
42. Pinna, F., *Supported metal catalysts preparation*. Catal. Today, 1998. **41**(1-3): p. 129-137.
43. Lok, C. M., *Novel highly dispersed cobalt catalysts for improved Fischer-Tropsch productivity*. Stud. Surf. Sci. Catal. , 2004. **147**: p. 283-288.
44. Satterfield, C. N., *Heterogeneous Catalysis In Industrial Practice*. 1991: McGraw Hill.
45. Nunan, J. G., Bogdan, C. E., Klier, K., Smith, K. J., Young, C.-W., and Herman, R. G., *Higher Alcohol and Oxygenate Synthesis over Cesium-Doped Cu/ZnO Catalysts*. J. Catal., 1989. **116**: p. 195-221.
46. *Handbook of Chemistry and Physics*. 90th Edition ed.: CRC.
47. Doesburg, E. B. M., Höppener, R. H., de Koning, B., Xiaoding, X., and Scholten, J. J. F., *Preparation and Characterization of Copper/Zinc Oxide/Alumina Catalysts for Methanol Synthesis*, in *Studies in Surface Science and Catalysis*, B. Delmon, P. G. P. A. J. and Poncelet, G., Editors. 1987, Elsevier. p. 767-783.
48. Aas, N. and Bowker, M., *Adsorption and Autocatalytic Decomposition of Acetic-Acid on Pd(110)*. J. Chem. Soc.-Faraday Trans., 1993. **89**(8): p. 1249-1255.
49. von Niekerk, J. N., Acta. Cryst., 1953. **6**(8): p. 720-723.
50. Mariño, F. J., Cerrella, E. G., Duhalde, S., Jobbagy, M., and Laborde, M. A., *Hydrogen from steam reforming of ethanol. characterization and performance of copper-nickel supported catalysts*. Int. J. Hydrogen Energy, 1998. **23**(12): p. 1095-1101.
51. Marino, F., Boveri, M., Baronetti, G., and Laborde, M., *Hydrogen production via catalytic gasification of ethanol. A mechanism proposal over copper-nickel catalysts*. Int. J. Hydrogen Energy, 2004. **29**(1): p. 67-71.
52. Wang, L., Li, D., Koike, M., Watanabe, H., Xu, Y., Nakagawa, Y., and Tomishige, K., *Catalytic performance and characterization of Ni-Co catalysts for the steam reforming of biomass tar to synthesis gas*. Fuel, 2013. **112**(0): p. 654-661.
53. Bridier, B., Lopez, N., and Perez-Ramirez, J., *Partial hydrogenation of propyne over copper-based catalysts and comparison with nickel-based analogues*. J. Catal. **269**(1): p. 80-92.
54. Pant, K. K., Mohanty, P., Agarwal, S., and Dalai, A. K., *Steam reforming of acetic acid for hydrogen production over bifunctional Ni-Co catalysts*. Catal. Today, 2013. **207**(0): p. 36-43.
55. Hu, X. and Lu, G. X., *Comparative study of alumina-supported transition metal catalysts for hydrogen generation by steam reforming of acetic acid*. Appl. Catal. B. **99**(1-2): p. 289-297.
56. Vogelaar, B. M., van Langeveld, A. D., Kooyman, P. J., Lok, C. M., Bonné, R. L. C., and Moulijn, J. A., *Stability of metal nanoparticles formed*

during reduction of alumina supported nickel and cobalt catalysts. Catal. Today, 2011. 163(1): p. 20-26.